STUDY

ON

MASS SPECTROMETER FOR DIRECT MEASUREMENT OF

THE UPPER-ATMOSPHERE COMPOSITION

by

Nobuyoshi FUGONO

Radio Research Laboratories

Ministry of Posts and Tellecommunications

August, 1970

Doctoral Thesis Kyoto University

PREFACE

The ionosphere consists of plasma generated mainly by the solar radiation. It extends from the altitude of about several tens to a few thousands kilometers and the importance of its role in communication over long distance on the earth never decreases even today when the communication satellites are also put to practical use. It is still worthwhile for practical and scientific purpose to make the characteristics of the ionosphere fully clear. The ionosphere is regarded as in an equilibrium state between ionization or excitation of the upper-atmosphere by the solar radiation and neutralization through various chemical reactions and dynamics. All parameters in these complex reactions must be known to understand the behabiour of the ionosphere.

Up to this time, the condition of the ionosphere has been expressed mainly by its measured electron density versus height. Of course, the electron density has a simple relation to the reflection of radio wave, and the most easily measured parameter to express the condition of the ionosphere. There are many species

of ions, however, with which electrons have parted, or neutral gases which are their parents. It may be said that the knowledge of the composition of the upper-atmosphere gives us a colorful information in comparison with electrons.

It was difficult to know the complicated composition of the upper-atmosphere by indirect measurements from the ground, because of their insensible motions. A powerful means, namely, the direct measurement by rocket-borne instruments was found after World War II. The mass spectrometry is one of the most effective method of the direct measurement of the upper-atmospheric composition.

In this thesis, mass spectrometers used in the direct measurement on space vehicles are reviewed in Chapter I. A new type of mass spectrometer which is expected to be suitable for long time flight space vehicles, is proposed and investigated both theoretically and experimentally in Chapter II. Various problems which are caused by direct measurements in the upper-atmospheric plasma, and their calibrations are studied in Chapter III. An apparatus which has been constructed for the calibration especially on the mass spectrometry,

is also introduced in the same chapter. Results of a rocket-borne experiment of the proposed mass spectrometer are described in Chapter IV together with the preflight experiment of the instrument. Finally in Chapter V, some conclusions and future prospects of these studies are mentioned briefly.

CONTENTS

PREFACE

CHAPTER 1. REVIEWS OF MASS SPECTROMETER USED IN SPACE VEHICLE..... 1

1.1 Introduction

.1 Outline of the Upper-Atmosphere..... 2

.2 Method to Measure the Upper-Atmosphere Composition..... 14

a. Absorption of Solar Ultra-Violet Radiation..... 14

b. Air-Glow..... 17

c. Chemical Release..... 28

d. Mass Spectrometry..... 29

1.2 Static Mass Spectrometer

.1 Deflection Type..... 33

.2 Time of Flight Type..... 40

.3 Ion Trap..... 43

1.3 Dynamic Mass Spectrometer

.1 Radio Frequency Type..... 49

.2 Quadrupole Field Type..... 55

.3 Resonant Type..... 65

1.4 Discussion..... 70

CHAPTER 2. MASS SPECTROMETER USING SPATIALLY PERIODIC STATIC FIELD..... 75

2.1 Introduction..... 76

2.2 Motions of Charged Particles Passing Through Spatially Periodic Static Fields

.1 Axially Symmetric Periodic Magnetic Field..... 77

.2 Axially Symmetric Periodic Electric Field..... 80

.3 Quadrupole Periodic Magnetic Field..... 83

.4 Quadrupole Periodic Electric Field..... 85

.5 Discussion..... 89

2.3 A Configuration of Mass Spectrometer Using Spatially Periodic Static Field..... 94

2.4 Calculation of Orbits of Charged Particles 102

2.5 Investigation in the Case of Finite Length of Sensor..... 109

2.6 Investigation into Actual Arrangement of Magnetic Field..... 111

2.7 Prototype..... 113

2.8 Experiment..... 117

2.9 Discussion..... 122

CHAPTER 3. PROBLEMS ACCOMPANIED WITH EXPERIMENTS ON SPACE VEHICLE AND ITS CALIBRATIONS..... 127

3.1 Introduction..... 128

3.2 Effects Originated by Invasion and High Speed Flight of Space Vehicle..... 129

.1 Effects of Aerodynamics..... 129

.2 Ram Effect..... 130

.3 Pressure Effect..... 136

.4 Potential and Field Effect..... 138

.5 Others..... 147

3.3 Influences Appeared in Data of Measurement

.1 Characteristics of Velocity..... 148

.2 Characteristics of Attack-Angle..... 153

.3 Characteristics of Potential..... 154

3.4 Characteristics for Active Species of the Upper-Atmosphere..... 161

3.5 Calibration

.1 Calibration as an Ordinary Mass Spectrometer..... 162

.2 Calibration for Characteristics Caused by High Speed Flight..... 164

.3 Calibration for Active Species..... 167

.4 Calibration System..... 174

a. Outline of the System..... 174
b. Generator and Supplier of Gas Species.. 177
c. Plasma Source..... 181
d. Main Vacuum Chamber..... 186
e. Standard Mass Spectrometer..... 191
f. Faraday Cup..... 193
g. Data Processing..... 193
h. Support Equipments..... 196

CHAPTER 4. EXPERIMENT OF SPATIALLY PERIODIC STATIC FIELD TYPE MASS SPECTROMETER ON BOARD JAPANESE SOUNDING ROCKET..... 197

4.1 Constitution of the Flight Instruments.... 198
4.2 Sensor..... 200
4.3 Electronic Circuits..... 205
4.4 Pre-Flight Calibration..... 209
4.5 Integration of Payload..... 213
4.6 Result of Flight Experiment..... 213
4.7 Discussion..... 217

CHAPTER 5. CONCLUDING REMARKS..... 223

ACKNOWLEDGEMENTS 227

REFERENCES 228

APPENDIX 247

CHAPTER 1

REVIEWS OF MASS SPECTROMETER

USED IN SPACE VEHICLE

1.1 Introduction

1.1.1 Outline of the Upper-Atmosphere (1)~(63), (120)~(122)

Before to mention of the subject, we may describe the condition of the upper-atmosphere and the reason why we need so many times of observation as in various times, seasons or years.

It may be appropriate to say that the upper-atmosphere of the earth is controlled by the sun. The circumstance of the upper-atmosphere, therefore, varies with the condition of the sun such as local time, season, latitude of an observing point or activity of the sun.

The outline of it can be learned by following various works. Figure 1.1 which is refered to CIRA (COSPAR, International Reference Atmosphere) 1965 model, edited by COSPAR (Committee on Space Research), shows the upper-atmospheric pressure distribution versus height. We can know that the pressure of 10^{-4} Torr is at about 100 km, and ordinary measuring techniques of mass spectrometry in vacuum are applicable in the higher atmosphere than this altitude.

The average temperature of neutral gas versus

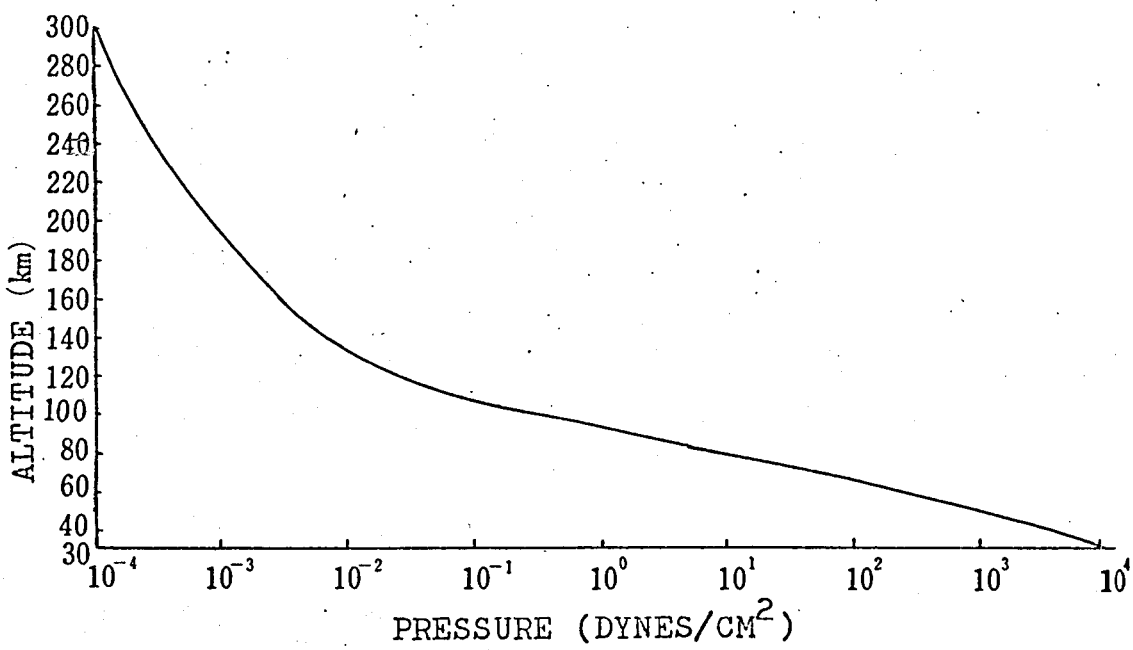

Figure 1.1 Upper-atmospheric Pressure versus height.

(after CIRA 1965)

height is show in Figure 1.2. In this figure, the curve marked as T_m is calculated with regard to the mean molecular weight at the height and T is not.

The atmosphere in lower altitude region is well mixed by wind or convection and it has the same composition as that of surface of the earth. Because of less frequent collision among the atmospheric molecules at the higher altitude, heavy molecules sink and light ones rise and the mean molecular weight consequently decreases with increase of height as shown in Figure 1.3. This phenomenon which is called diffusive equilibrium distribution begins at the height of about 100 km.

In the case of assumming neutral gas temperature, calculated ion and electron temperatures versus altitude are given in Figure 1.4 in both cases of the minimum sunspot number (a) and the maximum one (b).

Figure 1.5 shows a height distribution of composition of neutral molecules. The proportion of lighter weight atoms increase with altitude and atomic oxygen becomes dominant species in higher altitude than about 200 km. Atomic oxygen takes the most important role in F layer of the ionosphere.

The upper-atmospheric composition in the higher altitude is influenced by temperature, that is,

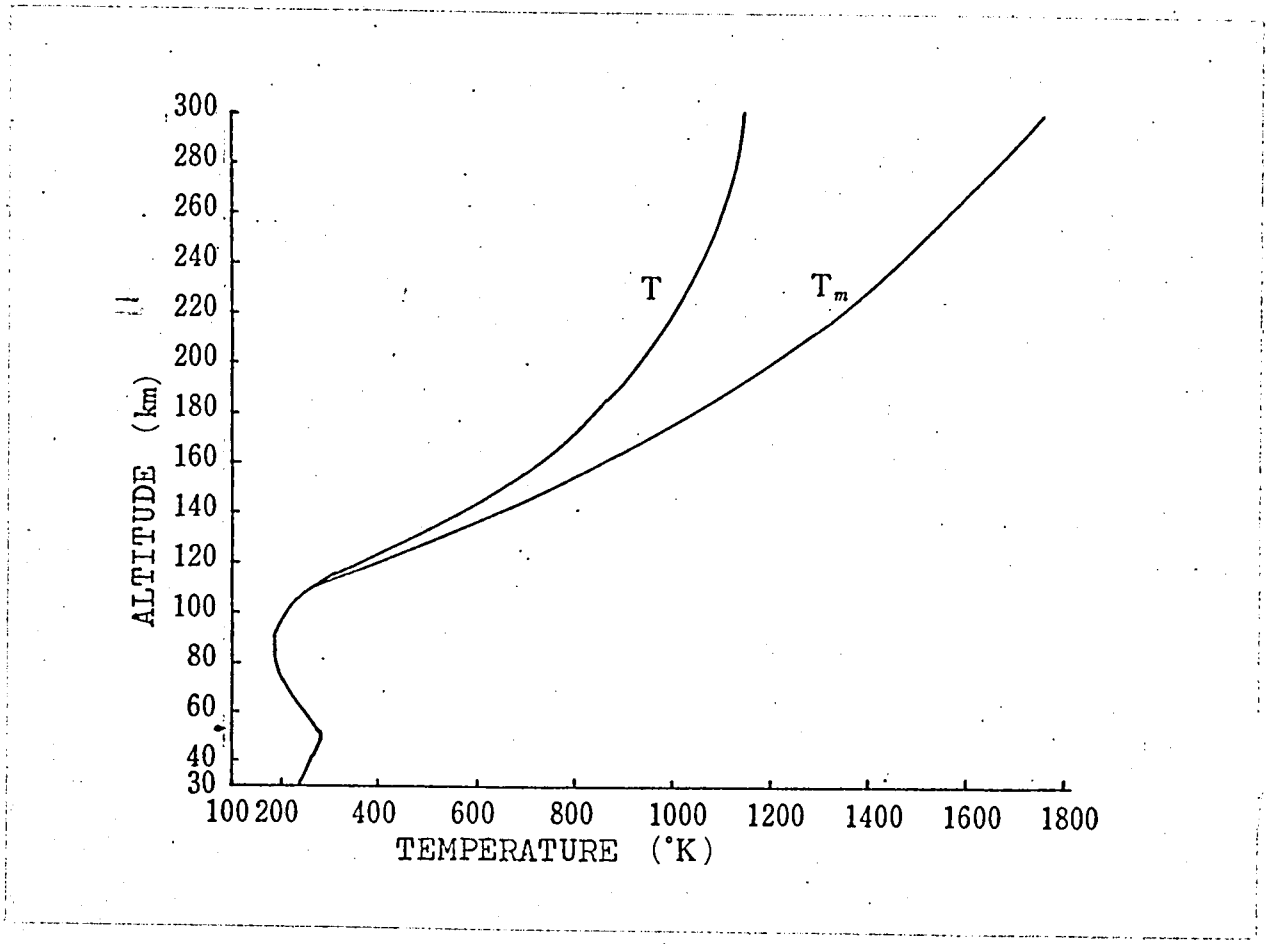

Figure 1.2 Profile of average temperature of neutral gas, T_m is calculated with regard to mean molecular weight shown in Figure 1.3.
(after CIRA 1965)

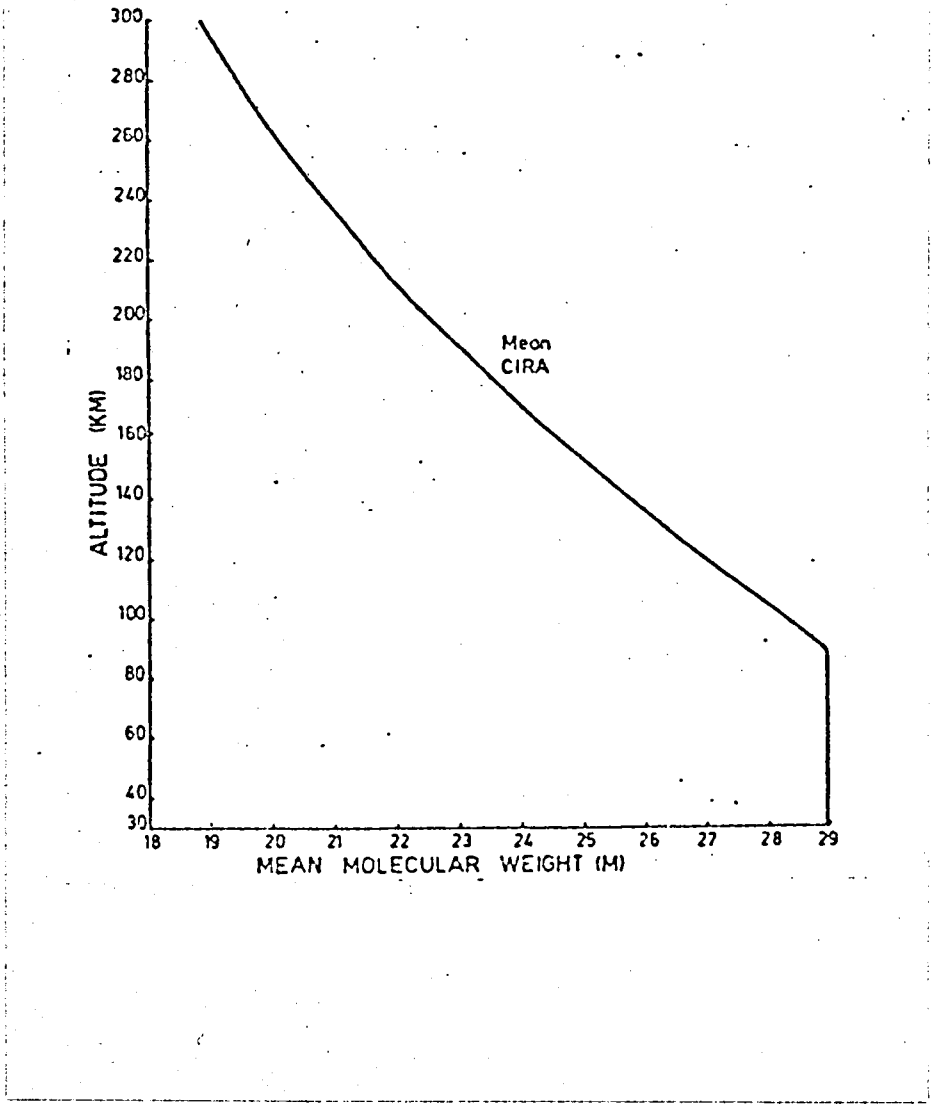

Figure 1.3 Mean molecular weight versus height.

(after CIRA 1965)

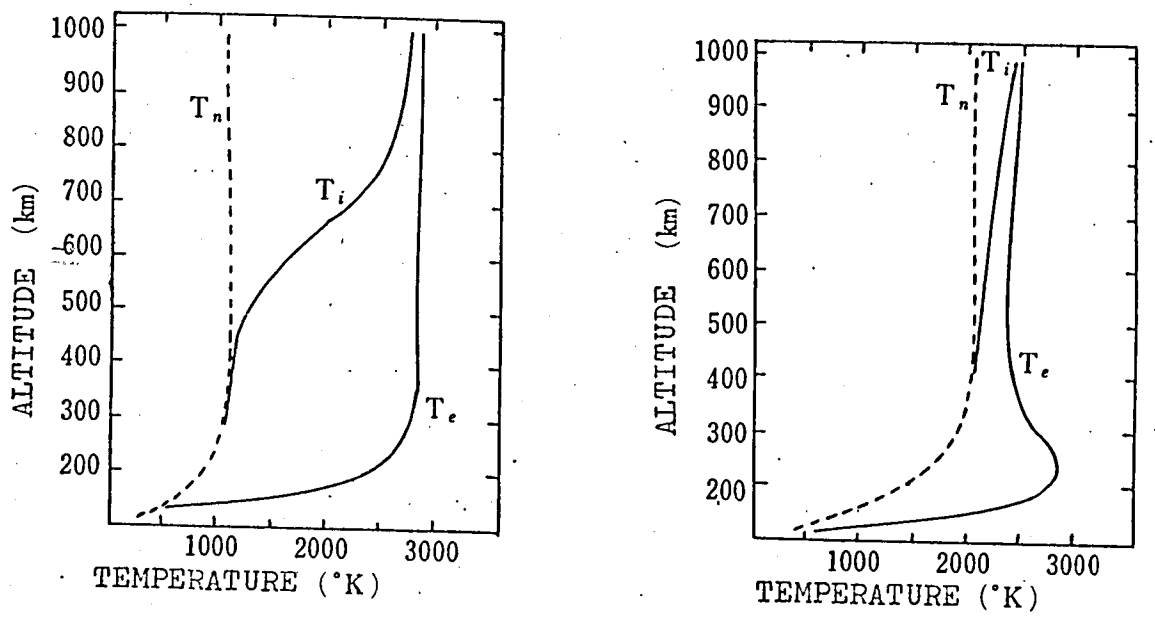

Figure 1.4 Calculated temperature profile of ion and electron, assuming neutral gas temperature.
(a) : in case of sunspot minimum
(b) : in case of sunspot maximum
(after Bowhill et al.)

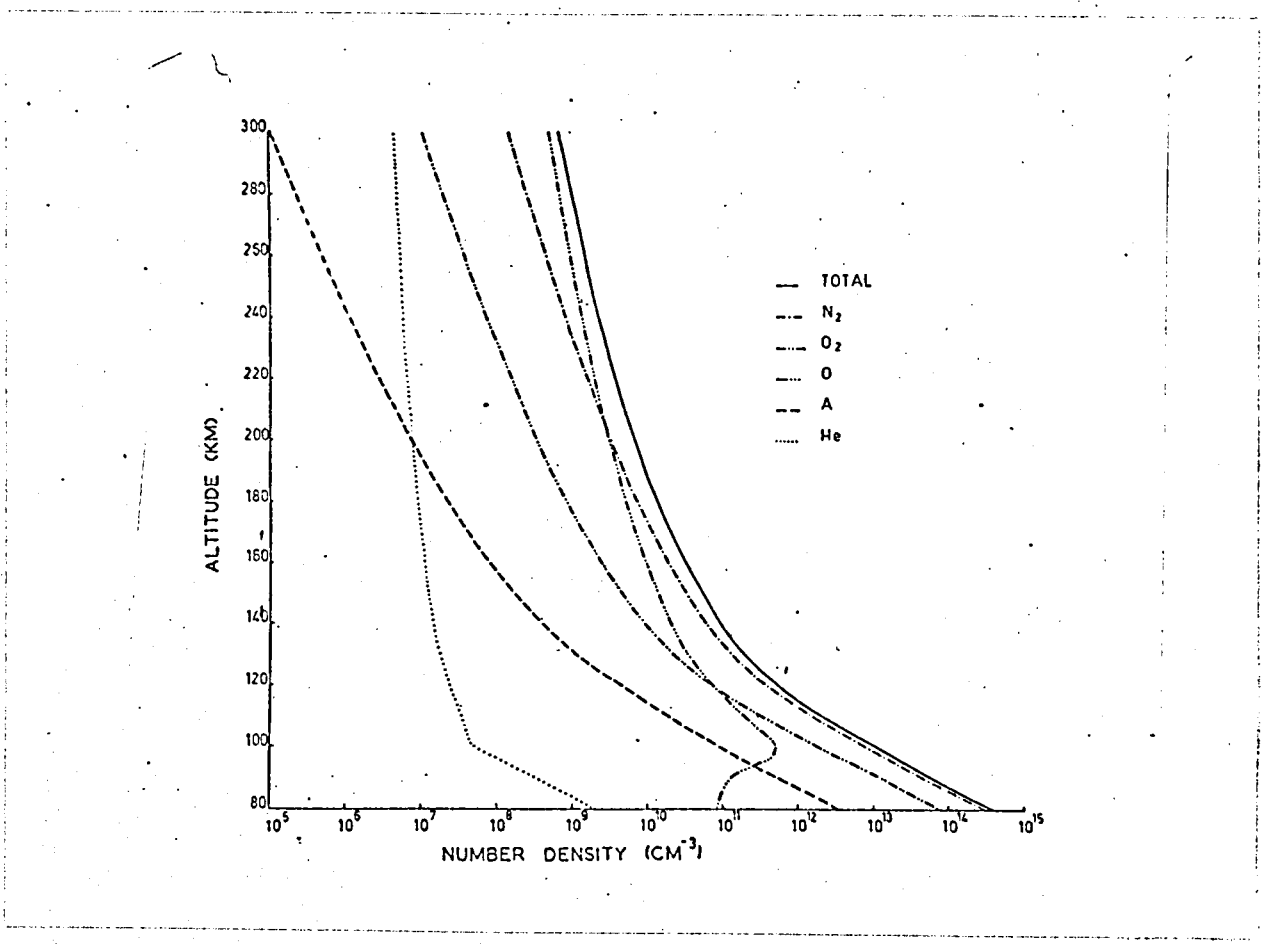

Figure 1.5 Height distribution of composition of neutral gases.
(after CIRA 1965)

condition of solar activity. Figure 1.6 shows the calculated concentrations of upper-atmospheric molecules in three cases assumming different temperature condition, suggesting the large influence of sun to the earth. During the term of active sun, the upper-atmosphere is heated and expands.

In the same conditions, the ion composition of the upper-atmosphere especially in topside ionosphere is calculated as shown in Figure 1.7. The transition heights of dominant ion are largely different in these three cases. And the transition mode also differs so that the helium ion can not be dominant at any height range in the quiet solar condition.

In lower altitude than about 500 km, that is, in the ionosphere, they are more complicated. It is well known that the ionosphere is composed of some layers which have specific features respectively. Their characteristics are predominant not only by the total electron density but also by the ion composition.

The results of direct measurement of ion composition of E and F regions by rocket borne mass spectrometer are shown in Figure 1.8, where (a) is of summer midnight and (b) is of winter morning. Figure 1.9 shows the result by Japanese sounding rocket. From these figures, we can

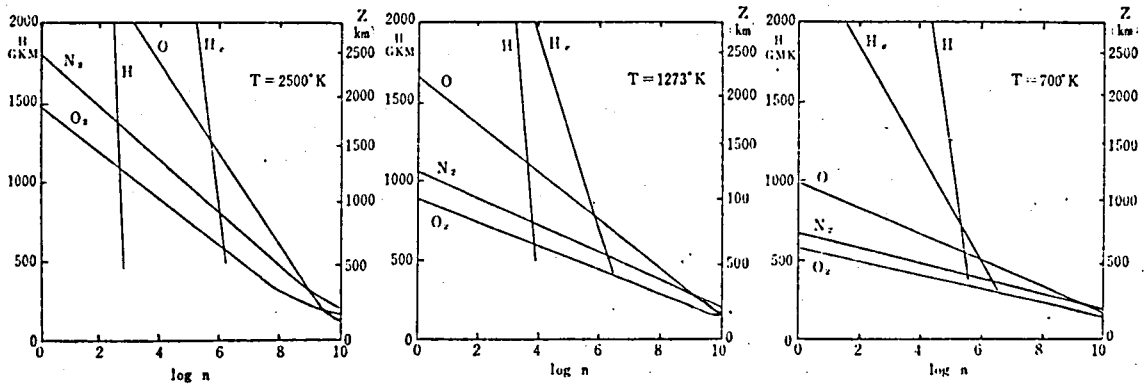

Figure 1.6 Calculated concentrations of the upper-atmospheric molecules versus height assuming three different temperatures. (after CIRA 1965)

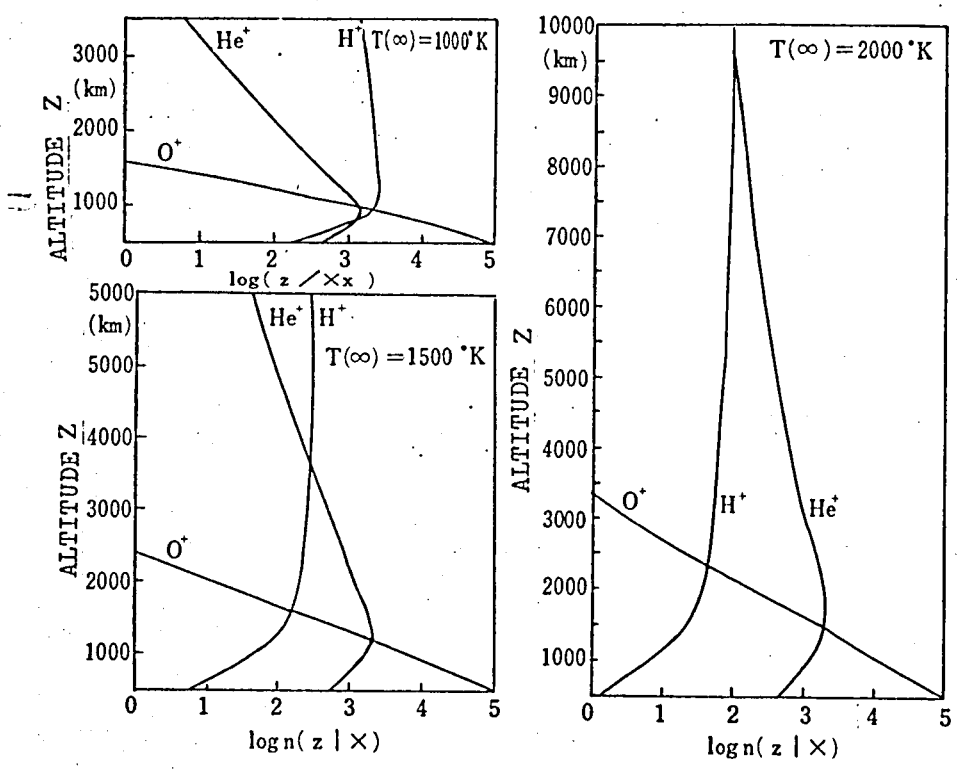

Figure 1.7 Calculated concentrations of ions in the topside ionosphere versus altitude, in cases of three different temperature.
(after Bates et al.)

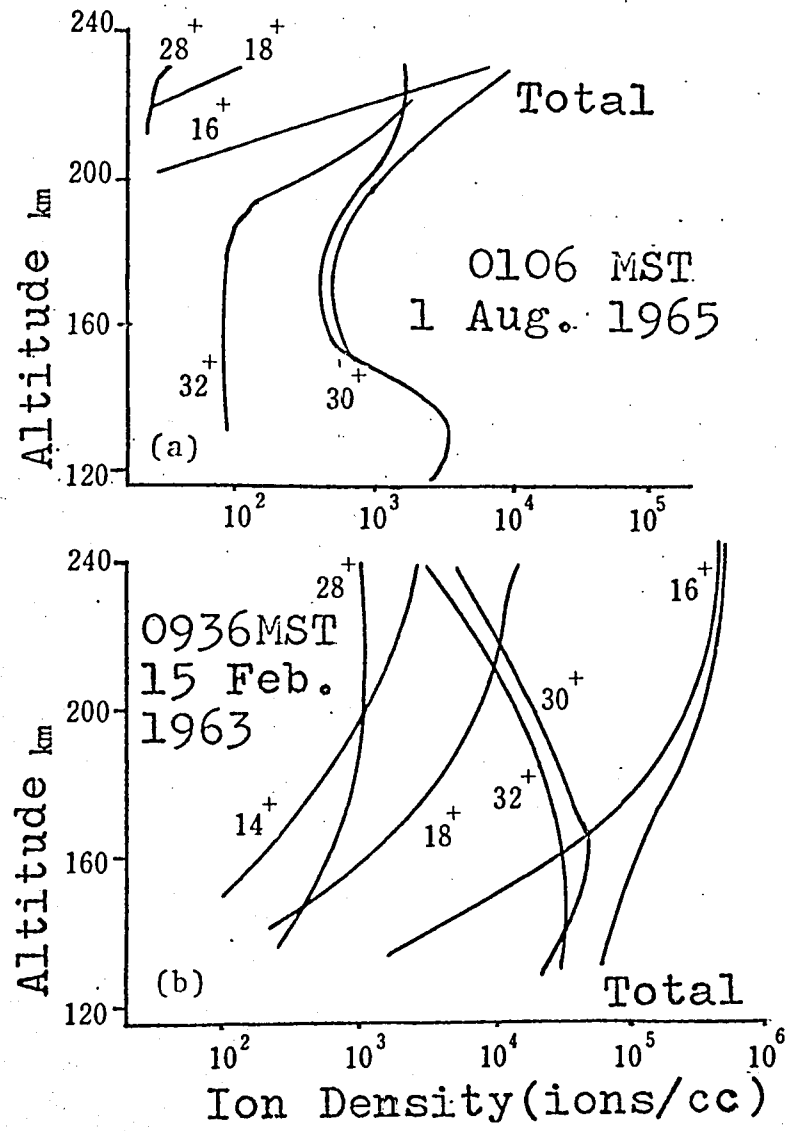

Figure 1.8 Ion composition of the upper-atmosphere of White Sands USA. measured by mass spectrometer

(a) : summer midnight,

(b) : winter morning .

(after Holmes et al.)

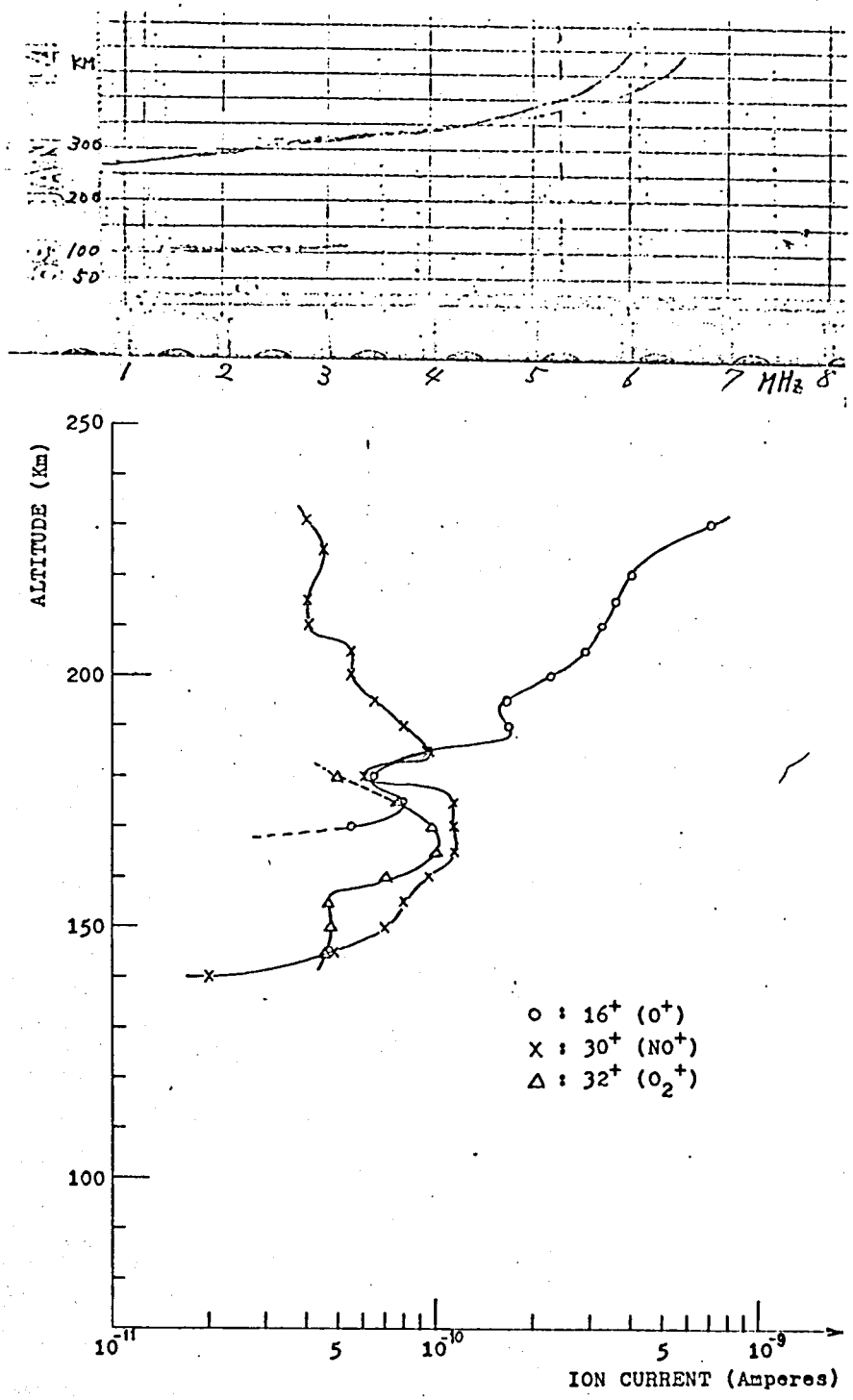

Figure 1.9 Ion composition measured by mass spectrometer borne in Japanese Kappa - 10 rocket and ionogram at a time during the flight.

find out that the dominant ion is nitric oxide ion or molecular oxygen ion in the E layer and atomic oxygen ion in the F layer. Figure 1.10, which is the result obtained by the same method as used in Figures 1.8 and 1.9, shows the ion composition in the F layer and the topside ionosphere.

Such a fact is also observed by the direct measurement by rocket borne mass spectrometer that the sporadic E layer is mainly composed by metal ion such as sodium, magnesium, alminium, silicon, potasium, calsium, nickel, iron and so on.

In the D layer, hydrated proton ions $H(H_2O)_n^+$, and rather complicated ions are also observed. Existence of considerable amount of negative ions is expected in this layer.

1.1.2 Methods to Measure the Upper-Atmosphere Composition

a. Absorption of Solar Ultra-Violet Radiation (64)~(69)

The solar radiations ionize or excite the upper-atmospheric atoms and molecules. In another word, solar radiations are absorbed by upper-atmosphere and its intensity decrease gradually with descending altitude.

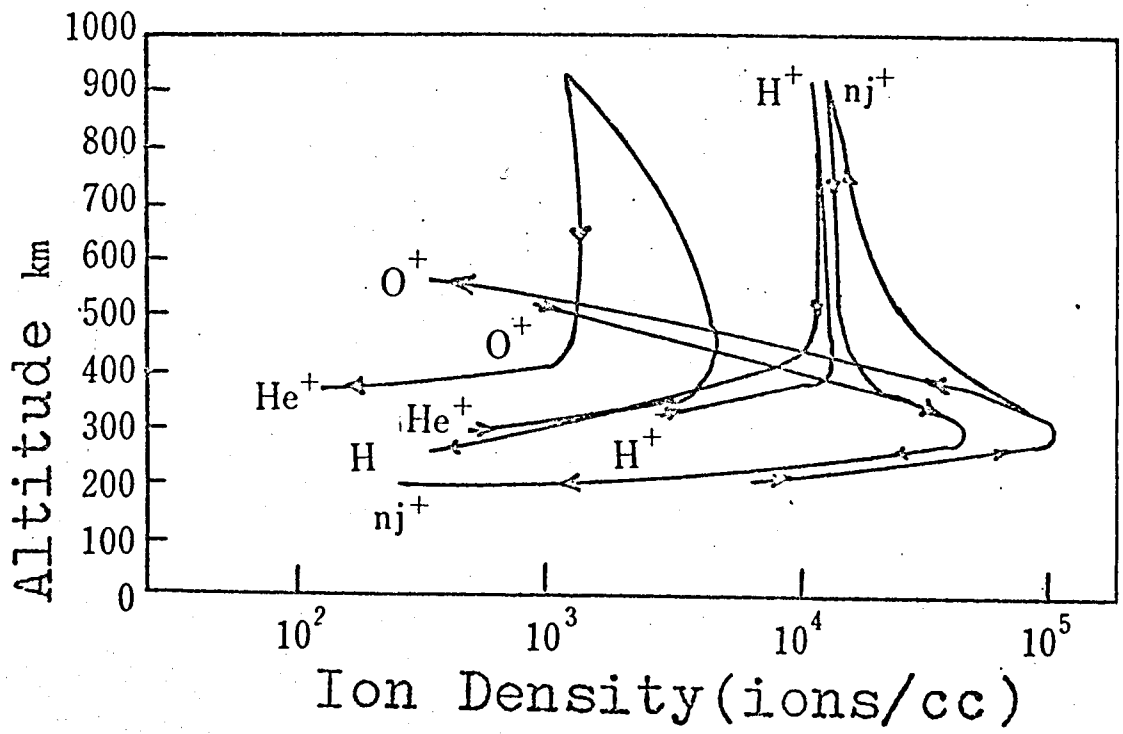

Figure 1.10 Ion composition of the topside ionosphere measured by rocket borne mass spectrometer. (after Hoffman)

The absorbing cross sections of upper-atmospheric atoms or molecules for ultra-violet rays at the various wave lengthes are well known by laboratory experiments. Consequently, density distribution of the upper-atmospheric species versus altitude can be obtained by measuring the variation of intensity of a ultra-violet ray with altitude by means of the instrument on board rocket.

There are various techniques for this purpose. For instance, various filtering materials such as LiF, BaF_2, Al_2O_3, CaF_2, MgF_2 permit ultra-violet rays of longer wave length than their specific cut-off wave lengthes to pass through. On the other hand, photo-ionization cross sections of various gases, such as nitric oxide or inert gases, are generally constant for considerable broad range of wave length shorter than ionization threshold. The measurement of adequate range of wave length is possible by using a combination of a filter and a gas ionization chamber. For shorter wave length range, some metal films are available as the window material. In this case photomultiplier, proportional counter or GM-counter are used as detecters.

Upper-atmospheric composition measurement by absorptions of solar ultra-violet rays is useful in the

regions where solar ultra-violet rays are strongly absorbed, that is, intensity of the rays changes abruptly with the thickness of the absorbing constituent of the atmosphere. According to the fact that the attitude of rocket refering to the sun affects largely on the sounding data, the attitude of rocket should be measured in every instance. The atitude control to make the sensor constantly point toward the sun, is desirable.

Table 1.1 shows nine ultra-violet lines which were observed in the range of 150 to 220 km at White Sands, USA., at 10^h04^m, on July 10, 1963, and their absorption coefficients to molecule nitrogen, molecule oxygen and atomic oxygen. Figure 1.11 shows observed count rate of 304 Å versus altitude as a example of these measurements. Number densities of N_2, O_2 and O which were calculated from these observation are presented in Table 1.2. Figure 1.12 also shows observed hydrogen Lymann - α (1216 Å) flux which was got at Woomera, Australia, at 09^h12^m, on December 6, 1963 and number density of molecular oxygen calculated from them versus altitude.

b. Air-Glow (70)$\sim$(72)

The brightness of night sky is due rather to radiations of upper-atmosphere than light of stars.

Wavelength Å	$\sigma(N_2)$, (10^{-18} cm^2)	$\sigma(O_2)$, (10^{-28} cm^2)	$\sigma(O)$, (10^{-18} cm^2)	Solar Emission Identification
1206.5	0	15	0	Si Ⅲ
1025.7	0.005	1.9	0	H Lyman β
977.0	0.9	3.7	0	C Ⅲ
833—835	~2	10	3.2	Unresolved blend of O Ⅱ and O Ⅲ lines
790.1	~15	23	3.3	O Ⅳ
629.7	18	25	12	O Ⅴ
584.3	19	22	13	He Ⅰ res. line
368.1	13	17	10.3	Mg Ⅸ
303.8	5.0	17	9.8	He Ⅱ Lyman-α

Table 1.1 Solar ultra-violet lines measured at White Sands, USA. at 10^h04^m, July 10, 1963, and their absorption coefficients. (after Hall et al.)

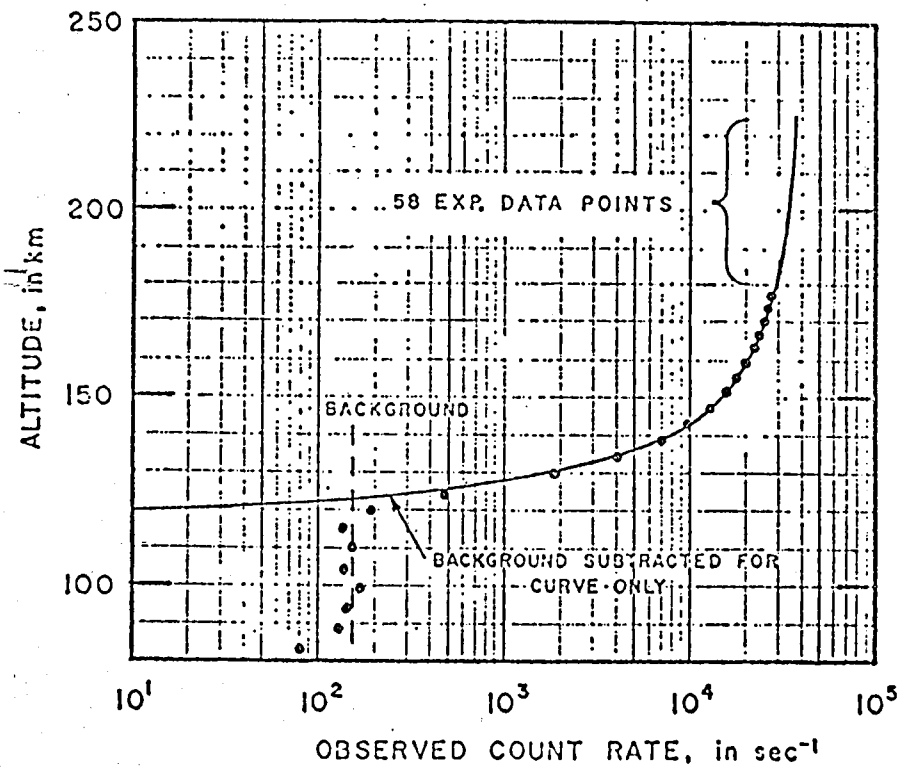

Figure 1.11 Count rates of 304 Å of solar radiation versus altitude observed in the experiment of Table 1.1. (after Hall et al.)

Altitude. (km)	Particle Number Densities. 10^9 particles/cm^3		
	N_2	O	O_2
150	21	21	3.3
160	12	13	2.1
170	7.0	7.8	1.2
180	4.5	5.8	0.77
190	3.0	4.5	0.48
200	2.0	3.5	0.30
210	1.3	2.8	0.19
220	0.8	2.2	0.11

Table 1.2 Calculated number density of N_2, O_2 and O according to the result of the experiment of Table 1.1. (after Hall et al.)

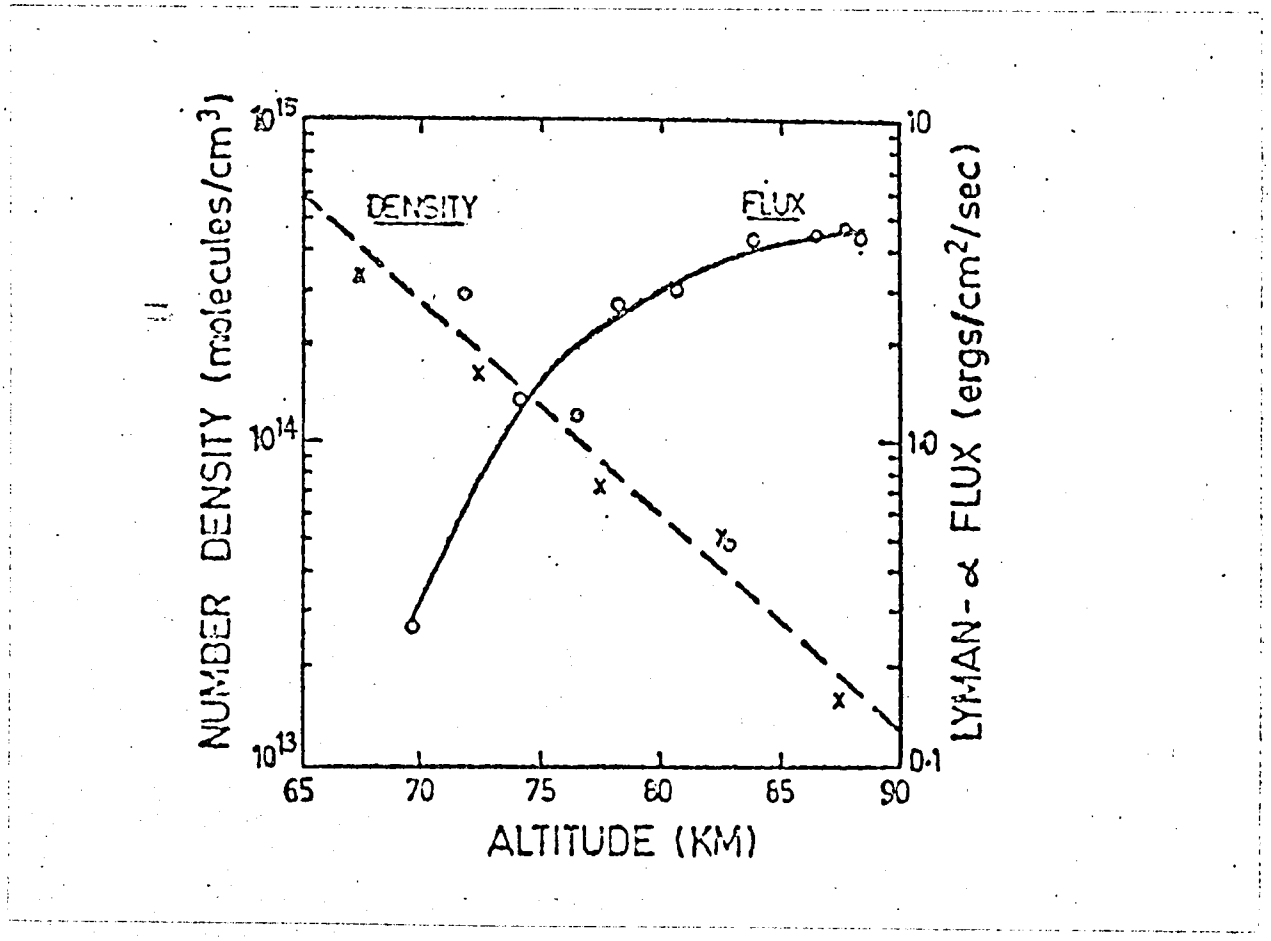

Figure 1.12 Observed Lymann - α flux at Woomera, Australia 09^h12^m, Dec. 6, 1963 and calculated number density of O_2 from the observation. (after Carver et al.)

These radiations are excited in both night and day. They are called night air-glow and day air-glow respectively.

It is considered that the generation of the air-glow is caused by

(1) scatter of solar radiation in the upper-atmosphere,

(2) radiation from the atmosphere which is excited or ionized by solar ultra-violet and X rays,

(3) radiation with chemical reactions in the upper-atmosphere,

(4) radiation from the atmosphere excited by cosmic ray or high energy particle.

(1) and (2) are mainly for day air-glow. Lymann - α is scattered by geocorona also in night.

The spectra of air-glow are composed of specific wave lengths for molecules or atoms of the upper-atmosphere. By observing the height distribution of the air-glow, therefore, the composition of the upper-atmosphere can be observed.

Combinations of a filter and a photomultiplier are used for instruments of this purpose. Various materials are used for photo-cathode according to the wave length range of the observing radiation.

The measurement of day air-glow must avoid the strong solar radiation. On the other hand, most of night air-glow are such weak as it is difficult to detect itself or to discriminate from star light, zodiacal light or albedo from the earth.

The light intensity which is measured by sensor of rocket borne air-glow detector changes with atitude or spin of rocket, because the apparent thickness of radiation layer of air-glow changes with direction of measurement, especially when rocket passes through the layer. It is, therefore, important to identify the attitude of rocket and desirable to controle it.

The important air-glows measured by rockets are
5577 Å (atomic oxygen) 6300 Å (atomic oxygen)
5893 Å (sodium) 2150 Å (γ-bands of nitric oxygen)
3914 Å (1st negative bands of molecular nitrogen ion)
2500 Å (Schumann-Runge bands of molecule oxygen).

Figure 1.13 shows intensity of 3914 Å versus altitude which is obserbed at Wallops, USA., at 16^h11^m on March 11, 1963. Height distribution of number density of molecular nitrogen ion calculated from Figure 1.13 is shown in Figure 1.14. At the same time, 6300 Å of atomic oxygen was observed as Figure 1.15.

Figure 1.16 shows γ-bands spectrum of nitric oxygen

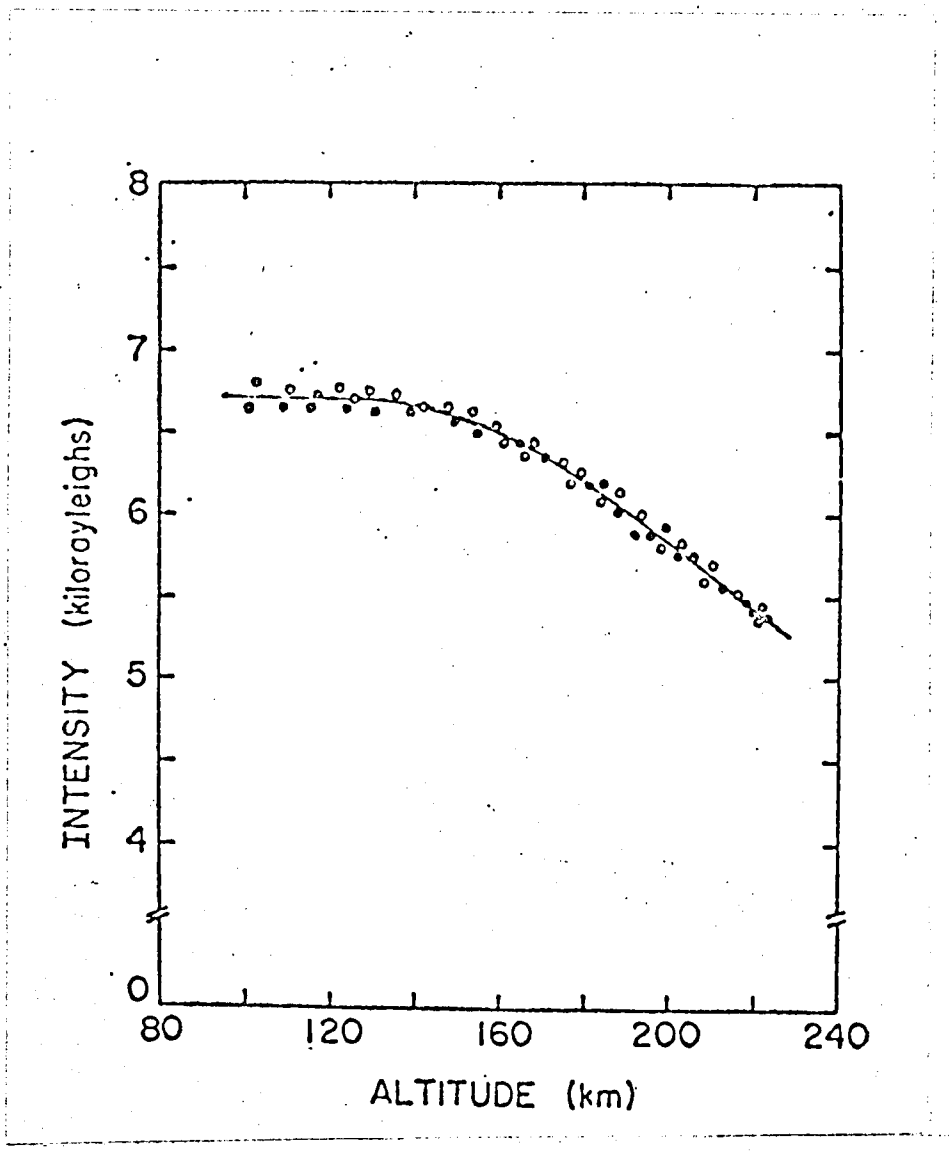

Figure 1.13 Intensity of air-glow of 3914 Å observed at Wallops, USA. 16^h11^m, Mar. 11, 1963. (after Zipf et al.)

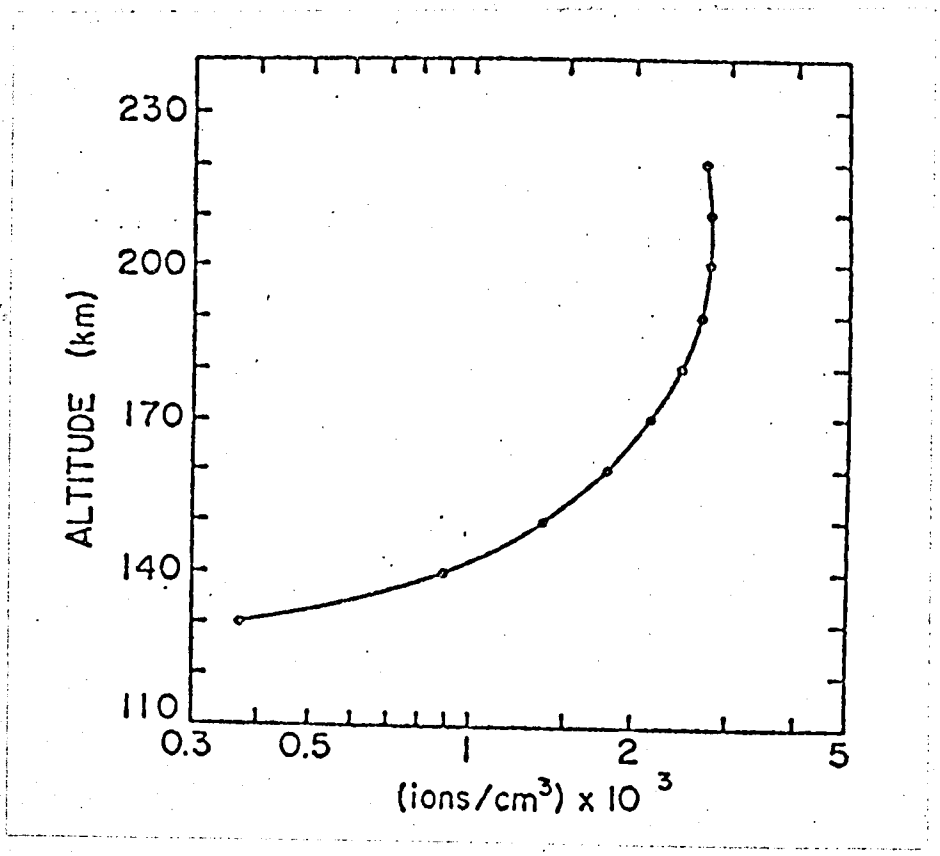

Figure 1.14 Height distribution of N_2 number density calculated from Figure 1.13.
(after Zipf et al.)

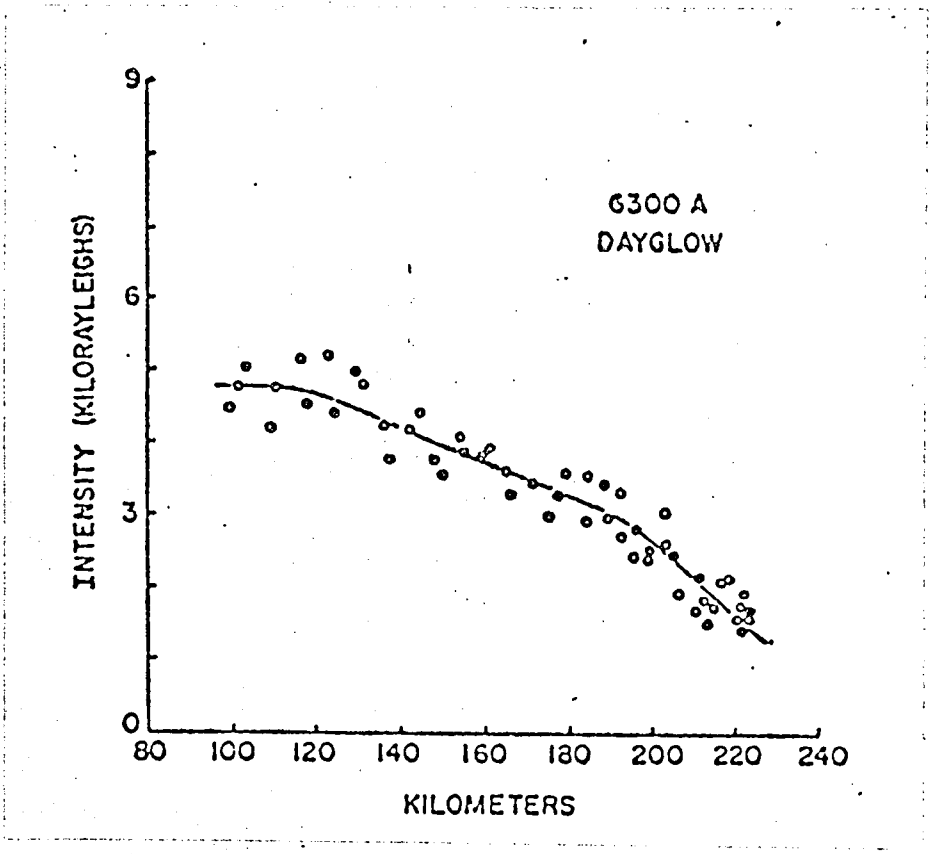

Figure 1.15 6300 Å air-glow of atomic oxygen observed in the same experiment of Figure 1.13. (after Zipf et al.)

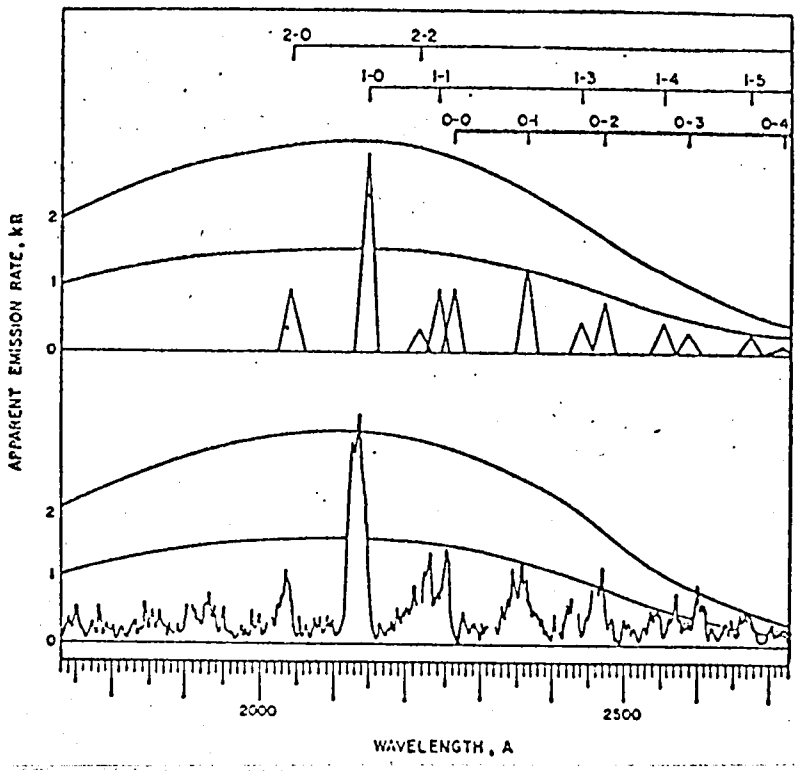

Figure 1.16 γ band spectrum of nitric oxygen air-glow observed at 146 km height by ultra-violet sweep spectroscope with its theoretical spectrum of upper half of the figure and curves in the figures are nonlinear characteristics of the instrument.
(after Barth)

which was observed at 146 km height by ultra-violet sweep spectroscope in the wave length from 1500 Å to 3200 Å, with its theoretical spectrum of upper half of this figure. The curves in the figure means non-linear characteristics of the instrument. This rocket was controlled in its attitude as pointing to zenith during ascent and to horizon during descent.

c. Chemical Release (73)∼(74)

In this method, the sodium vapour experiment is well known. This experiment, however, is for measurement of the wind and temperature in the range of 90 to 160 km, by observing the movement of strong D-line resonance radiation of sodium atoms from sun-shined sodium vapour cloud ejected into twilight upper-atmosphere from rocket.

Similar to this method, height distributions of some constituents of the upper-atmosphere are able to detect by ejecting some specific gases such as ethylene, acethylene or nitric oxide which emit the light of specific wave length as a result of chemical reaction with some constituent of the upper-atmosphere. The ground observations at plural points of trajectory of the intensity of the chemical radiation give the density

profile of the component of the upper-atmosphere. This method needs some assumptions and idealized model of the upper-atmosphere in the analysis of intensity of the radiation.

The ground observation is affected by weather and tends to have error. It is, however, a great merit that the payload of rocket is composed only of a gas container, a special nozzle and a valve controlled by timer.

For example, nitric oxide gas is used to measure atomic oxygen. The chemical reaction is

$$NO + O \rightarrow NO_2 + h\nu$$

Intensity of the radiation is such strong as the observation by photograph is possible in the region of existence of plentiful amount of atomic oxygen.

Table 1.3 shows parameters of a series of experiment with nitric oxide and the results are compared with data of mass spectrometer in Figure 1.17, normalizing at 120 km height.

d. Mass Spectrometry (121)~(123)

Mass spectrometer is the most powerful instrument not only for thin gas analyser, but also as analyser of liquid and even that of solid. Various types of mass

Name	Launch Time T, CST	Start of Release sec after Launch	Release Altitude (Start) (km)	Latitude (Start) (deg)	Longitude (Start) (deg)	Payload (net) (kg)	Tank Pressure (18°C) (atm)
Mabel	18h 00m 00s, Nov. 27, 1962	84.8	92.3	30.180	86.609	10.89	100
Dinah	22h 45m 00s, Dec. 3, 1962	80.7	90.0	30.130	86.686	11.34	100
Eva	04h 21m 00s, Dec. 6, 1962	79.2	88.6	30.228	86.620	10.91	100

Table 1.3 Parameters of a series of chemical release experiments with nitric oxide.
(after Golomb et al.)

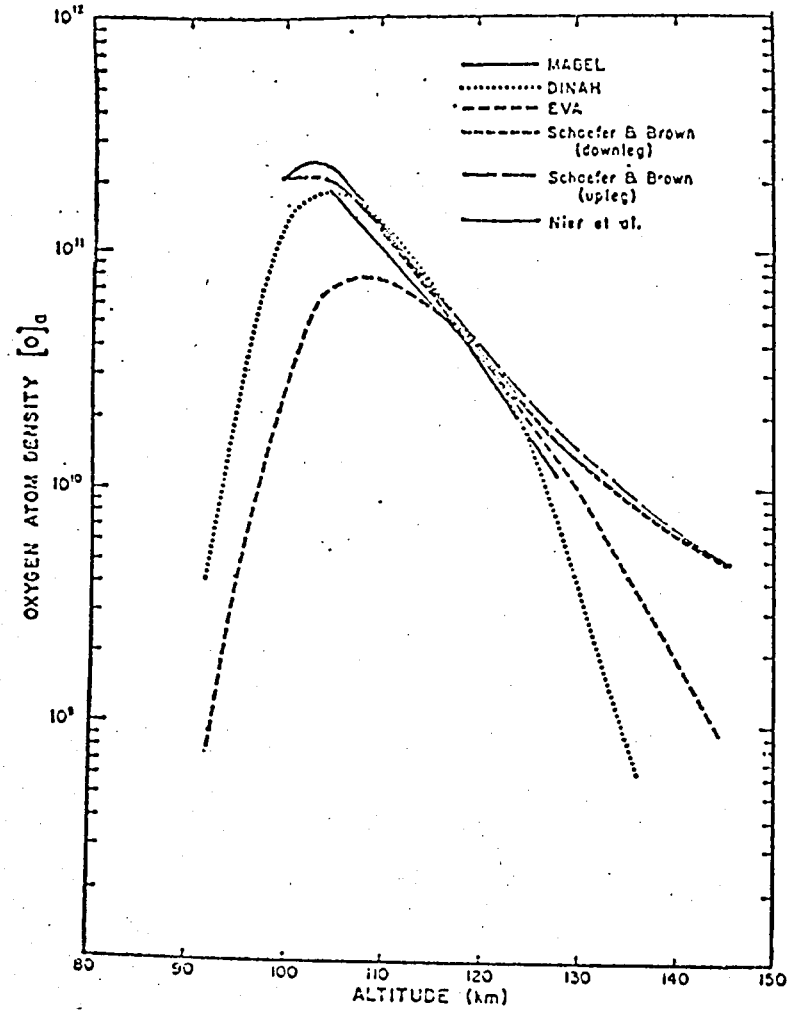

Figure 1.17 Nitric oxide concentration by chemical release experiments, compaired with mass spectrometric results.
(after Golomb et al.)

spectrometer are used in laboratory experiments. Mass spectrometers analyze the charge-mass ratio after ionizing the material to be analyzed by various method. Mass spectrometers make it possible to learn the wide mass range composition with one scanning spectrum.

When mass spectrometer is applied to measure the upper-atmospheric composition, it will bring more reliable information than other methods which have been described previously. The space use of mass spectrometer, however, contains many difficult technical problems. Space use instruments are commonly required its light weight, small sized, mechanical and thermal strength, stable and accurate operation, economical power consumption, and adaptable and reliable data to telemetering systems.

Besides these, high response and high sensitivity are generally required because the measuring object changes rapidly due to the high velocity of vehicle and the density of the surrounding plasma is low, respectively.

However excellent, therefore, it may be in laboratory, it does not necessarily mean suitable for space use. There are few which are adequate to space use among various type of mass spectrometer. Moreover, because they have individual merits and demerits, they may be

available in the respective case with suitable conditions such as in height range, mass range, sort of measuring objects or available vehicle. Details of their characteristics are discussed in following.

There are some problems of space use of mass spectrometer, in spite of its many excellence on measuring the upper-atmospheric composition. Direct measurement means that the upper-atmosphere or the ionospheric plasma is intruded by space vehicle as a impurity. The impurity runs with high velocity comparable or larger than ions or gases of environs. Consequently, the environment surrounding the space vehicle may differ from the original condition as it was and the instruments on the vehicle may give wrong results. Problems caused by these situations will be investigated in later.

1.2 Static Mass Spectrometer

1.2.1 Deflection Type (21)~(28), (75)~(78), (87)~(90)

This type of mass spectrometer analyses ions with

Lorentz force which charged particles running in the electric or magnetic field experience. The electric analyser, however, is used as velocity or energy analyser. The magnetic analyser which is used as a mass spectrometer, is usually called as magnetic sector type mass spectrometer. It has the longest history of mass spectrometers and it is the most reliable and precise mass spectrometer still today.

Figure 1.18 is a schematic picture of motion of charged particle travelling in transverse magnetic field, which expresses the principle of magnetic sector type mass spectrometer. A charged particle of mass number M and velocity v, is deflected along a circle of radius of curvature r, under magnetic field B. This relation is expressed as

$$M = \frac{e\,r}{m_p v} B \ , \qquad (1.1)$$

where e : charge unit,

m_p : mass of a proton,

or

$$M = \frac{e\,r^2}{2m_p V} B^2 \qquad (1.2)$$

where V : accelerating voltage.

It is seen from Equation (1.2) that heavier ions

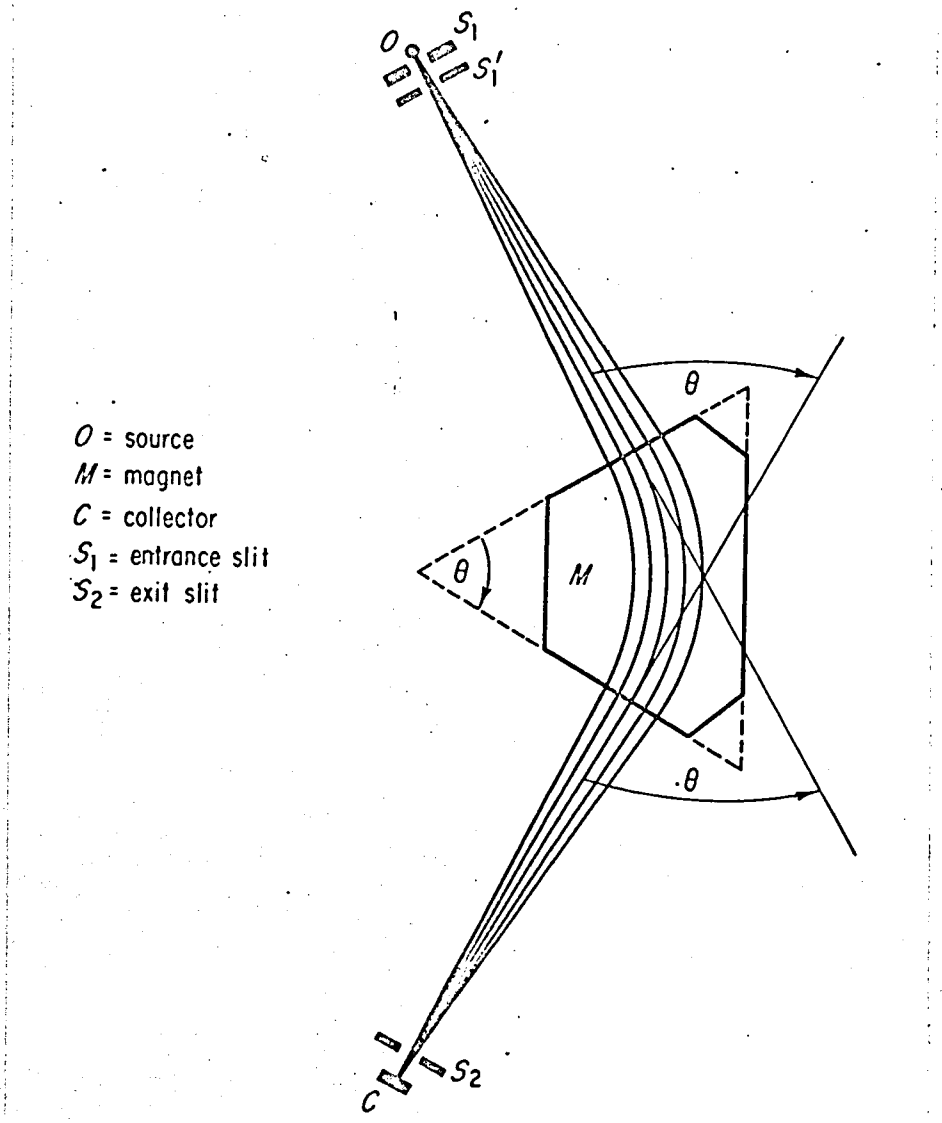

Figure 1.18 Schematic picture of principle of magnetic sector type mass spectrometer.

have larger radius and lighter ions have smaller radius in the same condition of V and B. Thus, when V or B is swept in its magnitude, the ions of different mass are focused on the collector through narrow slit successively from lighter to heavier or vice versa and a mass spectrum is gotten as a magnitude of ion current versus voltage or magnetic field, that corresponds to the mass number. Magnetic field scanning is commonly adopted especially for high resolution mass spectrometers because it is advantageous in mass discrimination and others. For space use, however, it is not suitable, because the electromagnet is heavy weight and needs plenty of electric power. The magnetic sector type of mass spectrometer on board space vehicle, therefore, uses permanent magnet and scans its accelerating voltage for getting mass spectra of the upper-atmospheric composition.

Merits of magnetic sector type of mass spectrometer as space use are that:

1. electronic circuit is simple and easy,
2. power consumption is little,
3. operation is stable and reliable.

On the other hand its shortcomings are that:

1. rather heavy in weight because of use of magnet,

2. precise mechanical alignment is necessary,
3. careful magnetic shielding is required because geomagnetic field is sometimes used for the determination of vehicle attitude by means of the geomagnetic aspectmeter in the same vehicle.

Figure 1.19 is a example of schematic diagram of rocket borne magnetic deflection type mass spectrometer. In this experiment, two different mass spectrometers were borne as seen in this figure. One is a single focussing type on the right hand and the other is double focussing type on the left. Double focussing type mass spectrometer employs both of electric and magnetic sector. The part of electric sector works as energy analyser and eliminates velocity aberration of the ion beam. Thus, the total performance as a mass spectrometer is improved. In this case, a sputter ion vacuum pump is employed to prevent from the dispersion of ion beam by collision with residual gas particles.

Figure 1.20 is schematic drawing of more simplified double focussing magnetic sector type mass spectrometer for satellite. In this case, multiple composition can be detected whereas neither magnetic field nor accelerating voltage is scanned. The ions come into the electric sector through a slit where they are refined

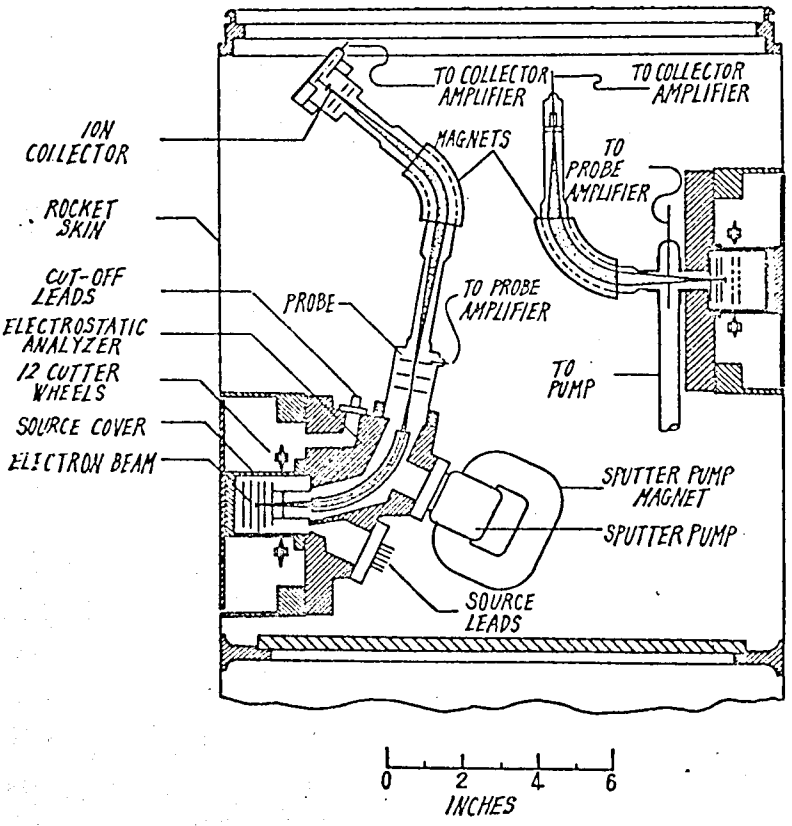

Figure 1.19 Schematic diagram of a example of rocket borne magnetic sector type mass spectrometers put in rocket body, left hand is double focussing and right hand is single focussing type. (after Nier)

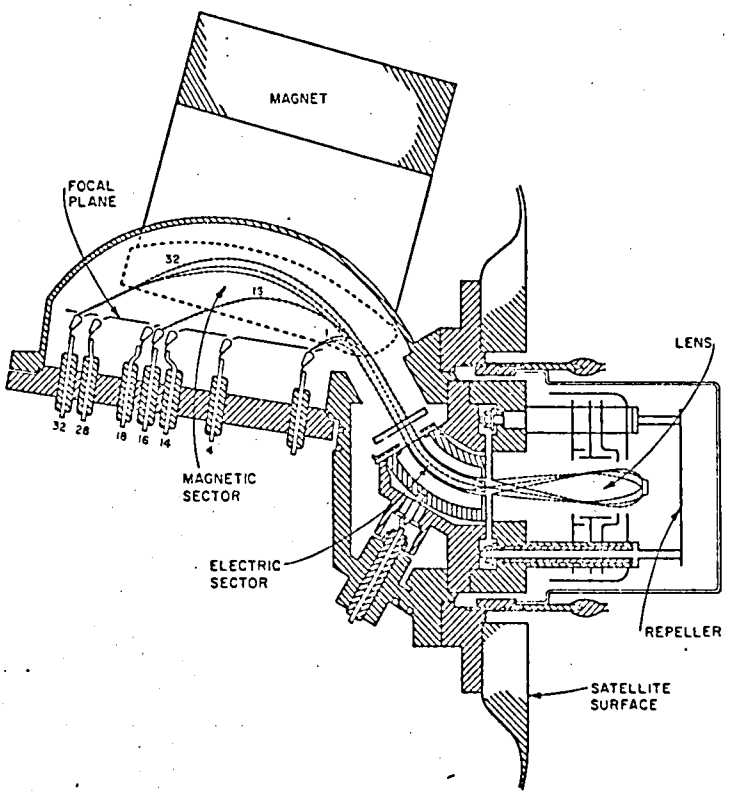

Figure 1.20 Schematic drawing of simplified double focussing magnetic sector type mass spectrometer for satellites.
(after Spencer et al.)

with its energy and then into the magnetic sector where they are sorted according to mass and measured by various collectors corresponding to mass numbers. These collectors are prepared for gas species expected its exsistence in the upper-atmosphere, and arranged at appropriate positions where these ions must strike with calculating their locus.

1.2.2 Time of Flight Type (87)∼(90), (140)

Although there may be opinions that time of flight type mass spectrometer is a dynamic mass spectrometer, it is classified here as a static mass spectrometer. Because in the dynamic mass spectrometer, some dynamic force should be applied on a particle in the analysing space. In this type of mass spectrometer, no dynamic force will be applied.

The principle of mass analysis of this type is that the velocity of charged particle accelerated by voltage is inversely propotional to square root of its mass, and the time of flight along a constant distance of the analyzed particle will be different according to its mass. There are some modified types.

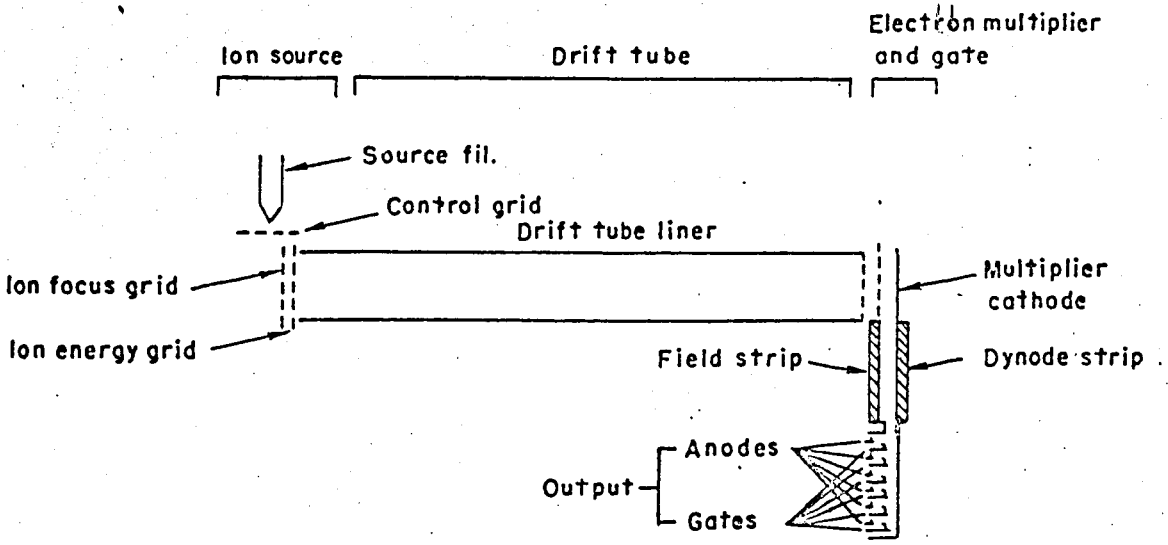

Figure 1.21 Schematic picture of pulsed beam time of flight type mass spectrometer for space use.

Figure 1.21 shows a schematic picture of pulsed beam time of flight type mass spectrometer for space use. The operating principle can be easily understood with this figure. The ions which are produced by electron bombardment are pulsively ejected by the accelerating voltage V into drift space of the length L. Time t which is taken to traverse the drift space by ion of mass number M is

$$t = \frac{L}{v} = L\sqrt{\frac{M\ m_p}{2e\ V}} \qquad (1.3)$$

where v : velocity of the ion,

m_p : mass of proton,

M : mass number.

Then, collector ion current versus time delay from the time of ejection at the entrance of drift space to the time of reaching to the collector gives a mass spectrum of the ions.

As this type of mass spectrometer has a good transparence of ion and high response, it is suitable to measure the phenomenon which changes rapidly or occurs suddenly. These are the capabilities which are required to the mass spectrometer to measure the upper-atmospheric composition.

Many difficult problems, however, lie in front of achievement of space use of time of flight type mass spectrometer. It needs a considerably long drift tube to achieve sufficient resolution, that is to make large time difference between successive ion components. Payload of space vehicle, however, must be small in volume.

Another difficulty is that telemeter of space vehicle ordinarily has poor response. The ions run very fast and it is difficult to make time lag of them from departure at ion source to arrival at collector longer than ten micro-second. The telemeter can not transmit those signals as full mass spectrum. Thus, as shown in Figure 1.21, multiple anodes with respective gates are used. By putting the start pulse into delay circuit which can make multiple delayed pulse, gates can successively be opened to the expected ions of different mass at the appropriate lag time which correspond to their arrival time by respective gating pulse and detected by collectors.

1.2.3 Ion Trap (79)~(85)

The thermal velocities of the upper-atmospheric

ions are smaller than velocity of satellite and comparable or rather small with the maximum velocity of sounding rocket. Therefore, the direct measurements of ion density with vehicle are largely affected by the velocity and reduction of measured data is complicated.

Though the ion trap is an instrument to improve these effects, simple composition of ion can be measured utilizing the vehicle velocity with it. As seen in Figure 1.22, a ion trap consists of two grids and a collector in a shape of plane or sphere.

The gradient of characteristic curve of collector current versus retarding voltage applied to the grid G_1, is inversely proportional to mass of ion, when the vehicle velocity is larger enough than thermal velocity of ions

$$\frac{dI}{dV} \propto \frac{-\alpha N e^2 A}{M m_p v} \qquad (1.4)$$

where α : transparency of grids,
N : number density of ions,
A : surface area of collector,
M : mass number of ions,
v : velocity of vehicle,
I : collector current,

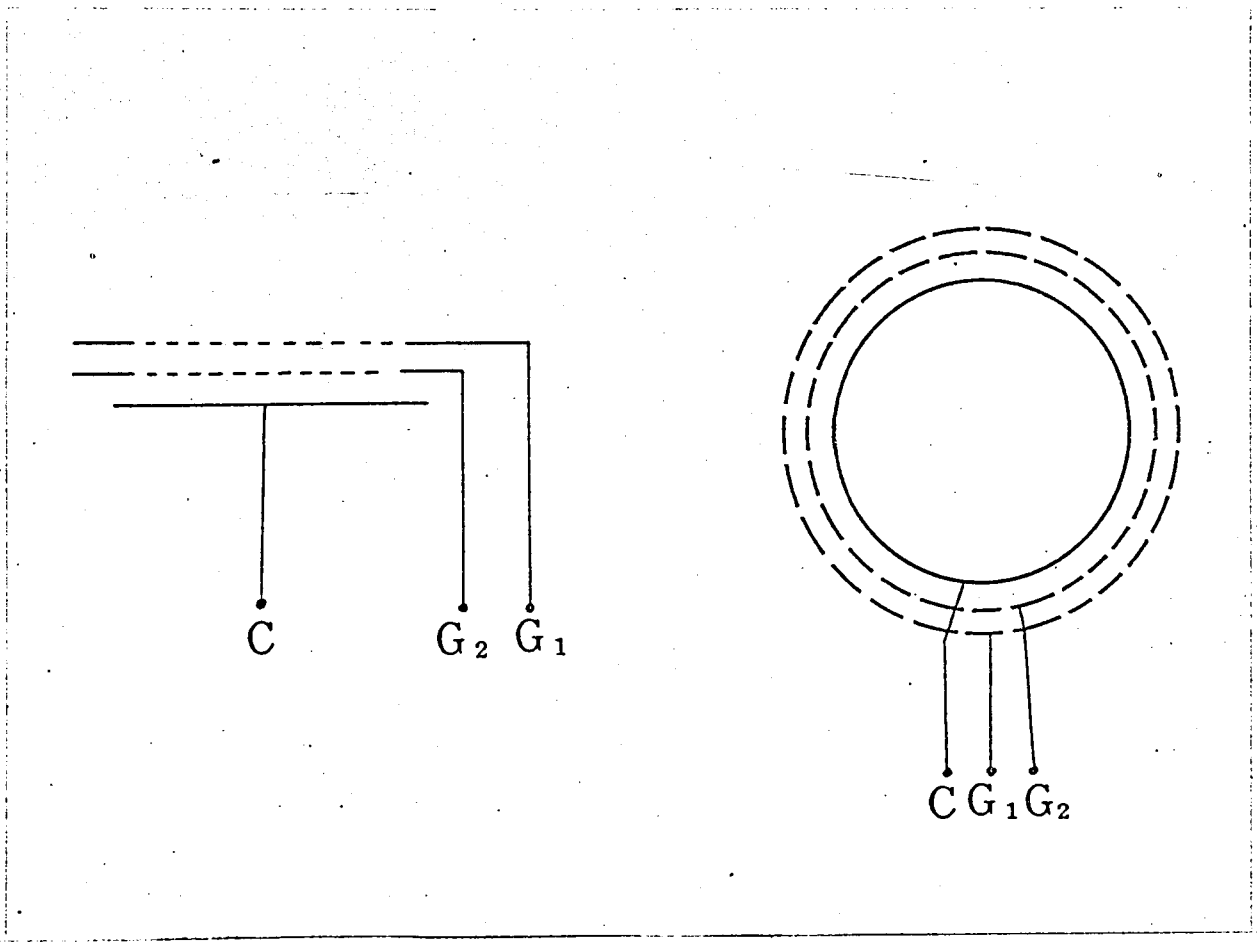

Figure 1.22 Schematic diagrams of planer and spherical ion traps.

V : retarding voltage of G_1,

m_p: mass of proton.

On the other hand, the retarding voltage which prevents the ions from attaining to the collecter is proportional to mass of ion

$$eV = \frac{1}{2} M m_p v^2 \qquad (1.5)$$

If only two species of ions exist in the upper-atmosphere and mass difference of them is large enough, collector current characteristics versus retarding voltage has two gradient and a step appears between them. According to the Equations (1.4) and (1.5), mass of the ions can be calculated by the gradients and the voltages at which the ions are stopped, and the ratio of number density of these two ions is estimated by the ion current at the step of characteristic curve.

The theoretically expected characteristic curves are shown in Figure 1.23 in the case of helium ion and atomic oxygen ion, and in Figure 1.24 of atomic hydrogen ion and helium ion. These characteristic curves are illustrated in various case of ratio of the ions.

As described above, the ion trap works as a simple mass spectrometer; however it is difficult to analyze ions in the case that multiple ions exist or mass number

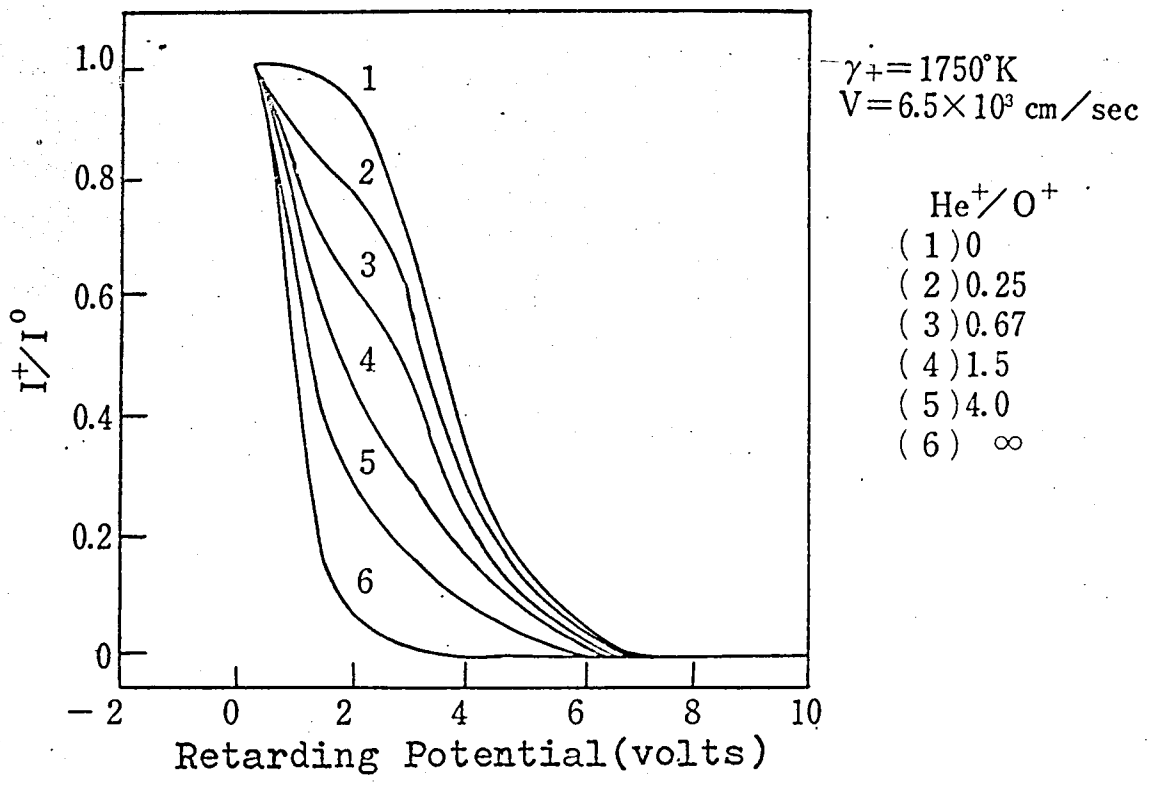

Figure 1.23 Theoretically expected characteristic curves of ion trap, in the case of helium ion and atomic oxygen ion.
(after Boudeau et al.)

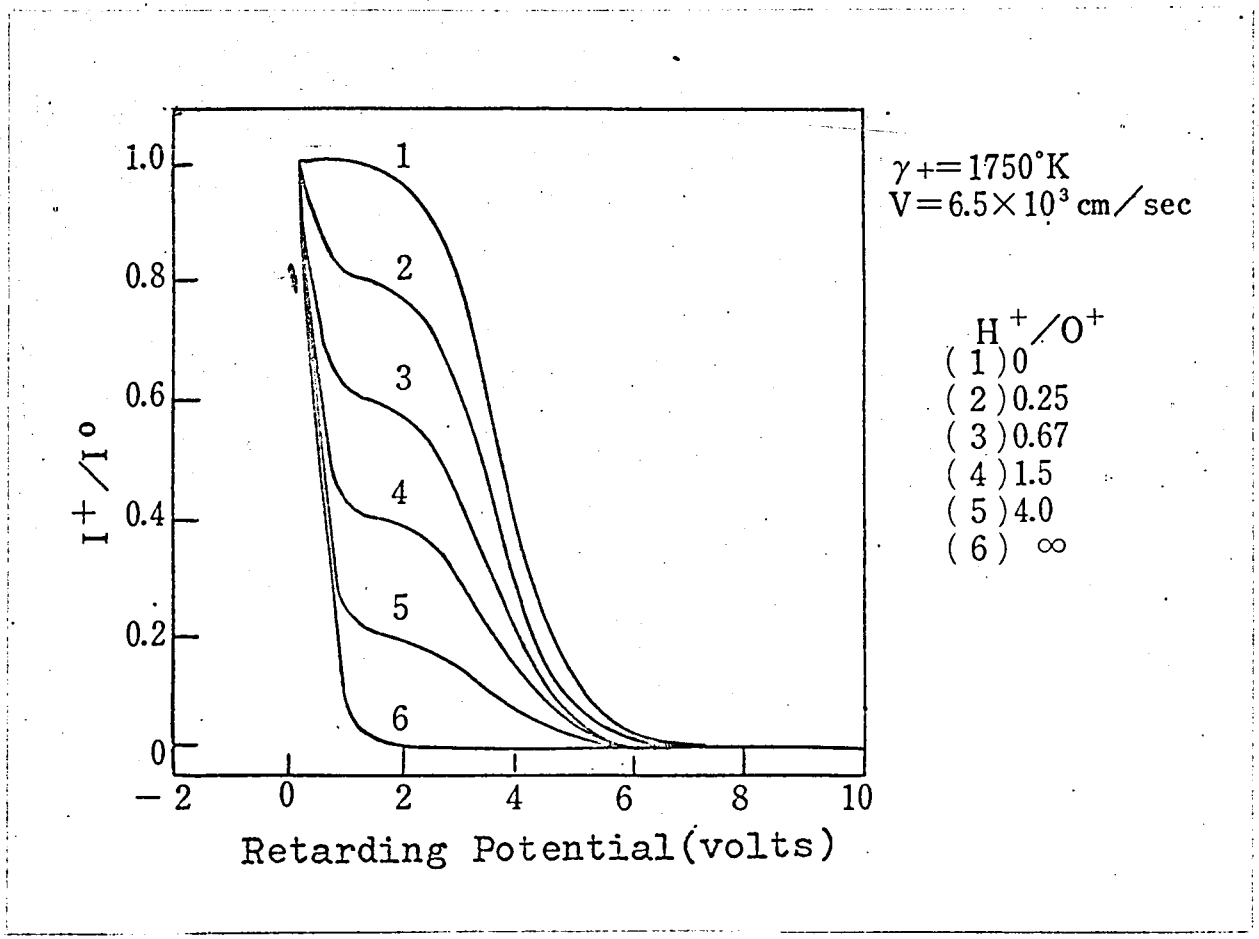

Figure 1.24 In the case of atomic hydrogen ion and atomic oxygen ion.
(after Boudeau et al.)

of ions is close. Moreover, it is not so easy to analyze data gotten from experiment even in the case of simple composition of ions as expected theoretically. Accuracy and reliability of measured data can not be evaluated as regular mass spectrometer. Ion trap was used as a simple mass spectrometer in Ariel satellite of the United Kingdom.

1.3 Dynamic Mass Spectrometer

1.3.1 Radio Frequency Type $\begin{matrix}(29)\sim(52),\ (87)\sim(101),\\ (121)\sim(126)\end{matrix}$

There are various types of mass spectrometer which analyze ions by means of radio frequency field. Most of them utilize the exchange of energy between radio frequency field and ions passing through the field.

Among these mass spectrometers, Bennett type mass spectrometer has been frequently used for space observation. Bennett type of mass spectrometer is a sort of linear accelerator and its principle is a combination of energy exchange effect between RF-field and ions, with time of flight effect.

Figure 1.25 is a schematic diagram to explain the operating principle of Bennett type mass spectrometer. Radio frequency voltage is applied to the center grid refering to the both side grids of each triplet. Ions are accelerated by voltage and reached to the grids from left hand of this figure. Assuming that any change of ion velocity affected by RF-field is smaller enough than its mean velocity, the energy that the ion gets from RF-field during passing through the triple grids, is given as :

$$\Delta W = v \left[\frac{e V_{rf}}{s} \left\{ \int_0^{s/v} \sin(\omega t+\theta)\,dt - \int_{s/v}^{2s/v} \sin(\omega t+\theta)\,dt \right\} \right]$$

$$= \frac{2e V_{rf}}{\frac{s\omega}{v}} \left(\cos \frac{s\omega}{v} - 1 \right) \cos\left(\frac{s\omega}{v} + \theta \right) \quad (1.6)$$

where v : mean velocity of ion,

V_{rf} : peak value of RF voltage,

s : spacing between the adjacent grids of triplet,

ω : angular frequency of RF voltage ($= 2\pi f$),

θ : phase of RF voltage at the instance that the ion reaches the first grid of triplet.

When RF voltage V_{rf}, frequency f, and grid space s are fixed, ΔW is function of v and θ. Therefore, the

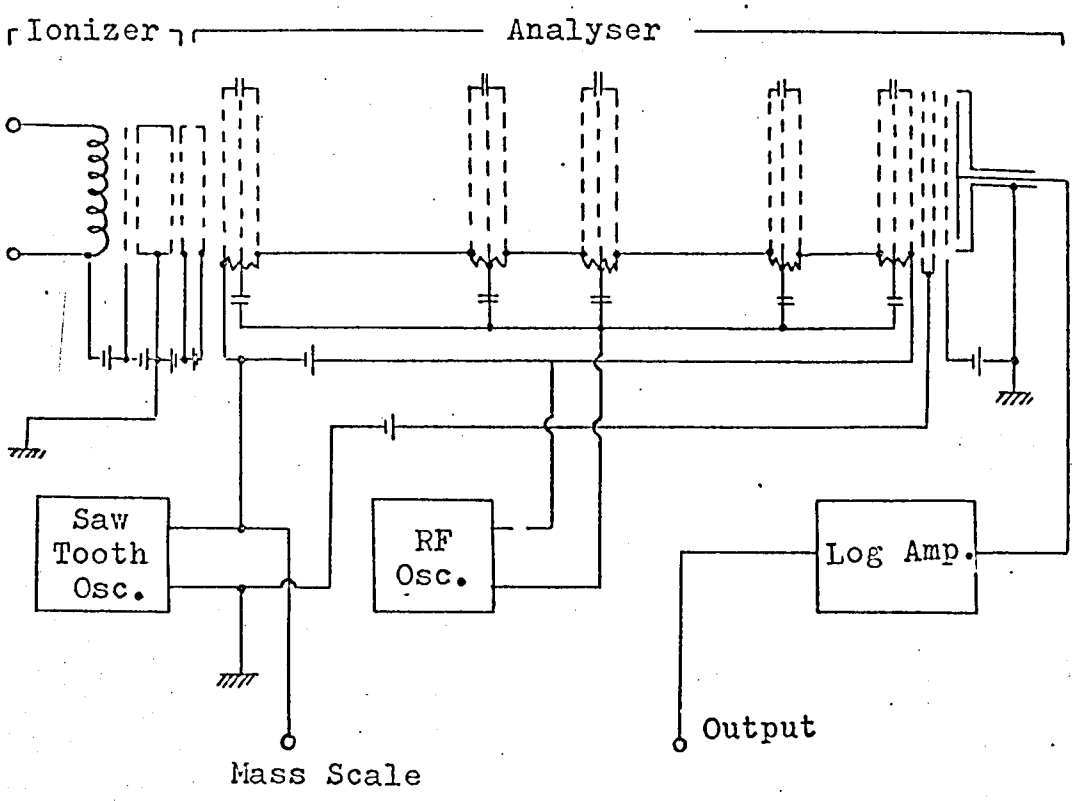

Figure 1.25 Schematic illustration of operating principle of Bennett type mass spectrometer.

maximum of ΔW is obtained from Equation (1.6) as follows:

$$\Delta W_{max} = \frac{2e\ V_{rf}}{\frac{s\omega}{v_o}} \left(1 - \cos \frac{s\omega}{v_o} \right) \qquad (1.7)$$

where

$$\frac{s\omega}{v_o} + \theta_o = \pi \qquad (1.8)$$

from

$$\frac{\partial(\Delta W)}{\partial \theta} = 0 ,$$

and

$$\frac{s\omega}{v_o} \sin \frac{s\omega}{v_o} + \cos \frac{s\omega}{v_o} = 1 \qquad (1.9)$$

from

$$\frac{\partial(\Delta W)}{\partial v} = 0 .$$

From Equation (1.8) and (1.9), we obtain

$$\frac{s\omega}{v_o} \simeq 2.33 , \qquad \theta_o \simeq 0.81 \qquad (1.10)$$

where v_o : mean velocity of the ion that the energy is given as ΔW_{max}, that is, of the ion that satisfies optimum condition,

θ_o : phase of RF voltage at the instance that the ion of optimum condition reaches the first grid of triplet.

Provided that DC inverse voltage is superposed so as to deprive the energy of ions given in Equation (1.7), ions under optimum condition have the constant velocity of v_o at an entrance and an exit of the triplet and the remaining ions are retarded. The DC bias voltage V_b is estimated as :

$$V_b = \frac{2\left(1 - \cos\frac{s\omega}{v_o}\right)}{\frac{s\omega}{v_o}} V_{rf} \simeq 1.45\, V_{rf} \qquad (1.11)$$

Practically, as shown in Figure (1.25), the energy transfer repeats a few times and a equipotential drift space of which transit angles of ions under the optimum condition to the RF-field are $n \times 2\pi$, is inserted among these energy transfer regions. Length of the drift space is shown as :

$$d = n\frac{v_o}{f} - 2s \qquad (1.12)$$

where n : integer.

Consequently, in this system, ions satisfying the optimum condition at the first stage keep the same condition at the succesive stages and the other ions are retarded more and more.

Finally, if a grid is held to the retarding

potential V_r which allows only ions under the optimum condition to pass through, these ions can reach the collector and others are driven back. V_r can be given as :

$$V_r = N \times 1.45 \times V_{rf} \times \alpha \qquad (1.13)$$

where N : number of stages,

α : positive parameter less than unity which determins resolution of the mass spectrometer and is also related to sensitivity of it.

The potential V which accelerates ions to the velocity v_o, is given as :

$$e V = \frac{1}{2} M m_p v_o^2 \qquad (1.14)$$

From Equation (1.10) and (1.14), we obtain the mass number M, of the ions under optimum condition is calculated as

$$M \simeq \frac{0.2636 \text{ V (volts)}}{s^2 \text{ (cm)} \ f^2 \text{ (M H}_z\text{)}} \qquad (1.15)$$

Accordingly, the relative abundance of ions with different masses can be obtained by varying V or f.

V is generally swept from a technical reason in the case of space use.

The shortcomings of the Bennett type mass spectrometer for space use are that any focussing force does not affect on ions, thus, analysis as to radial motion of ions is impossible and because of using large number of grids, the transparency of ions becomes worse especially of the active ions such as atomic oxygen.

On the other hand, this type of mass spectrometer satisfies almost all technical merit for space use.

Figure 1.26 shows a rocket borne five stage Bennett type mass spectrometer of Japan.

1.3.2 Quadrupole Field Type (53)∼(63), (87)∼(90), (102)∼(109), (121)∼(123)

About twenty years ago, it was discovered in Brookhaven National Laboratory that proton beam was strongly focussed by alternative magnetic field intensity of which is rather weak than in the case of uniform magnetic field. Since that time, this phenomenon has been studied as a lens effect of charged particle, especially electron focussing problem in space charge effect dominant field.

Figure 1.26 Photograph of rocket borne five stage Bennett type mass spectrometer of Japan.

On the other hand, Paul et al. proposed a mass filter with this principle, so called as Pauls Massenfilter or Quadrupole Type mass spectrometer. This is composed of four poles parallel to the ion beam shown in Figure 1.27 as cross sectional schematic view. Their curvature are hyperbola shown as

$$x^2 - y^2 = \pm r_o^2 \qquad (1.16)$$

The opposite pairs of electrodes are connected together. When one pair is applied with voltage which is superposed direct voltage V_{dc} and ratio frequency voltage $V_{rf}\cos\omega t$

$$\phi = V_{dc} + V_{rf} \cos\omega t \qquad (1.17)$$

and the other is applied with

$$-\phi = -(V_{dc} + V_{rf} \cos\omega t) \qquad (1.18)$$

the electric fields in the space among the four rods separated by $2r_o$ are

$$E_x = -(V_{dc} + V_{rf}\cos\omega t)\frac{2x}{r_o^2} \qquad (1.20)$$

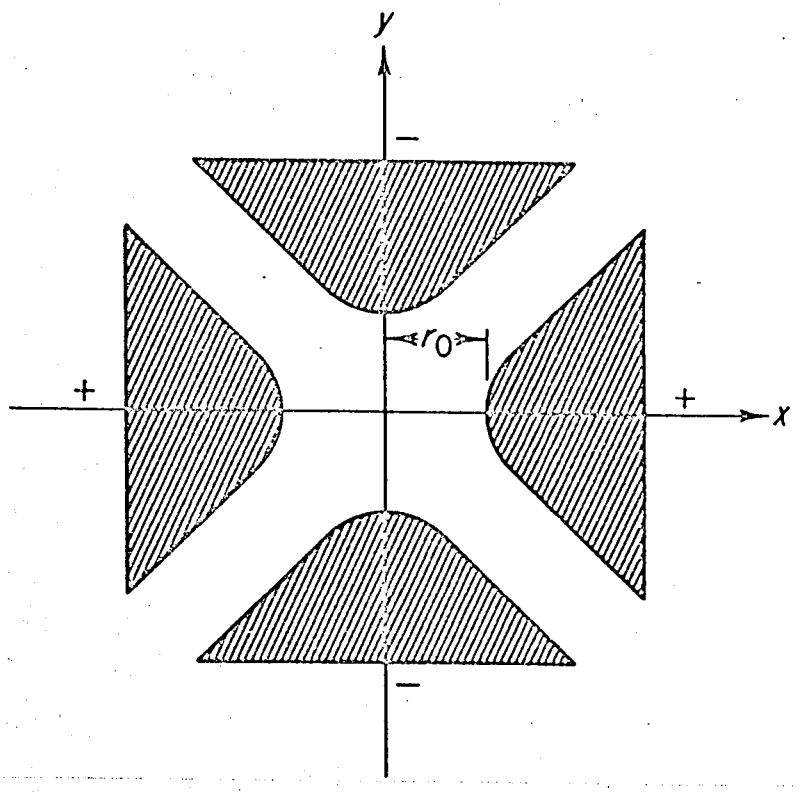

Figure 1.27 Cross sectional schematic view of quadrupole.

$$E_y = (V_{dc} + V_{rf}\cos\omega t) \frac{2y}{r_o^2} \qquad (1.21)$$

$$E_z = 0$$

Therefore, the equations of motion of charged particle in the field are following as :

$$M m_p \frac{d^2 x}{d t^2} + \frac{2e}{r_o^2} (V_{dc} + V_{rf}\cos\omega t) x = 0 \qquad (1.22)$$

$$M m_p \frac{d^2 y}{d t^2} - \frac{2e}{r_o^2} (V_{dc} + V_{rf}\cos\omega t) y = 0 \qquad (1.23)$$

$$M m_p \frac{d^2 z}{d t^2} = 0 \qquad (1.24)$$

They are rewritten with $T = \frac{\omega t}{2}$ as following :

$$\frac{d^2 x}{d T^2} + \frac{8e}{M m_p r_o^2 \omega^2} (V_{dc} + V_{rf}\cos 2T) x = 0 \qquad (1.25)$$

$$\frac{d^2 y}{d T^2} - \frac{8e}{M m_p r_o^2 \omega^2} (V_{dc} + V_{rf}\cos 2T) y = 0 \qquad (1.26)$$

$$\frac{d^2 z}{d T^2} = 0 \qquad (1.27)$$

Equations (1.25), (1.26) are the form of Mathieu's differential equation defined as :

$$\frac{d^2 x}{d T^2} + (a + 2q \cos 2T) X = 0 \qquad (1.28)$$

Solutions of the Mathieu's differential equation are, as well known, stable or unstable according to the value of parameters a and q.

Therefore ions which are ejected into the space among these poles, travel with constant velocity in z derection and focus into or diverge from center of the space as respective condition given in following :

$$a = \frac{8 e V_{dc}}{m_p r_o^2 \omega^2 M} \qquad (1.29)$$

$$q = \frac{4 e V_{rf}}{m_p r_o^2 \omega^2 M} \qquad (1.30)$$

Ions under the focussing condition can reach collector of the mass spectrometer.

The stable and unstable condition with a and q are shown in Figure 1.28. From Equation (1.29) and (1.30),

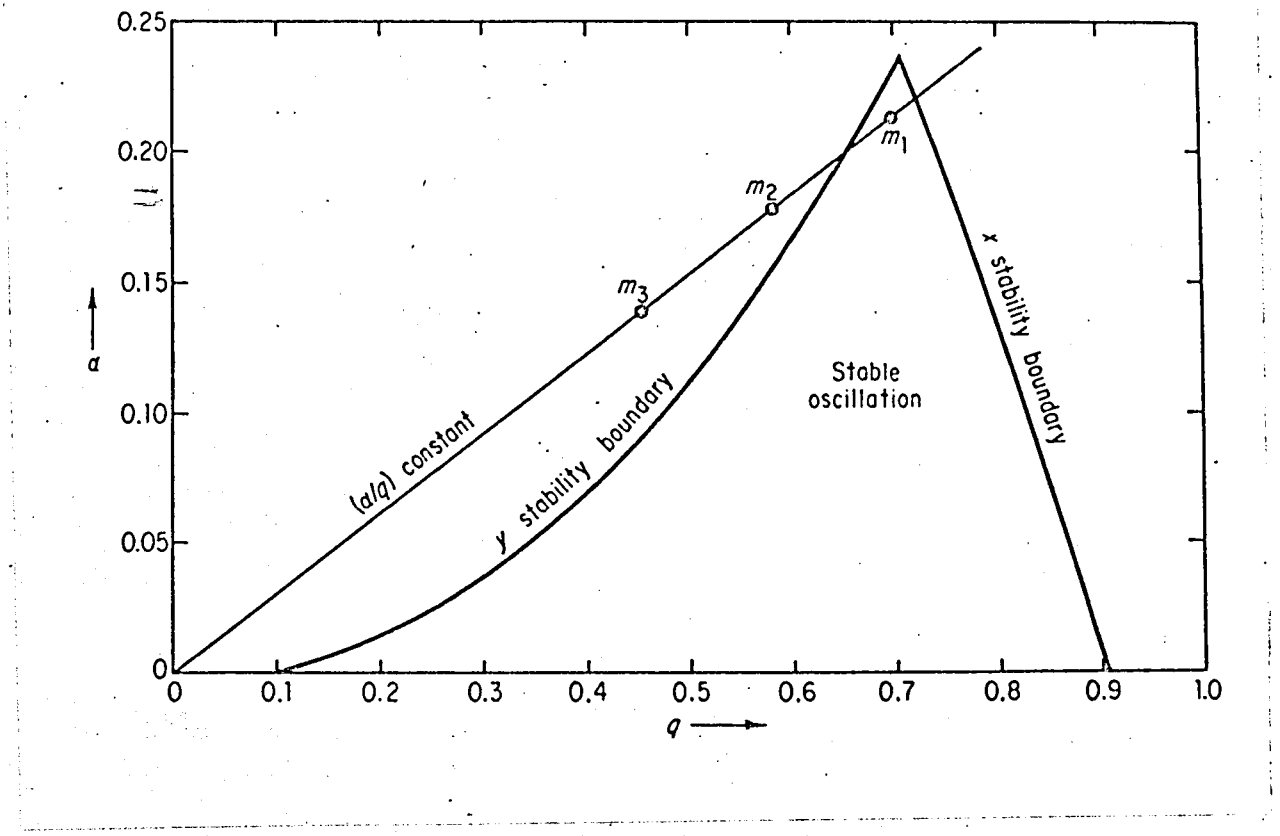

Figure 1.28 Stability diagram of quadrupole mass spectrometer.

and Figure 1.28, it is recognized that the straight line given as

$$\frac{a}{2q} = \frac{V_{dc}}{V_{rf}} = k \text{ (constant)} \qquad (1.31)$$

crosses the stable region and the shorter the straight line in the stable region gives the higher the resolution of the mass spectrometer. In condition of $k \simeq 0.167$ the line touches the apex point of stable triangle and no ion can reach to the collector at the larger value of k than 0.167 .

In order to use as a mass spectrometer which covers wide mass range, it is apparent from Equation (1.29),(1.30) and (1.31) and Figure 1.28 that V_{dc} and V_{rf} must be varied in wide range while the relation between V_{dc} and V_{rf} of Equation (1.31) is sustained.

There are two difficulties to adopt mass spectrometer of this type as space use. One is that the electronic circuit must supply V_{dc} and V_{rf} in wide range, maximum value of V_{rf} is usually required about 500 volt and ratio of V_{dc} / V_{rf} should not change in whole of swept range because the fluctuation causes directly changes of sensitivity and resolution of the mass spectrometer. The other is that the sensor must be constructed very

precisely parallel without any distortion and twist. These difficulties are serious problems for space purpose which requires small power consumption, stable operation and mechanical strength.

In recently, however, in spite of these difficulty, many space scientists have come to adopt this type of mass spectrometer. In Japan, we also use it for observation of ion composition of the lower ionosphere and observation neutral composition of the upper-atmosphere.

One of the demerit of this type as a mass spectrometer is that pattern coefficient of the mass spectrum varies with change of k factor defined in Equation (1.31), that is with its resolution. To improve this phenomenon, some techniques are applied, for example, superposing constant bias voltage on V_{dc}.

Practically, due to a difficulty to make poles which have hyperbolic surface, columns are used as shown in Figure 1.29, When the diameter of these columns is selected in proper to their distances, electric field in the space among the poles in which ions travel is not so different from the case of hyperbolic surface as it gives serious effect on ion motion. Moreover, to avoid difficulty of setting of poles, circular concave electrodes are developed which is able to make from one

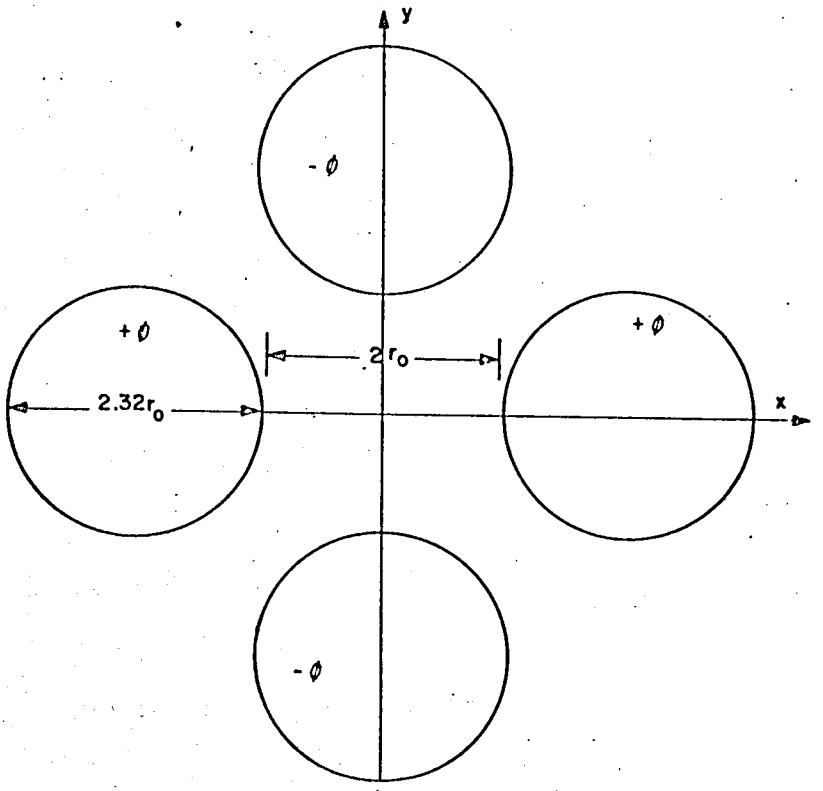

Figure 1.29 Cross sectional schematic diagram of conventional quadrupole.

column and does not need troubles of setting up, and we adopted this type for space experiment mentioned above.

There are some type of mass spectrometer using similar principle. The one is called monopole mass spectrometer as shown in Figure 1.30. This has some merits comparring to quadrupole type. For example, it is not necessary to maintain the ratio V_{dc} / V_{rf} so restrict as the case of quadrupole type. Severe restriction of injection angle of ion is a difficalty of this type, especially for space use. Recently, however, it begins to be used for rocket borne mass spectrometer.

Another type, socalled mini Q, has three dimensional feature as shown in Figure 1.31. It is also considered as a sort of resonant type. The distinctive feature of this type is that ions under resonant condition are trapped for long time while the others are eliminated out of the field. Though it has only short history, it will have many applications in many fields, of course also in space.

1.3.3 Resonant Type (86)∼(90), (121)∼(123)

Many types of resonance of charged particle are

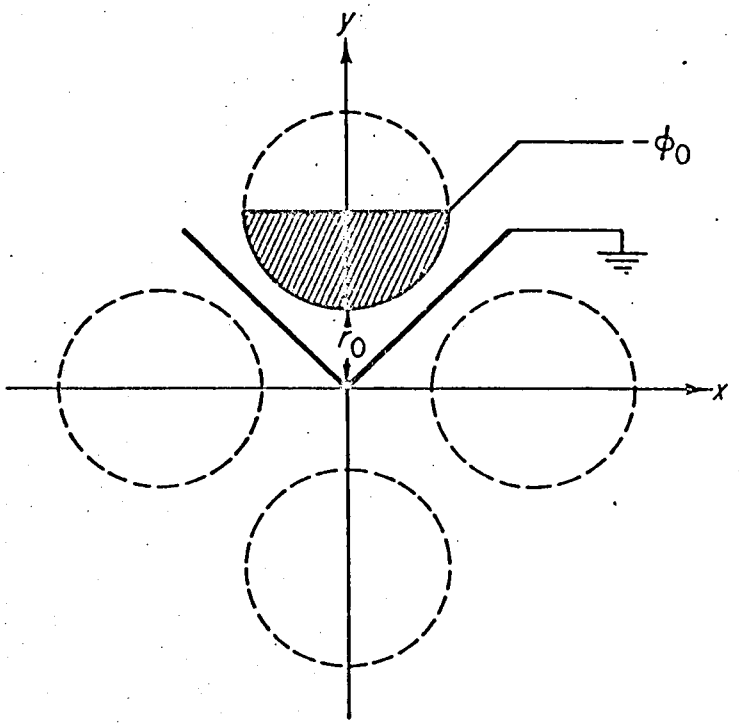

Figure 1.30 Cross sectional schematic diagram of monopole mass spectrometer.

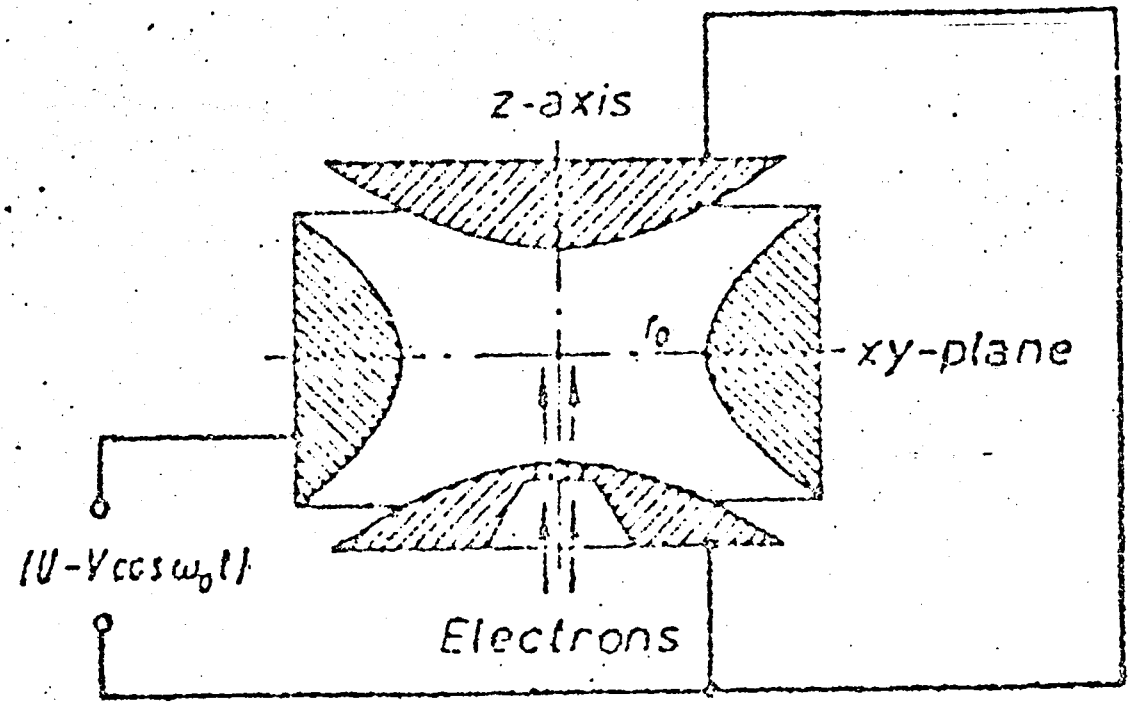

Figure 1.31 Cross sectional schematic diagram of mini - Q.

considered and there are many types of mass spectrometer using these resonance. A mass spectrometer using the ion cyclotron resonant phenomenon has been used as a rocket born payload. This is called " omegatron " and its schematic illustration is shown in Figure 1.32.

The operating principle is the same as cyclotron accelerator. Ions made by electron bombardment in an analysing space are oscillated by radio frequency field applied to the walls of the analyser, which are parallel to magnetic field B. The motion of ions of mass number M, which satisfy the cyclotron resonant condition in the magnetic field B with angular frequency of applied RF voltage ω_c, is described as

$$\frac{e\,B}{m_p M} = \omega_c = 2\pi f_c \qquad (1.32)$$

synchronize with RF-field, and the ions gain energy from it. Consequently, the radius of oscillation of the ions grows up and ions collide against the collector. f_c of Equation (1.32) is called as ion cyclotron frequency of ion of mass number M in magnetic field B.

As seen from Equation (1.32), the frequency of RF voltage must be swept for scanning mass range. Although it is very difficult to generate RF voltage with a flat

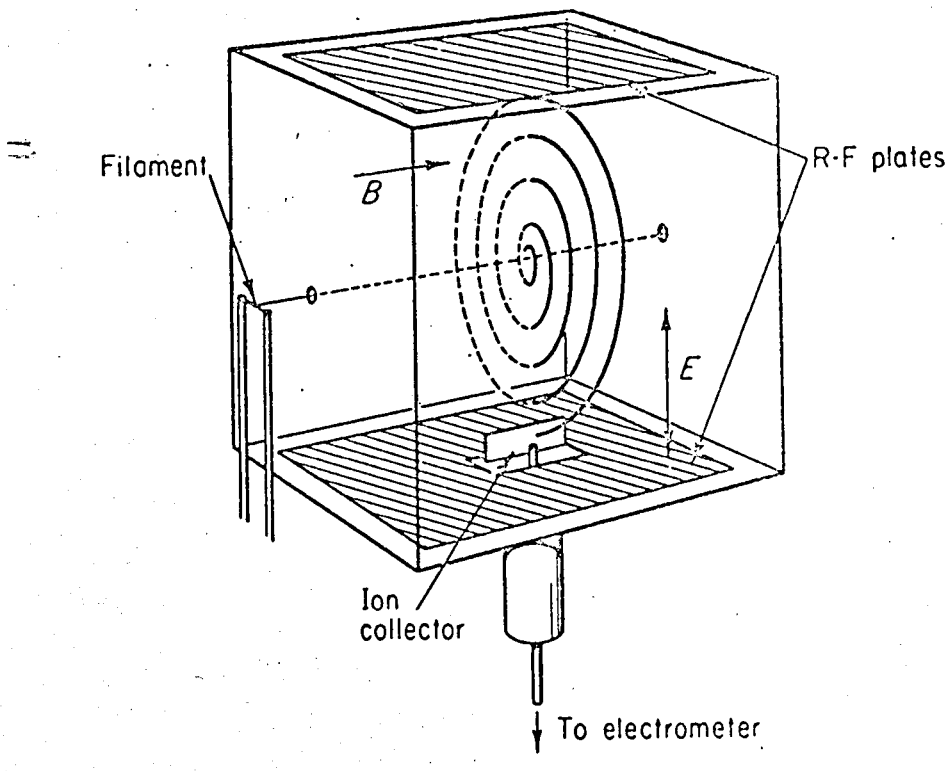

Figure 1.32 Schematic diagram of principle of omegatron.

voltage characteristics covering widely swept frequency range, the characteristics of the omegatron mass spectrometer depend largely on its voltage value or fluctuation. It is the merit of this type of mass spectrometer for space use that ions are made in its analyzing space and the ambiguities in the ion source can be neglected.

1.4 Discussion (87)∼(90), (121)∼(123)

Mass spectrometers which have been used in direct measurement of the upper-atmosphere composition are reviewed as above. They have respective characteristics and it is difficult to say, in short, which is the most suitable for our purpose. Among mass spectrometers described above, some of them are not frequently used because of their shortcomings which are serious obstacle for space application.

Then, the characteristics of magnetic sector type, Bennett type and quadrupole type are briefly compared and discussed from the point of view of space use.

The sensor of quadrupole type is the lightest and

smallest, while the magnetic sector type is the heaviest due to its permanent magnet.

As for a sensitivity, Bennett type has rather high characteristics. Though transparency of Bennett type is worse, area of inlet has no limit. On the other hand, the orifice of quadrupole type and magnetic sector type must be narrow to get excellent characteristics, especially in resolution. Grids of Bennett type disturb the ion motion and they are particularly undesirable to measure active species.

Magnetic sector type has the simplest electronic circuit and is smallest power consumption while quadrupole type is the worst case on these points. Stability and reliability of operation which are important for long term measurement such as a satellite observation are related to the complexity of electronic circuit.

An undesirable appearance of pseudo spectrum by the harmonic relation of the applied RF voltage is the most important problem of Bennett type.

Wide dynamic range is requiered in space observation, so it is desirable that the sensitivity and resolution can be adjusted in a sensor with some electronic techniques. Operation mode of mass spectrometer on a satellite must be selected by command system, because

the conditions of objects of measurement change widely with time, day, season, altitude of vehicle or latitude of the earth.

Bennett type is weakly affected by its attitude compared with other type because of its large cross section of beam. Velocity of vehicle gives different effect on them, that is, mass scale moves in magnetic sector type, while resolution becomes worse in quadrupole type. In Bennett type, the both effects will appear in the same time.

It is impossible to decide the most excellent one. In earlier era of space observation, Bennett type was the most popular mass spectrometer on space vehicle, and recently quadrupole type is frequently employed getting over technical difficulty. In future, quadrupole type will be more frequently used, but the merit of Bennett type that it does not need an electron multiplier, must not be forgotten.

And for satellite, the stability of operation, simplicity of circuit and small power consumption of magnet sector type are important, though it can not electronically change its resolution and sensitivity. It is desirable in satellite observation to control resolution and sensitivity at the analyser with command

from the earth. A mass spectrometer which has such characteristics as required above is developed as described later.

We are carrying out the direct measurement of the upper-atmospheric composition. The Bennett type mass spectrometer without electron multiplier is used to measure the ion composition of E and F layer of the ionosphere by Kappa - 9M rocket, the quadrupole mass spectrometer is used for measurement of ion composition of the lower ionosphere and neutral composition and a new type of mass spectrometer will be used for top side of the ionosphere and satellite.

CHAPTER 2

MASS SPECTROMETER USING

SPATIALLY PERIODIC STATIC FIELD

2.1 Introduction

Various types of mass spectrometers are used for direct measurement of the upper-atmosphere. Besides general qualifications which are commonly required to instruments for space use, the mass spectrometer for this purpose is required with high response characteristics, high sensitivity and wide dynamic range, in consequence of its measuring object which covers various sorts of masses. A suitable type of mass spectrometer, therefore, will be adopted for respective purpose, such as altitude range, sorts of vehicle, object and so on.

For a long time experiment, that is on a satellite, the most important conditions are high reliability and stability of instruments and small power consumption. High reliability depends directly on the simplicity of electronic circuit. The simple electronic circuit generally consumes small electric power. Static mass spectrometer, especially magnetic sector type satisfies these conditions. However, it cannot electronically control the resolution and sensitivity but mechanically. The electronic control of resolution at sensor with command signal from the earth is necessary to choose the

most suitable operating condition at the position where satellite is running and to get wide dynamic range of the experiment.

To develop a mass spectrometer for satellite which has such characteristics as simple electronic circuit like as magnetic sector type and as changable resolution with electronic methods, we had surveyed motions of charged particles in periodic fields and proposed a new type of mass spectrometer of a configuration which is superposed quadrupole spatially periodic magnetic field and quadrupole electric field. According to the results, we made the mass spectrometer and tried to use in laboratory and in space.

2.2 Motion of Charged Particles Passing Through Spatially Periodic Static Fields

(110), (111), (114)~(116), (128)~(132)

2.2.1 Axially Symmetric Periodic Magnetic Field

At first, the case of an axially symmetric periodic magnetic field as shown in Figure 2.1 is investigated. It is assumed here that : axial velocity of charged

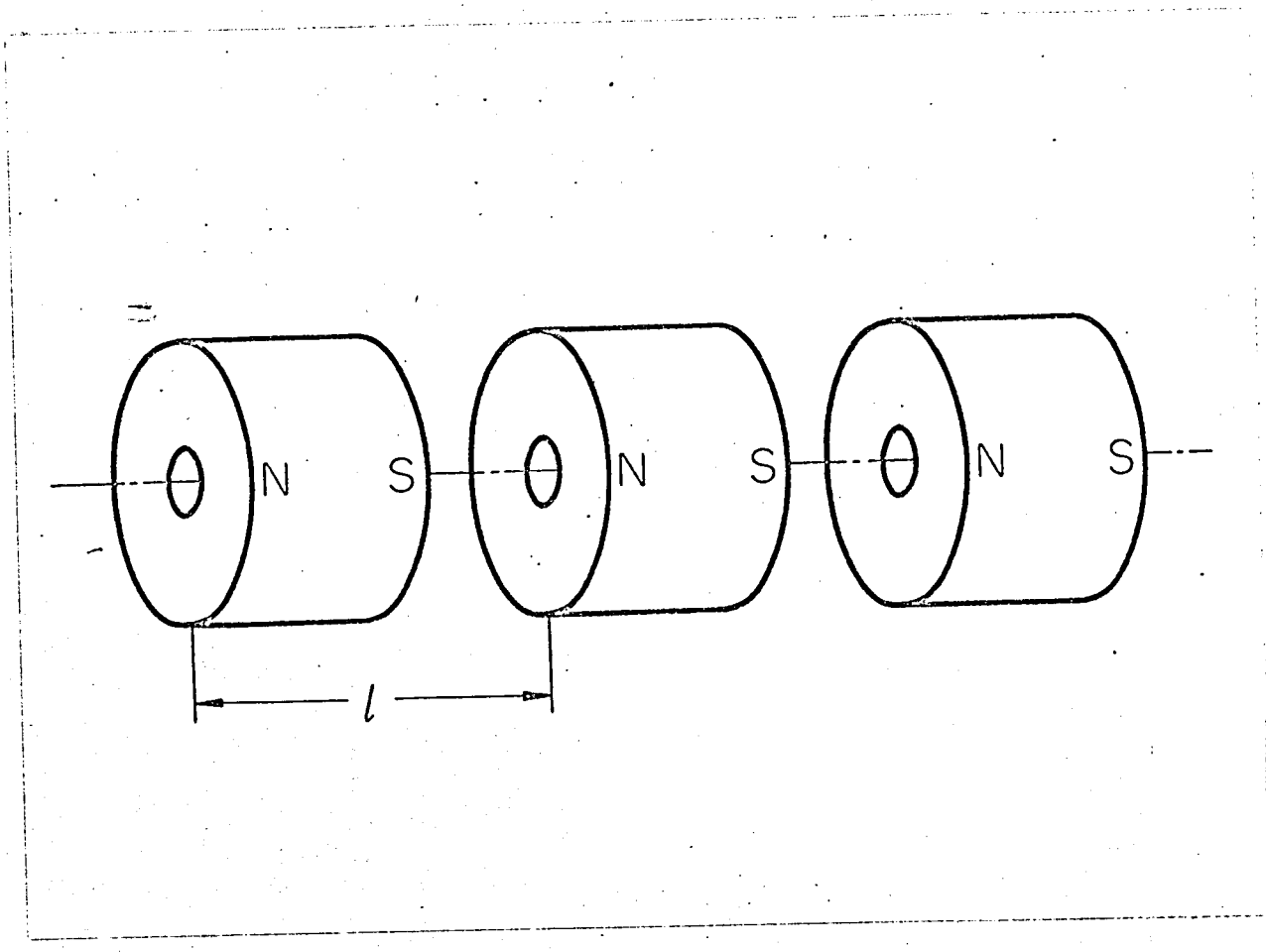

Figure 2.1 Schematic illustration of arrangement of axially symmetric periodic magnetic field.

particles is constant and a distance of a period of motion of charged particles along the axis is larger than diameter of the beam.

Assuming the magnetic field change as sinusoidal in z direction, it might be given as :

$$B_z = B_o \cos kz \qquad (2.1)$$

where B_o : magnetic field of peak value that is at magnetic pole,

k : $2\pi/\ell$ (ℓ: length of a period of the magnetic field),

z : axial distance.

The equation of motion of a charged particle in cylindrical coordinate is shown as

$$m_p M \left\{ \frac{d^2 r}{dt^2} - r\left(\frac{d\theta}{dt}\right)^2 \right\} = er \frac{d\theta}{dt} B_z - eE_r \qquad (2.2)$$

where

$$\frac{d\theta}{dt} = \frac{e}{m_p M} B_z$$

m_p : mass of proton

M : mass numbers

e : electronic charge

As eE_r means the force which is subjected by space

charge effect, it is able to neglect in the case of thin density of charged particle. Therefore

$$\frac{d^2r}{dt^2} - 2r\left(\frac{e}{m_pM} B_o \cos kz\right)^2 = 0 \qquad (2.3)$$

From the asumption as previously mentioned

$$t = z/v \quad \text{and} \quad kz = s$$

then

$$\frac{d^2r}{ds^2} - \left(\frac{ekv}{m_pM} B_o\right)^2 (1 + \cos 2s)r = 0 \qquad (2.4)$$

(111), (112),
(114)~(116),
(128)~(132)

2.2.2 Axially Symmetric Periodic Eledtric Field

Although in the case of axially symmetric periodic Electric field as shown in Figure 2.2, the axial velocity of a charged particle is not constant. It is assumed that the velocities of charged particles is equal at the same cross section of the beam. Providing voltage on the axis varies as :

$$V(z) = V_o + V_1(1 - \cos kz) \qquad (2.5)$$

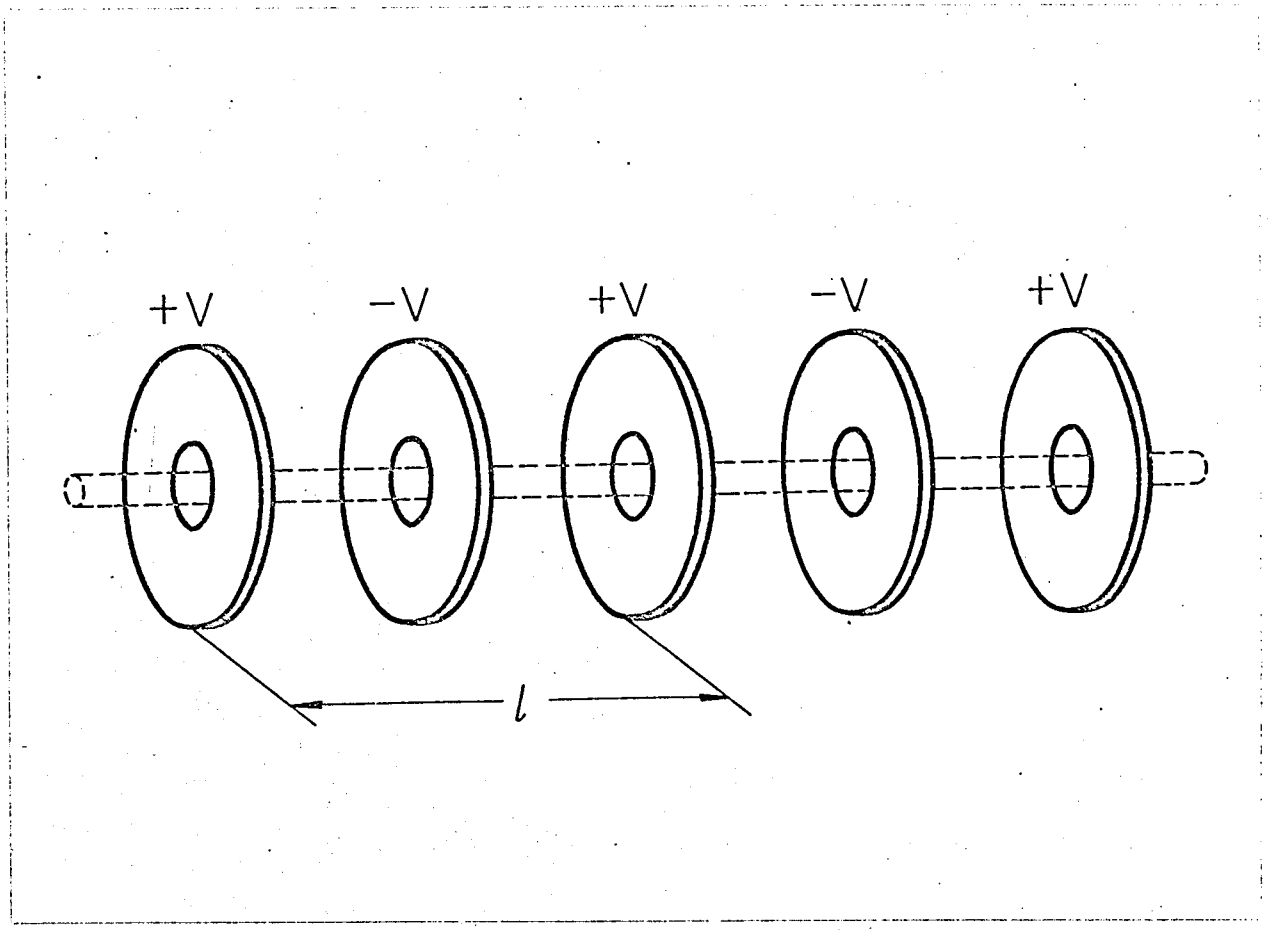

Figure 2.2 Schematic illustration of arrangement of axially symmetric periodic electric field.

the voltage adjacent to the axis is given approximately as :

$$V(z,r) = V(z) - \frac{1}{4}\frac{d^2V(z)}{dz^2} r^2 \qquad (2.6)$$

The equation of motion of radial direction of a charged particle near the axis is :

$$m_p M \frac{d^2r}{dt^2} = e \frac{dV(z,r)}{dr} \qquad (2.7)$$

then

$$\frac{d^2r}{dt^2} = - \frac{e}{2m_p M} \frac{d^2V(z)}{dz^2} r \qquad (2.8)$$

Because the axial velocity of charged particles is larger enough than the radial velocity, the following equation is derived

$$\frac{d^2r}{dz^2} + \frac{1}{2V(z)} \frac{dV(z)}{dz} \frac{dr}{dz} + \frac{1}{4V(z)} \frac{d^2V(z)}{dz^2} r = 0 \qquad (2.9)$$

Again, it is transformed by $kz = s$, $R = krV(z)^{1/4}$ under the conditions of $V_o \gg V_1$

$$\frac{d^2R}{ds^2} + \frac{3}{32}\frac{V_1^2}{V_o^2}(1 - \cos 2s)R = 0 \qquad (2.10)$$

2.2.3 Quadrupole Periodic Magnetic Field (110), (111), (114)~(116), (128)~(132)

In the case of quadrupole periodic magnetic field as shown in Figure 2.3, adoptation of the rectangular co-ordinate is rather convenient than cylindrical co-ordinate. The axial direction is taken as z axis. When a period of the magnetic field ℓ is larger than the radius of beam, components of the magnetic field is given as :

$$B_x = \frac{B_o}{r_o} y \cos kz$$

$$B_y = -\frac{B_o}{r_o} x \cos kz \qquad (2.11)$$

$$B_z = k \frac{B_o}{r_o} xy \sin kz$$

Providing components of velocity of the ion passing through the field are

$$v_x, v_y \ll v_z = v$$

equations of motion of the ions are described as

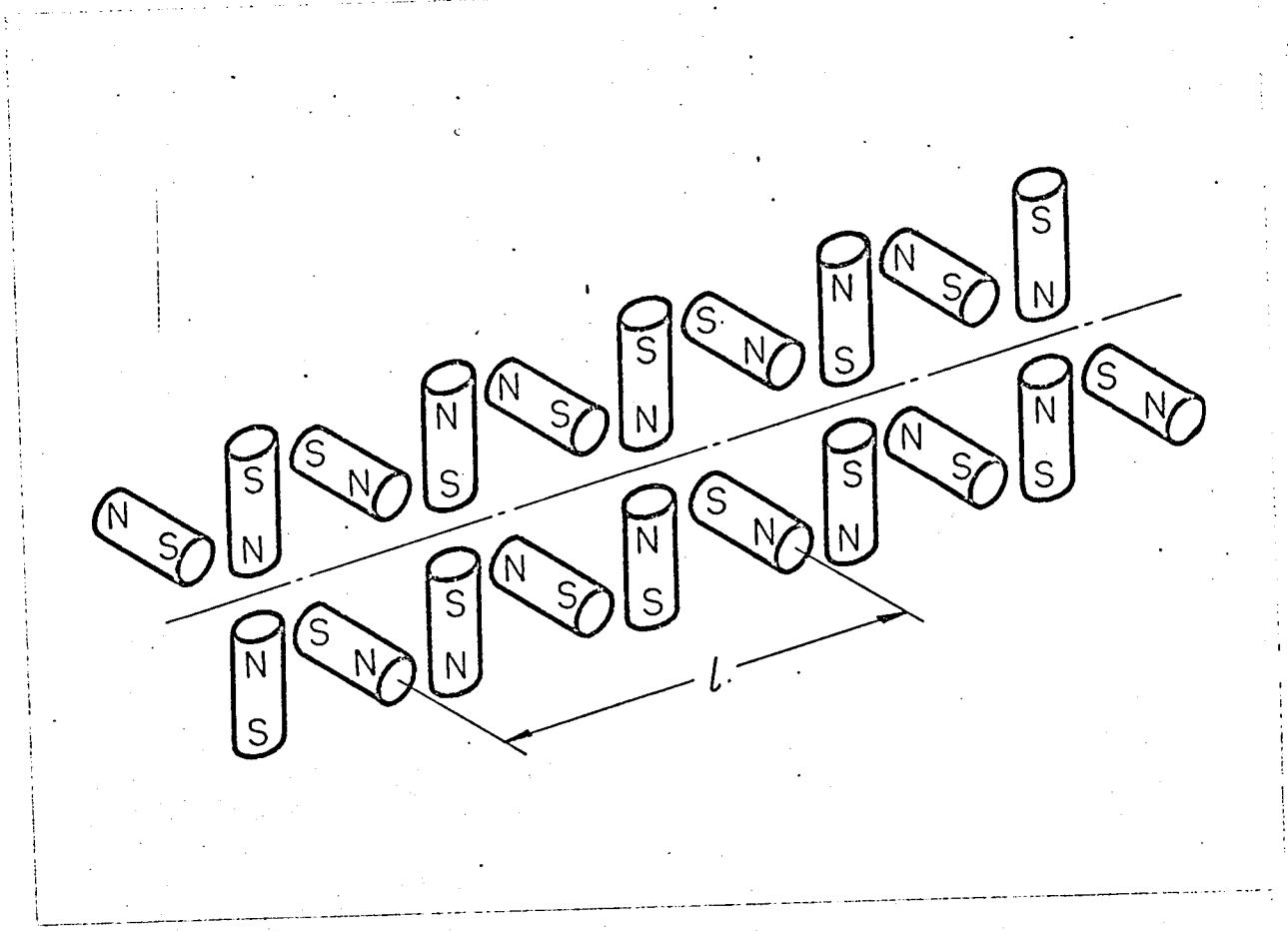

Figure 2.3 Schematic illustration of arrangement of quadrupole periodic magnetic field.

$$\frac{d^2x}{dt^2} + \frac{eB_o}{m_p M r_o} vx \cos kz = 0$$

$$\frac{d^2y}{dt^2} - \frac{eB_o}{m_p M r_o} vy \cos kz = 0 \qquad (2.12)$$

where r_o : radius of beam.

After transformation of variable as $z = vt$, $kz = 2s$ they are written as

$$\frac{d^2x}{ds^2} + \frac{4eB_o}{m_p M r_o k^2 v} (\cos 2s)x = 0$$

$$\frac{d^2y}{ds^2} - \frac{4eB_o}{m_p M r_o k^2 v} (\cos 2s)y = 0 \qquad (2.13)$$

2.2.4 Quadrupole Periodic Electric Field (111), (112), (114)~(116), (128)~(132)

Components of electric field which is made by quadrupole periodic electric field as shown in Figure 2.4 are given as follows under simillar asumption as previous :

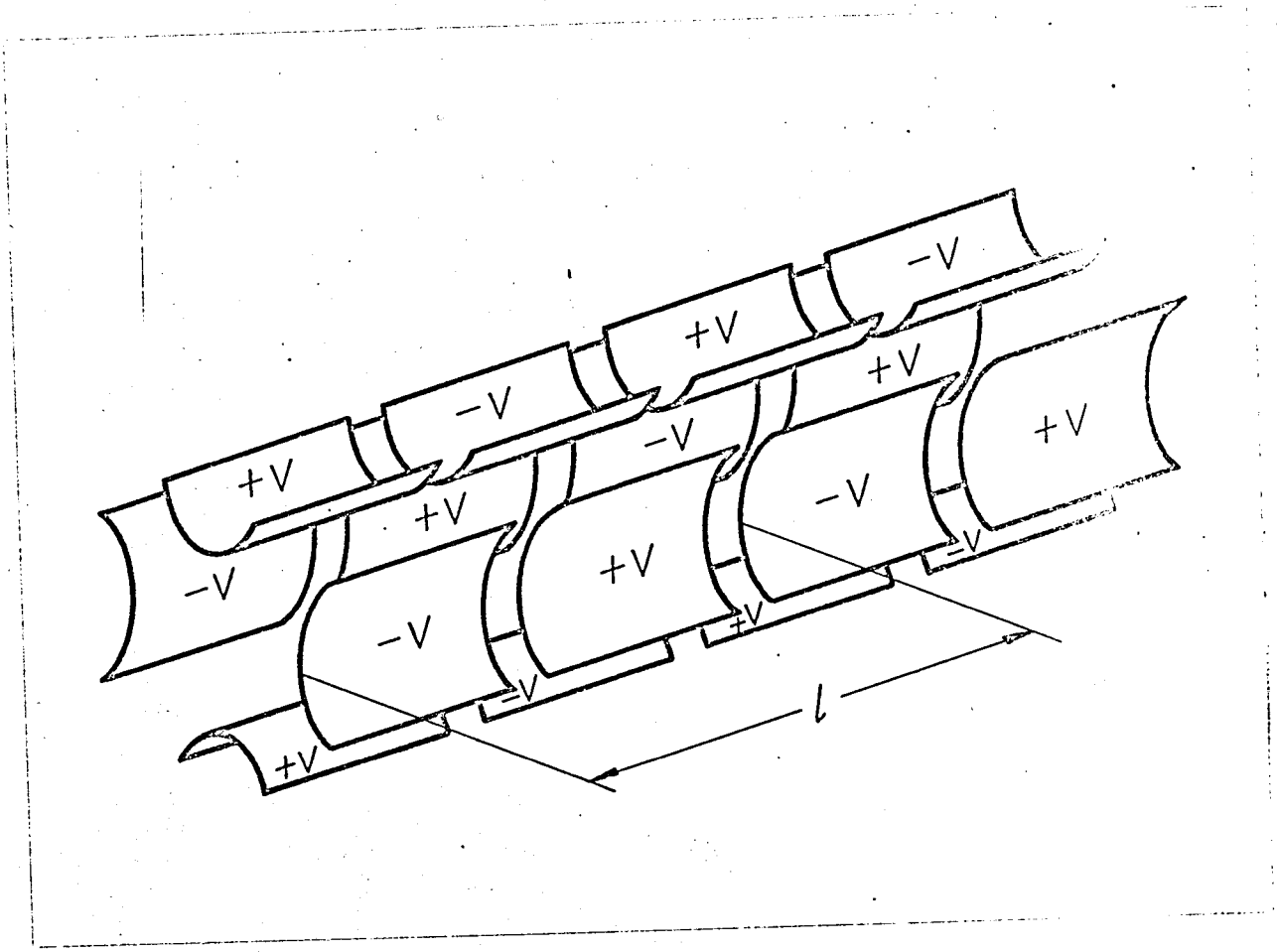

Figure 2.4 Schematic illustration of arrangement of quadrupole periodic electric field.

$$E_x = \frac{2V}{r_o^2} x \cos kz$$

$$E_y = -\frac{2V}{r_o^2} y \cos kz \qquad (2.14)$$

$$E_z = -\frac{kV}{r_o^2} (x^2 - y^2) \sin kz$$

As same as previous subsection 2.2.3, lines of force draw hyperbola. The equations of motion of ions which pass through the field are that :

$$\frac{d^2x}{dt^2} + \frac{2eV}{m_p M r_o^2} (\cos kz)x = 0$$

$$\frac{d^2y}{dt^2} - \frac{2eV}{m_p M r_o^2} (\cos kz)y = 0 \qquad (2.15)$$

It is apparent from Equation (2.14) that the electric field becomes to zero on the axis of the beam. Therefore, it is considerable that $v_z = v$ is constant in the vicinity of the axis. By the replacement of variables with $t = z/v$, $kz = 2s$ under the same asumption as previous, Equations (2.15) are written as

88 項欠

$$\frac{d^2x}{ds^2} + \frac{8eV}{m_p M r_o^2 k^2 v^2}(\cos 2s)x = 0$$

$$\frac{d^2y}{ds^2} - \frac{8eV}{m_p M r_o^2 k^2 v^2}(\cos 2s)y = 0 \qquad (2.16)$$

2.2.5 Discussion (114) (116)

The resultant equations of previous subsections such as Equation (2.4), (2.10), (2.13) and (2.16) are resemble. They are the differential equation which has a coefficient of periodic function.

Such a sort of differential equation is generally written as :

$$\frac{d^2x}{dt^2} - [\, a - 2q\phi(t) \,]x = 0 \qquad (2.17)$$

and it is called Hill's differential equation.

To the special case as $\phi(t) = \cos 2t$, it is the well known Mathieu's differential equation. That is

$$\frac{d^2x}{dt^2} - (\, a - 2q \cos 2t \,)x = 0 \qquad (2.18)$$

Page 88 is skipped by numbering miss.

The solution of Equation (2.18) is called as Mathieu function and it shows stable or unstable according to the values of coefficient of Equation (2.18), a and q. The condition is illustrated in a diagram as shown in Figure 2.5 which is called as Mathieu's Butterfly Diagram. The hatched areas are stable regions of the solution and the others give unstable solution.

Equation (2.4) is in the case of

$$a = -2q = \left(\frac{ekv}{m_p M} B_o \right)^2 \qquad (2.19)$$

Equation (2.10) is

$$a = 2q = -\frac{3}{32} \frac{V_1^2}{V_o^2} \qquad (2.20)$$

Equations (2.13) are

$$a = 0 , \quad q = \frac{2eB_o}{m_p M r_o k^2 v} \qquad (2.21)$$

and Equations (2.16) are in the case of

$$a = 0 , \quad q = \frac{4eV_1}{m_p M r_o^2 k^2 v^2} \qquad (2.22)$$

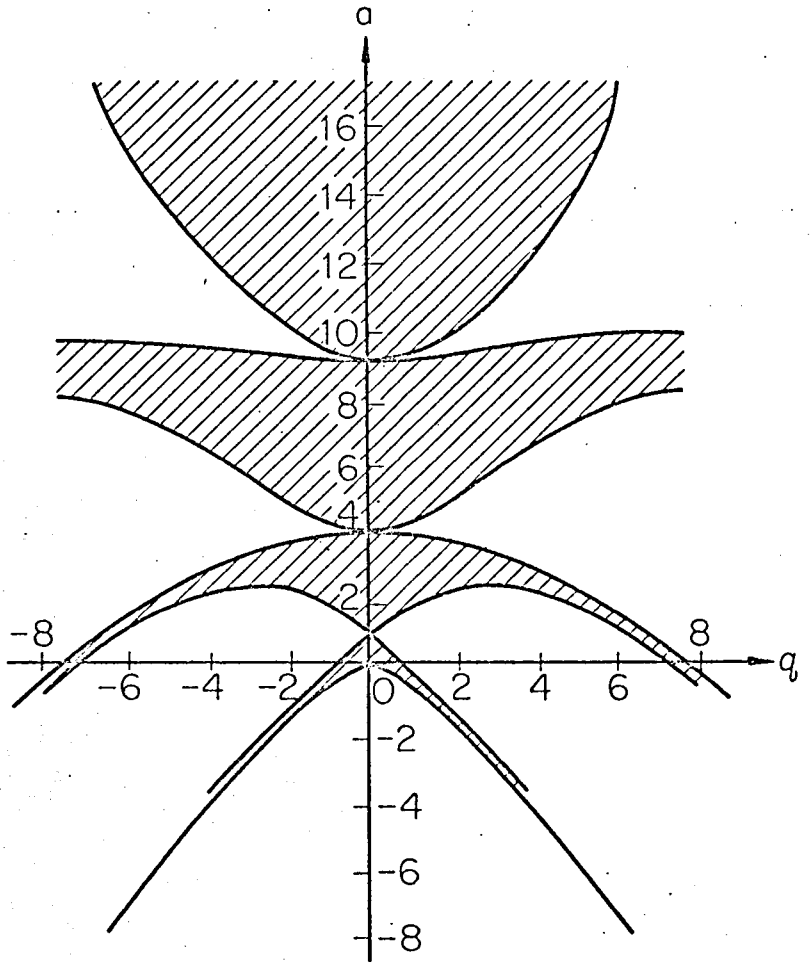

Figure 2.5 Mathieu's Butterfly Diagram.

92 項欠

It is apparent from these equations that they vary on each operating line of the diagram when the parameters change. The operating line is $a = -2q$ for Equation (2.19) and is $a = 2q$, $a = 0$ and $a = 0$ for Equations (2.20), (2.21) and (2.22) respectively. As seen from Equations (2.19).....(2.22), according the changes of the conditions such as k, v, M, B_o, V_1 or V_o, the operating condition is determined at a point on each operating line, and the solution is given in stable or unstable, that is, the beam of the charged particle is converged or diverged corresponding to the point of the diagram.

As learned from Figure 2.5 and Equations (2.19)..... .....(2.22), if the basic configuration of field is used for mass analysis, there are the probability that ions of different mass are focussed in the same condition. Consequently, they can not be used as a mass spectrometer but some proper combination of them will achieve a mass spectrometer.

Page 92 is skipped by numbering miss.

2.3 A Configration of Mass Spectrometer Using Spatially Periodic Static Field (113)∼(115), (117), (128)∼(132)

In the previous section, motions of charged particles in basic cases of periodic static field are investigated. They are unable to have individually the function as a mass spectrometer. Some appropriate combinations of them, however, in which behavior of ions is different and complicated from the basic cases, are promising to analyze the mass or energy of ions.

A configuration among them which is superposed quadrupolar periodic magnetic field and quadrupolar electric field, as schematically illustrated in Figure 2.6 is proposed for a mass spectrometer. The line of force of the electric and magnetic field in the cross-section at a magnet position are shown in Figure 2.7 (a) and (b) respectively.

It is assumed that the variation of the magnetic field with the z-axis follows the cosine law, the radius of beam of ions through the field, r_o, is much less than the period of the magnetic field ℓ, and without losing generality, the relation between the velocity components of ions can be expressed as v_x, $v_y \ll v_z = v$.

Under these condition, the equations for the

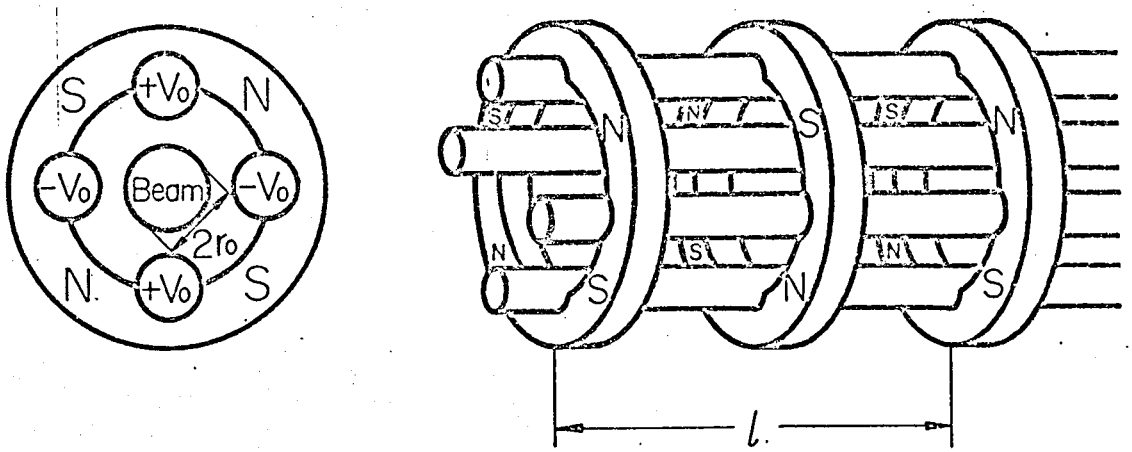

Figure 2.6 Schematic illustration of proposed configuration superposed quadrupolar periodic magnetic field and quadrupolar electric field.

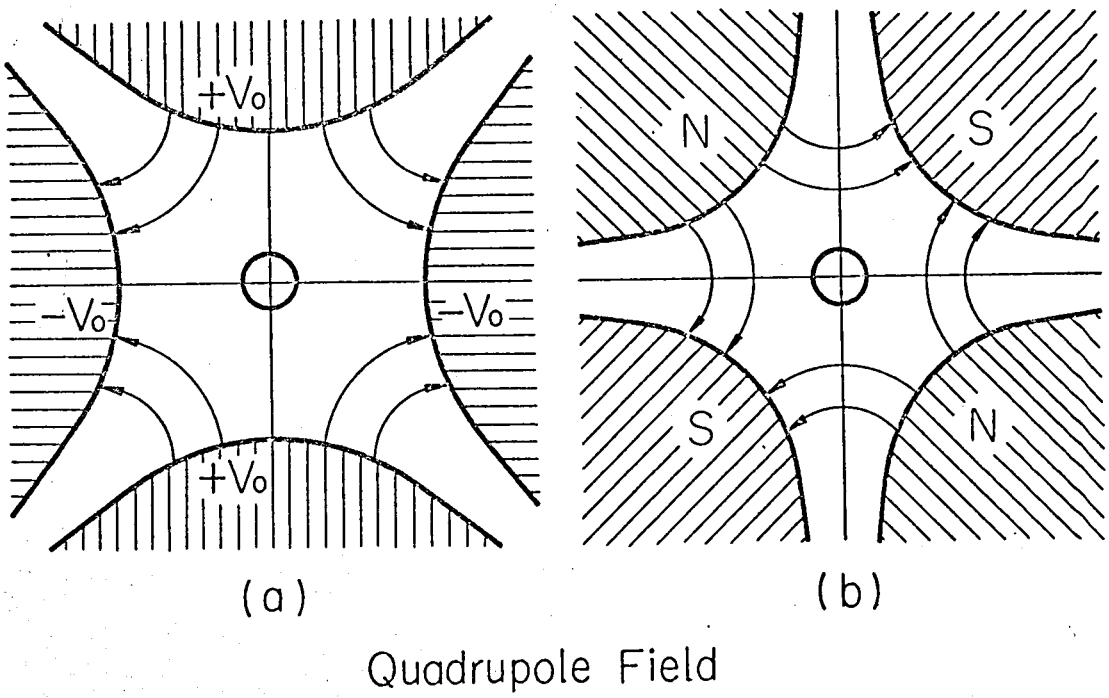

Figure 2.7 Line of force of electric (a) and magnetic (b) fields in the cross section at magnet.

magnetic field are the same as Equations (2.11) and the equations for the electric field are given as follows :

$$E_x = -\frac{2V_o}{r_o^2}x$$
$$E_y = \frac{2V_o}{r_o^2}y \qquad (2.23)$$

Therefore, the equations of motions for the ions which pass through these fields are :

$$\frac{d^2x}{dt^2} + \frac{2eV_o}{m_p M r_o}x + \frac{eB_o}{m_p M r_o}v\left(\cos\frac{2\pi}{\ell}z\right)x = 0$$
$$\frac{d^2y}{dt^2} - \frac{2eV_o}{m_p M r_o}y - \frac{eB_o}{m_p M r_o}v\left(\cos\frac{2\pi}{\ell}z\right)y = 0 \qquad (2.24)$$

Under the same assumptions as in the previous sections, providing $vt = z$, $z/\ell = \tau$, Equations (2.24) become as :

$$\frac{d^2x}{d\tau^2} + \frac{e\ell^2}{\pi^2 m_p M r_o^2 v^2}\left(2V_o + r_o B_o v\cos 2\tau\right)x = 0$$
$$\frac{d^2y}{d\tau^2} - \frac{e\ell^2}{\pi^2 m_p M r_o^2 v^2}\left(2V_o + r_o B_o v\cos 2\tau\right)y = 0 \qquad (2.25)$$

These equations are rewritten with accelerating voltage V_A ($= \frac{m_p M v^2}{2e}$) as :

$$\frac{d^2x}{d\tau^2} + \frac{\ell^2}{\pi^2 r_o^2 V_A}\left(2V_o + r_o B_o \sqrt{\frac{2eV_A}{m_p M}}\cos 2\tau\right)x = 0$$

$$\frac{d^2y}{d\tau^2} - \frac{\ell^2}{\pi^2 r_o^2 V_A}\left(2V_o + r_o B_o \sqrt{\frac{2eV_A}{m_p M}}\cos 2\tau\right)y = 0 \qquad (2.26)$$

These are Mathieu equation which have no specific relations between a and q. Accordingly, as understood from Equations (2.25) or (2.26) and Figure 2.5, the region of " Butterfly diagram " which gives stable solutions at the same time to the x and y directions is the hatched area of Figure 2.8. Therefore, ions having the operational condition in the above region have converged trajectories and can be trapped by its collector.

When dimensions of sensor of the mass spectrometer are taken as ℓ = 2 cm, r_o = 0.2 cm, coefficient of Mathieu equation a and q are given as

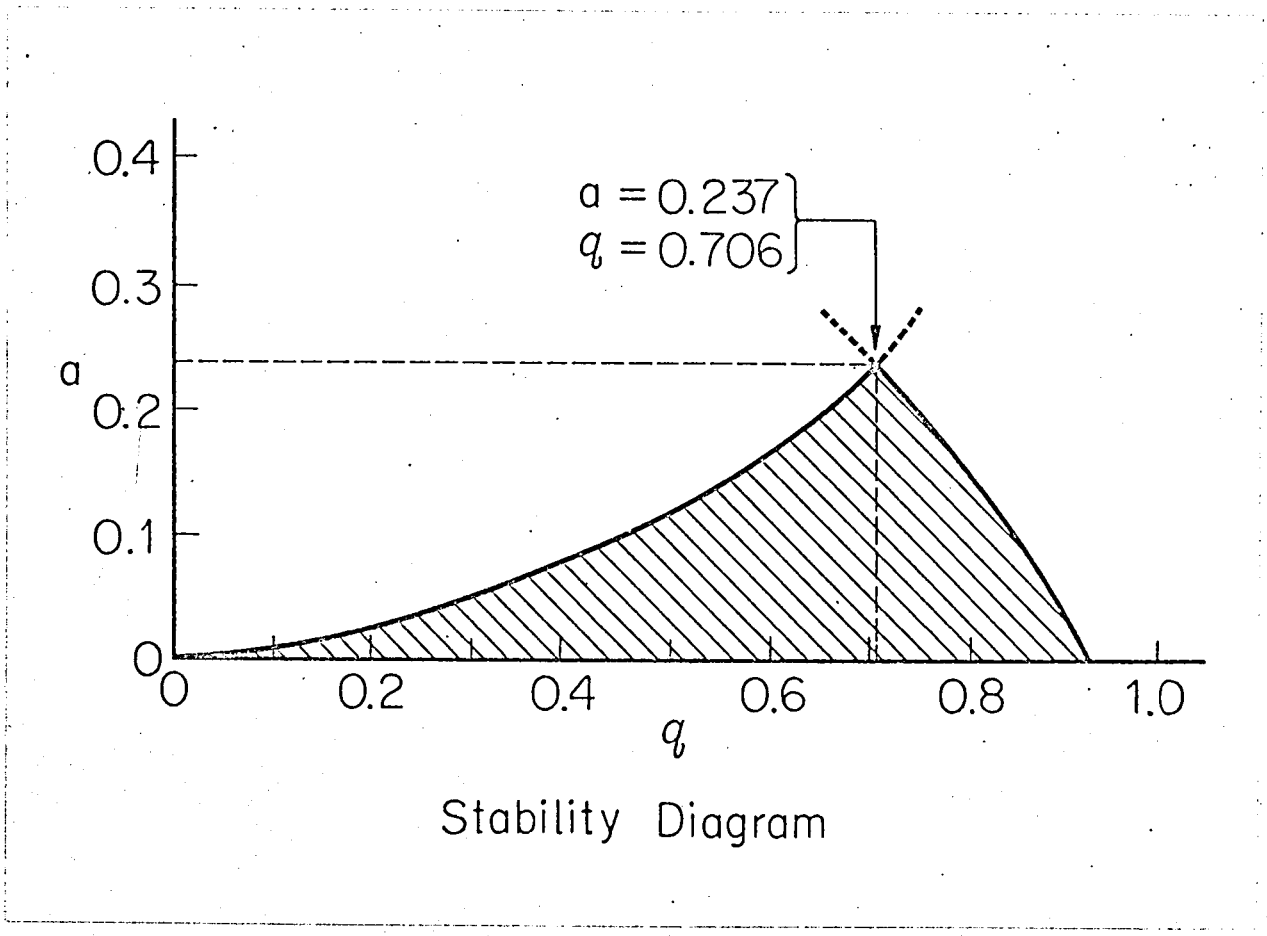

Figure 2.8 Stability diagram charged particle in the mass spectrometer.

$$a \simeq 10 \frac{V_o}{V_A}$$

$$q \simeq 0.7 \times 10^{10} \frac{B_o}{\sqrt{V_A M}} \qquad (2.27)$$

where V_o and V_A : in volt,

B_o : in Wb / m^2.

Therefore, when B_o is constant value and V_A is varied for scanning of mass range, a mass spectrum can be obtained. Thus the quantites V_o, V_A and B_o are realizable even if the velocity of ions v might be much greater than that of the space vehicle.

Some available combinations may be considered in the similar condition under some limits. Equations of motion of charged particles passing through the field of the similar shape of electrodes using only electric field as illustrated in Figure 2.9 are described as :

$$\frac{d^2x}{d\tau^2} + \frac{\ell^2}{\pi^2 r_o^2 V_A}(V_o + V_1 \cos 2\tau)x = 0$$

$$\frac{d^2y}{d\tau^2} - \frac{\ell^2}{\pi^2 r_o^2 V_A}(V_o + V_1 \cos 2\tau)y = 0 \qquad (2.28)$$

The stable region of the configuration is the same as

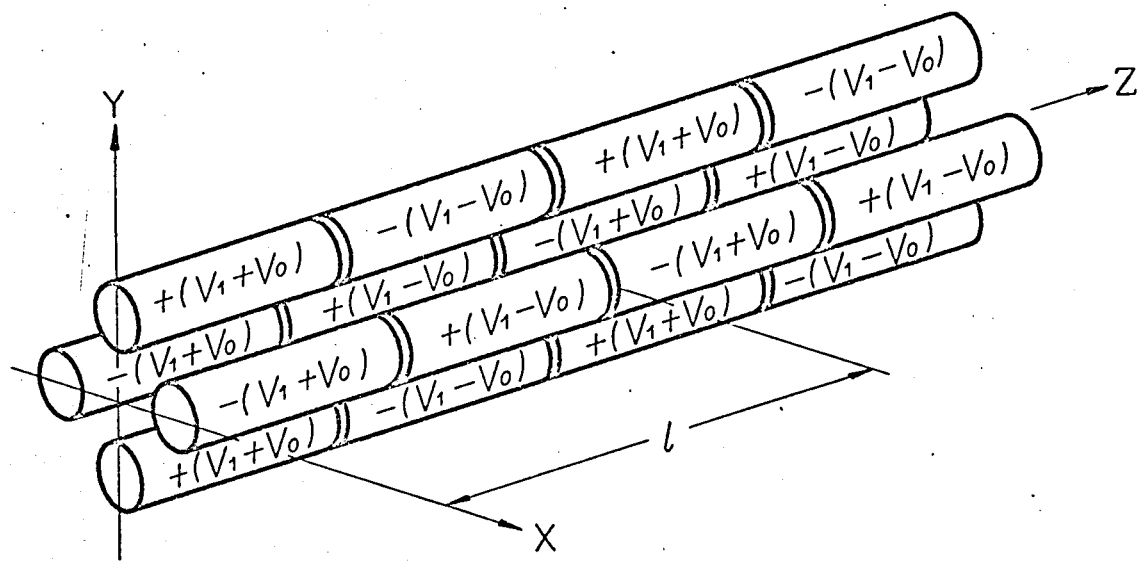

Figure 2.9 Schematic illustration of energy analyser.

Figure 2.8 and as seen from Equations (2.28) it analyzes incident energy of charged particles, that is, it is used not as mass spectrometer but as energy analyser.

When the velocity of a space vehicle on which the energy analyser is installed, is faster enough than thermal velocity of ions, it can be used as mass spectrometer utilizing the velocity as ion trap. In such a case, it is much more excellent than ion trap.

(114), (115), (117), (128)~(132)

2.4 Calculation of Orbits of Charged Particles

The trajectories of charged particles passing through the configuration of the field as shown in Figure 2.6 and 2.7, that is, the solution of Equation (2.26) is calculated by electronic computer with various conditions. Although the Mathieu's differential equation is generally solved by developing into infinite series of two families as well known, we adopted direct calculation of the differential equation by electronic computer. The details of the method adopted for the purpose is described in the appendix.

Though many calculations have been done under

various conditions of parameters, only some typical results are shown in following. The trajectories of ions in Figure 2.10 show the aspects of divergence of H^+ and O^+ ions under the convergent condition of He^+ ion. Figure 2.11 shows the trajectories of the same kind of ions as Figure 2.10 for higher resolution with varying a, e.g. V_o.

From these two figures, the influence of different operational condition is apparent especially on the trajectories of the convergent ions and it seems that the convergent ion trajectories show a laminar flow.

Figure 2.12 includes the case of heavier ions that is, it shows trajectories of NO^+, N_2^+ and O_2^+ ions on the convergent condition of NO^+ ions besides that of He^+, H^+ and O^+ ions. The initial position of these ions is assumed to be about 1.5 mm apart from the axis and the radial component of initial velocity is zero. This figure shows that to analyze the higher mass of ion, the longer configuration of sensor of the mass spectrometer is required.

All of previous results are in the case where the ions are injected into the orifice of the mass spectrometer in various positions and only with the velocity component parallel to the z axis. Because

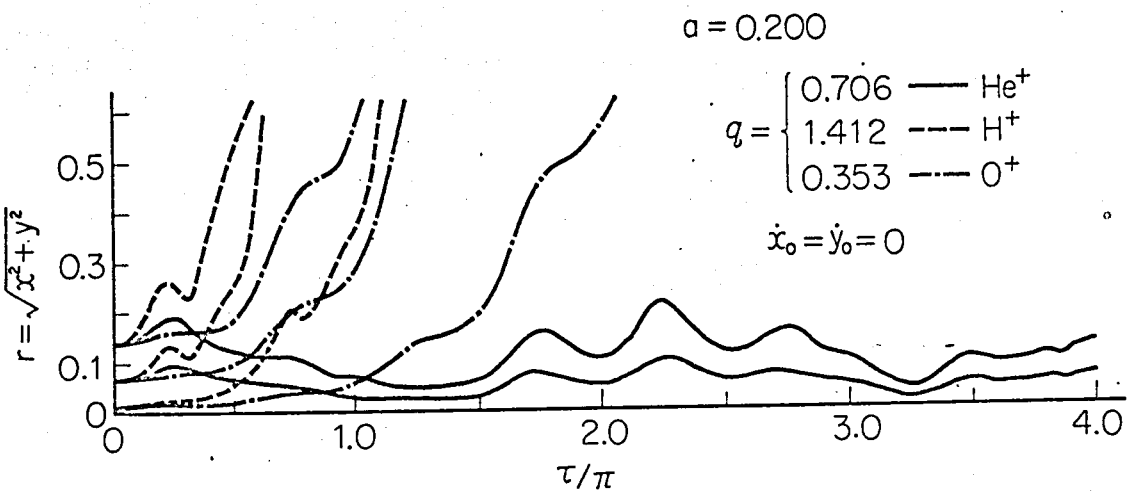

Figure 2.10 Trajectories of H^+, He^+ and O^+ ions under convergent condition of He^+ ion.

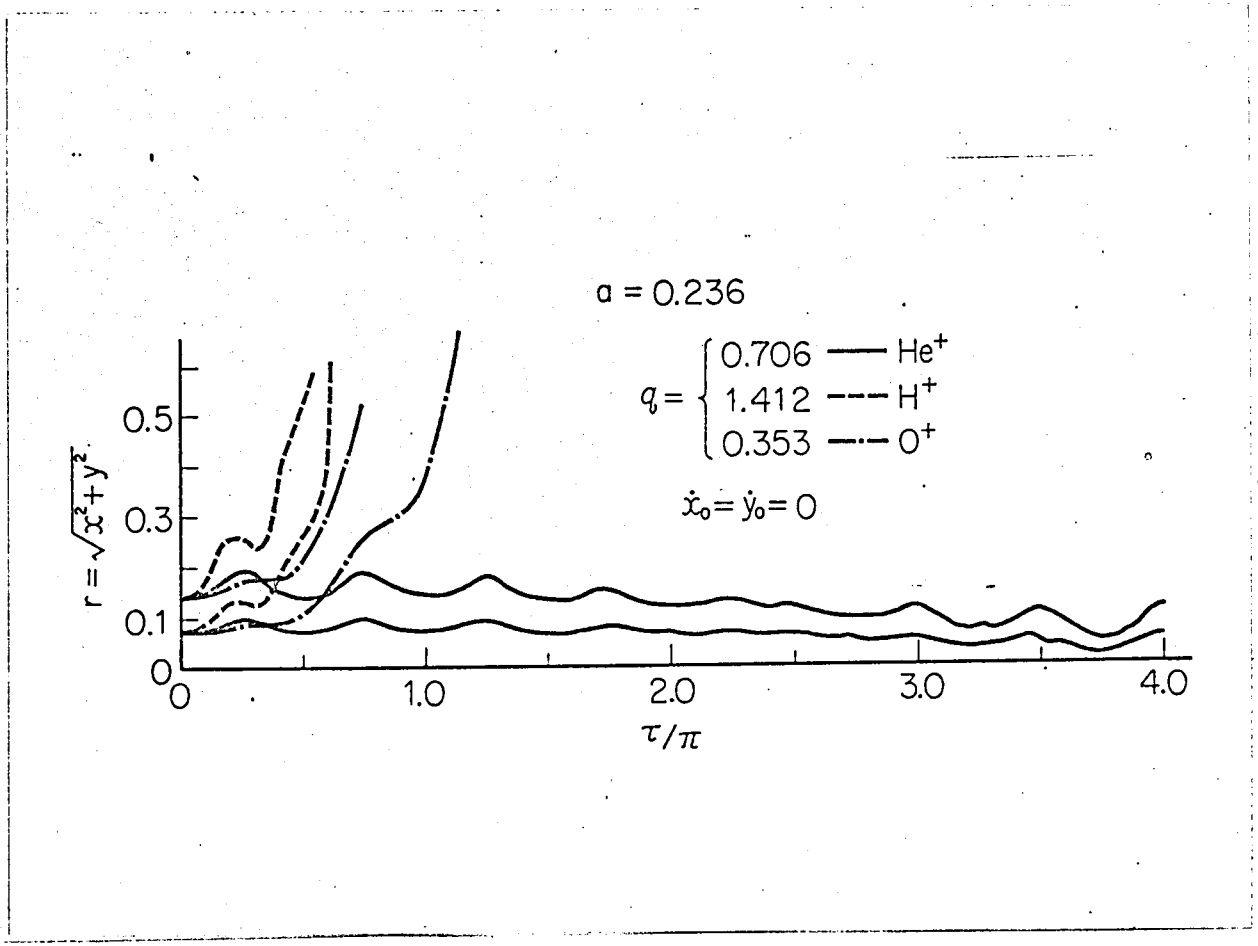

Figure 2.11 The same as Figure 2.10 but higher resolution.

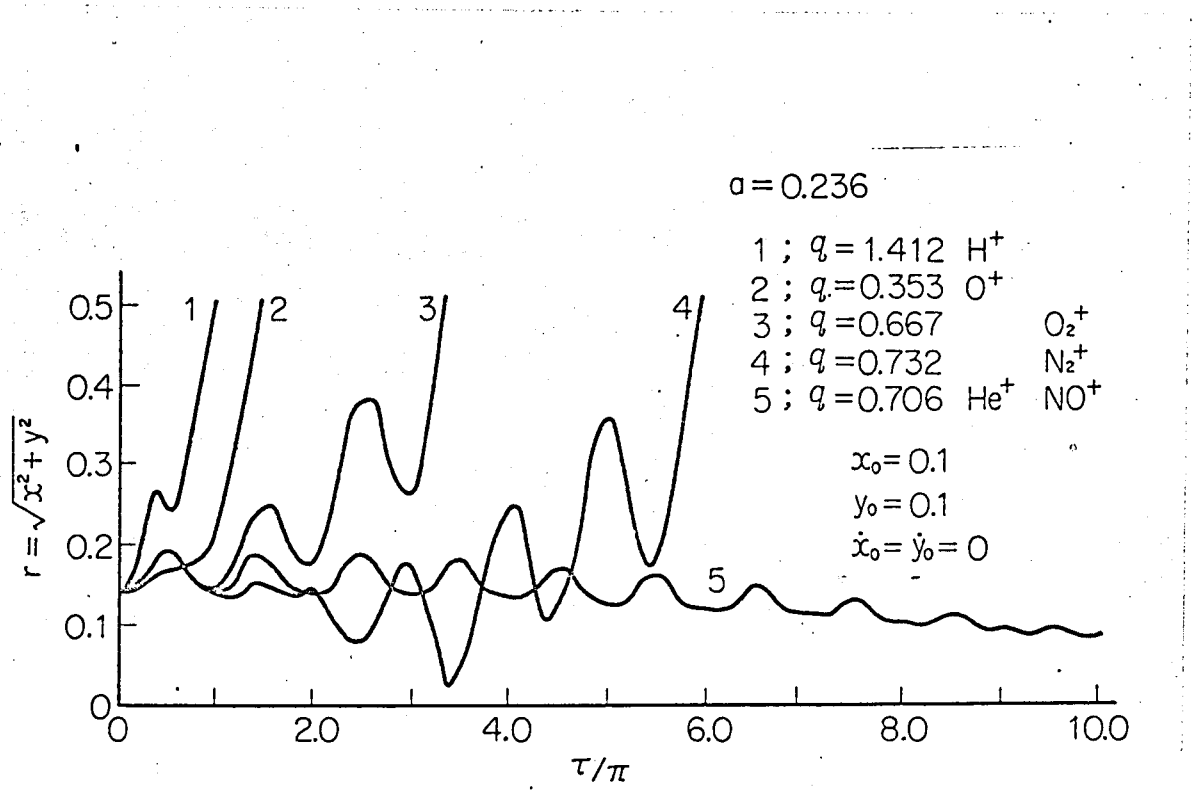

Figure 2.12 Trajectories of H^+, He^+ and O^+ ions under convergent condition of He^+ ion and NO^+, N_2^+ and O_2^+ ion under stable condition of N_2^+ ion.

the direction of flight of the space vehicle installing the mass spectrometer sensor is not always coincide with the derection of axis of the sensor, the velocity component perpendicular to the z axis should be taken into consideration. Although details of this characteristics called as characteristics of attack angle will be mentioned in Chapter III, Figure 2.13 is shown as an example of theoretical calculation of the characteristics.

In this case, the axial component of the initial velocity for He^+ ions is 5×10^4 m/sec and the angle between the axes of the sensor and vehicle with the velocity of 8×10^3 m/sec is assumed to be 10 degrees. It is apparent that the trajectories vary with its incident condition, even the ions of convergent condition slowly diverge and the laminar flow is disturbed.

Although these figures shown previously are illustrated only according to the departure from the center of the beam, that is, $r = \sqrt{x^2 + y^2}$, the actual trajectories show complicated behaviors in three dimensional one.

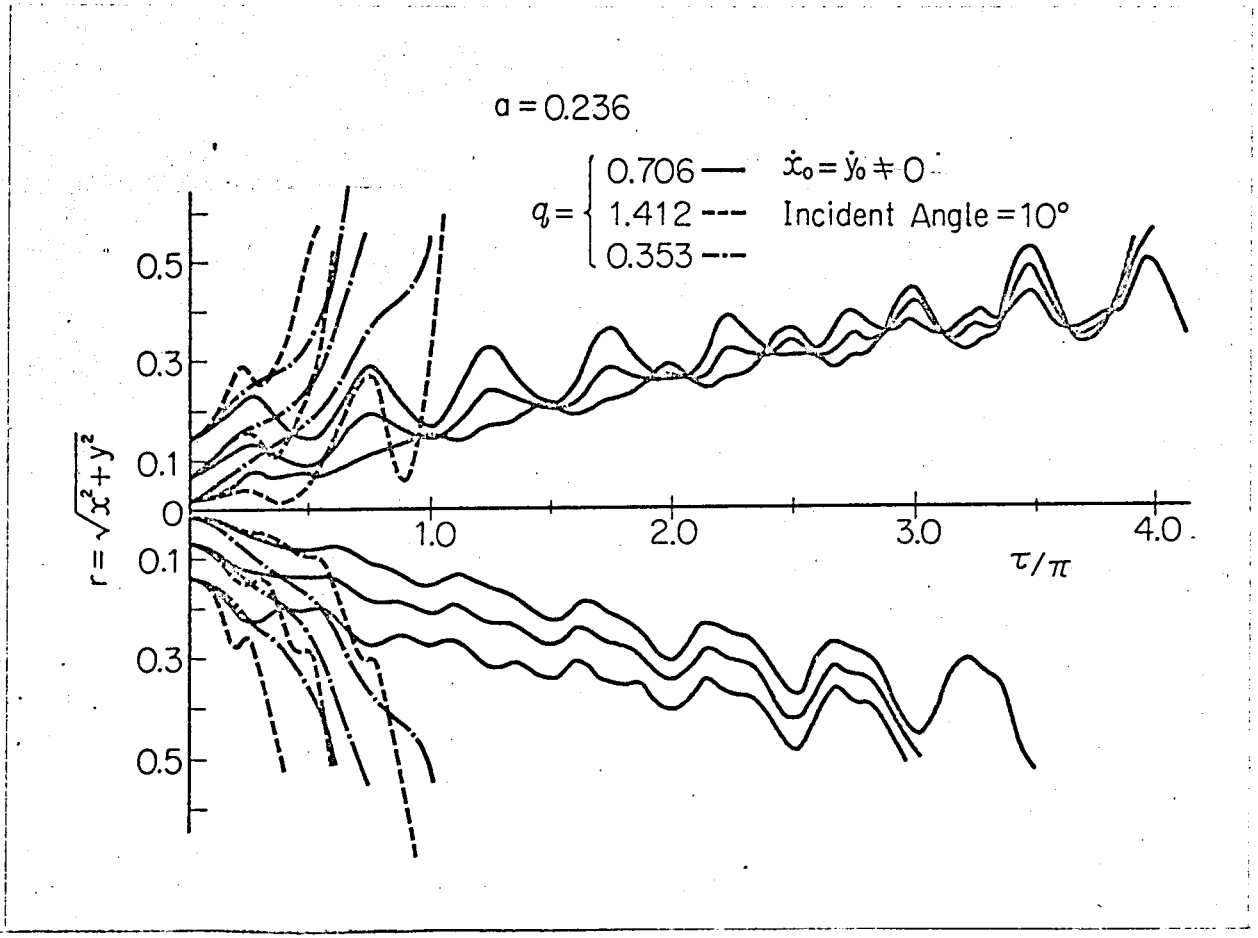

Figure 2.13 Trajectories of ions of oblique injection, that is, characteristics of attack angle.

2.5 Investigation in the Case of Finite Length of Sensor (114), (115), (118), (128)∼(132)

As mentioned previously, the stability condition of the solution of Equation (2.26) is given by the hatched area of Figure 2.8. It holds good, however, in such case that the magnetic and electric fields continue infinitely along the z direction and the circumstance is different from actual finite length of the sensor. Though the number of times that ions are subjected to the field, decrease with a sensor of finite length and it is expressed as growing inferior resolution, a finite length sensor must be used in actual instrument.

The data which are used in designing optimum configuration of sensor and give a suitable operational condition to the sensor, are required. For this purpose the deformation of the stable region in Figure 2.8 in the case of infinite length must be investigated. The results of calculations are shown in Figure 2.14.

It is seen from the figure that the phenomena of the flat appex of the triangular boundaries mean lowering of the resolution and different operational conditions from that of Figure 2.8 must be chosen as the number of magnetic poles decrease.

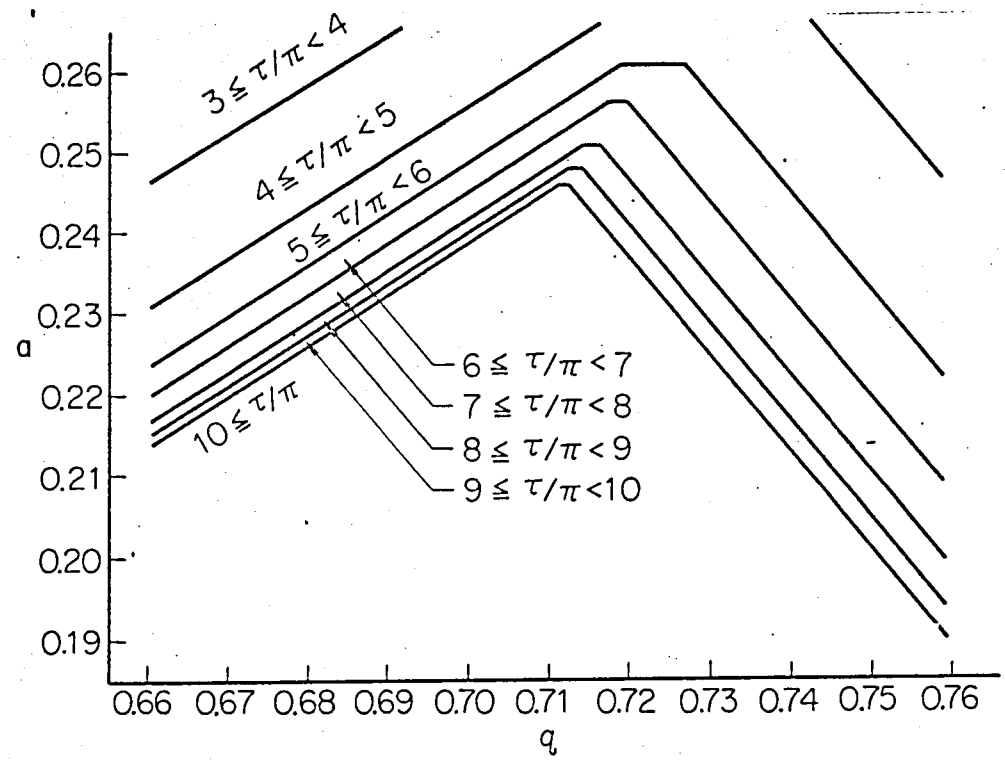

Figure 2.14 Stability diagram for various length of sensor.

2.6 Investigation into Actual Arrangement of Magnetic Field (114), (115), (118), (128)~(132)

All of above calculation have been done on the assumption that the periodic magnetic fields vary in cosine law along z axis. However, in actual, the magnetic poles are arranged discretely, and the shapes of magnetic field generated by these poles will vary according to the shape, dimension or interval of the poles.

To investigate for such cases, some stability conditions are calculated for the several cases that the variations of magnetic field along z axis are from periodically rectangular to triangular figure in which sinusoidal form is contained. Results of the calculation is shown in Figure 2.15. In this figure the magnified appex parts are illustrated.

It is apparent from this figure that the stable condition or stable region does not change essentially but the stable region shifts in parallel to the parameter q. Consequently, it is learned that the difference of the shape of magnetic field make only shift of mass range and give no influence on the operation as a mass spectrometer.

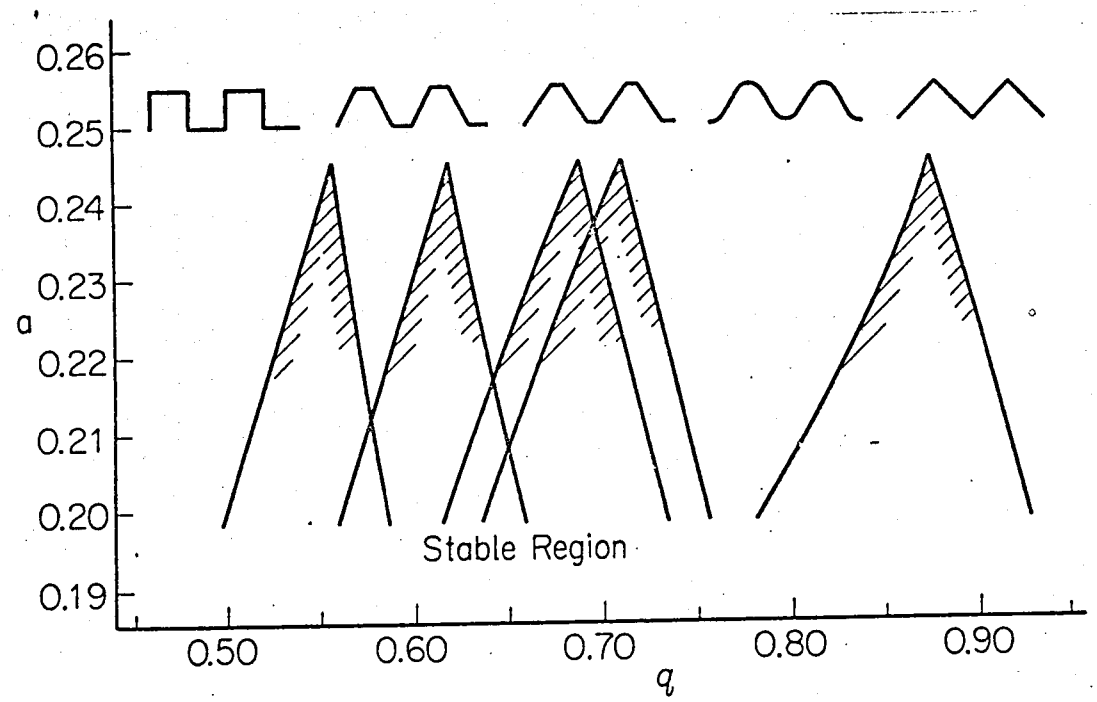

Figure 2.15 Stability diagram for various shape of periodic magnetic field.

Thus, there is no necessity of serious consideration of the shape or arrangement of magnetic poles.

2.7 Prototype (115), (118), (119)

According to the result of previous sections, a first prototype of a sensor of the mass spectrometer was constructed as shown in Figure 2.16. Though mechanical precision and accuracy of magnetic field were not necessarily satisfactory, experiments showed the evidences that the sensor worked as a mass spectrometer.

Then, second prototype production which is schematically shown in Figure 2.17 was done with special emphasis on mechanical precision of magnetic poles, electrodes and their fabrication and accurate magnetization of the poles.

Figure 2.18 shows a set of quadrant magnetic poles. The accuracy of magnetization of the poles are defined by fluctuation of the magnetic field at the center of adjacent two poles as ± 2.5 % of the provided magnetic field.

Figure 2.16 Photograph of primary prototype of the mass spectrometer.

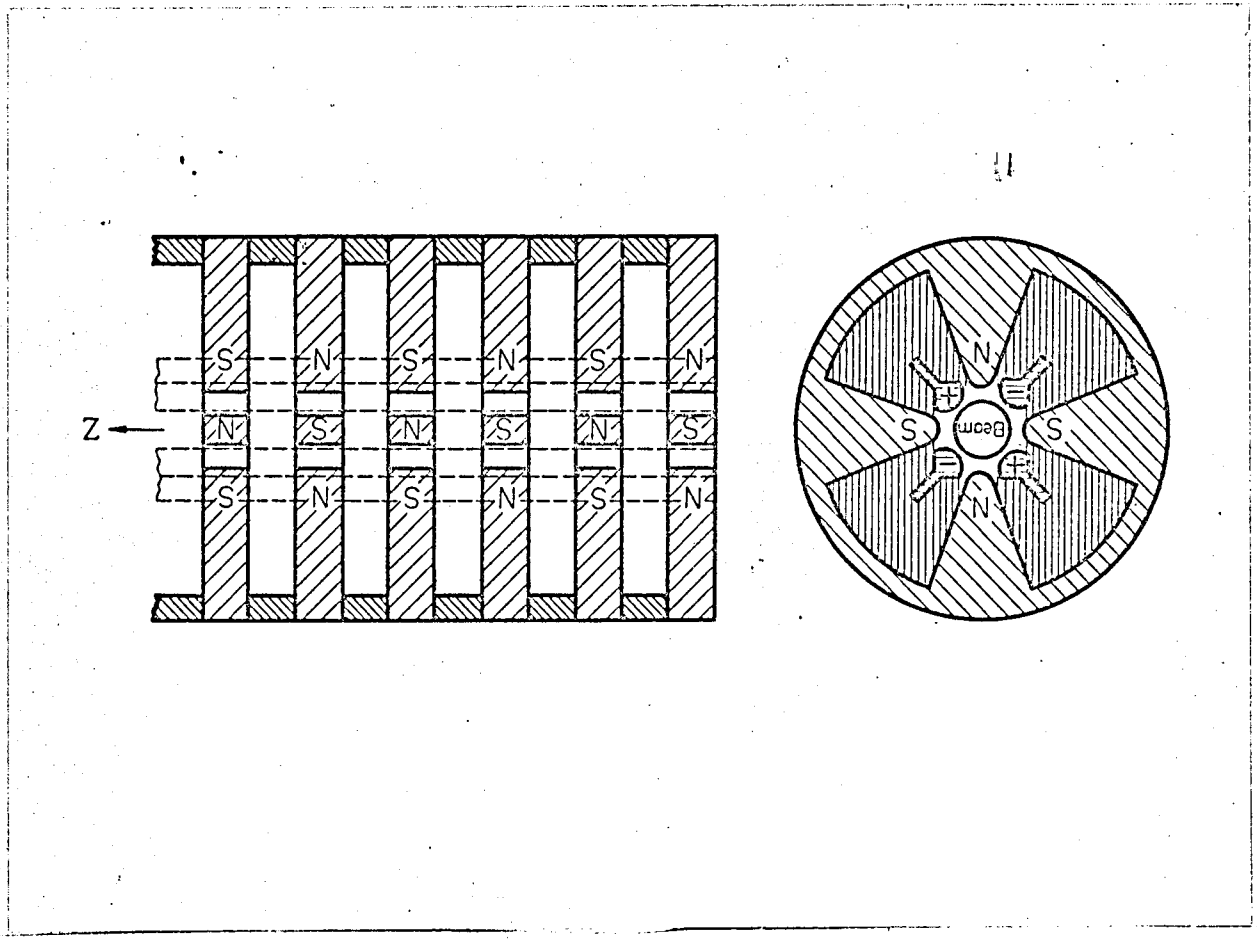

Figure 2.17 Diagram of secondary prototype.

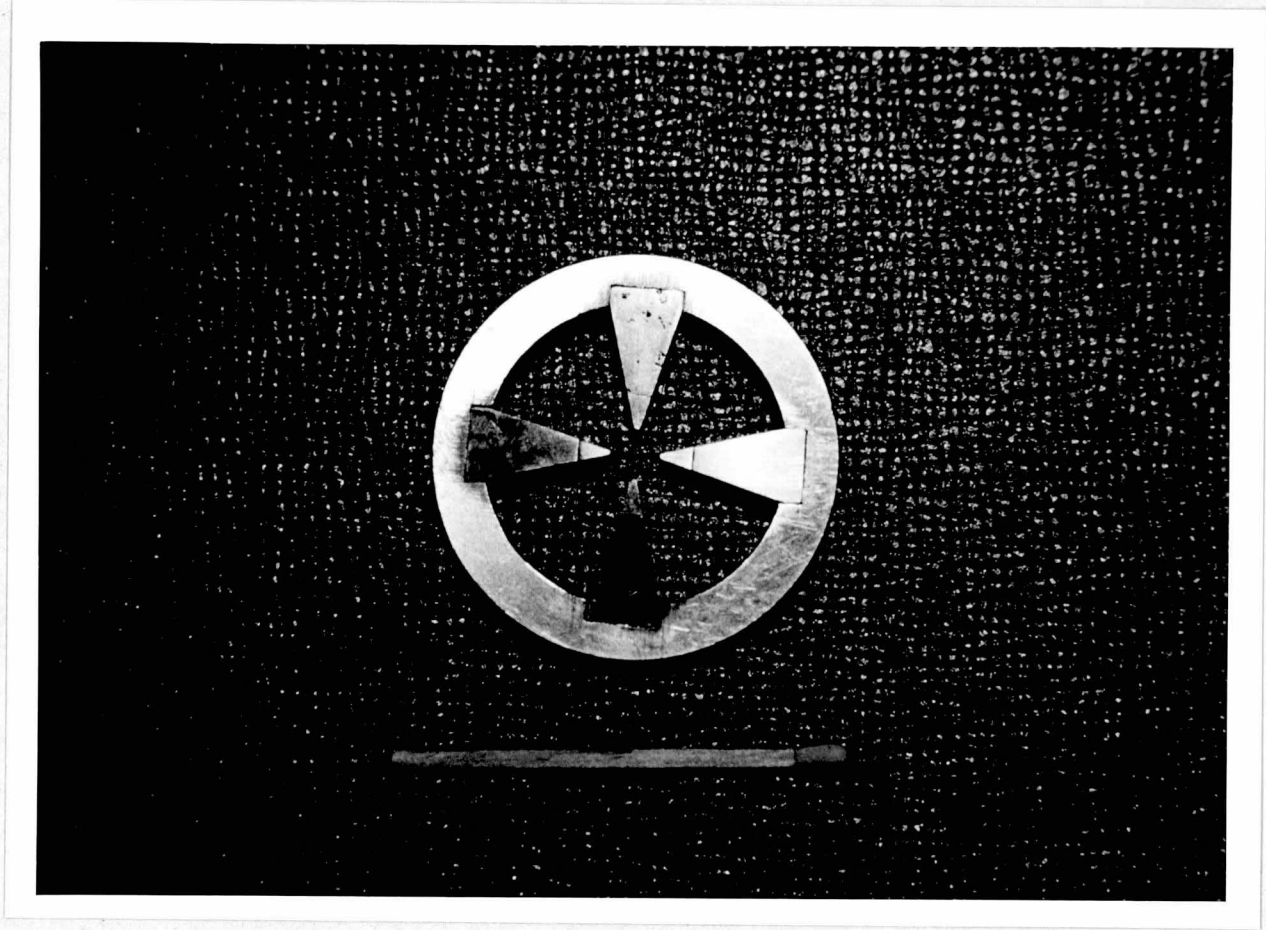

Figure 2.18 Set of quadrant magnetic poles of secondary prototype.

The electrodes shown in Figure 2.19, the cross section of which is the shape of a leaf of maidenhair tree, are supported between each adjacent two poles.

The fabricated mass spectrometer of second prototype is shown in Figure 2.20. This is the final form and the sensor used for flight experiment was basically the same as this, though the insulating material was different.

2.8 Experiment (115), (119)

Laboratory experiments have been done with the sensor of secondary prototype model. Figure 2.21 shows two spectra which were gotten in the space chamber of the Institute of Space and Aeronautical Science, University of Tokyo. The view in the chamber of the experiment is shown in Figure 2.22. The spectrum of (a) was gotten in hydrogen molecule atmosphere of 10^{-5} Torr and by special type of back diffusion plasma source. The spectrum of (b) was in the case that helium gas was introduced and the other condition and operational parameter was the same as those of spectrum

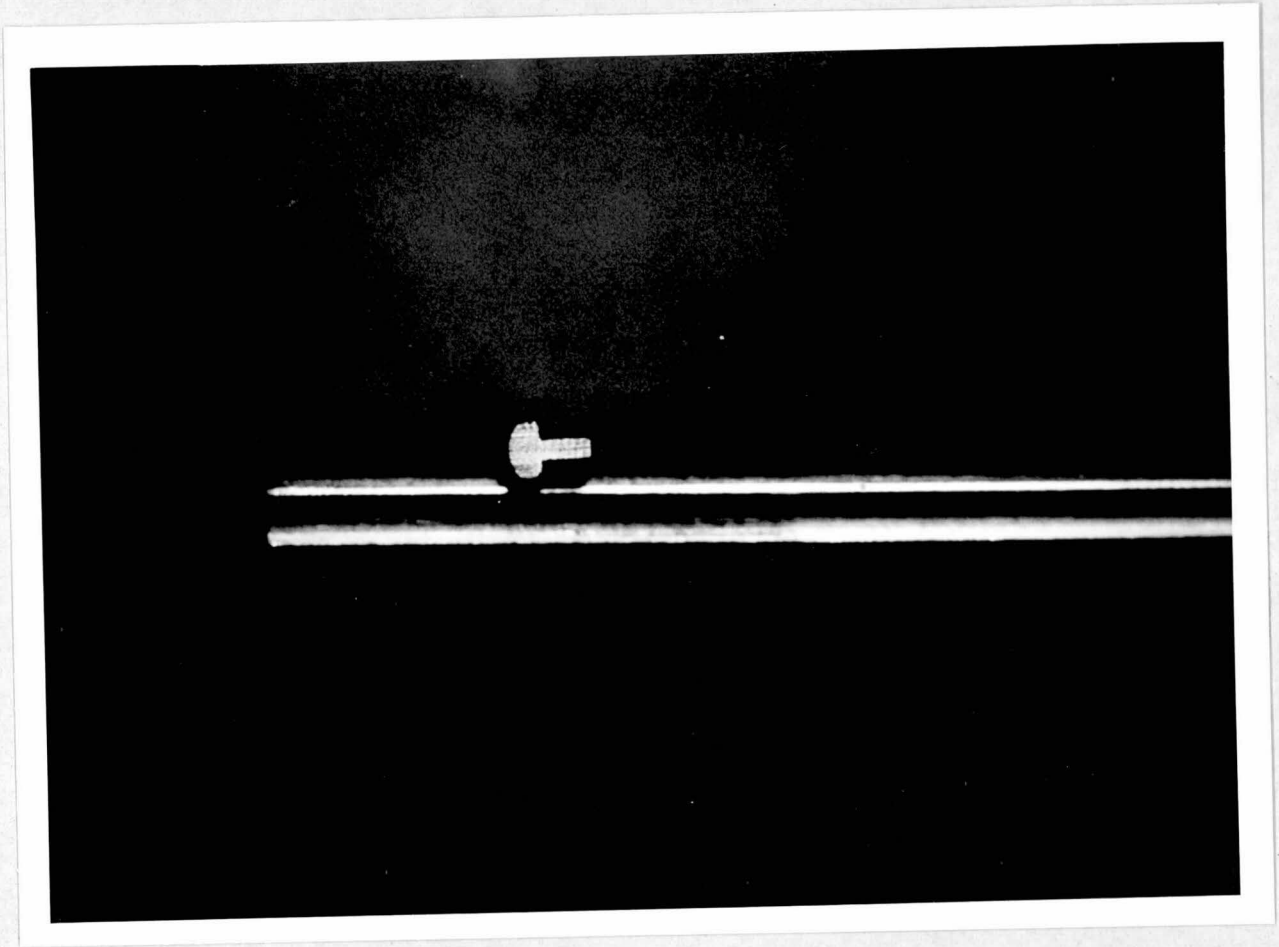

Figure 2.19 Electrode of secondary prototype.

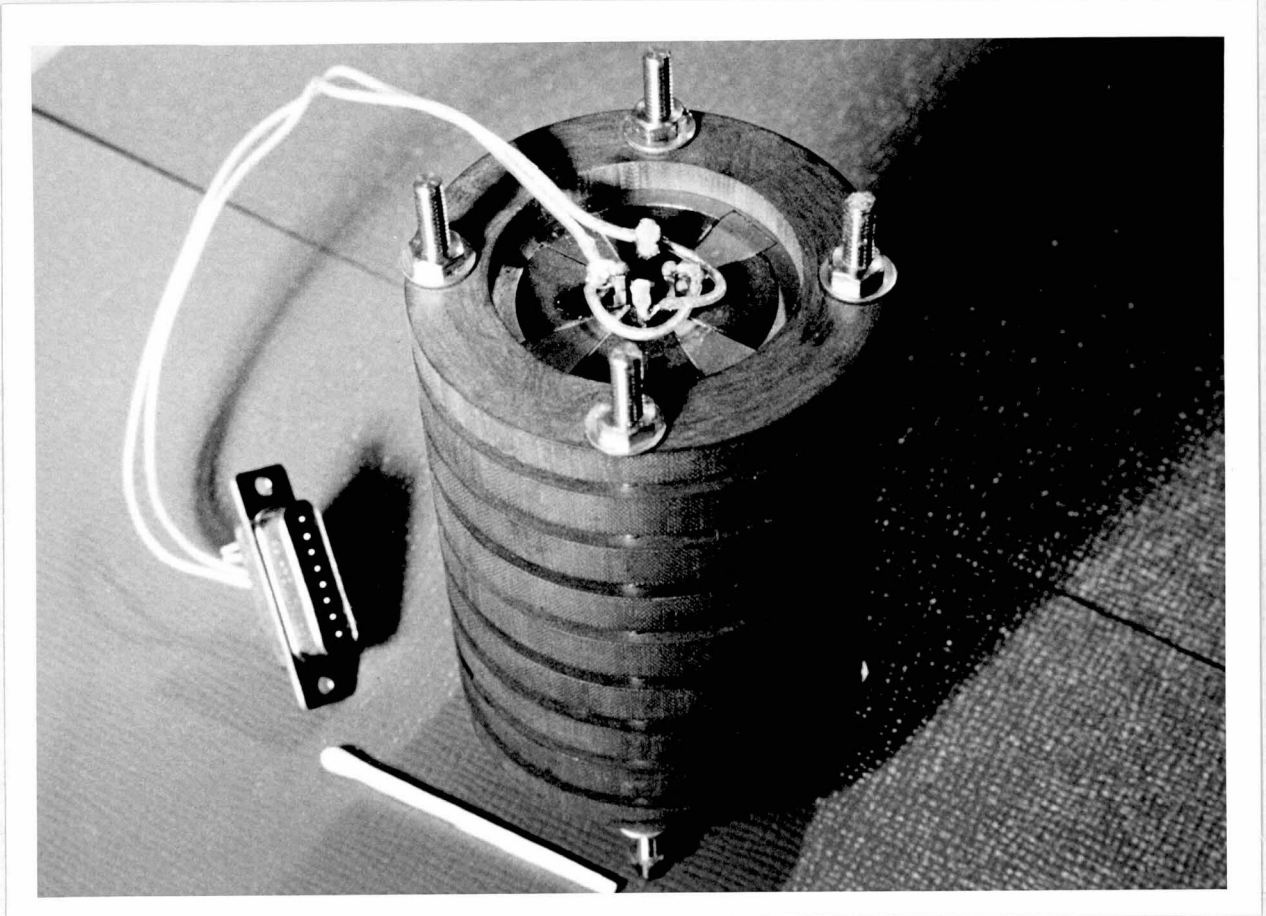

Figure 2.20 Photograph of set up of secondary prototype of the mass spectrometer.

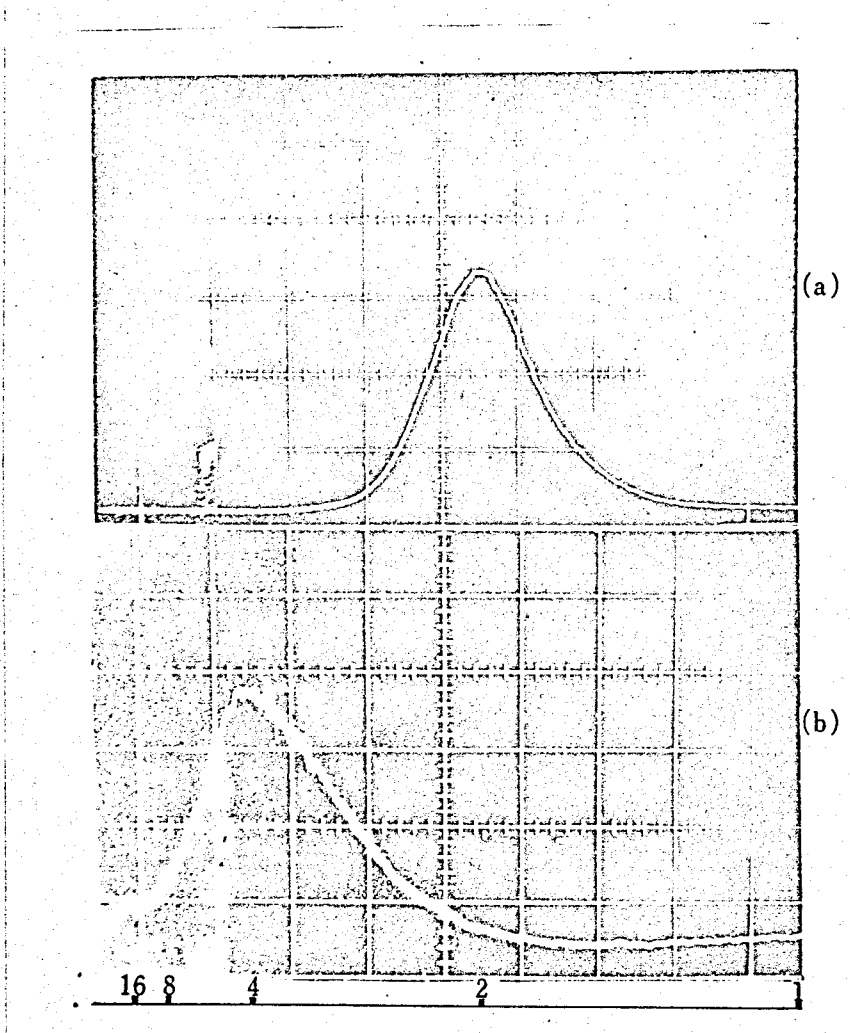

Figure 2.21 Mass spectra gotten in space simulation chamber of H_2^+ ion (a) and He^+ ion (b).

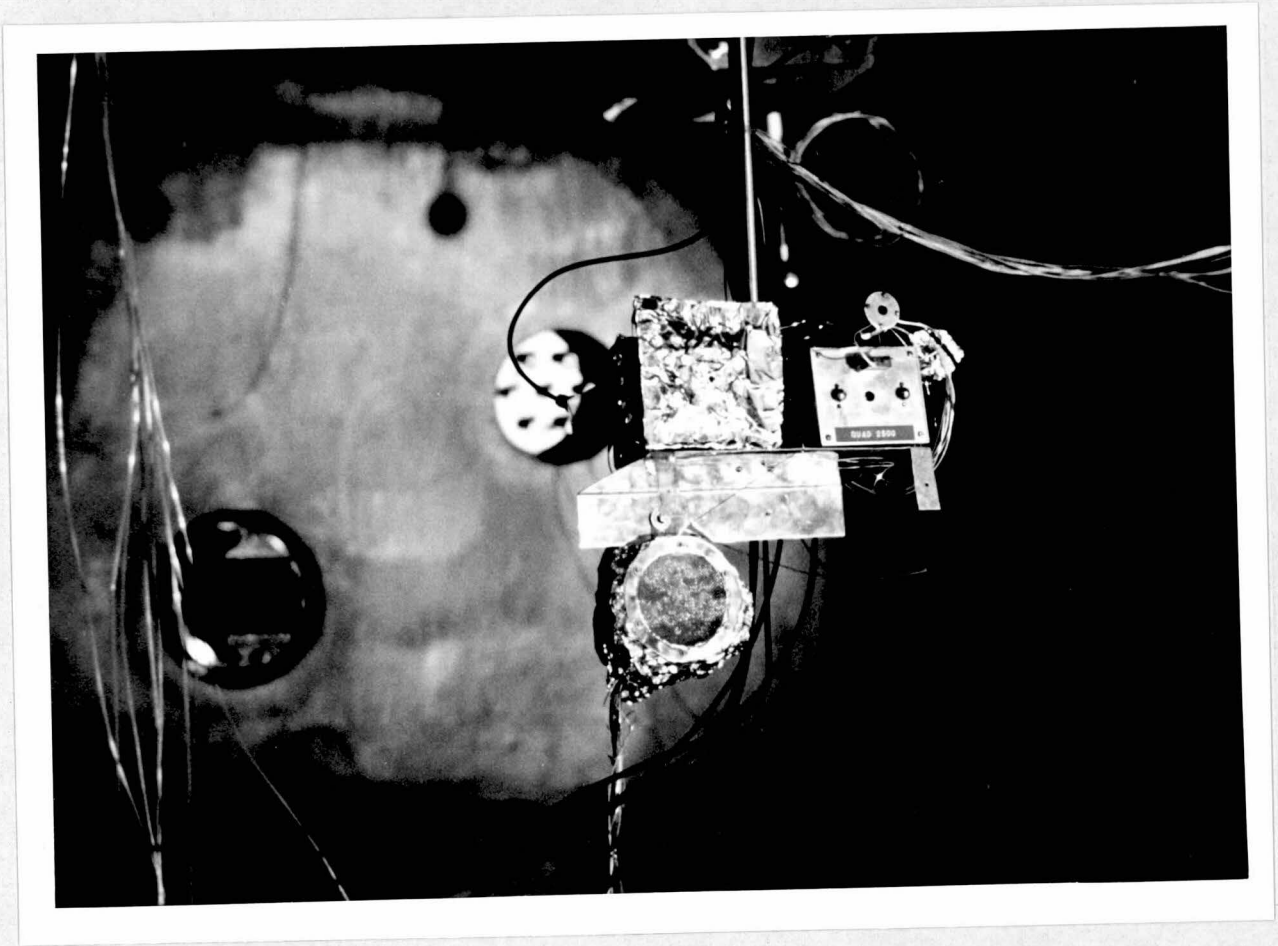

Figure 2.22 Photograph in the space simulation chamber under the experiment of Figure 1.21.

of (a). These spectra were got under the condition that the resolution was set its minimum value, because the inadequate dimension of the orifice of the mass spectrometer caused the split of ion spectrum at high resolution.

Figure 2.23 shows the mass spectra for hydrogen molecule ion and helium ion which were got in the calibration system described in detail later. The resolution of the sensor was set at maximum value and the results of Figure 2.23 were satisfactory for our purpose.

2.9 Discussion

The purpose of development of this type mass spectrometer was that it had the merits of static mass spectrometer such as small power consumption, simple electronic circuit and stable operation, and that it was able to vary electronically its operational mode such as resolution or sensitivity at the sensor stage.

It can be said that the configuration of this type of mass spectrometer achieves these purpose

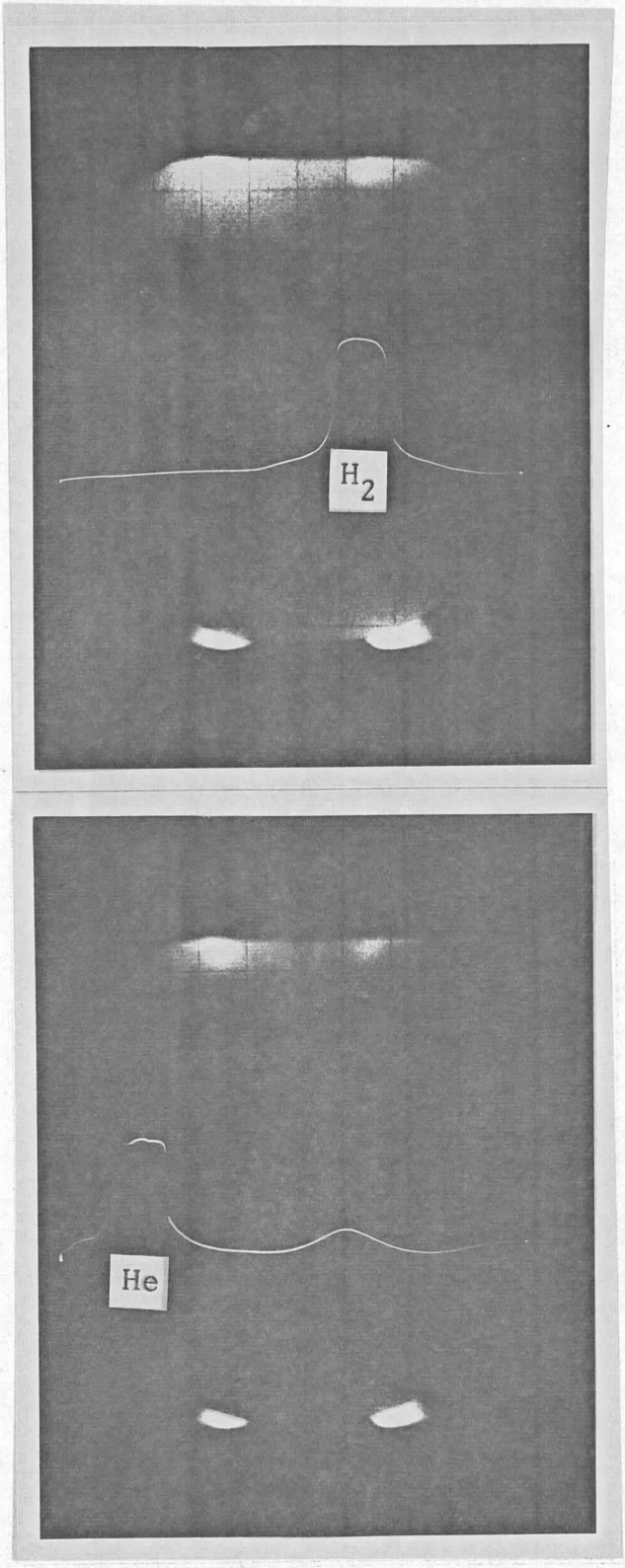

Figure 2.23 Mass spectra of higher resolution.

satisfactorily. The power consumption and electronic circuit ~~is~~ are the same as that of magnetic sector type of mass spectrometer and consequently, its stability is also the same condition.

On the other hand, the resolution is changeable by only varying potential V_o on the electrodes which is given by dividing accelerating potential V_A, because their ratio is proportional to parameter a.

The sensitivity is not so affected by varying the resolution as expected below to the critical value of V_o.

The dimensions of the sensor are about 5 cm in diameter, 8 cm in length which is the case of 4 stage and about 1 kg in weight including magnetic shielding.

The transparency, namely, sensitivity is rather good than expected and the extra-ordinal mass discrimination is not observed by the Bennett type mass spectrometer.

Achievement of the mechanical precision and accurate magnetization is the most difficult thing and shortcomings of the type of mass spectrometer.

As easily seen from its configuration, the leakage flux of magnetic poles is essentially small because the magnetic field is concentrated at the end of quadrupole.

Consequently, though the excellency of this type of

mass spectrometer in laboratory is still indistinct because of containing unknown quantities, many merits are expected in the utilization in space in spite of a few difficulties.

CHAPTER 3

PROBLEMS ACCOMPANIED WITH EXPERIMENTS ON SPACE VEHICLE AND ITS CALIBRATIONS

3.1 Introduction

Mass spectrometry in the upper-atmosphere to measure its composition is the most direct measurement, that is, it selects one by one the analyzed particle. Though it is expected to accomplish precise measurement, there are still many problems that various errors are contained in results of measurement because the space vehicle installing instruments invades into objects of the measurement and runs with high speed in it. These problems composed many scientific and engineering ones.

As a method to solve them, it is the best way to remove the origins of these troubles. It is, however, usually difficult and a counterplan of one problem may cause another trouble.

It is also important to comprehend the substances of the phenomena and to make a detail calibration for the measured value, so as to make the precise measurement possible inspite of existence of these troubles.

It is very interesting to learn the various phenomena which are arisen by the invasion and high speed running of space vehicle in the upper-atmospheric plasma. Many works have done about them. The purpose of this

chapter is not to investigate in detail about them, but to review clearly their physical meaning and to understand the degree of importance of them on results of the measurement. Based on the full understanding of these problems, appropriate methods and systems will be established to calibrate instruments and data.

3.2 Effects originated by Invasion and High Speed Flight of Space Vehicle

3.2.1 Effects of Aerodynamics (57)

In the case of high speed motion in the atmosphere, aerodynamic effects are important not only in flight trajectory but in mechanical vibration or heating on flight body. In our purpose, however, they should be grasped as another problem especially in high altitude, that is in the altitude range in which collision of atmospheric particle is rare, for instance in the altitude range of diffusive equilibrium condition.

Still important problems they are in lower range than that. It is well known that impingement of a mass

of gas into stationary gas generates plasma. In the lower ionosphere, it is naturally considerable that flight body or its shock wave gives some changes to the ambient atmospheric composition and errors to results of the measurement.

For example, it is expected that hydrated proton ions, $H^+(H_2O)_n$ which are supposed to exist in a large amount in the lower ionosphere, are subjected to dissociation and measured as hydrated proton ions of smaller molecular weight or some other species. Similar effects are expected in measurement of negative ions in the lower ionosphere.

For calibration of the effects, plasma wind tunnel should be used but detail calibration will be very difficult.

3.2.2 Ram Effect (122)~(125), (134)

Although problems on measurement of the upper-atmospheric particles on the space vehicle running with high speed are essentially the subject of mutual relationship among the vehicle and various particles in the upper-atmospheric plasma, we can only detect about

them or their effects with various influences which arise on the measured data from them.

Considering from the view point of measurement of the upper-atmospheric parameter, these effects give us the results which are different from real state of the space. Calibrations for errors of the data are finally necessary.

Velocity of a satellite is about $7 \sim 8 \times 10^3$ m/sec, though it depends on the orbit of a satellite and that of sounding rocket is rather small. As an example, parameters of Japanese sounding rocket are shown in Table 3.1.

On the other hand, the most probable velocity V_m of a particle is given as :

$$V_m = \sqrt{\frac{2\,k\,T}{m}} \qquad (3.1)$$

where m : mass of the particle,

T : temperature of the particle,

k : Boltzmann constant.

When temperature of the upper-atmosphere is 1500 °K, the velocity of the particles is roughly estimated as

electron : 2×10^5 m/sec

H : 5×10^3 "

Name	Diameter (mm)	Payload weight (kg)	Max. velocity (m/sec)	Max. altitude (km)	Flight time (sec)	Launch. angle (deg.)
MT-135	137	2	136	50	217	75
S -160	160	5	1516	80	279	78
S -210	210	12	1716	120	328	75
S -300	314	39	1930	170	398	76
S -350	364	48	2104	216	453	76
K-8L(2nd)	166	22	1770	145	371	80
K-8 (2nd)	250	70	1805	182	422	80
K-9M(2nd)	255	33	2435	327	565	80
K-10(2nd)	420	132	2073	237	486	78
L-3H(2nd)	767	137	2596	377	661	78
L-3H(3rd)	548	80	5397	1995	1790	78
L-4S	for satellite					
M-4S	for satellite					

Table 3.1 List of Japanese sounding rockets.

O : 1.2×10^3 m/sec

NO : 9×10^2 "

The velocity of particles V_p except for electron is smaller than vehicle velocity V_v , though that of electron is larger enough than V_v .

As shown schematically in Figure 3.1, therefore, the component of ion velocity of the direction of sensor axis at the orifice of sensor of mass spectrometer V_i is

$$V_i = V_v \cos\theta + V_p \cos\alpha \qquad (3.2)$$

where α : angle between direction of ion velocity and axis of sensor,

θ : angle between ram direction of the vehicle and axis of sensor namely, attack angle.

It is apparent that V_i varies with V_v and θ , when $V_v \gg V_p$. And in wake side of the space vehicle, such a phenomenon happens that ions can not arrive to the vehicle. Namely, ions can not enter the region of wake shown in Figure 3.2, after ions swept out with the vehicle, where $\tan\varphi = V_v / V_m$.

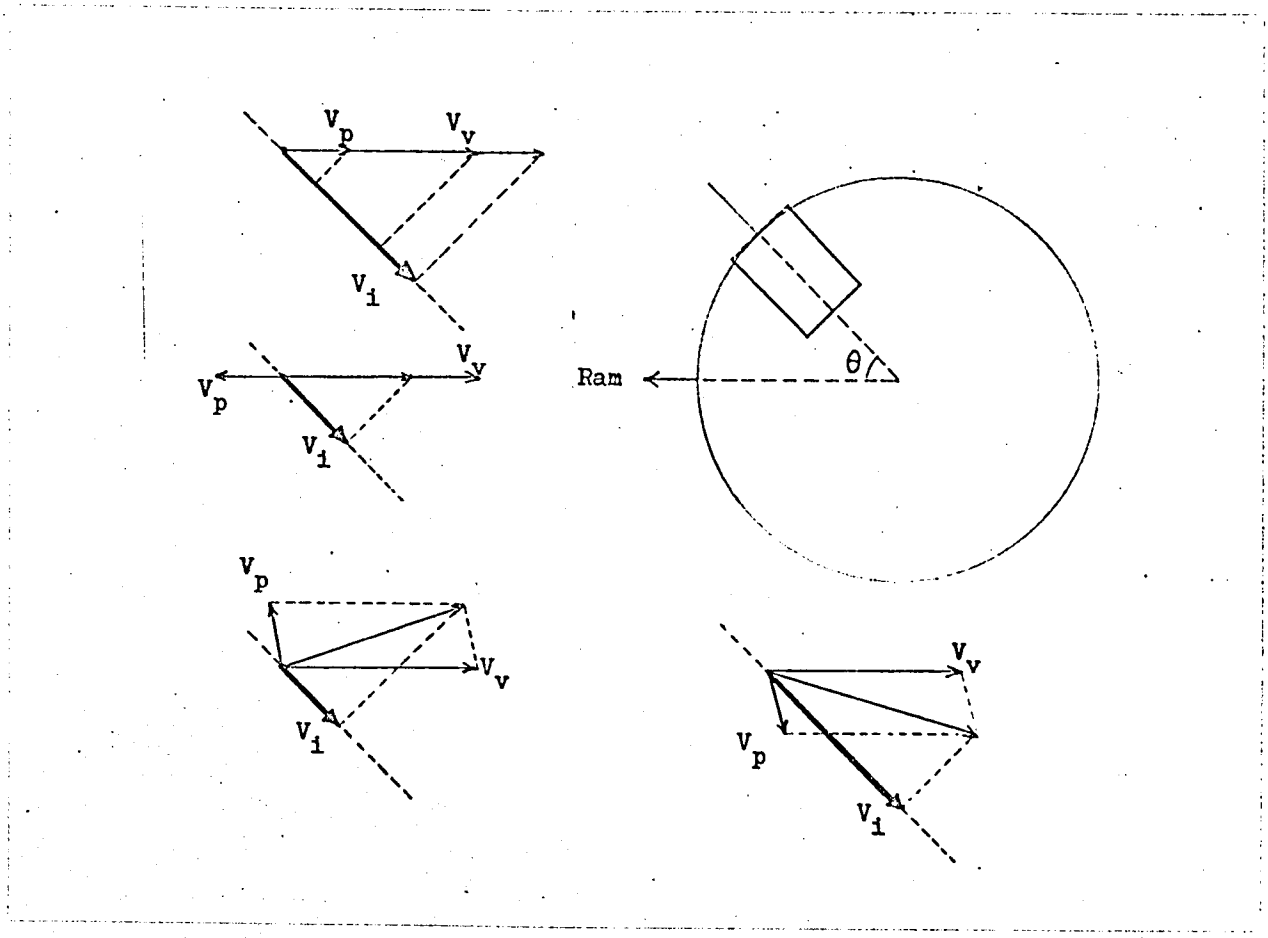

Figure 3.1 Schematic illustration of ram effect.

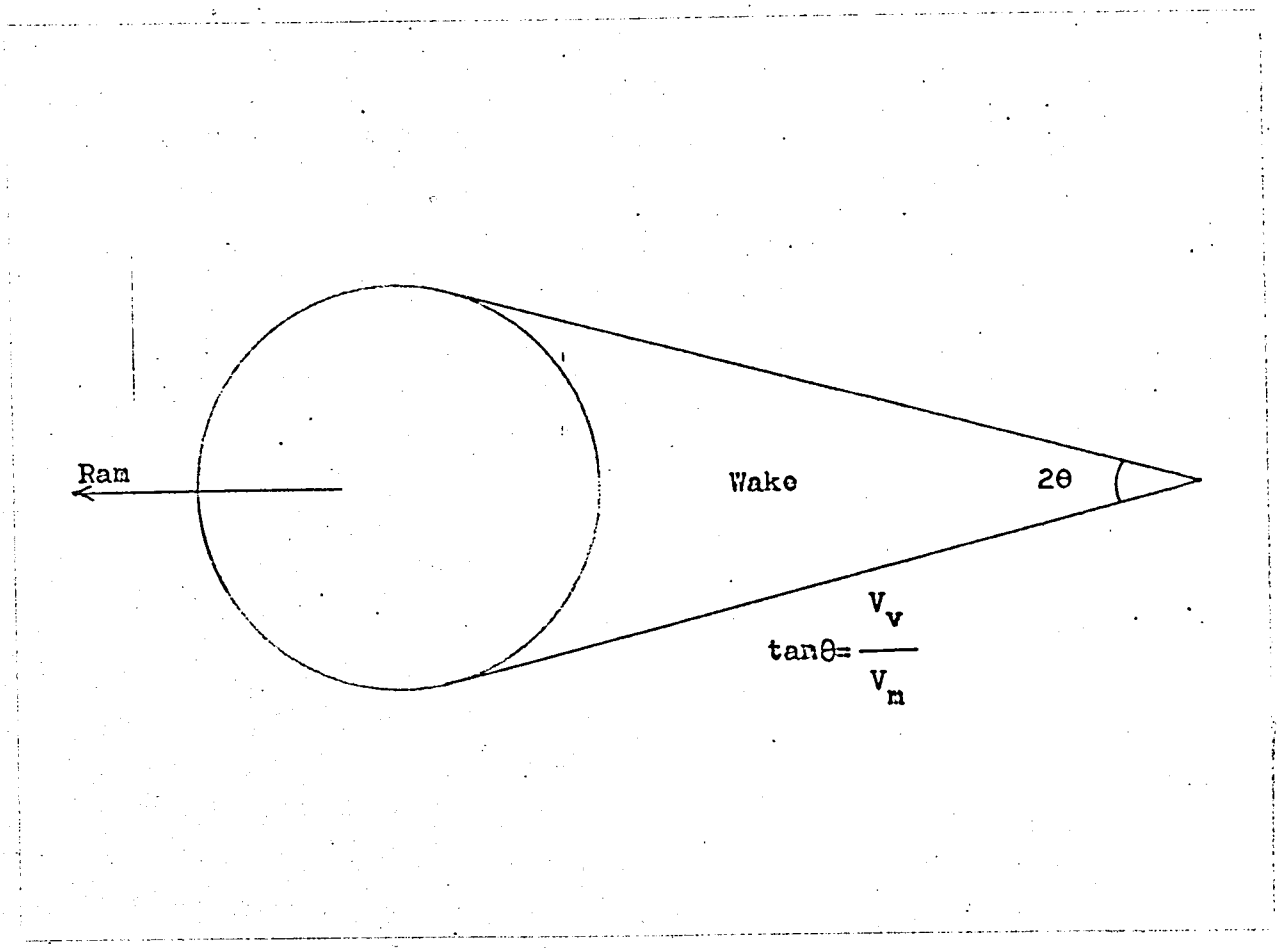

Figure 3.2 Region of wake of space vehicle.

3.2.3 Pressure Effect (122)∼(125), (134)

As described previously, because the vehicle velocity is rather larger than the thermal velocity of particles except for electron, particles are bunched in front of the vehicle and depleted behind it, as if tadpoles are swept away with ladle, as shown in Figure 3.3.

The equation which explains conceptually the pressure at a front of vehicle, P, may be represented on the ram vector as :

$$P = k \sum n T + 2 V_V^2 \sum n m \qquad (3.3)$$

where n : number densities of the particles.
The second term becomes larger than first term which expresses the pressure on a body at rest, when V_V is larger than thermal velocity of particles. The force which gives drag to a satellite is out of the serious question for direct measurement because of small density of particles, though it is the direct force.

It is rather important that ion current which is collected through an orifice of a mass spectrometer by a motion of space vehicle with high speed and may be

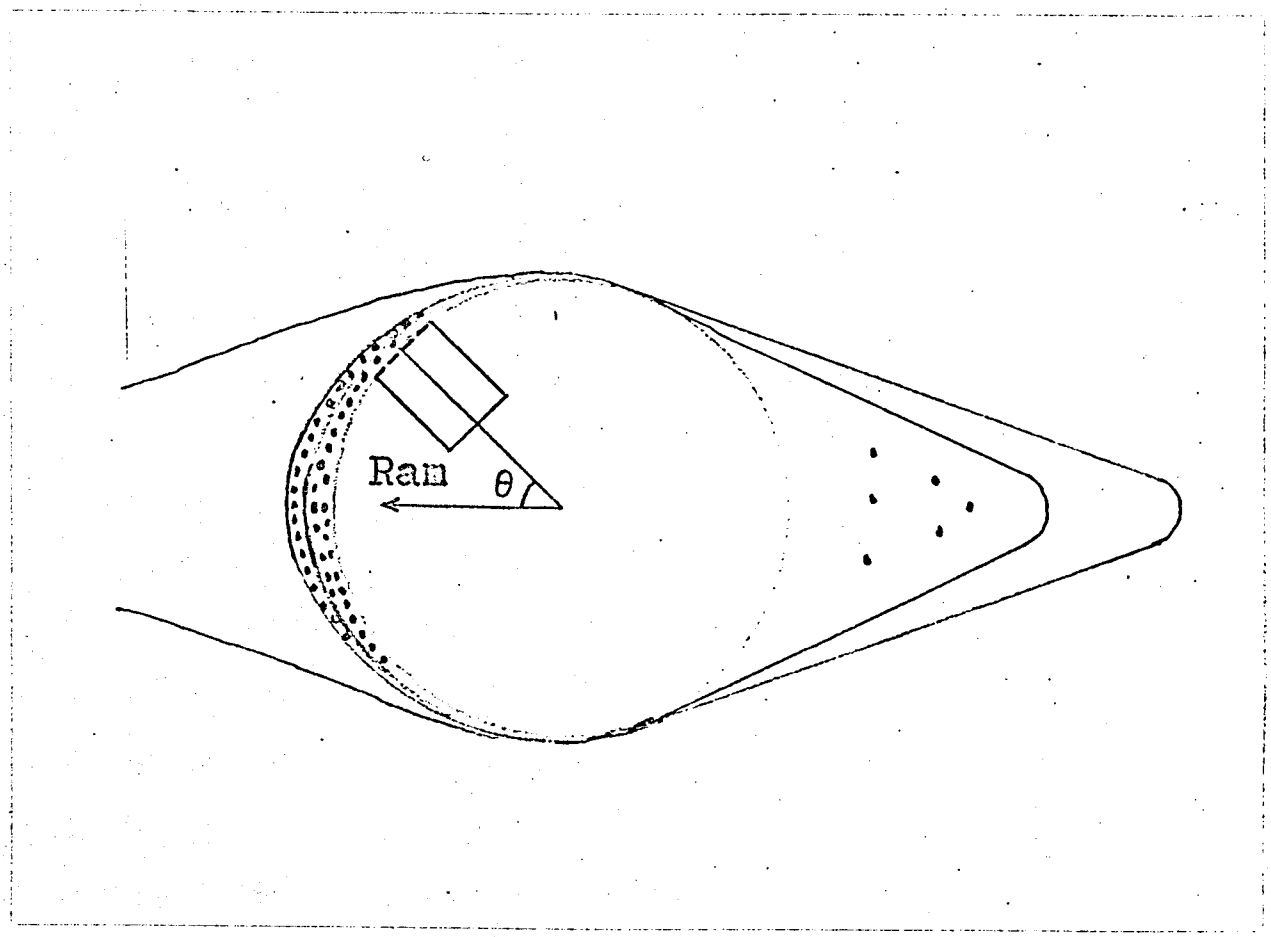

Figure 3.3 Schematic illustration of prassure effect.

expressed simply as

$$i_r = e\, n\, A\, V_v \cos\theta \qquad (3.4)$$

where A : area of orifice of mass spectrometer,
is larger than the ion current which flows into surface of body at rest in the upper-atmospheric plasma. The problem concerning the ion current will be mentioned in following subsection.

3.2.4 Potential and Field Effect (122)~(125), (133)~(135)

When a body is placed at rest in the upper-atmospheric plasma, electron and ion currents flow from plasma to the body. The body will acquire a net negative charge or negative equilibrium potential due to the large thermal velocity of the electrons compared to the thermal velocity of the ions. The electron current to the body is produced only by those electrons which are energetic enough to overcome the equilibrium potential. At equilibrium, the total current to the body is zero with the electron current balanced by the positive ion current.

Due to the small thermal velocity of the ions, the

region surrounding the body depletes electrons as shown in Figure 3.4. It will have a net positive charge and is called as an ion sheath.

Since at equilibrium the total current to a body immersed in a neutral plasma is zero, a negative potential must exist on the body which is represented for simplified situation as :

$$\phi = \frac{k\,T_-}{2\,e} \ln \frac{T_-\,M_+}{T_+\,M_-} \qquad (3.5)$$

where T_- : electron temperature,

T_+ : ion temperature,

M_- : mass of electron,

M_+ : mass of ion.

However, it differs from actual condition. As a space vehicle runs in plasma with high velocity, different treatment should be necessary between front and rear of a vehicle, ion and electron, different size or shape of vehicle and so on.

Photo-emission by intense solar radiation can not be neglected. Besides these, many factors which give influences on the potential of a space vehicle and consequently cause changes of the sensitivity of measurements, should be considered, such as a secondary

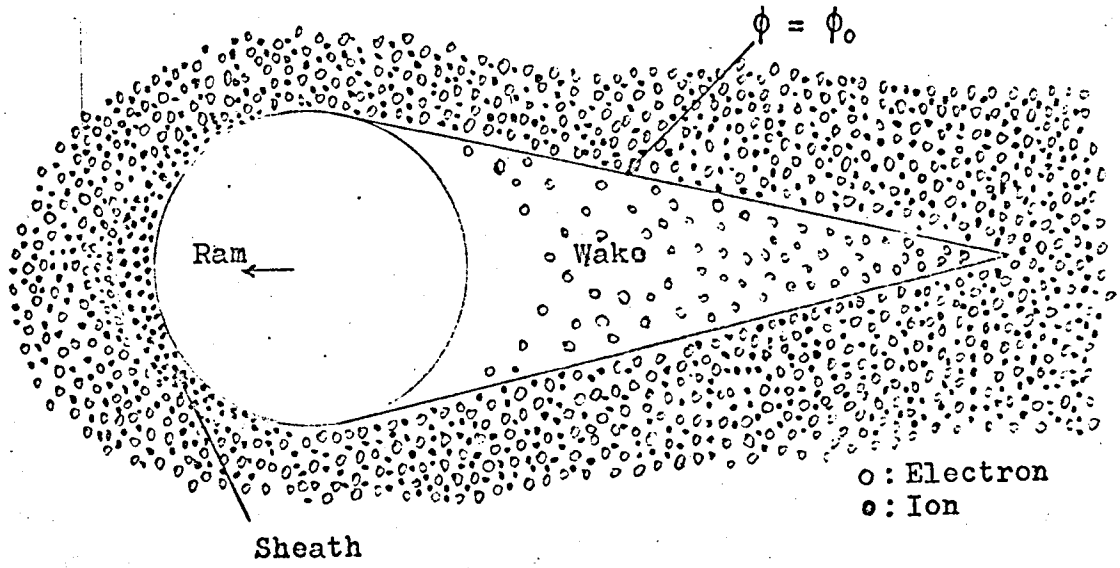

Figure 3.4 Schematic illustration of circumstance of charged particle around a space vehicle.

emission from the surface of the vehicle due to the cosmic ray bombardment, surface temperature of the vehicle, radio emission from antenna of the vehicle and so on.

In the case of the moving body, potential on a space vehicle also should reach to an equilibrium. When the total current to the body is zero.

$$I_- + I_+ + I_m = 0 \qquad (3.6)$$

where I_- : electron current,

I_+ : ion current,

I_m : miscellaneous current.

These currents are respectively given following a theory of plasma physics and condition of the upper-atmosphere, sun, vehicle and so on. Both of I_- and I_+ must be dealt differently according to the sign of charge of vehicle. In calculation of I_+, the velocity of vehicle must be regarded. As for I_-, it can be disregarded when a size of the vehicle is small enough.

When the velocity and size of space vehicle are large and region of wake in which ions can not enter is large as shown in Figure 3.4, the sink of potential in the wake region can not be neglected. In such a case,

special consideration should be paid in estimation of I_-, because electrons which can enter to the wake region are limitted to high energetic electrons enough to overcome the potential.

As an example, assuming that the vehicle is a negative charged sphere and small enough to Debye length L,

$$L = \sqrt{\frac{\epsilon_o \, k \, T}{n \, e^2}} \qquad (3.7)$$

currents are represented as :

$$I_- = \frac{1}{2}\sqrt{\pi} n_- e r^2 V_{m-} \exp.(\phi e / kT_-) \qquad (3.8)$$

$$I_+ = \sqrt{\pi} n_+ e r^2 V_{m+} \left[\frac{\sqrt{\pi} V_{m+}}{V_v} \mathrm{erf}\left(\frac{V_v}{V_{m+}}\right)\left(\frac{\phi e}{kT_+} + \frac{V_v^2}{V_{m+}^2} + \frac{1}{2}\right) + \exp.\left\{-\left(\frac{V_v}{V_{m+}}\right)^2\right\}\right] \qquad (3.9)$$

where

$$\mathrm{erf}(x) = \frac{2}{\sqrt{\pi}} \int_0^x \exp.(-y^2)\,dy \qquad (3.10)$$

$$y = \sqrt{\frac{2 \, e \phi}{m+}} \qquad (3.11)$$

r : radius of vehicle,

n_- : electron density,

n_+ : ion density.

Providing $I_m = 0$, the relation between the normalized potential of vehicle versus Mach number which is the normalized velocity of vehicle is shown in Figure 3.5.

In the case that the size of vehicle becomes large and the sheath in front of vehicle and negative potential in the wake should be considered in the estimation, the normalized vehicle potential versus Mach number is shown in Figure 3.6. In such a condition as the large photo-emission current from surface of vehicle under intensive solar emission, $I_m \neq 0$ and a vehicle may be charged in positive potential.

Assuming the parameters of the upper-atmosphere in which the vehicle runs, the potential of the vehicle and ion current which flows into an orifice of the mass spectrometer can be estimated.

Further, when an attracting voltage is applied on the orifice of the mass spectrometer, strong fields are generated, and quantity of current into the mass spectrometer will change largely as shown in Figure 3.7.

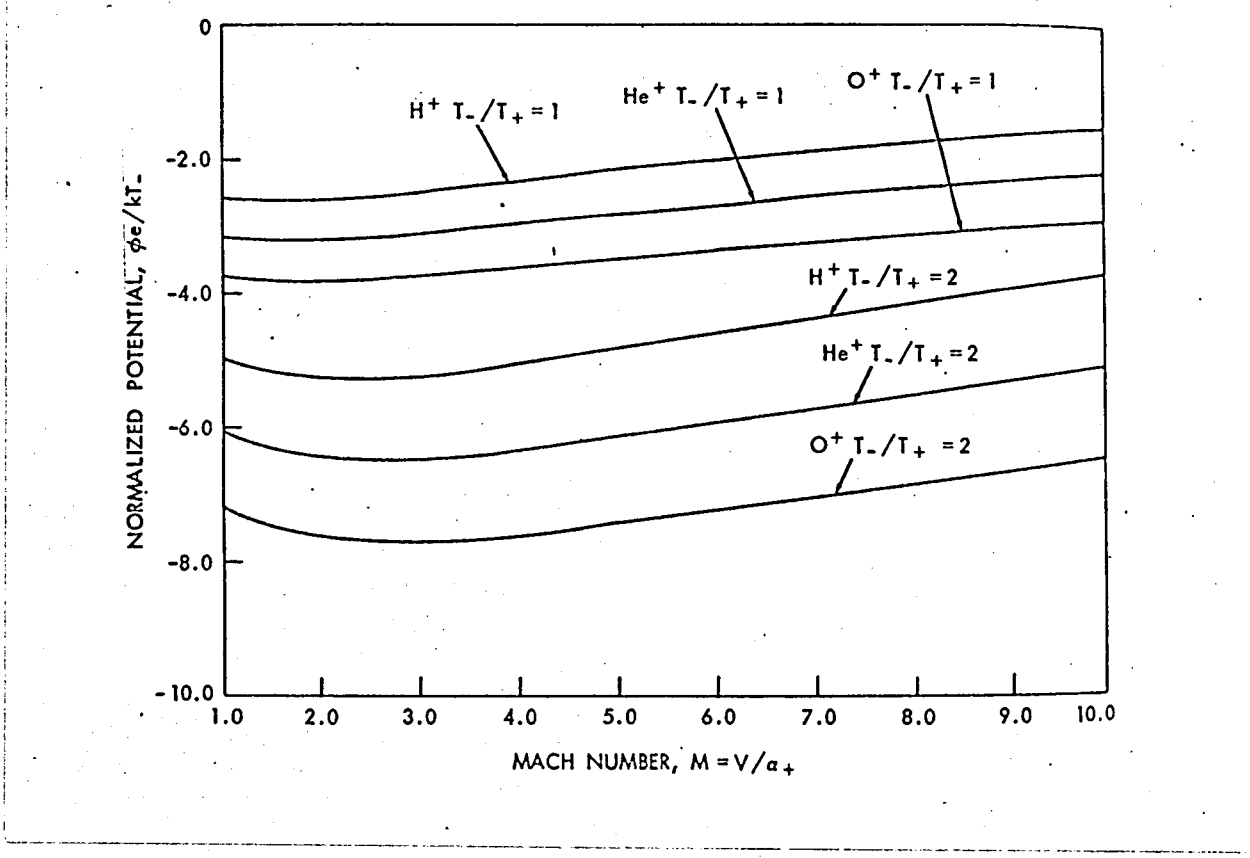

Figure 3.5 Normalized potential of vehicle versus Mach number, assuming the vehicle is negative charged small sphere, where V means V_v and α_+ is V_{m+} . (after Whipple)

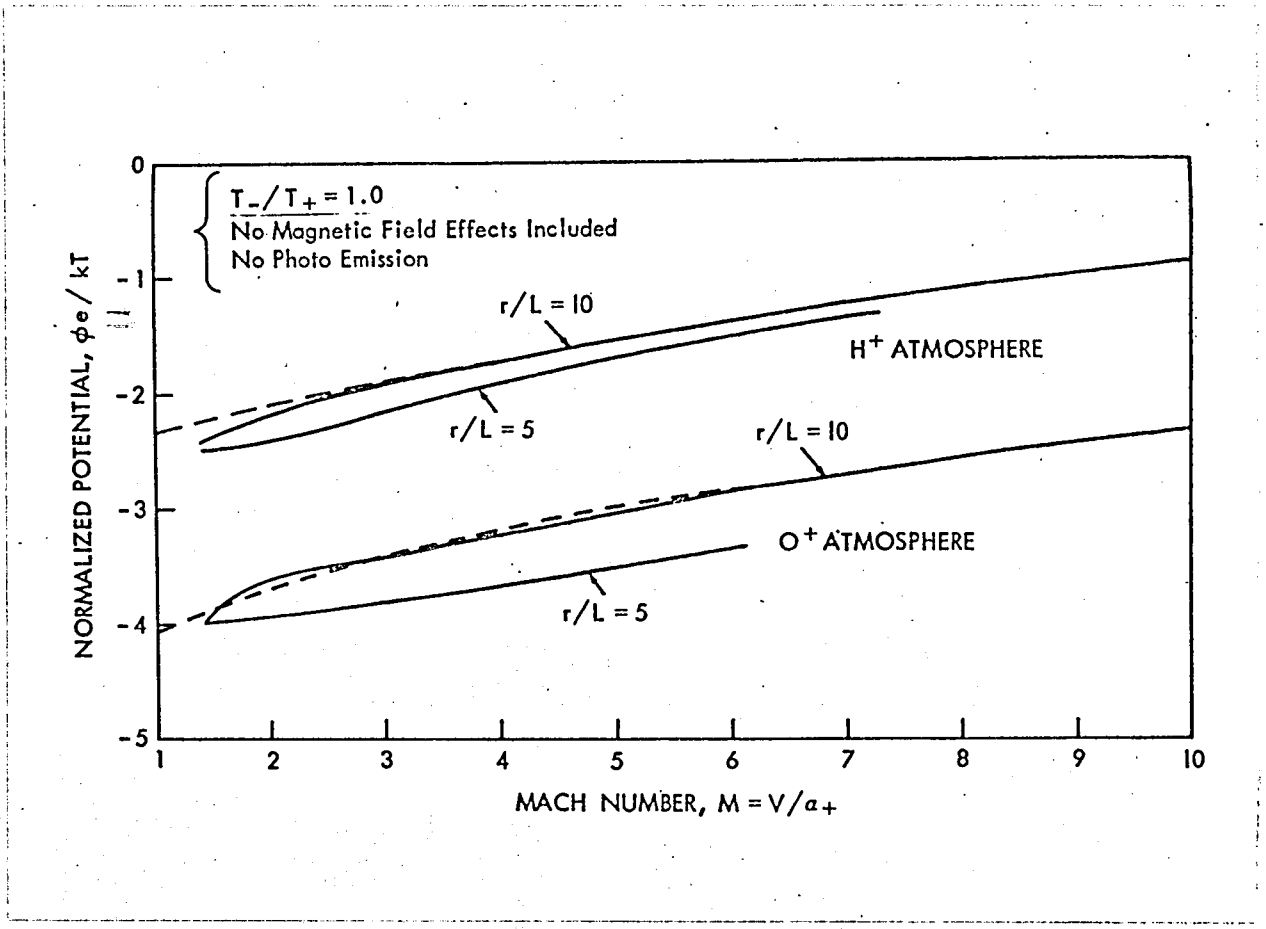

Figure 3.6 Normalized potential of vehicle versus Mach number, when radius of vehicle r is larger than Debye length L, smoothed line and dotted line come from different assumption at the calculation. (after Whipple)

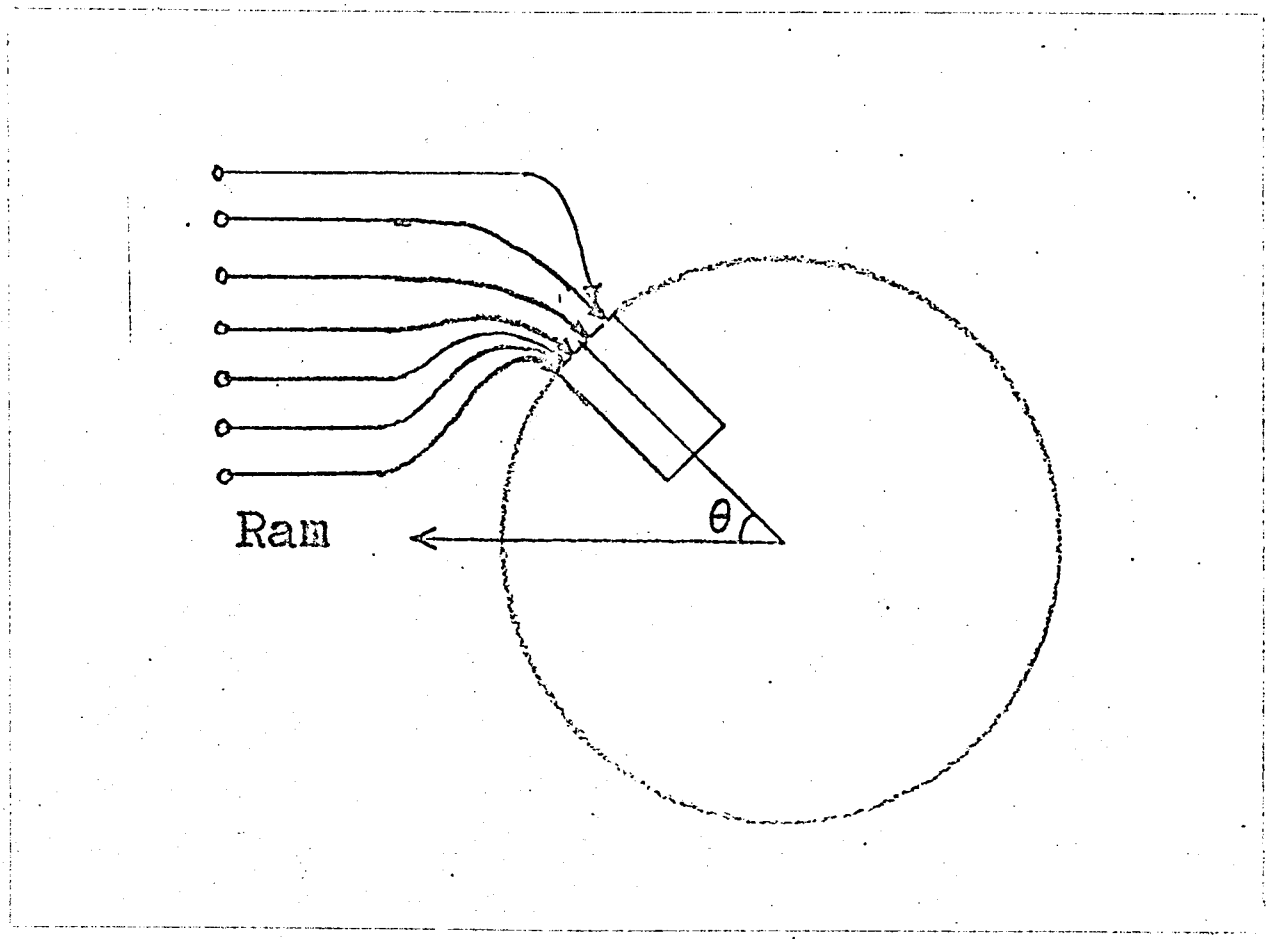

Figure 3.7 Schematic illustration of field effect.

3.2.5 Others

As a space vehicle is composed of various materials, the influences of out-gases which are exhausted from these materials, can not be neglected. The origins of gases are expected as contamination of surface of the instruments, evaporation from organic materials, vapour from embers of rocket motor in special cases and so on.

Among these things, various organic materials might change its quality, sublimate and exhaust a considerable quantity of gases for a long term, as a result of applying of intense solar radiation in vacuum circumstance. The possibility is unable to be disregarded that those materials are detected by mass spectrometer, after dissociating or reacting with some constituents of the upper-atmosphere.

As an attempt to escape from those effects, a satellite which was sealed hermetically in stainless steel container with specially treated surface have tried for a precise measurement of circumstance on the satellite.

On the other hand, some sorts of chemisorption might occur at the surface of special materials of a satellite which is cleaned up by solar radiation and

vacuum as a result of long stay in the upper-atmosphere. In such a condition, an active species around the satellite might be depleted by this reaction.

3.3 Influences Appeared in Data of Measurement

3.3.1 Characteristics of Velocity (122)~(125)

As understood from previous section, it is difficult to deal with characteristics appeared in data modulated by the effect of velocity, attack angle and potential separately. That is, the velocity of a satellite gives influences both on characteristics of attack angle and of potential. Though they are described separately in the following three subsections, their content are not so clearly separated as the subtitles.

As the velocity, with which ions pass through the analysing part, is sum of the velocity by accelerating voltage on grids or slits and the velocity of the space vehicle, the mass spectrometer whose mass range is scanned by accelerating voltage, for example Bennett

type, time of flight type or magnetic sector type, is affected by the velocity of vehicle in its mass range. As a matter of course, the operating condition must be determined as to be able to neglect the influence. However, there is the limit from various technical reasons.

As an example, Figure 3.8 shows calculated result of the energy gain of ions versus the change of ion velocity when the species which should be selected, is hydrogen ion by using the three-stages Bennett type mass spectrometer. Figure 3.9 and Figure 3.10 also show the same situations when the species which should be selected are atomic oxygen ion and nitric oxide ion respectively.

It is apparent from the figures that in the case of heavier ion, a shift of mass scale by a few per-cent change of the velocity gives a possibility of serious mistake in the determination of ion species. Therefore, a careful treatment should be required to the data of direct measurement. They are not serious in sounding rockets, but some adequate steps are need for a satellite especially of excentric orbit.

In the case of the Bennett type mass spectrometer, the retarding voltage which is the most important for

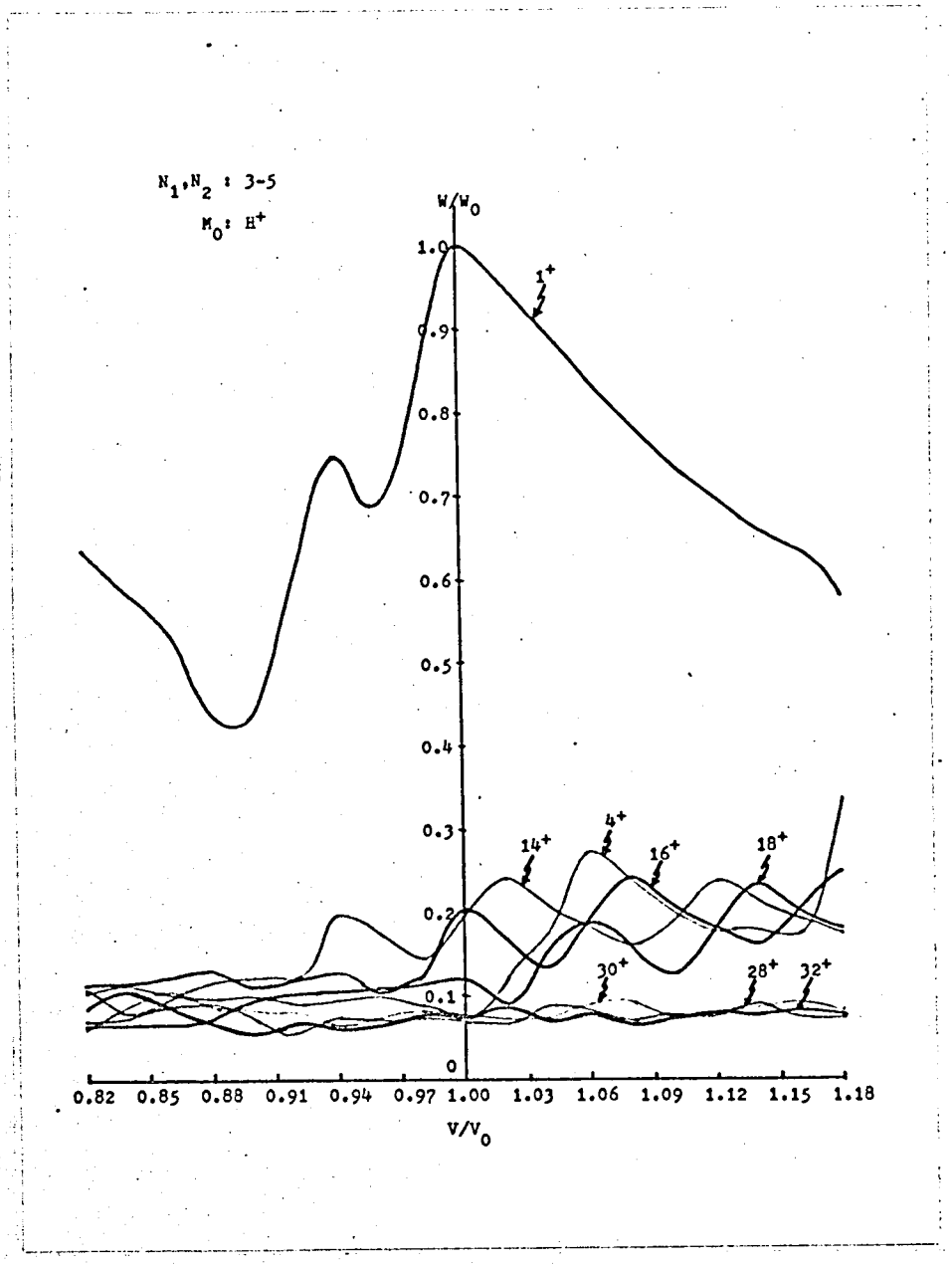

Figure 3.8 Calculated result of energy gain of ions versus the shift of ion velocity for Bennett type mass spectrometer when ion of optimum condition is H^+.

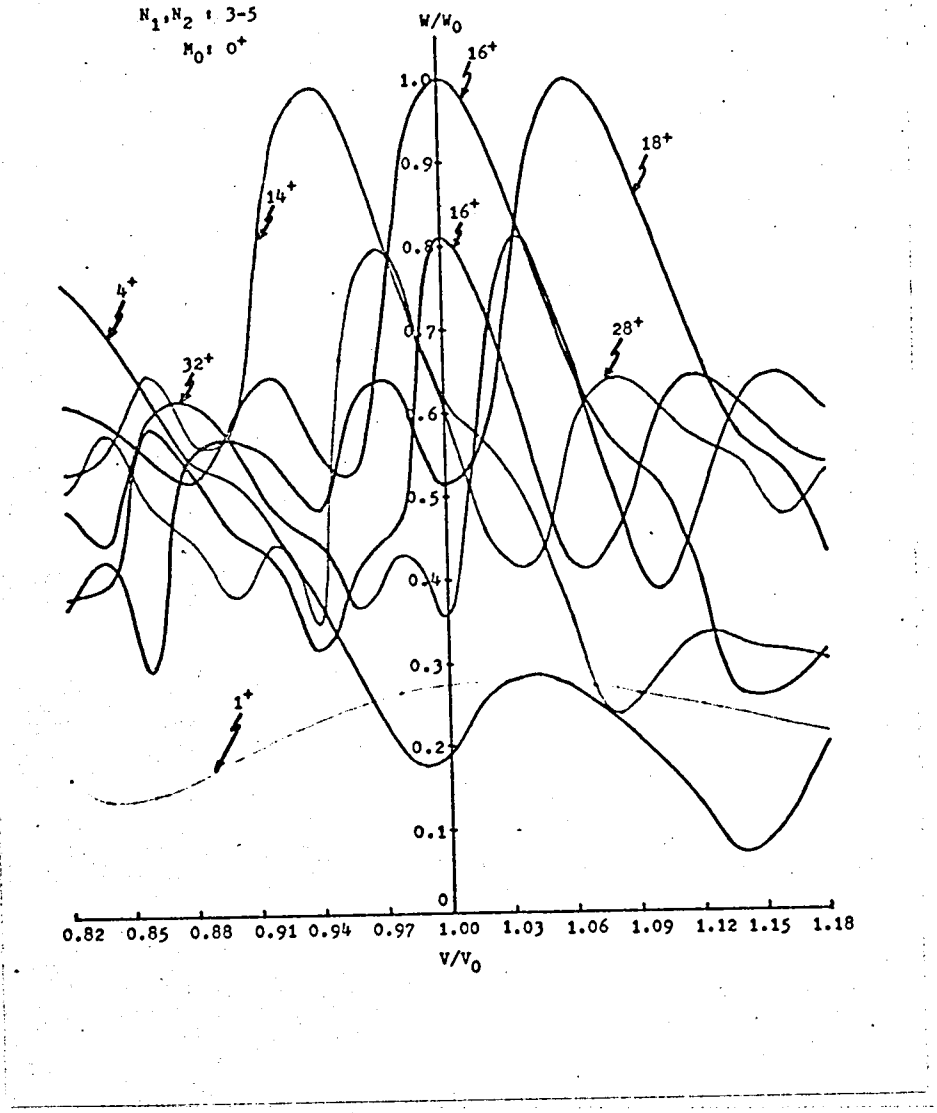

Figure 3.9 Similar result as Figure 3.8, when optimum ion is O^+.

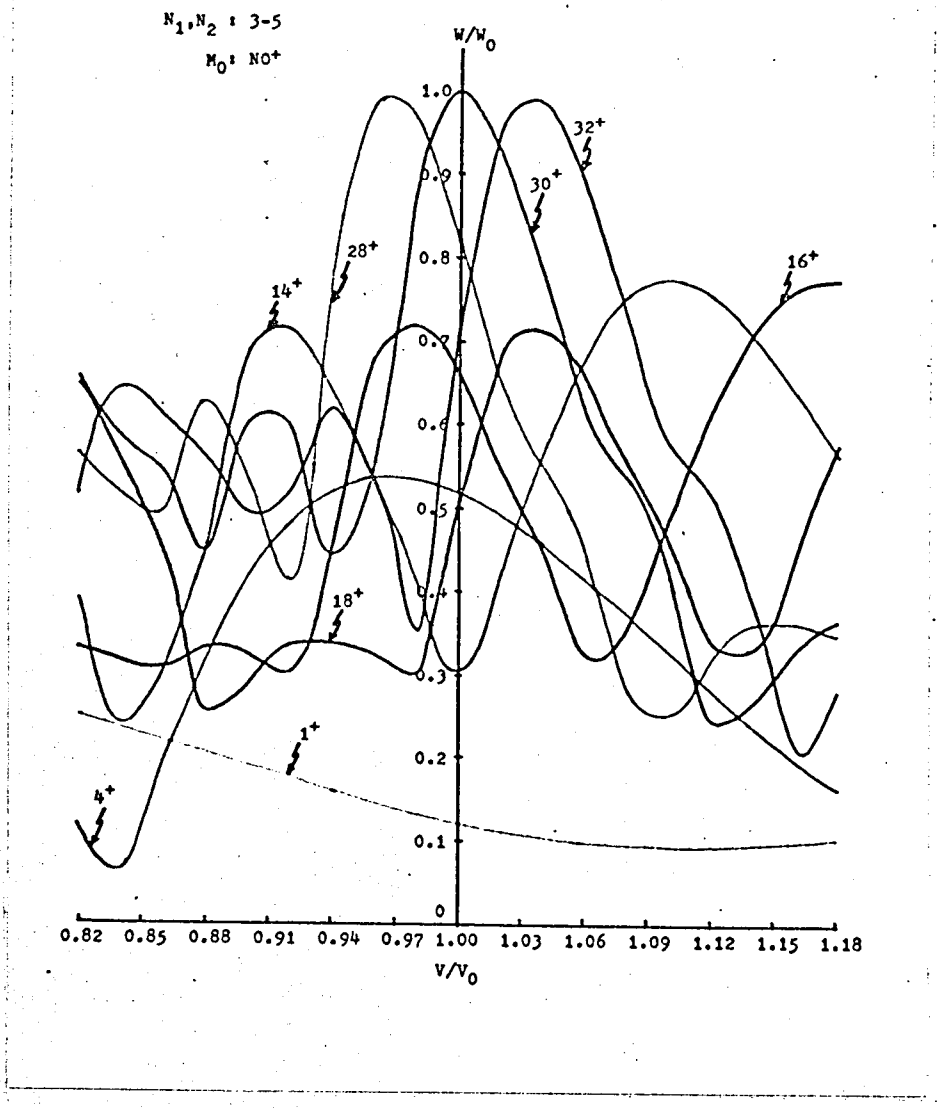

Figure 3.10 Similar result as Figure 3.8, when optimum ion is NO^+.

analysis becomes effectively lower value according to the initial ion velocity and harmonic peaks appear in the spectrum as a result of getting worse of resolution. As a example, when the velocity of a space vehicle is 8×10^3 m/sec, effective lowering of the returding voltage is 0.3 volts for H^+, 1.3 volts for He^+ and 5.3 volts for O^+. These values can not be neglected.

3.3.2 Characteristics of Attack Angle (122)∼(125)

As expected in previous section, the influence of angle between ram direction of the satellite and axis of the mass spectrometer, so called an attack angle, can not be neglected because the velocity of a satellite is larger than the velocity of particles.

The characteristics of attack angle is affected not only by its angle but also by shape and size of the space vehicle, operating mode of the mass spectrometer, sorts and structure of the mass spectrometer, way of installation on the vehicle, surface condition of the vehicle, or parameters of circumstance of the vehicle such as electron and ion temperature, electron and ion density, ion composition

and so on.

Therefore a calculation with some simple assumptions cannot apply to a real case. It is significant, however, to understand the outline of the characteristics and to make design and calibration of the instruments by the results of model calculation.

Figure 3.11 shows proton ion flux at the orifice of a mass spectrometer normalized by ion flux of ram direction versus attack angle. The parameter is ion temperature of the upper-atmosphere and various conditions are shown as in the figure. Figure 3.12 shows the same characteristics of atomic hydrogen, helium and atomic oxygen as a parameter.

As seen in these figures, characteristics of attack angle differs between species of ions even in the same condition and the characteristics depend on various conditions of the satellite and its circumstance. The calibration, therefore, must be done with the ions which are expected in the upper-atmosphere and for all of parameters.

3.3.3 Characteristics of Potential (122)∼(125), (133)∼(135)

The potential and field around a satellite might

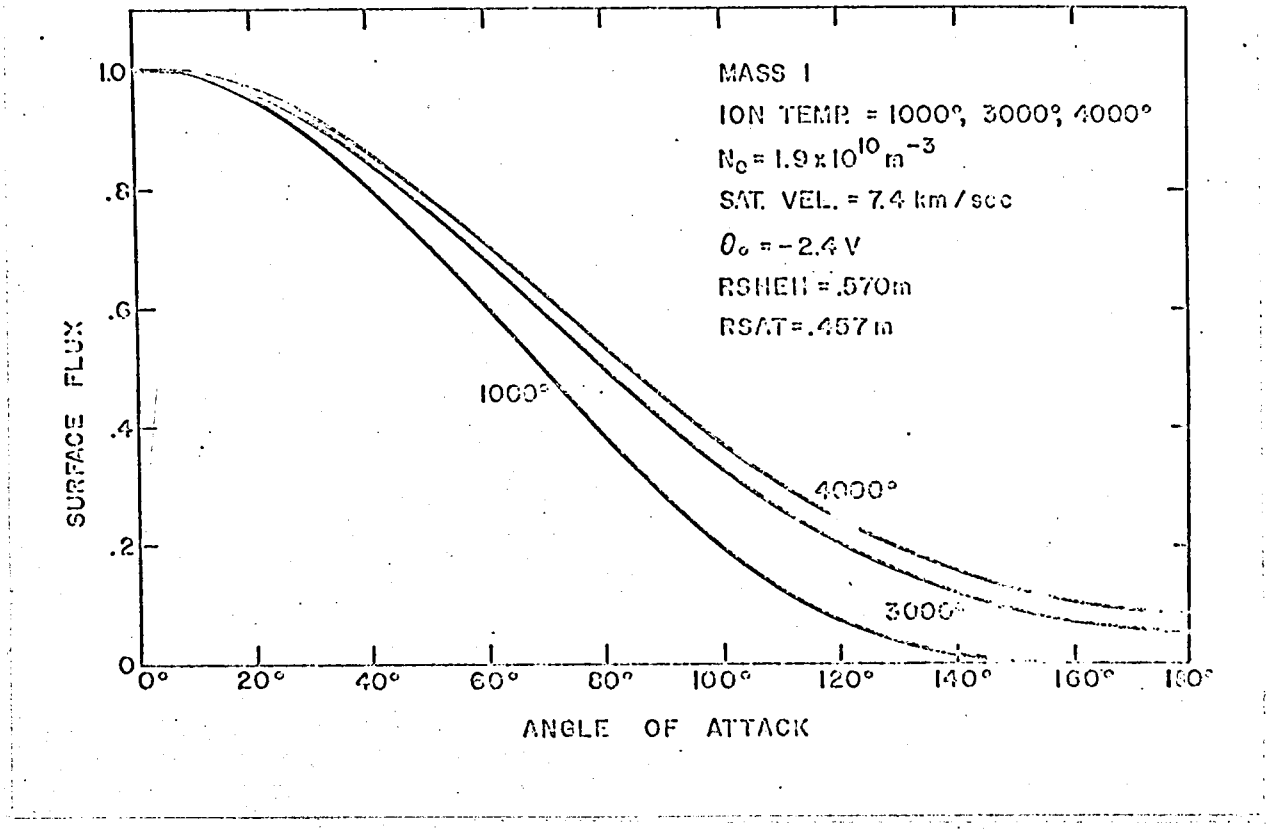

Figure 3.11 Calculated proton flux at the orifice of mass spectrometer normalized by ion flux of ram direction versus attack angle under various ion temperature as parameter, where θ_o means velocity of vehicle, RSHEH is radius of sheath and RSAT is radius of the satellite. (after Scott)

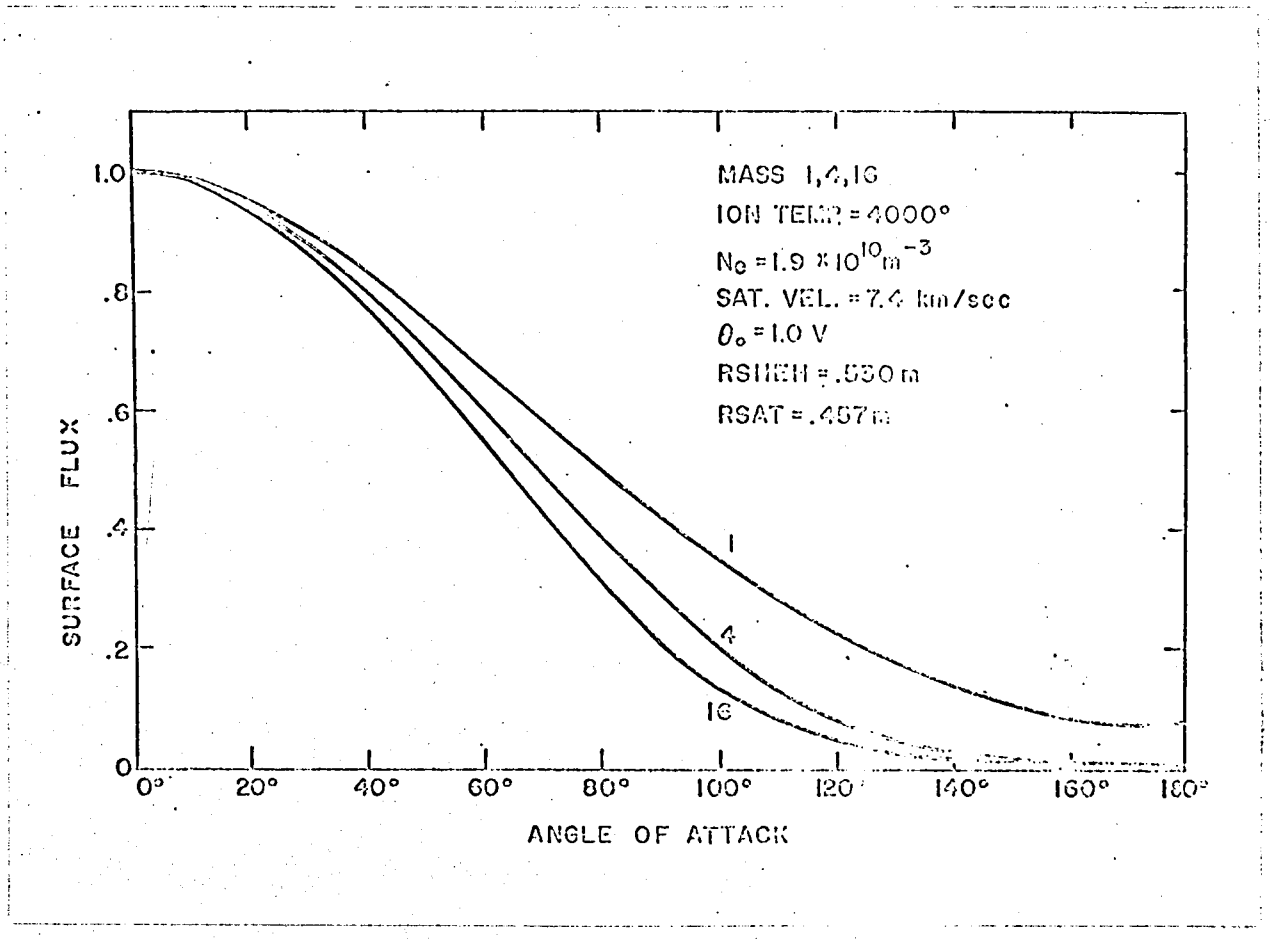

Figure 3.12 Characteristics of attack angle of O^+, He^+ and H^+. (after Scott)

be complicated and differ from calculations with simplified model or simulation experiments, because various potentials are applied on probes, sensors or antennas of instruments installed in the space vehicle.

Figure 3.13 shows the characteristics of attack angle on atomic hydrogen ion collection with the vehicle potential as a parameter. The larger negative potential of the vehicle gives the smaller ion flux difference in the characteristics of attack angle, as seen in this figure. In addition, the attracting voltage applied on the orifice of a mass spectrometer may increase the tendency.

Figure 3.14 shows normalized output ion current of the 5-stage Bennett type mass spectrometer which is used for measurement of the ionospheric ion composition on Japanese sounding rocket versus attack angle when the attracting voltage is 50 volts. It is assumed in the calculation that radio frequency field on grids of the mass spectrometer does not give any influence on the characteristics of attack angle. In Figure 3.15, the same characteristics is shown in the case of a mass spectrometer of different size from that of Figure 3.14, such as 2 times in diameter and about 1/3 in length.

It is seen from these figures that attracting

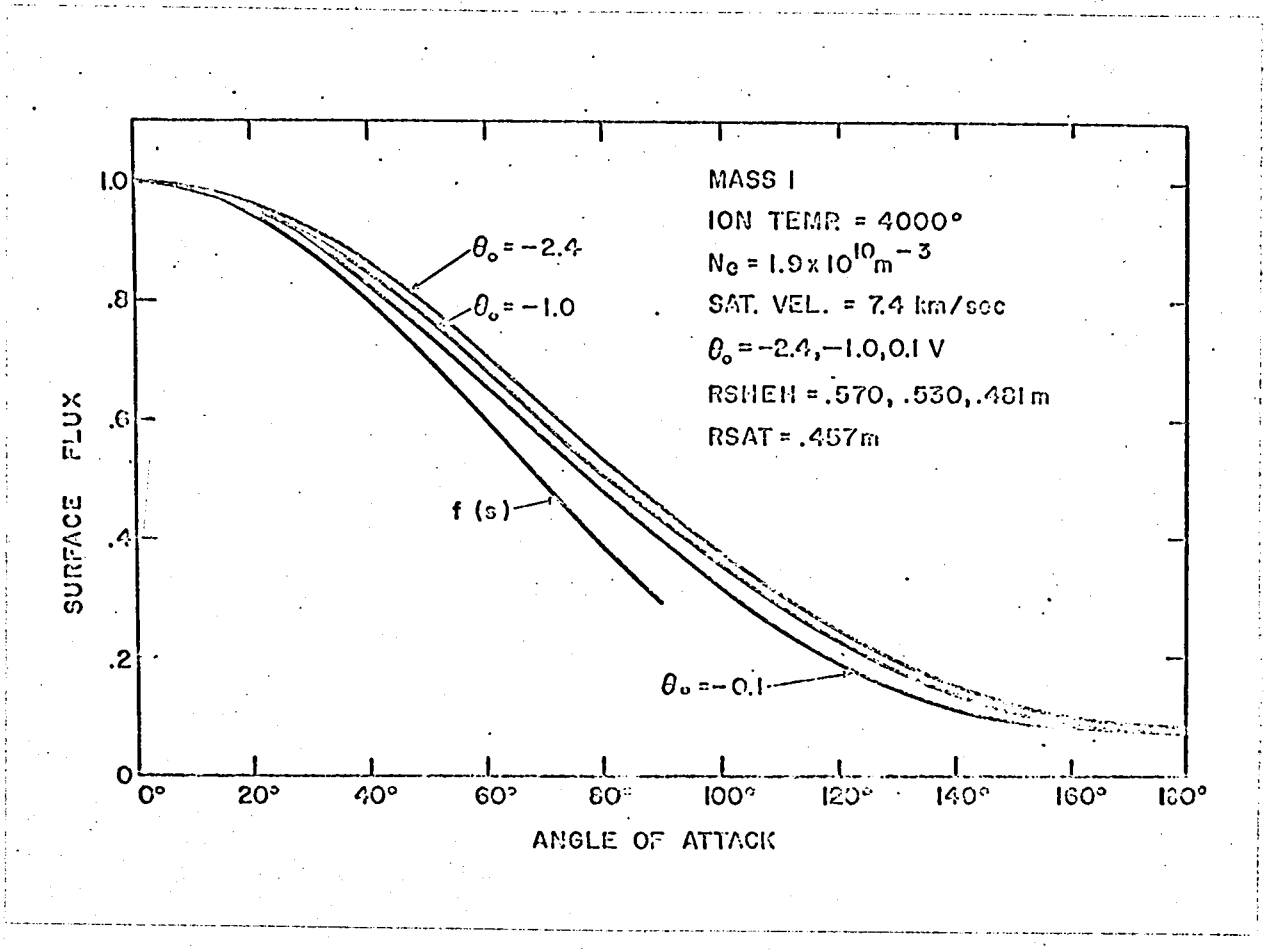

Figure 3.13 Characteristics of attack angle of H^+ with vehicle potential as a parameter.
(after Scott)

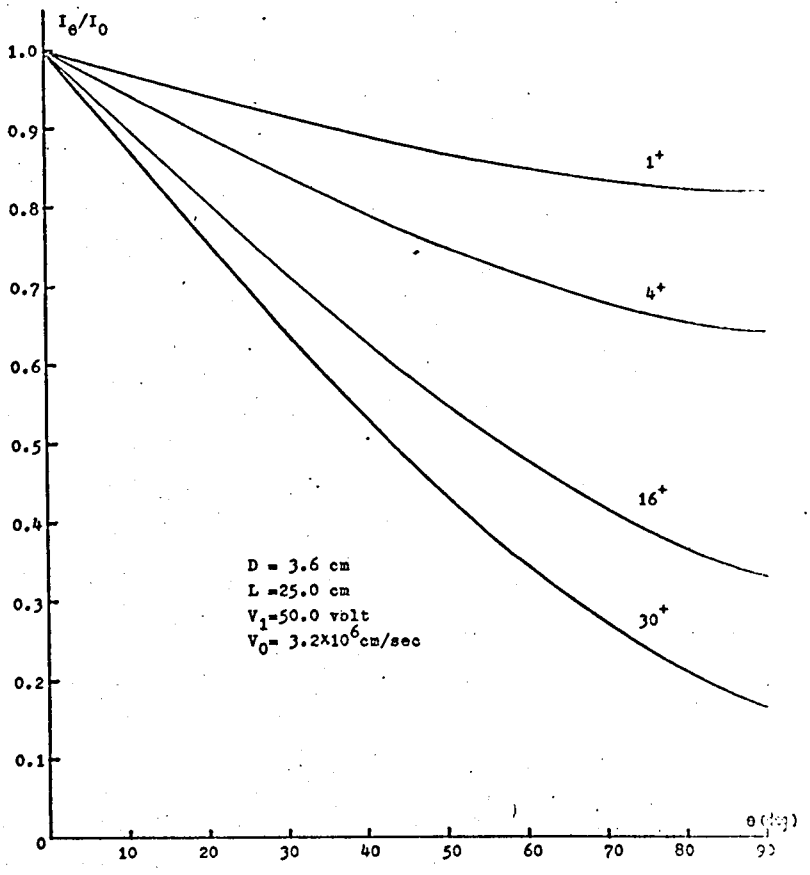

Figure 3.14 Normalized collector current of Bennett type mass spectrometer for Japanese sounding rocket versus attack angle, where D is diameter of sensor, L is its length, V_1 is draw-in-voltage and V_o is velocity of optimum ion in the sensor.

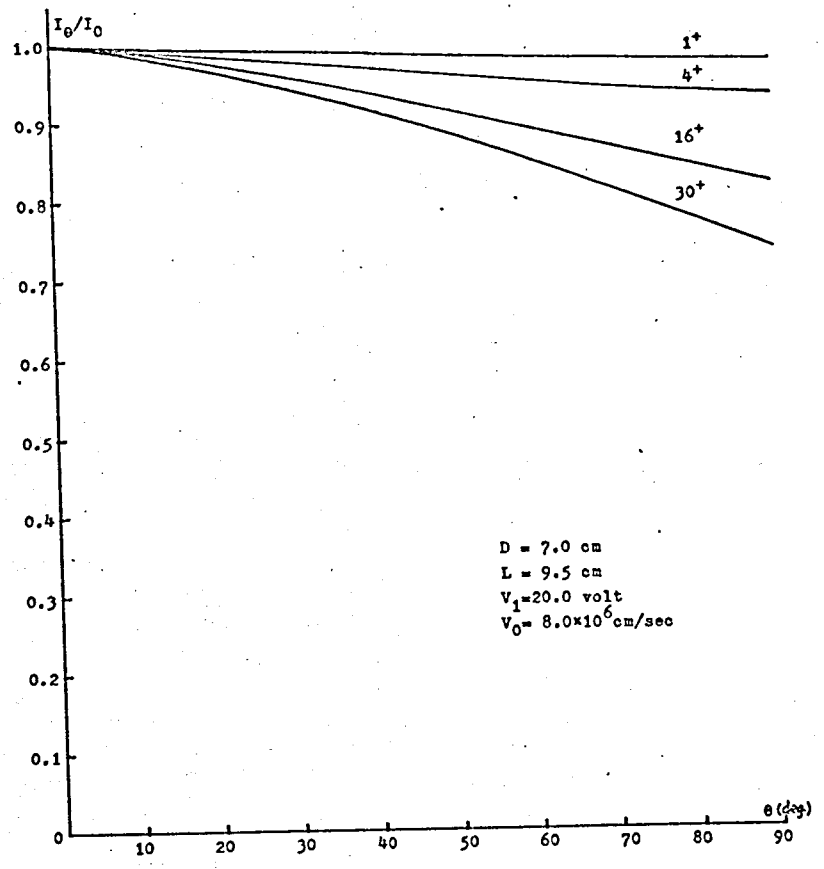

Figure 3.15 Similar result of satellite borne Bennett type mass spectrometer.

voltage improves characteristics of attack angle and in the case of Bennett type mass spectrometer the characteristics depend largely on a dimension of the sensor. They are, however, only the result of calculation under some assumption and simplified situation and actual characteristics are affected by more complicated condition. They show only a general tendency of these characteristics.

3.4 Characteristics for Active Species of the Upper-Atmosphere (122)∼(125), (136)∼(155)

In the upper-atmosphere, some species which can not exist at the ground surface are important constituents. Among them, atomic oxygen is one of the most important species of the ionosphere and it is said that mass spectrometric measurements of it give smaller value than expected density. Though many reasons are suspected with it, main origin of the loss must appear in the ion source of the mass spectrometer. Therefore it depends on size and dimension of the ion sorce or inlet of it, wall temperature of it, electron energy

and so on.

It is said, that the reaction coefficient which has been got in laboratory experiments under higher pressure cannot be applied to the reaction in the upper-atmosphere, especially for active species as atomic oxygen. The mechanism of reaction in the upper-atmosphere where the pressure is rather low, might differ from that in higher pressure. At least, the results of upper-atmospheric atomic oxygen measured by mass spectrometer on space vehicle are suspected. This is one of the most important and difficult problem on direct measurement of the upper-atmospheric composition by mass spectrometer.

3.5 Calibration

3.5.1 Calibration as an Ordinary Mass Spectrometer

There are various type of mass spectrometer which is from the simple type such as used for analyzing residual gases in vacuum or for observing the upper-atmosphere composition, to the large scale mass

spectrometer which is used for analyzing radio active isotopes or for deciding structure of large molecular organic matters having score thousand of resolution.

No mass spectrometer has uniform sensitivity to all masses or species of ions, that is, it has the mass discrimination. The mass discrimination characteristics is due to analyser itself and its ion source.

Mass spectrometers, in which the analyzing principle depends on transit velocity in analyser and the sweep of accelerating voltage is used to scan of mass range, have the sensitivity dependence on the value of accelerating voltage.

On the other hand, in the case of a quadrupole type mass spectrometer which does not depend on the ion velocity in its analyzing principle, the transparency decreases for ions of large masses when the inclination of operating line, shown in Figure 1.28, is made steeply in order to improve its resolution.

Although the motion of charged particle in the analyzing field of a mass spectrometer is enough investigated, there are many obscure points on ionizing action in an ion source. Though the ionizing efficiencies of various species of nutral particles have the maximum at various different voltage, the ionization

voltage applied in an ion source is an average value. Effective ionizing voltage or sample rate of ions to an analyser depend on size, dimension and temperature of an ion source and difference of composition between inside and outside of an ion source.

It is the most serious that there is no standard ion source. The evaluation of pattern coefficient of a mass spectrometer is usually done refering to magnetic field scanned sector type mass spectrometer which has the longest history and is considered to be reliable. We used a magnetic field scanned sector type mass spectrometer as a first standard and a quadrupole mass spectrometer as a second standard.

3.5.2 Calibration for Characteristics Caused by High Speed Flight (122)∼(125)

In this purpose, it is the most important problem how to make the condition which appears around a space vehicle in the upper-atmosphere. As it is imposible to make actual condition of high speed flight of the vehicle in the laboratory, it is simulated by making plasma beam which has the similar composition,

temperature and density as expected in the upper-atmosphere and is accelerated in a parallel beam.

A plasma wind tunnel may be available for simulation of lower altitude such as D layer of the ionosphere. In the simulation for higher altitude, a plasma beam of proper characteristics flowed in vaccum chamber may be available.

It is rather difficult to make a plasma beam of slow speed as a space vehicle and high density as the ionosphere. A plasma beam of high density and slow velocity is practically made by the ways that a dense plasma is generated by dischange in rather high pressure gas and ejected into the test place of high vacuum. It is impossible, however, to satisfy both conditions of velocity and density. An experiment is usually done with rather high velocity plasma and correction will be done afterward. The plasma beam must be parallel and homogeneous inside a cross-section which is large enough for a calibrating sensor. The measurements of parameters of the generated plasma flow are also important for precise calibration.

Figure 3.16 shows an example of result of measured characteristics of attack angle of Bennett type mass spectrometer for molecular hydrogen ion. It was done

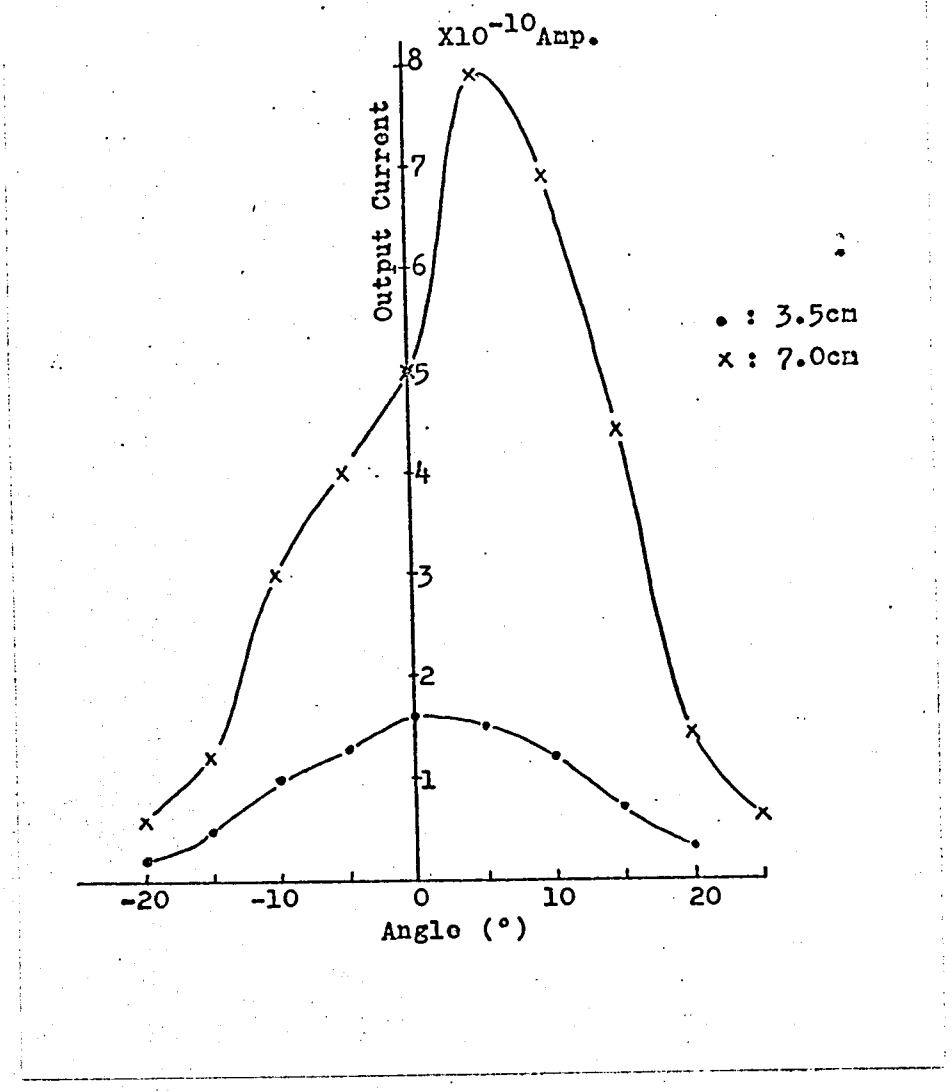

Figure 3.16 Result of laboratory experiment for characteristics of attack angle of two Bennett type mass spectrometers.

in the " Space Chamber " of the Institute of Space and Aeronautical Science, University of Tokyo, which has 2 meters in diameter and 3 meters in length. Figure 3.17 is a view of the sensor in the chamber. The asymmetry of the result is supposed not by the asymmetry of plasma-beam, but by the interface of some parts of equipment. A back diffusion type plasma source was used and energy of the ion is 30 eV. The corrected result of Figure 3.16 due to the ion velocity is shown in Figure 3.18.

3.5.3 Calibration for Active Species (122)∼(125), (127), (136)∼(155)

As described previously, the error in the measurement of active species is one of the most serious problem of the upper-atmospheric mass spectrometry. There are two ways to attain a accurate measurement. One is to develop an excellent instrument, especially, ion source. The other is to calibrate a usual mass spectrometer in the atmosphere, whose composition is accurately measured by some other means.

As for the former way, various types of ion source were tried changing their sizes, structures, or

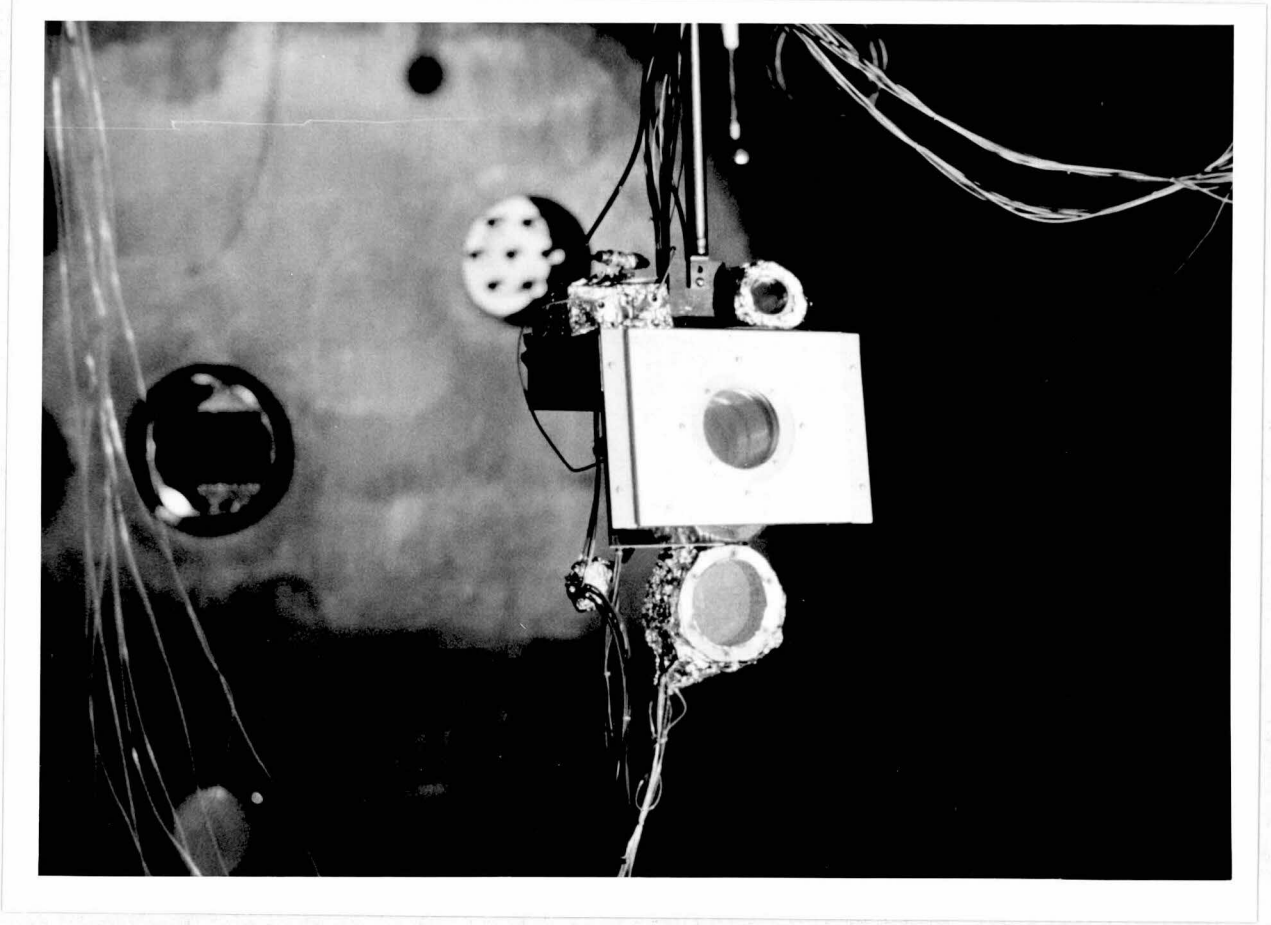

Figure 3.17 Photograph of mass spectrometers in " Space Chamber " under experiment for characteristics of attack angle.

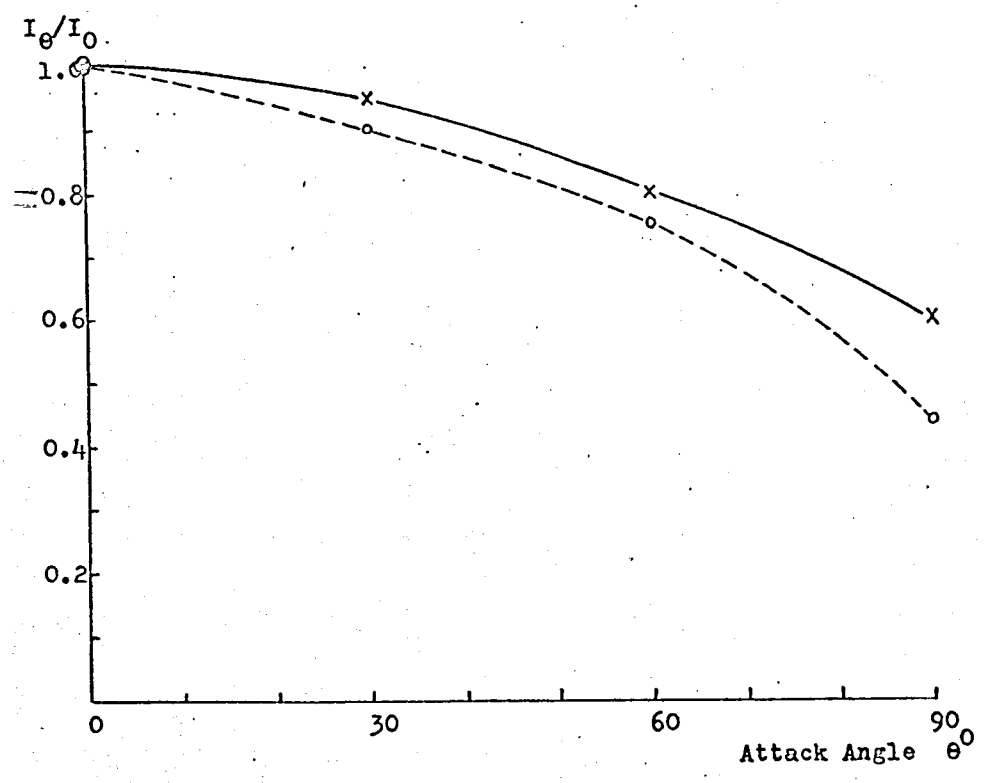

Figure 3.18 Characteristics of attack angle from the result of Figure 3.16 after correction of ion velocity.

materials. Recently, a helium cooled ion source was tried. In this ion source, helium gas is flowed along the wall of the ion source to avoid reactions or losses at the wall surface of high temperature. We adopted, however, the later way. The calibration procedure for atomic oxygen is following.

The atomic oxygen is generated by NO (nitric oxide) titration method, details of which will be described in the following subsection. The production rate of atomic oxygen can be known acculately by the precise measurement of the flow rate of nitric oxide. However, as the pressure in the qualtz pipe at which atomic oxygen generated is about at 1 Torr, and the pressure around the mass spectrometer must be lower than 10^{-4} Torr, the differential pumping is done through a pin-hole between these two position.

Therefore, the density of atomic oxygen in the atmosphere surounding the mass spectrometer is to be calibrated precisely by some means. We adopted a method for this purpose to measure a change of resistance of a thin metal film caused by a chemisorption at the surface. The occurrence of the phenomenon called adsorption or chemisorption depends on the combination of metals and gases. In Table 3.2, the activity of

	O_2	C_2H_2	C_2H_4	CO	H_2	CO_2	N_2
A {Ca, Sr, Ba, Ti, Zr, Hf, V, Nb, Ta, Cr, Mo, W, Fe, (Re)}	+	+	+	+	+	+	+
B_1 Ni(Co)	+	+	+	+	+	+	−
B_2 Rh, Pd, Pt, (Ir)	+	+	+	+	+	−	−
C Al, Mn, Cu, Au	+	+	+	+	−	−	−
D K	+	+	−	−	−	−	−
E {Mg, Ag, Zn, Cd, In, Si, Ge, Sn, Pb, As, Sb, Bi}	+	−	−	−	−	−	−
F Se, Te	−	−	−	−	−	−	−

Table 3.2 List of activities of chemisorption of metal surface to gases in room temperature. (after Keii)

chemisorption of metals for various gases in room temperature is shown. Then, some kind of metal can be chosen for this purpose.

In the case of Cd and oxygen, the change of an electrical resistance of cadmium film, ΔR, is

$$\frac{\Delta R}{R} = \alpha \frac{N(O_2)}{N(Cd)} , \qquad (3.12)$$

where R : resistance of Cd film,

α : parameter of the reaction and approximately 4,

$N(O_2)$: number of adsorbed oxygen,

N(Cd) : total number of cadmium atom.

Figure 3.19 shows a example of resistance change of cadmium film by adsorption of oxygen.

As the atomic oxygen generated by NO titration method is mixed with only molecule nitrogen, this method to measure the density of atomic oxygens is effective and the accurate measurement is expected. Practically, the thin metal film is made by sputtering on glass plate in vacuum.

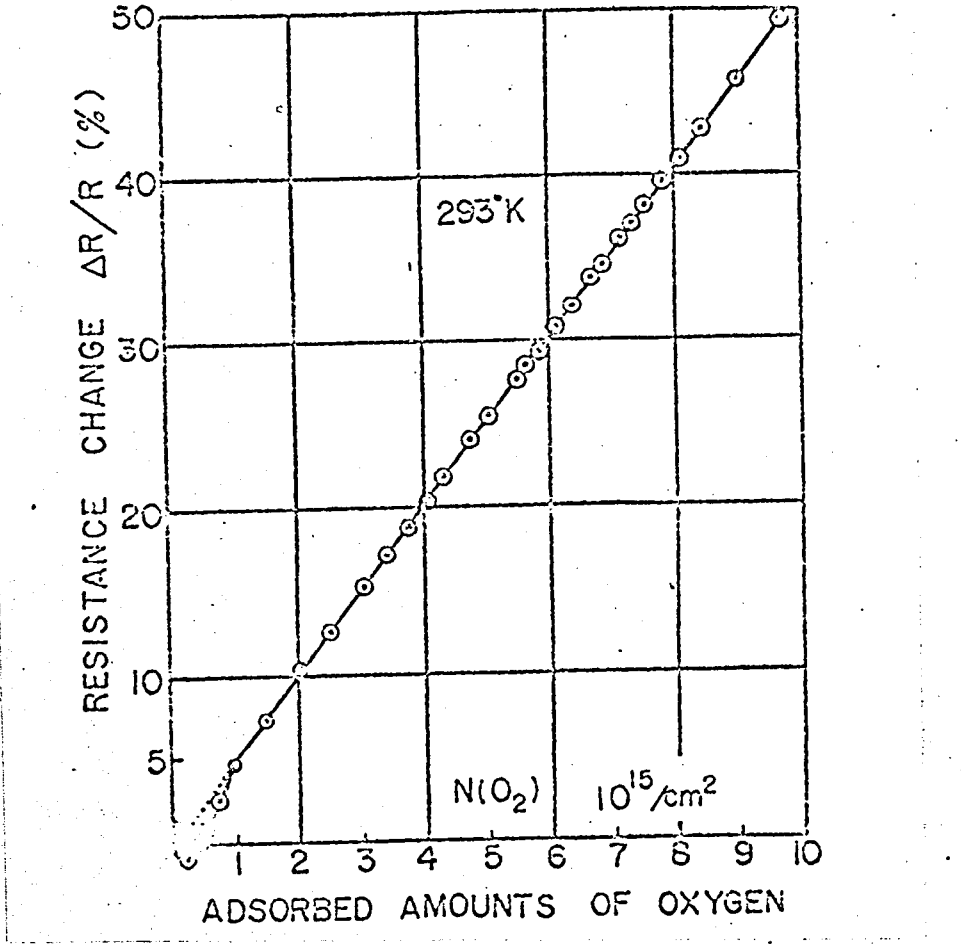

Figure 3.19 Experimental result of resistance change of Cd thin film versus adsorption of atomic oxygen. (after Onchi)

3.5.4 Calibration System

a. Outline of the System (122)∼(125)

According to a necessity of pre-flight calibration of a mass spectrometer for the upper-atmosphere measurement as described previously, a system of apparatus for this purpose is constructed. This calibration system is made of three parts, gas supplier, plasma source and calibration chamber, as shown in Figure 3.20.

The gas supplier sends all kinds of gases to the plasma source which are expected to exist in the upper-atmosphere. The flow of gases except for atomic species is automatically controlled at a proper rate. This apparatus is able to generate, hydrogen, nitrogen and oxygen in atomic state.

At the plasma source, ions are generated by high frequency discharge or electron bombardment and ejected into the calibrating vacuum chamber with some suitable energy which is adjustable.

In the chamber, there are a turn table which is installed at the bottom of it and on which a mass spectrometer for flight is calibrated, a movable Faraday

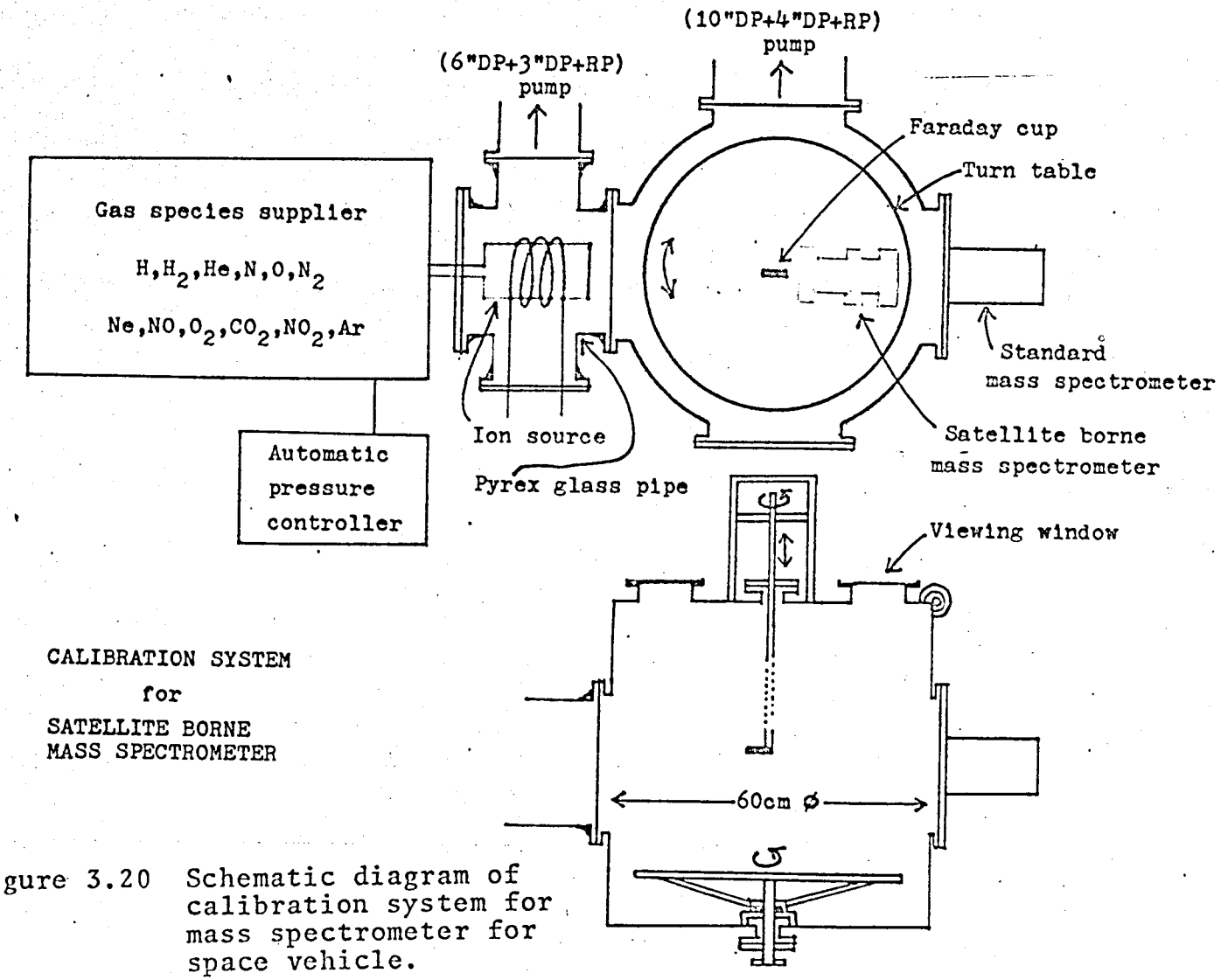

Figure 3.20 Schematic diagram of calibration system for mass spectrometer for space vehicle.

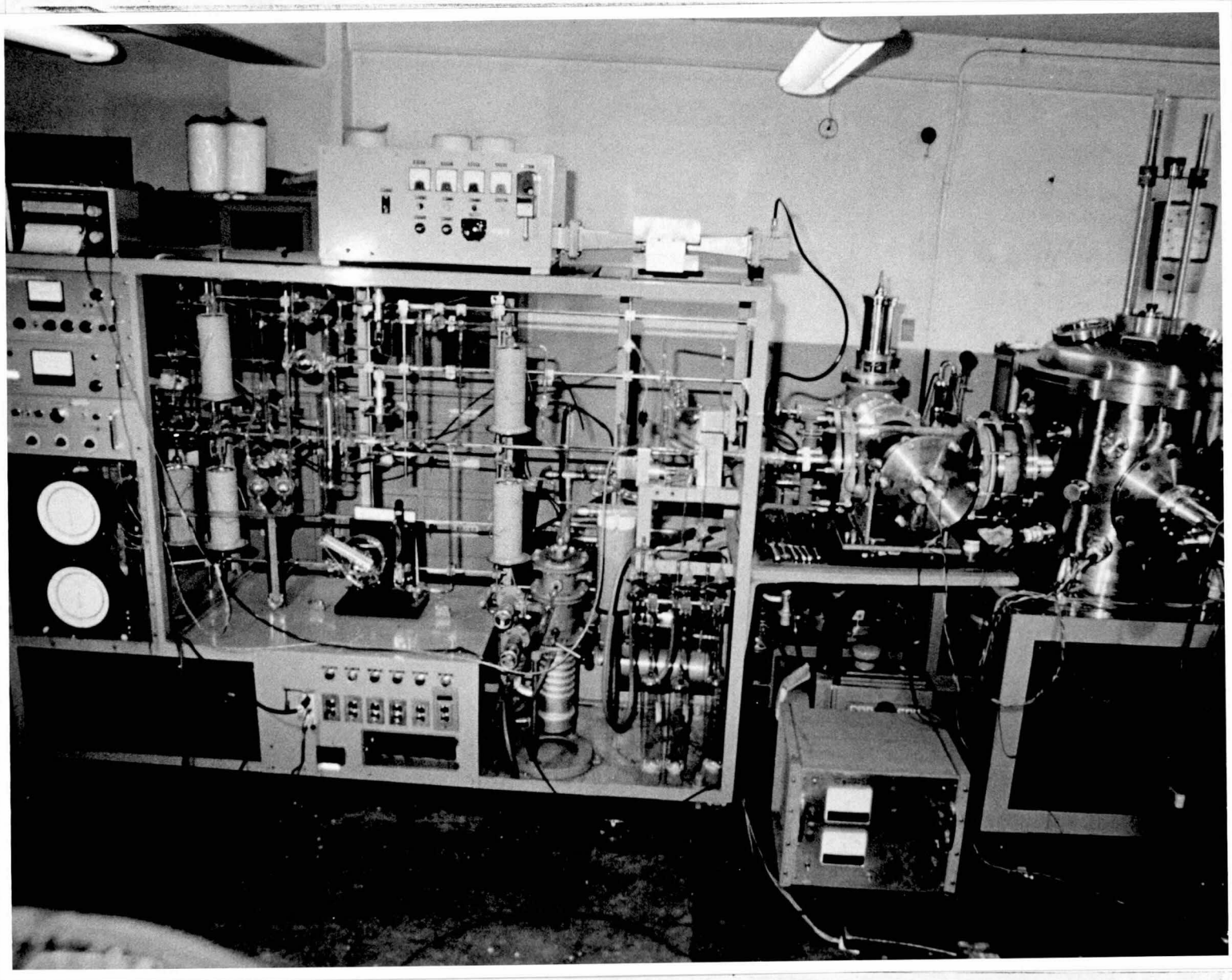

Figure 3.21 A view of calibration system.

cup which checks the homogeneity of density and energy of ion beam, and a standard mass spectrometer which is composed of a magnetic sector type and a quadrupole type to diagnoses the composition of the beam. The calibration system is shown in Figure 3.21.

b. Generator and Supplier of Gas Species $\begin{matrix}(122)\sim(125),\\(136)\sim(155)\end{matrix}$

The schematic diagram of the apparatus is shown in Figure 3.22. It has two functions. One is the supplier of various gases with constant flow. Gases are supplied from gas container and flow through motor driven needle valve which composes a closed automatic control loop with a vacuum gauge or a flow meter and electronic circuits. This control system keeps the pre-set value of pressure or flow rate with a good response.

The other is the generator of hydrogen, nitrogen and oxygen in atomic state. The atomic oxygen generating system takes a large part of the apparatus, which is the well known NO titration method. Atomic nitrogen is generated by excitation of molecular nitrogen in a qualtz pipe which thrusts through a microwave cavity. The capacity of the magnetron microwave oscillators of

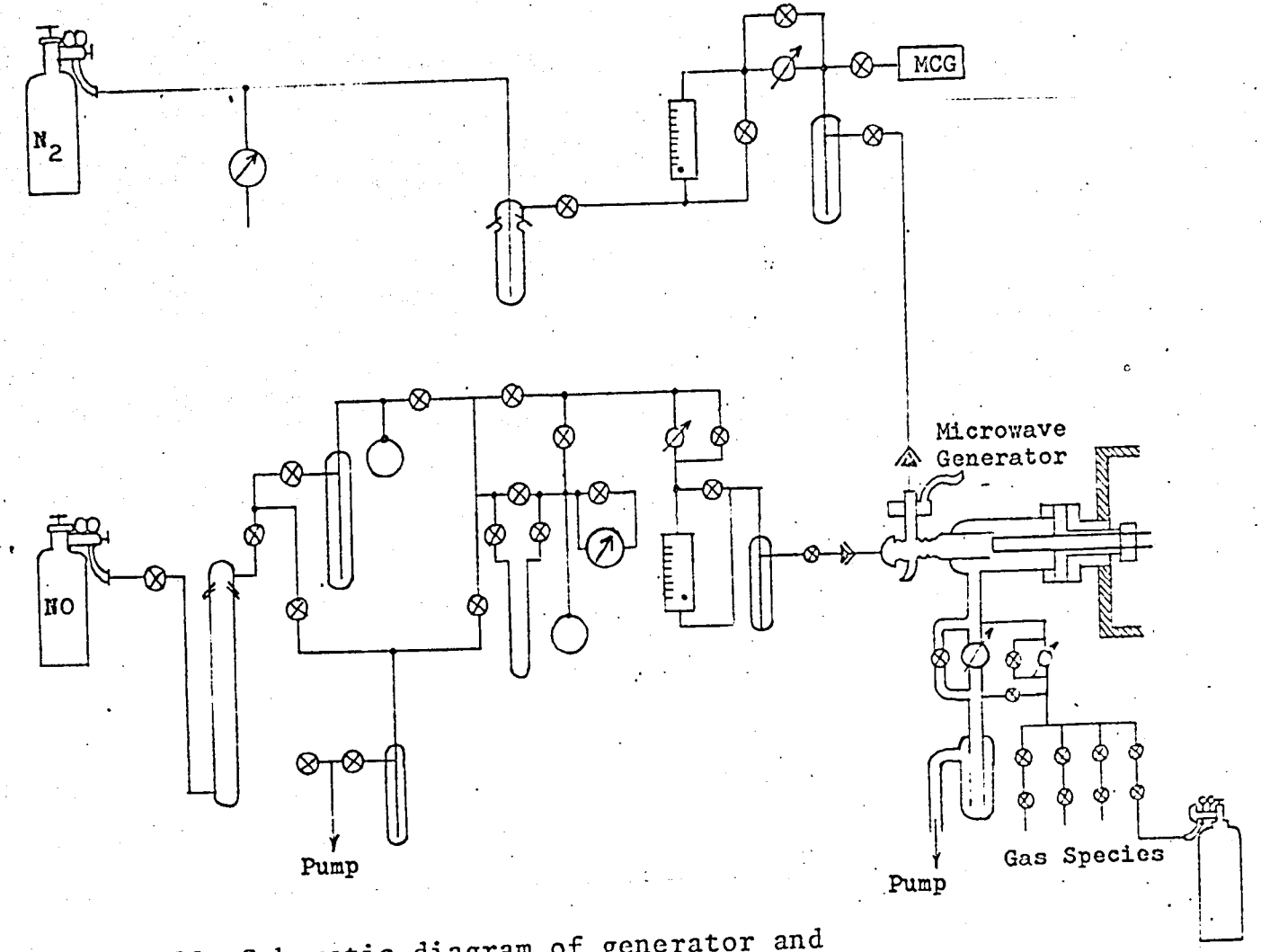

Figure 3.22 Schematic diagram of generator and supplier of gas species.

2.4 GH_z is about 800 Watt though it is usually operated at about 200 Watt. A circulator is adopted in the wave guide circuit and protects the oscillator from the reflection power from the exciting cavity which is absorbed at non reflecting terminal. By this excitation, atomic nitrogen of a few percent of molecular nitrogen flow is generated.

When nitric oxide is injected into down stream of the excitation, reaction (1) generates atomic oxygen.

Reaction (1) $N + NO \rightarrow N_2 + O$ (3.13)

$k_1 = 22 \times 10^{-11}\ cm^3 molecule^{-1} sec^{-1}$

(2) $N + O + M \rightarrow NO + M + h\nu$ (3.14)

$k_2 = 5 \times 10^{-23}\ cm^6 molecule^{-2} sec^{-1}$

(3) $NO + O \rightarrow NO_2 + h\nu'$ (3.15)

$k_3 = 3 \times 10^{-17}\ cm^3 molecule^{-1} sec^{-1}$

(4) $NO + O + M \rightarrow NO_2 + M$ (3.16)

$k_4 = 6 \times 10^{-32}\ cm^6 molecule^{-2} sec^{-1}$

The resultant atomic oxygen reacts with reaction (2) and radiates blue light in the case of excess of atomic nitrogen. When nitric oxygen is surplus, greenish

yellow light is emitted by reaction (3). When no excess exist, that is, quantity of atomic nitrogen and nitric oxygen is equal, these light diminish. At the moment, there are only atomic oxygen and molecular nitrogen in the down flow of reacting spot. Although the generating rate of atomic nitrogen from molecular nitrogen is indistinct, it is clear from above discussion that the production rate of atomic nitrogen is able to know accurately by measuring precisely the flow rate of nitric oxygen. The flow rate L is given by the relation of

$$L = \frac{C\Delta P}{\Delta t} , \qquad (3.17)$$

where C : volume of the reservior of nitric oxygen,

Δt : period of an experiment,

ΔP : pressure difference of the reservior during Δt.

Atomic nitrogen of equal content to the atomic oxygen will be supplied to the chamber, if nitric oxide flow is stopped as the condition of those glow faded out. Precise control of titrating condition is effectively achieved not by needle valves in the route of molecular nitrogen and nitric oxide but by microwave power output, because of difference of their response. As it is

apparent from the reactions from (1) to (4) that the reaction rate of (1) is faster enough than other reactions, the generated atomic oxygen can reach to the orifice of plasma source without loss.

c. Plasma Source (122)~(125)

Gases from gas supplier are ionized at the ion source which is located between the frame of gas supplier and the main chamber. It is composed of a " reducer cross pyrex pipe of 9 and 6 inches " and three types of ion source such as RF discharge type, electron bomberdment type and back diffusion type as shown in Figures 3.23, 3.24 and 3.25 respectively. Those are able to be installed in the pipe alternatively.

The ion sources of the former two types ionize the gas at high pressure about 10^{-2} or 10^{-3} Torr in the ion source and the ions are extracted through many holes and ejected into main chamber with proper velocity which is given at the final grid. In the case of the latter type of the ion source, dense gas is flowed against the ionizing space and unionized residual gas is exhausted by vacuum pump after ions taken out by electric field.

Figure 3.26 shows RF type ion source. RF power is

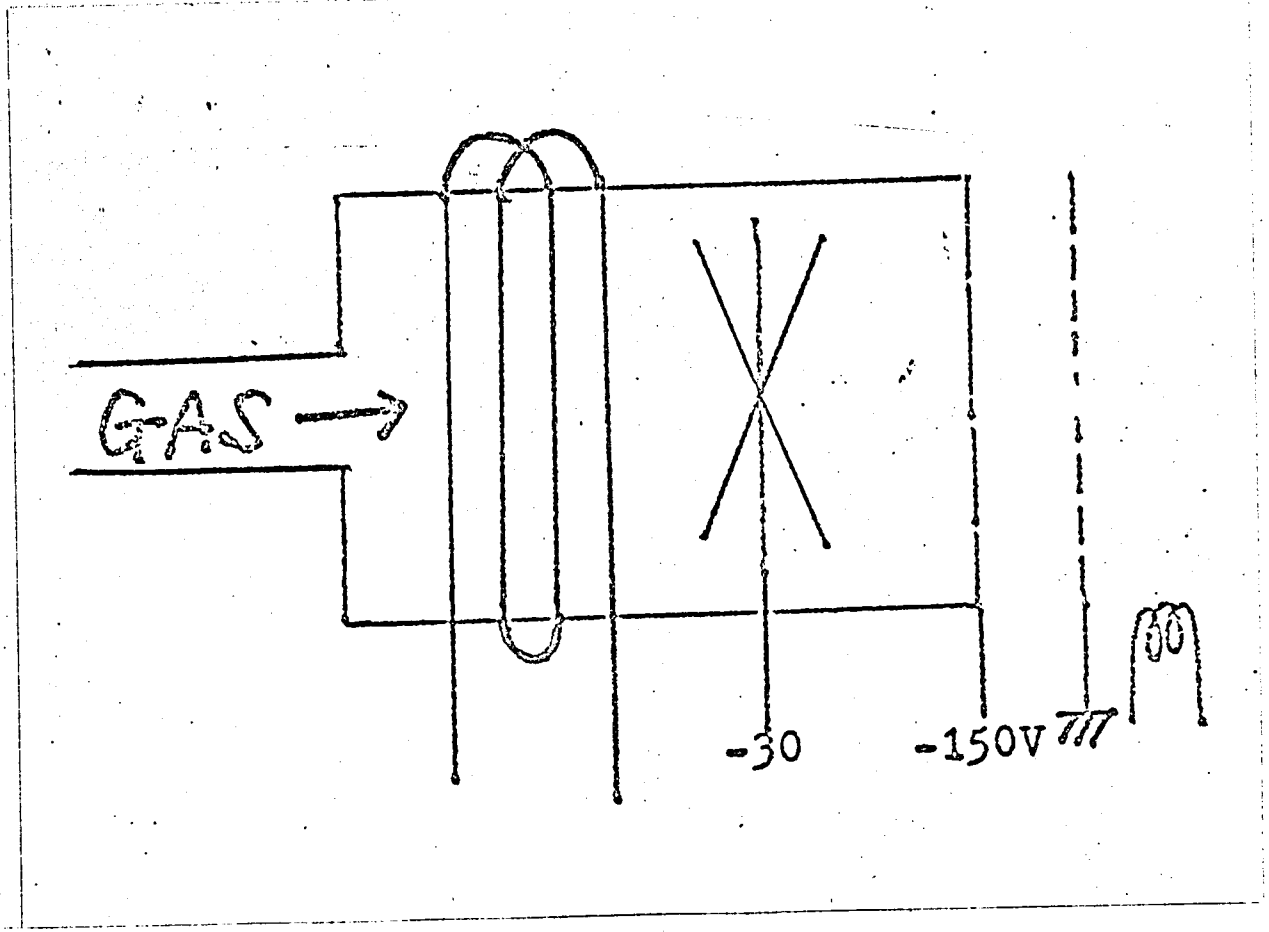

Figure 3.23 Schematic diagram of radio frequency plasma source.

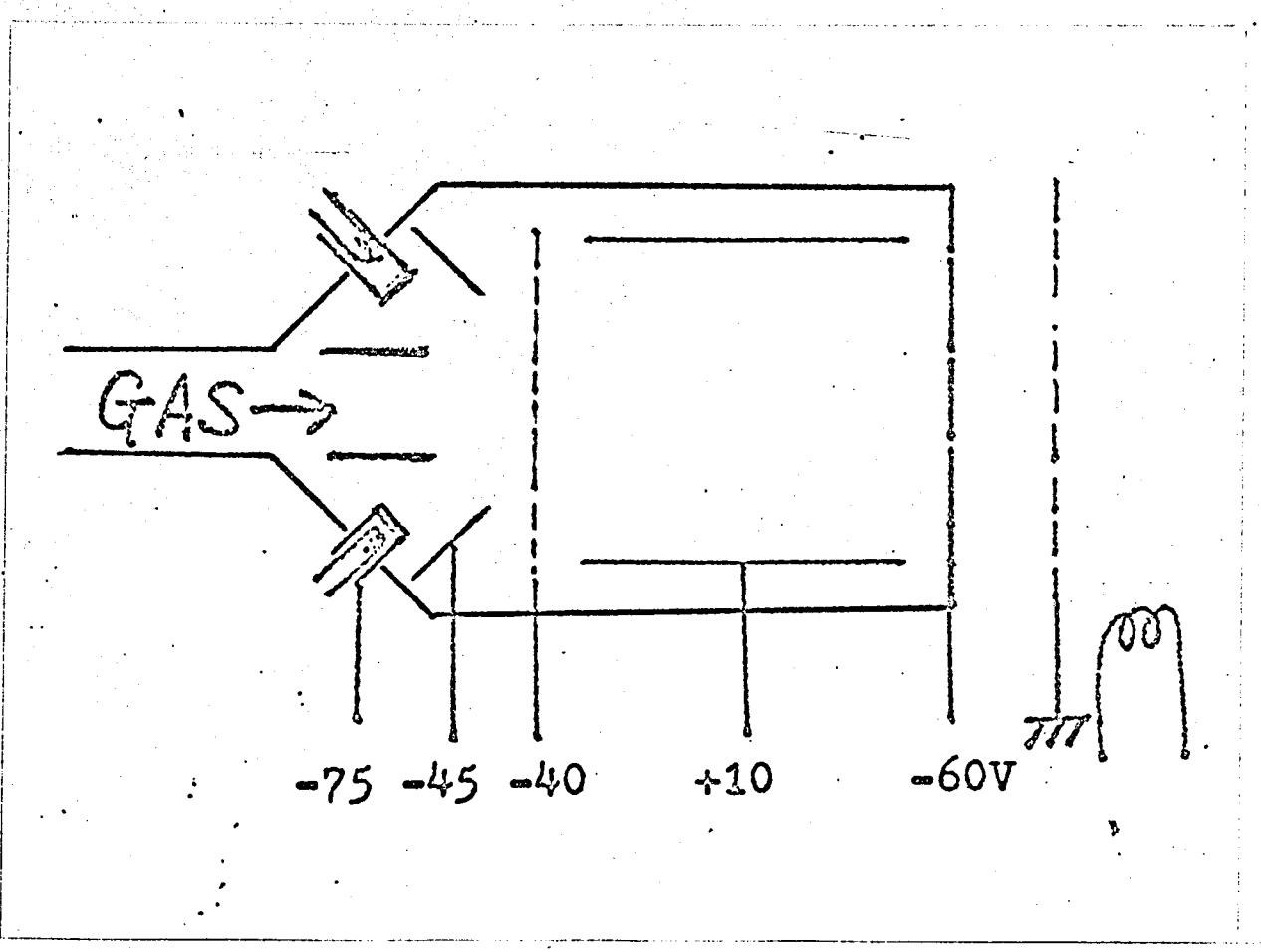

Figure 3.24 Schematic diagram of plasma source by electron bomberdment.

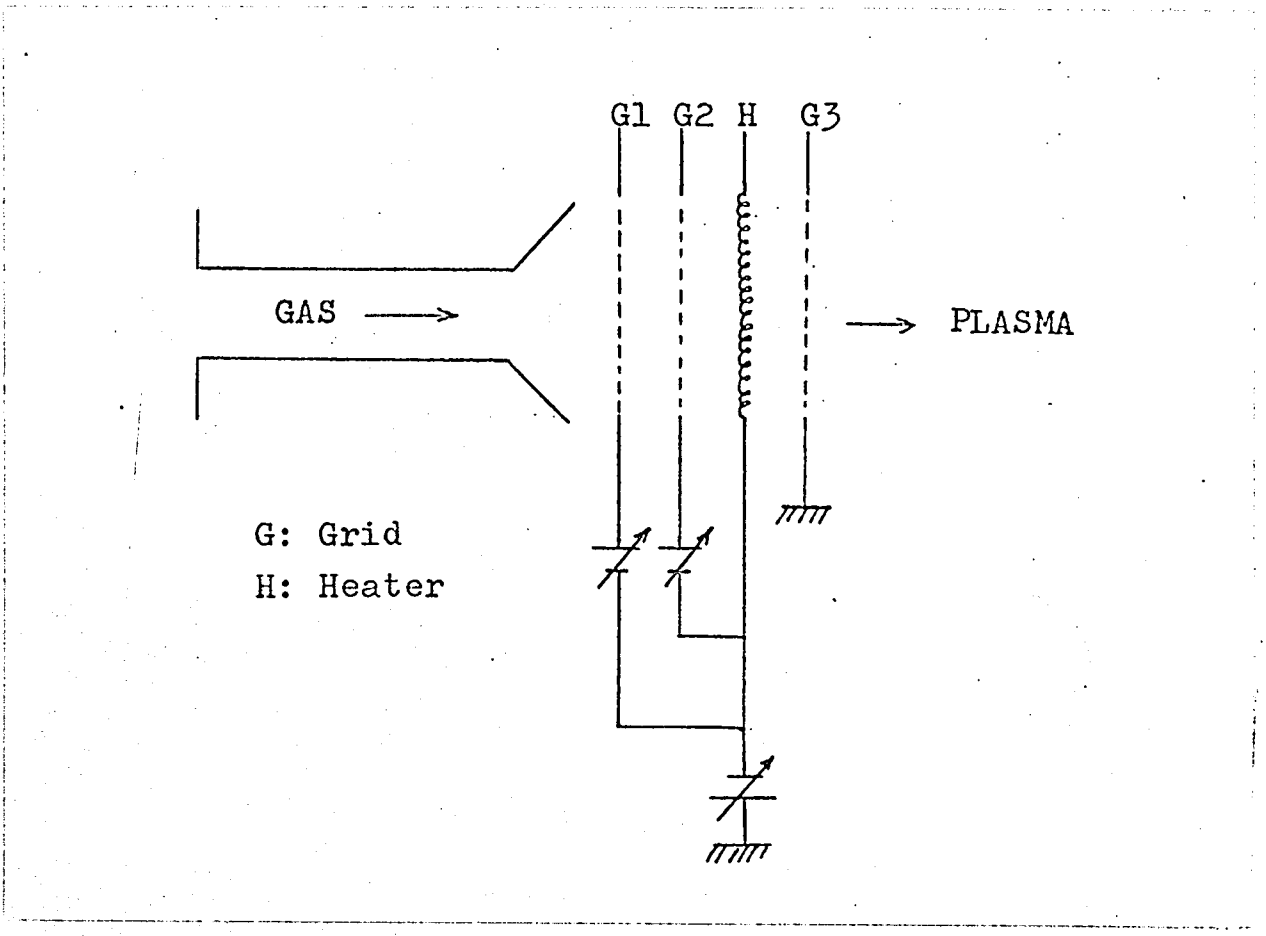

Figure 3.25 Schematic diagram of back diffution type ion source.

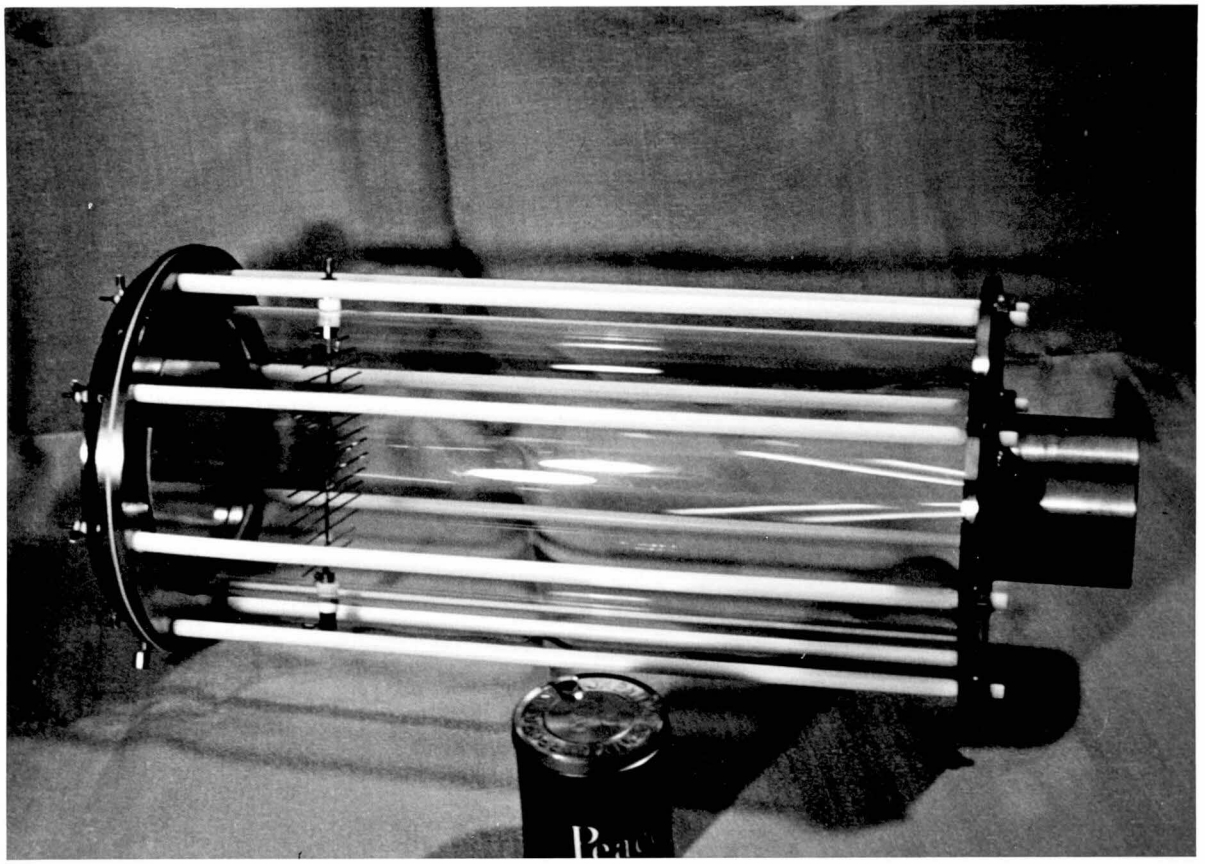

Figure 3.26 Photograph of RF - plasma source.

supplied by water cooled coil wound at outside of pyrex cylinder of the ion source. RF oscillator used for this purpose has 1 kW of power capacity at 14.5 MH_z. Front view, final power stage and circuit diagram of the oscillator are shown in Figure 3.27, 3.28 and 3.29 respectively. Figure 3.30 shows electron bomberdment type ion source.

d. Main Vacuum Chamber

Main vacuum chamber of the calibration system is 60 cm both in diameter and height as shown in Figure 3.20. It has a turn table at the bottom which can bear about 30 kg of weight. The turn table can be rotated from outside of the chamber with accuracy of 0.5 degree of its angle.

A stainless steel rod of 1 cm in diameter pierces through the ceiling of the chamber, rotates in any direction, moves up and down within 50 cm and bears 10 kg of hanging load. At the side of the chamber, four of 250 mm flange and twenty of 70 mm " conflat flange " are arranged.

Figure 3.27 A view of RF generator for plasma source.

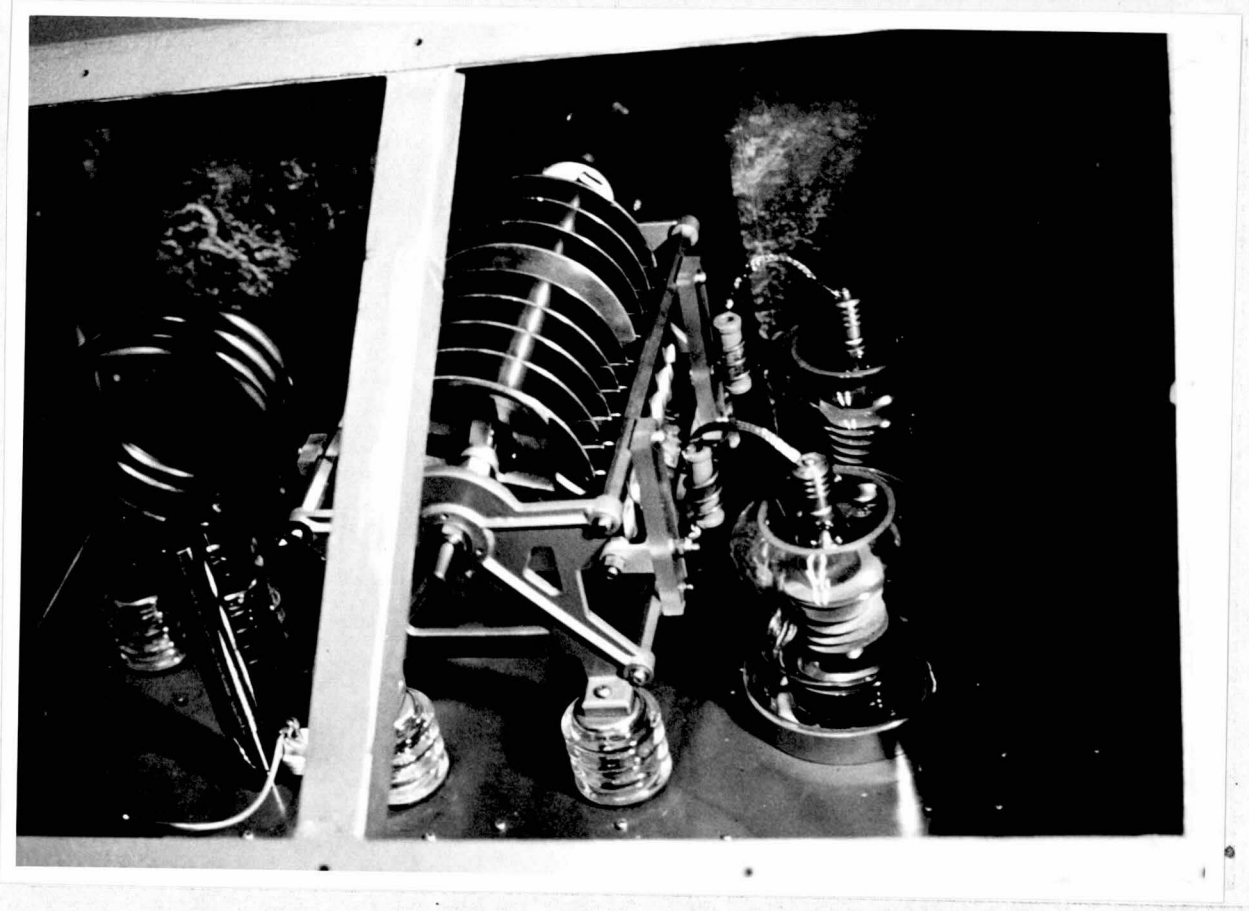

Figure 3.28 A close-up view of final stage of RF generator.

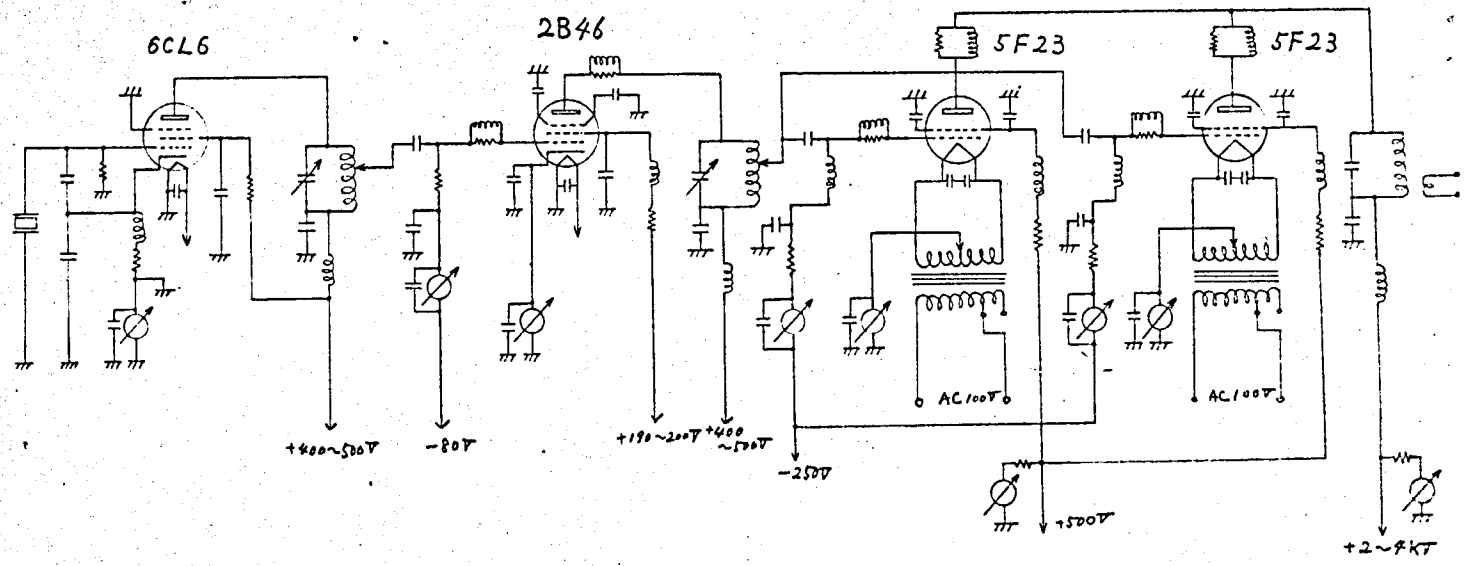

Figure 3.29 Circuit diagram of RF generator.

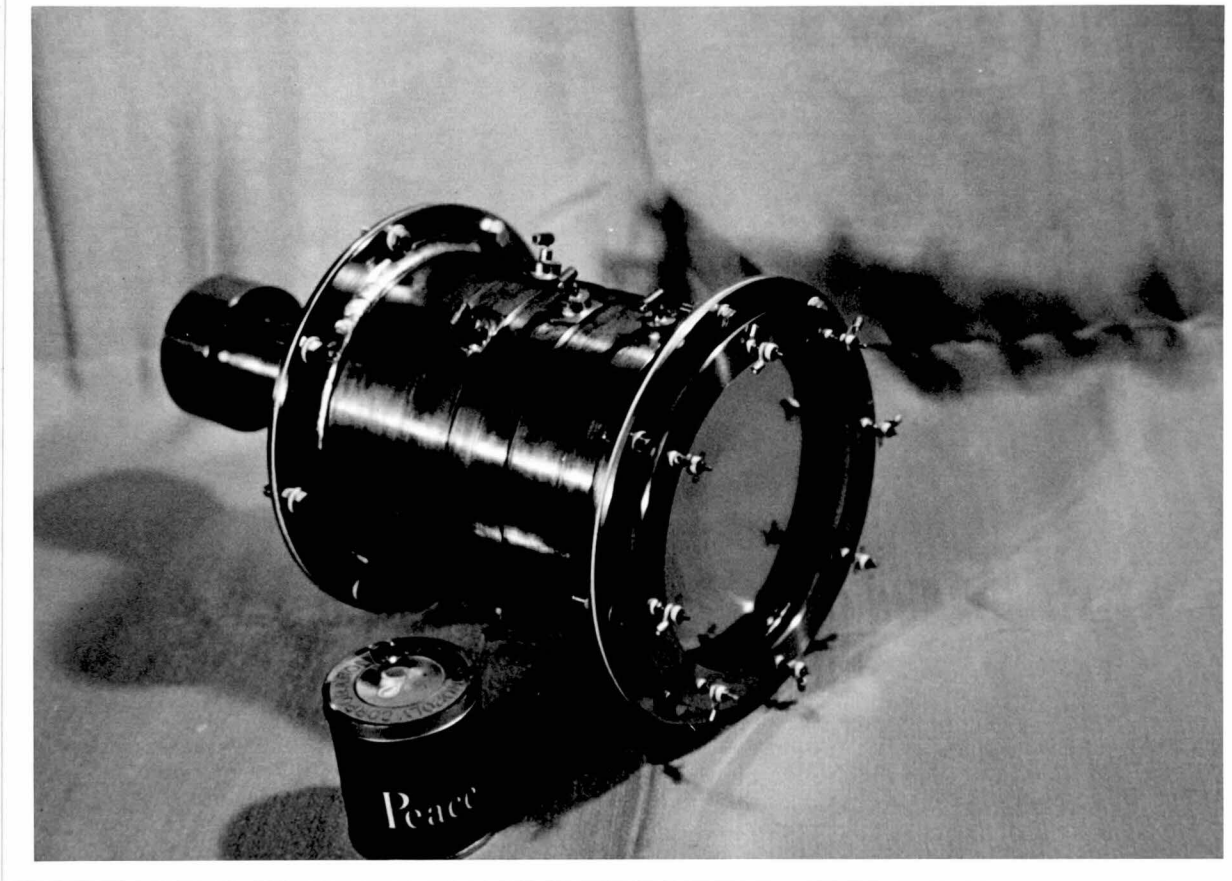

Figure 3.30 Photograph of plasma source of electron bomberdment.

e. Standard Mass Spectrometer

The composition of the ion beam which is used in the calibration system in which a space borne mass spectrometer is calibrated must be fully analysed before a calibration experiment.

A combination of a magnetic sector type and a quadrupole type mass spectrometer is used for a standard. A quadrupole type mass spectrometer is generally used during calibration experiment, because an influence on light ion beam by the leakage flux exists in a magnetic sector type mass spectrometer. The quadrupole mass spectrometer, however, usually has a large mass discrimination which depend on its operating condition especially on setting of its resolving power. Then the pattern coefficient of the quadrupole mass spectrometer is calibrated by scanning magnetic field sector type mass spectrometer. The outline of characteristics of these mass spectrometer are as follows.

Magnetic sector type mass spectrometer

mass range : 1∼200 m/e

resolution $M/\Delta M$: $\geqq 100$

scanning : available both magnetic field scan

and accelerating voltage scan
3 m sec ~ 30 min.
automatic repetition and manual start

sensityvity : 10^{-13} Torr with secondary electron multiplier

sensor : ion orbit of 5 cm in radius and 75° in deflection angle

special specification : potential of ion orifice is always zero volt and high voltage is applied on the sector

leakage magnetic flux : less than 3 gauss at 1 meter from orifice of the sensor

Quadrupole type mass spectrometer

mass range : 1~750 m/e

resolution : ≧2M and ≧500

sensitivity : 5×10^{-15} Torr with secondary electron multiplier

scan rate : 25 m sec ~ 30 min.
automatic and manual

dynamic range : 10^{7}

f. Faraday Cup

In order to check a homogeneity of density and energy of the ion beam over its cross-section, a sort of Faraday cup of small diameter is mounted at the end of a movable rod in main chamber. The schematic diagram of the sensor and pre-amplifier is shown in Figure 3.31.

g. Data Processing

Calibration with this system will be done under various parameters which are expected to give a serious influence to a mass spectrometer measurement on a space vehicle. A lot of data got by calibration experiment must be utilized effectively for the reduction and analysis of observation data on a space vehicle with various parameter such as information of orbit or trajectory of space vehicle, attitude or temperature of space vehicle and various geophysical parameters. For such a purpose a considerable scale of data processing and conputing system is necessary and a system as shown in Figure 3.32 was planned and is in progress..

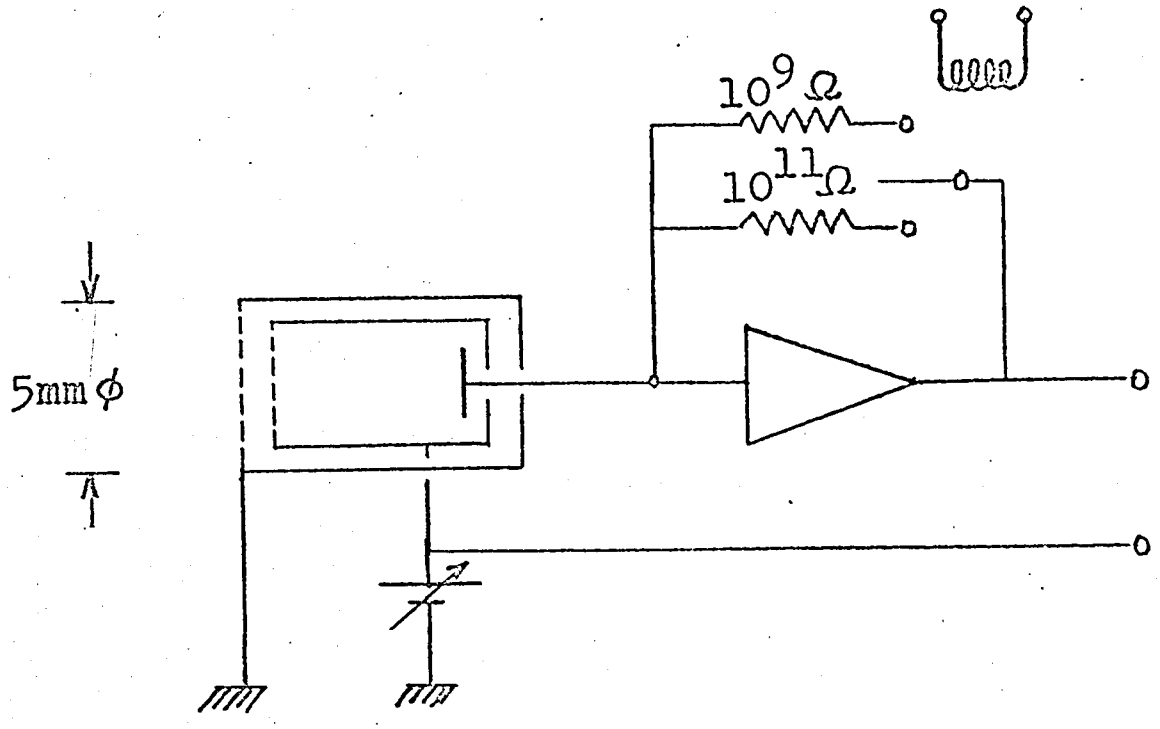

Figure 3.31 Schematic diagram of Faraday cup and its amplifier.

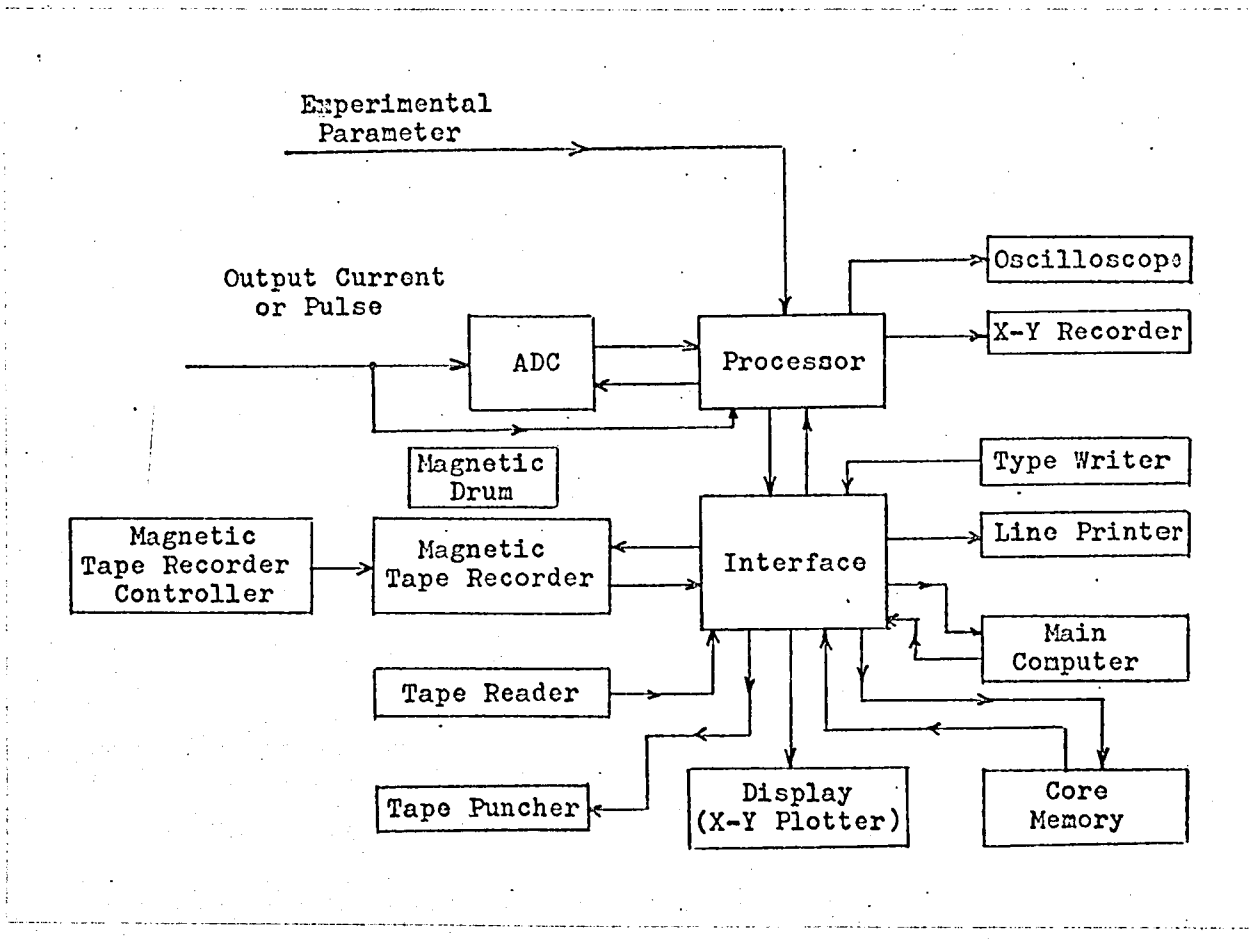

Figure 3.32 Diagram of data processing system under contemplation.

h. Support Equipments

Many and various support equipments or instruments is used for the calibration experiments. Only vacuum pumping equipments, however, are described here. The ion source and main vacuum chamber have two lines of vacuum pump system such as 10 inch and 4 inch oil diffusion pump and oil rotary pump, and 6 inch and 2 inch oil diffusion pump and oil rotary pump. The latter system is perfectly protected from failure of electric and water supply. Then, the latter system is operated continuously always and the former powerful system is operated only during experiment, especially of gas flow. The final vacuum which can achieve by full operation is about 10^{-8} Torr. The gas supplier uses a 4 inch oil diffusion pump and oil rotary pumps besides these.

CHAPTER 4

EXPERIMENT OF SPATIALLY PERIODIC STATIC FIELD TYPE MASS SPECTROMETER ON BOARD JAPANESE SOUNDING ROCKET

4.1 Constitution of the Flight Instrument

The total constitution of the system of the flight type instrument borne in Lamda-3H-6 rocket is schematically illustrated as a diagram in Figure 4.1.

Accelerating voltage V_A was applied to the orifice of the sensor and the voltages applied to the quadrupole electrodes, $V_A + V_o$ and $V_A - V_o$ were made by dividing the accelerating voltage. These voltage were scanned from 0 to about -300 V in 2 second.

The ions which passed through the mass spectrometer sensor were ejected into the channel type secondary electron multiplier, of which the high voltage of -3 kV was applied to its entrance. The current gain of the multiplier was about 10^6 or higher. This type of multiplier does not need voltage dividing resistor and it is smaller and easier use than ordinally electron multiplier of BeCu dinodes. The output current was received by a high input impedance pre-amplifier and log-amplifier.

The power supplying switch of high voltage circuit was separated from the power switch of the other circuits and it turned on by a signal from program timer borne in the rocket after about 5 second from a

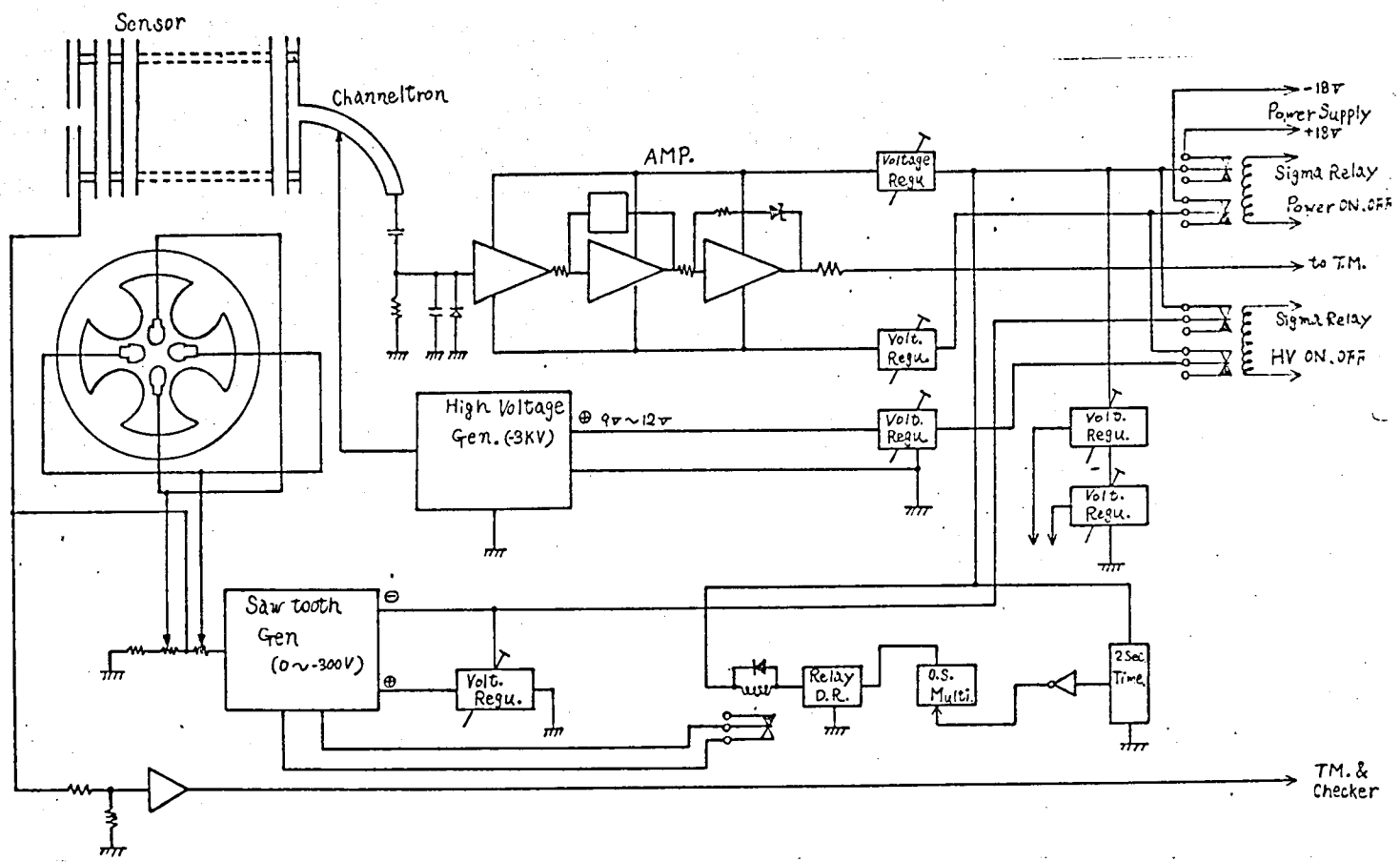

Figure 4.1 Diagram of rocket borne instrument of spatially periodic static field type mass spectrometer.

burning out of final rocket motor, the altitude being about 200 km.

The payload of the mass spectrometer for Lamda-3H-6 rocket is shown in Figure 4.2. It was composed of two parts, such as sensor, electron multiplier and pre-amplifier part and the other electronic circuit part. These size were 80 mm in diameter and 200 mm in height for sensor part and 200 mm in diameter and 100 mm in height for electronics part. The total weight was about 2.5 kg.

4.2 Sensor

The drawing for fabrication of sensor and its magnetic shield which were used for the experiment is shown in Figure 4.3. A schematic drawing of the sensor part is illustrated in Figure 4.4. The magnetic shield is used as an aperture of orifice and outlet of the sensor. Therefore, the magnetic shield was applied the accelerating voltage of ions and the outer case was at the rocket potential. The leakage flux was smaller enough than one tenth of geomagnetic field at about 10

Figure 4.2 Photograph of the mass spectrometer for Lamda-3H-6 rocket.

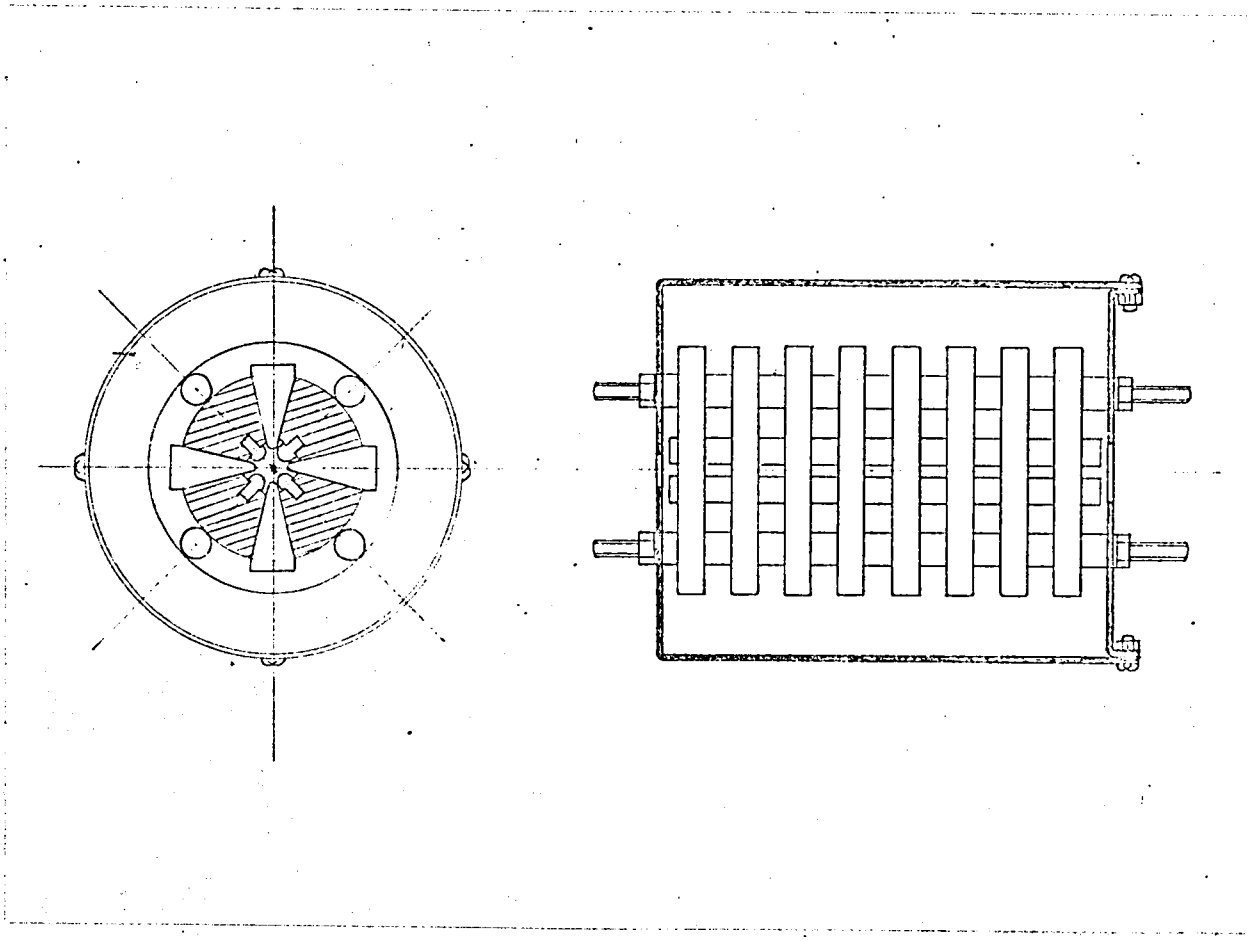

Figure 4.3 A drawing of sensor of the mass spectrometer.

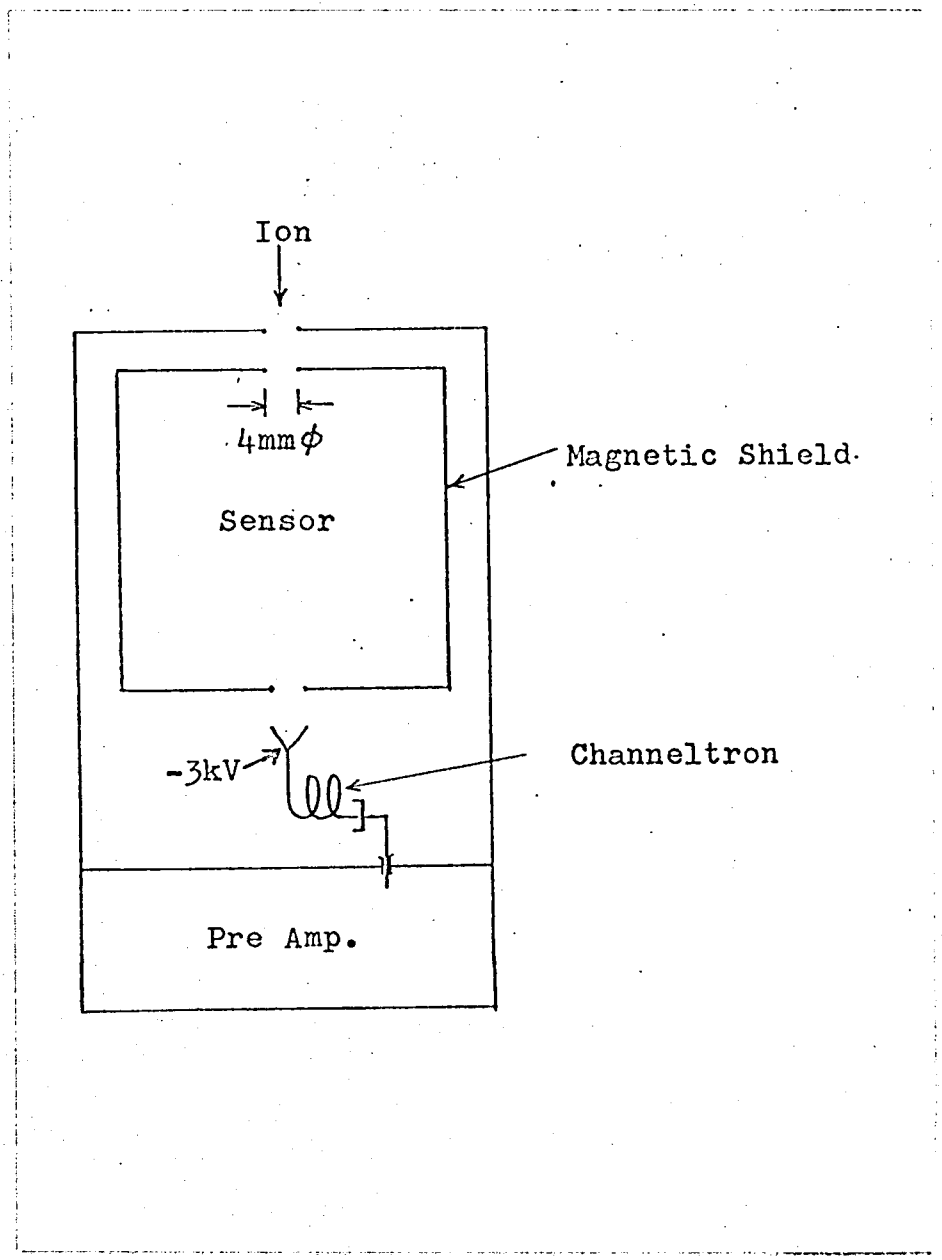

Figure 4.4 Schematic diagram of sensor part.

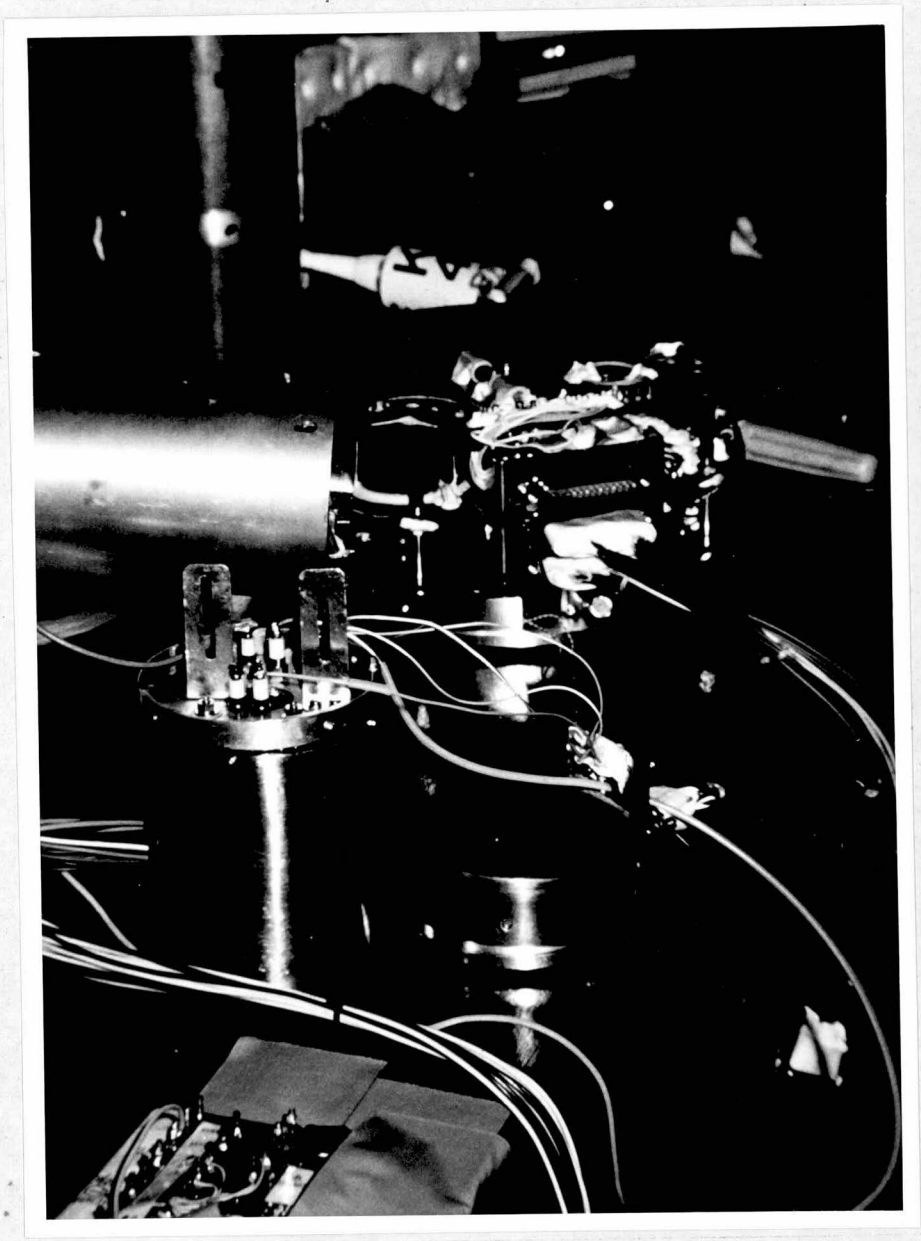

Figure 4.5 Photograph of sensor part under overhaul.

cm away from the orifice. Figure 4.5 shows an inside view of the sensor case.

4.3 Electronic Circuits

The electronic circuits which controlled the sensor and amplified the output signal were all solid state. Figure 4.6 is a circuit diagram of the pre-amplifier, log-amplifier and output buffer-amplifier. The pre-amplifier was of 10^6 ohm input impedance and of zero decibel gain. The dynamic range of the log-amplifier was about 4 orders, that is, input voltage of the range from 1 mV to 10 V corresponding to the range of 1 V to 5 V in the output. The output analog signal was sent by a FM-PM VHF telemeter.

The circuit diagram of sawtooth generator of -300 V is shown in Figure 4.7 and its timing circuit in Figure 4.8. High voltage of about -400 V was made by DC-DC converter and sawtooth voltage of $0 \sim -300$ V was directly made by a Miller integrating circuit with high voltage transistor. The sawtooth voltage was divided in a proper ratio and supplied to the sensor and

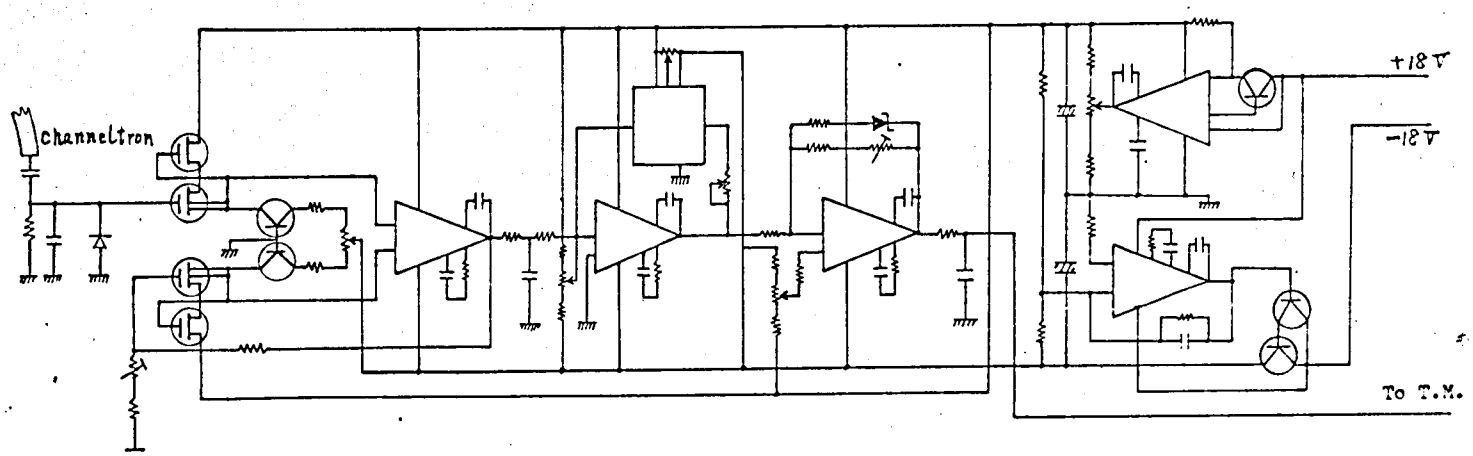

Figure 4.6 Circuit diagram of amplifier.

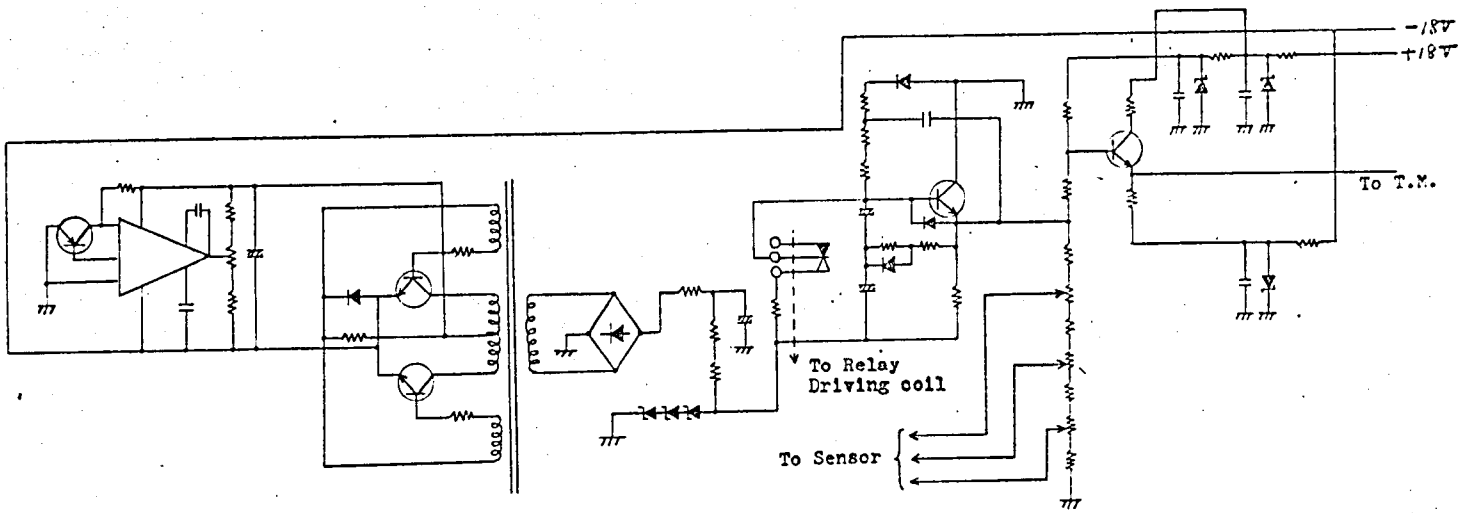

Figure 4.7 Circuit diagram of Sawtooth generator.

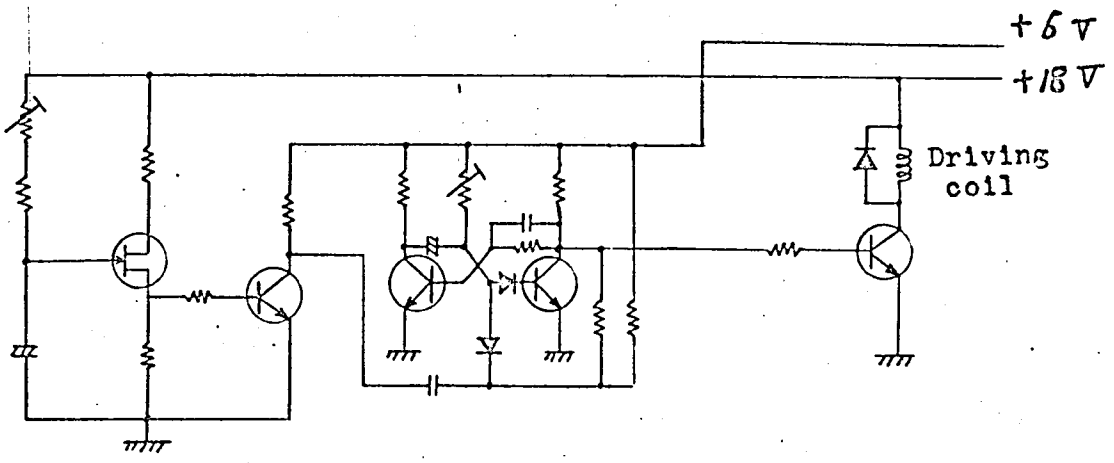

Figure 4.8 Circuit diagram of timing pulse generator.

telemeter. The resolution can be varied by changing the dividing resistor. The timing circuit drove the relay of sawtooth generating circuit in each 2 second. The high voltage of -3 kV was also made by DC-DC converter as shown in Figure 4.9.

The simple circuits described above are all electronics which are necessary for this type of mass spectrometer. Figure 4.10 shows a part of electronic circuit removed its case cover.

4.4 Pre-Flight Calibration

The pre-flight calibration was done by means of the calibration system described above. The purpose of the calibration was to insure its normal operation and to record the characteristics or voltage at the various point of the circuit to be used for data reduction such as sawtooth voltage as shown in Figure 4.11, characteristics curve between input and output of log-amplifier, linearity of amplifiers, accurate voltage of high tension circuit, sensitivity, resolution and so on. Figure 4.12 shows output at the collector of channeltron.

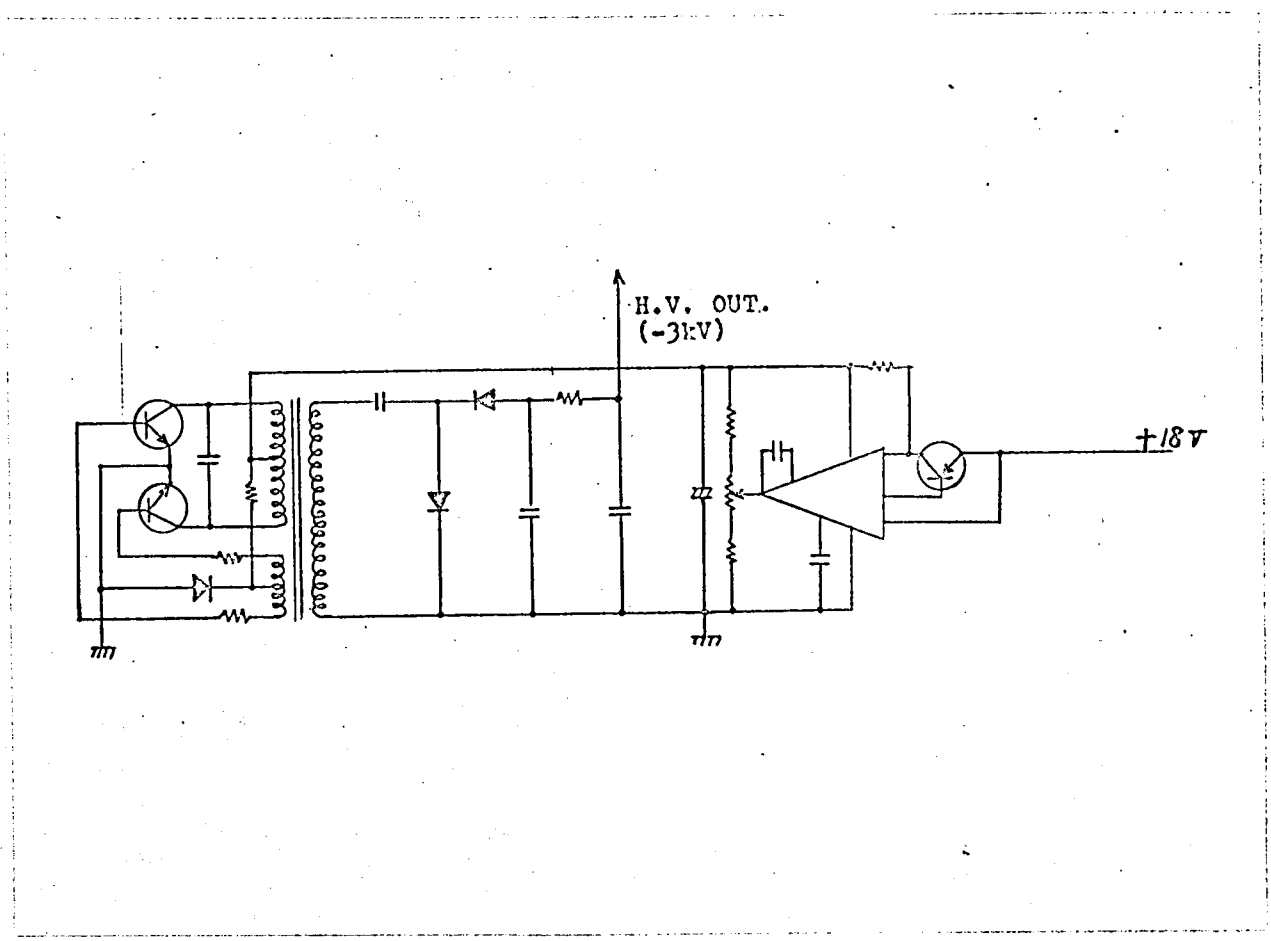

Figure 4.9 Circuit diagram of high tension circuit of 3 kV.

Figure 4.10 Photograph of electronics part.

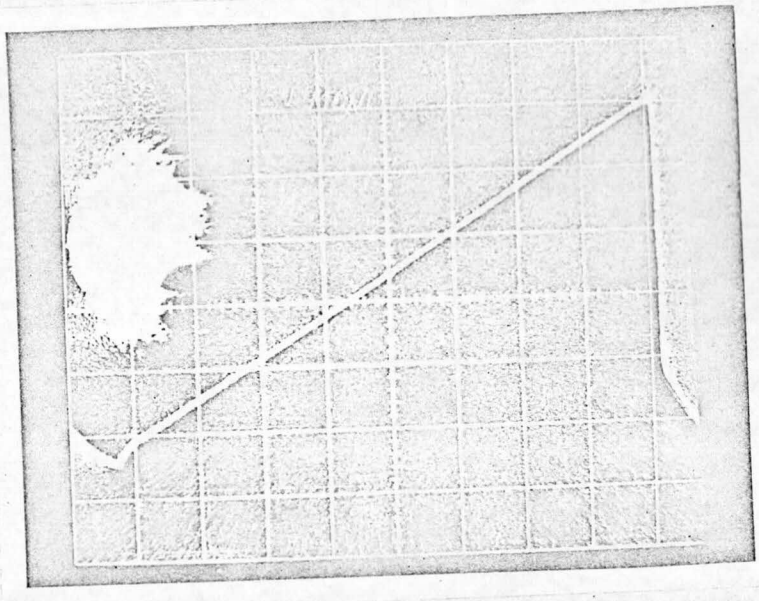

Figure 4.11 Oscilloscope trace of sawtooth accelerating voltage under pre-flight calibration.

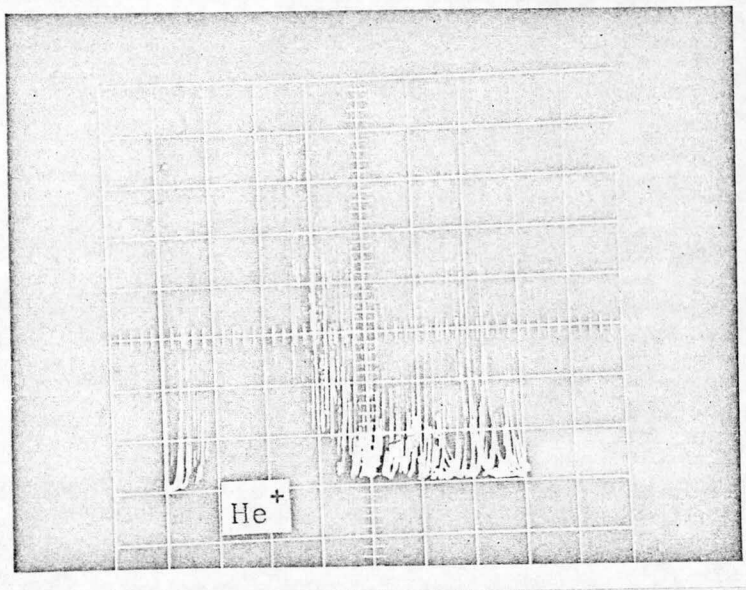

Figure 4.12 Oscilloscope trace of output signal at the collector of channeltron of the mass spactrometer in Helium atmosphere.

4.5 Integration of Payload

After installed and integrated in the rocket with many other instruments as shown in Figure 4.13, the payload was tested in various ways, such as mechanical vibration, shock, electronic operation and so on. The sensor of the mass spectrometer was installed at the top of the Lamda-3H-6 rocket. Figure 4.14 is the close up view of the sensor on the rocket.

4.6 Result of Flight Experiment

The mass spectrometer was flown by Lamda-3H-6 rocket shown in Figure 4.15, in January , 19, 1970. Though the performance of the rocket was good, the output ion current of the instrument was saturated after the moment of turning on the high voltage circuit to supply the high voltage to the channeltron. This condition continues during passing through the peak and falling down to about 500 km. After then, the saturating current rather decreased and ion mass peaks began to appear in the data though unexplained current

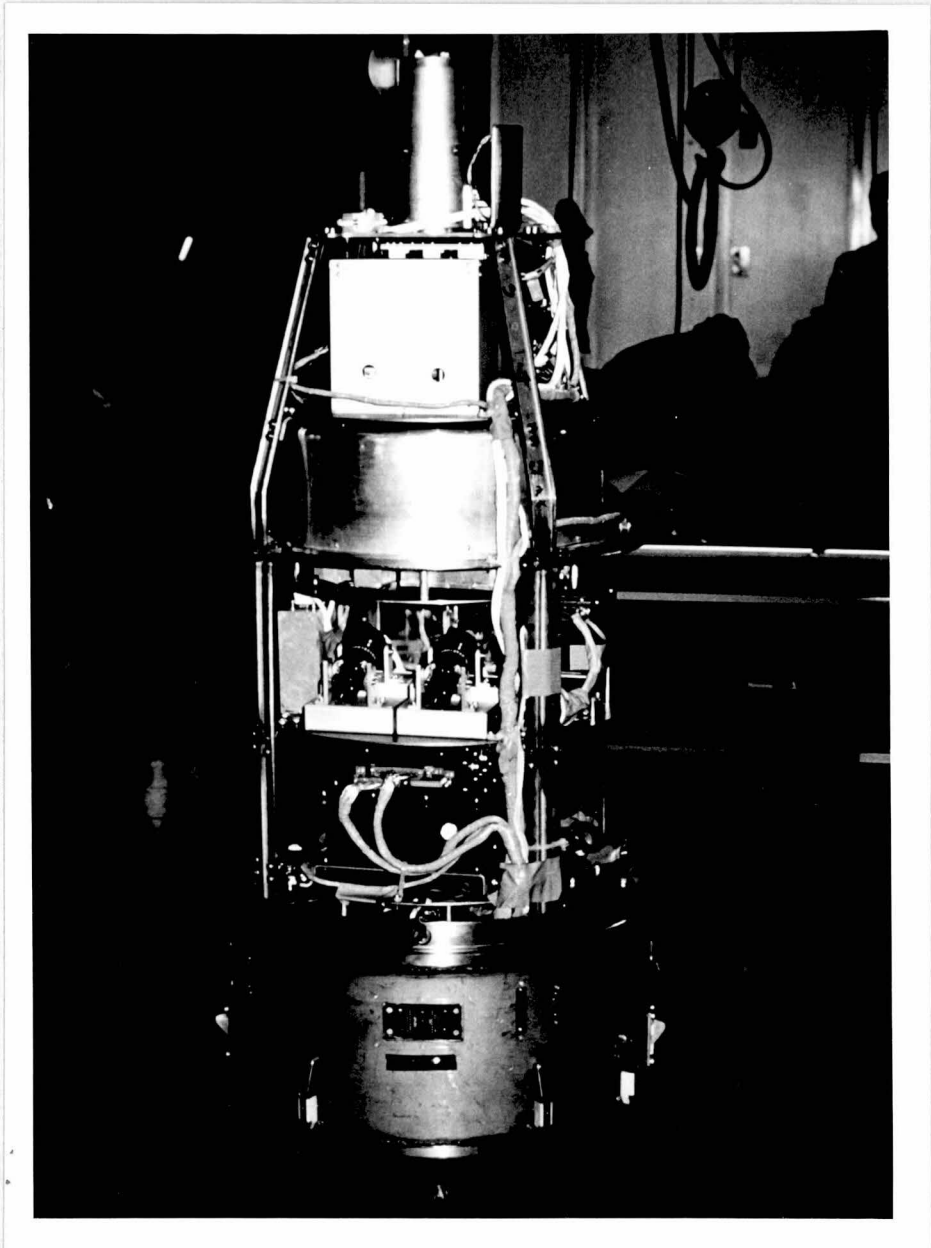

Figure 4.13 Assembled payload of Lamda-3H-6.

Figure 4.14 Close-up view of the mass spectrometer sensor on the rocket.

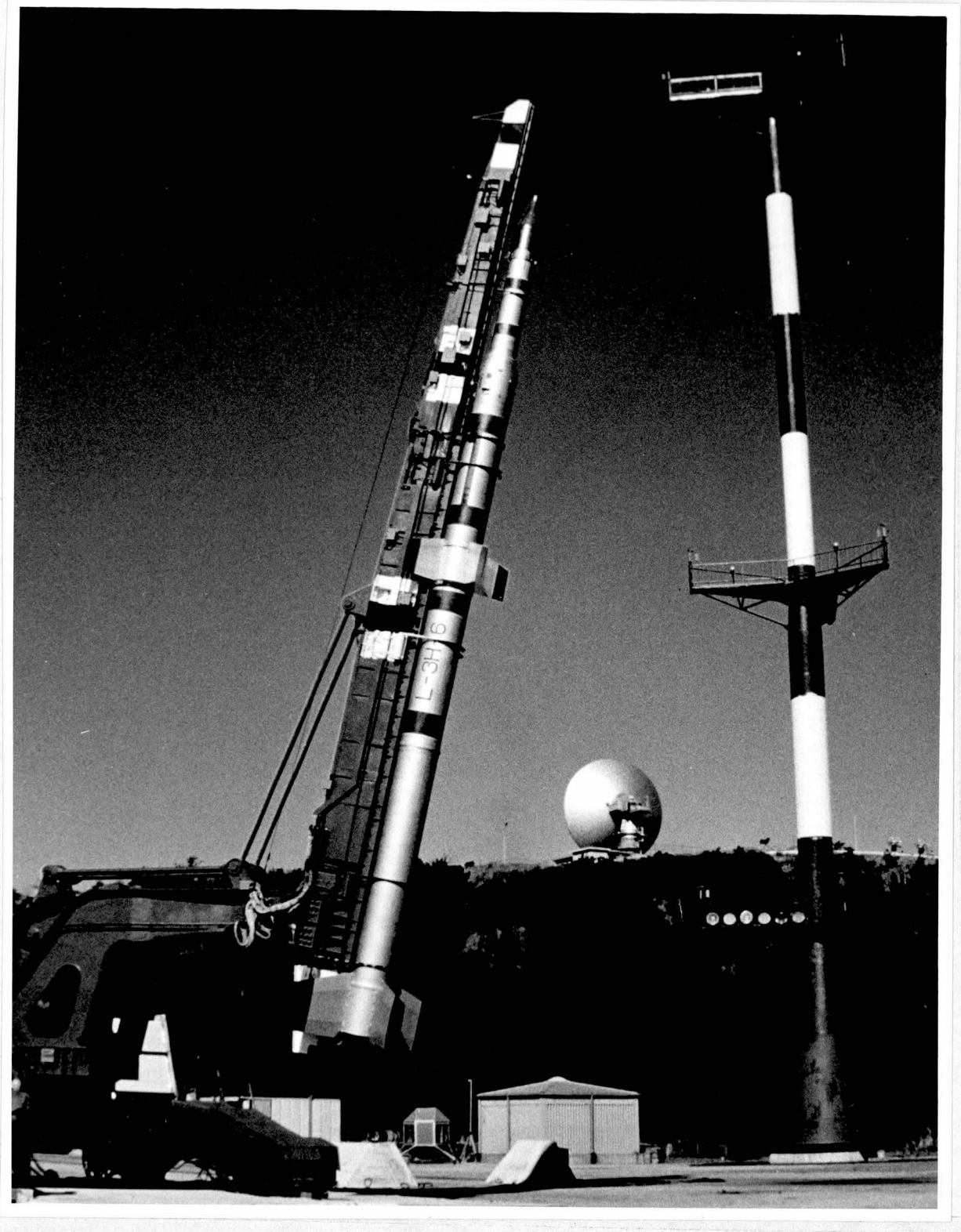

Figure 4.15 Lamda-3H-6 rocket on the launcher.

which was modulated by scanning of acceleration voltage superposed on the mass spectra. The telemetered raw data ~~is~~ are shown in Figure 4.16. In these spectra, the peaks of atomic oxygen ion which is expected as the dominant constituent at those altitude, clearly appear. Though it is not precise due to the superposed unknown current, the content of atomic oxygen is estimated more than 10^3 ion/cc.

4.7 Discussion

Though the normal operation of mass spectrometer sensor was verified in the final stage of the flight, the cause of the saturation of the ion current should be ascertained for future experiments.

It is supposed that the trouble was caused by the orifice aperture of the sensor. The sensor had been fabricated as schematically shown in Figure 4.4 but it was changed in the final integration before flight as shown in Figure 4.17, because it was conjectured that if a discharge of high voltage would occure in the electron multiplier due to slow evacuation in the

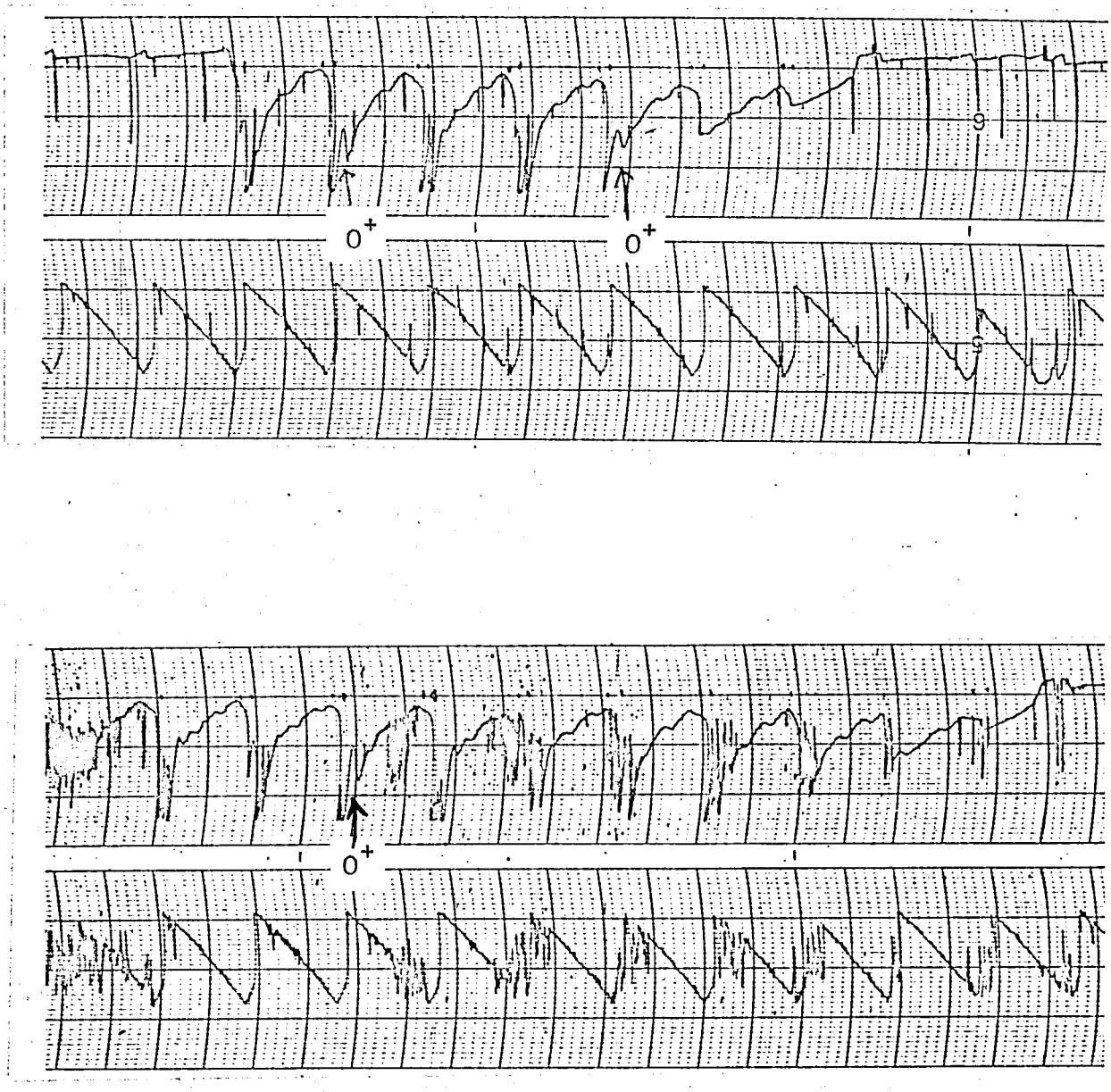

Figure 4.16 Data gotten from the flight experiment. They were gotten at about 400∼300 km of decent. Atomic oxygen ion peaks clearly appear.

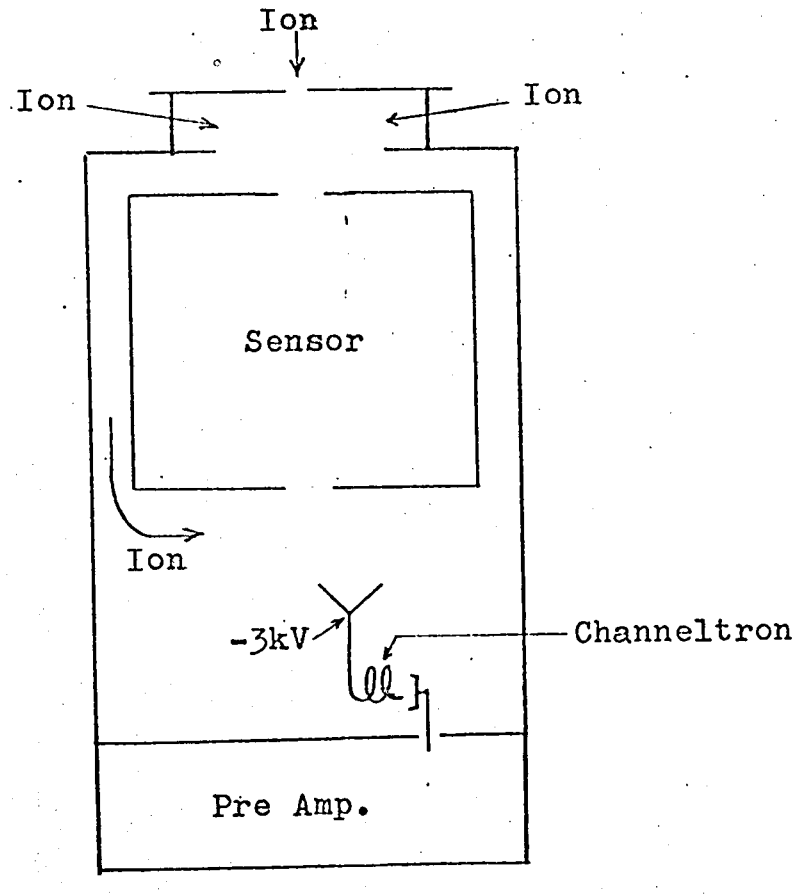

Figure 4.17 Schematic illustration of the sensor part in flight and of supposed phenomenon which caused saturation of ion current.

sensor case, it might disturb other electronicses. After this change, the orifice of the case was hold by four slender poles and orifice of the sensor on which the accelerating voltage applied was revealed to the ionospheric plasma.

It is confirmed now that the saturation was occured by the ions which were directly collected by the channeltron on which attracting high voltage was applied, without passing through the mass spectrometer as shown in Figure 4.17. The process how the ions reached from the orifice to the channeltron, is not yet clear, though many possibilities were investigated such that ions passed between case and magnetic shield or secondary ions were made by collision between the accelerated ionospheric ions and residual gases in the case. However, it is ascertained by the supplementary experiment in the calibration system described above that the same condition of saturation occurs with the sensor of lifted orifice and that the normal operation is achieved when the orifice is set following the original design. Moreover it is recognized that the operation in the wake mode reduces the saturation.

Consequently, the problem of saturation of ion current will be solved by the original structure of the

orifice. To solve the trouble of discharge, the sensor of the mass spectrometer will be put in anevacuated container as schematically shown in Figure 4.18. The inside of the container is evacuated by vacuum pump. After chipcutting the container to integrate the payload in the rocket, the vacuum is sustained by getter and the orifice will be opened at a high altitude in a trajectory for measurement. This method will be adopted in next experiment. It will be carried out by Lamda-3H-7 rocket in January 1971.

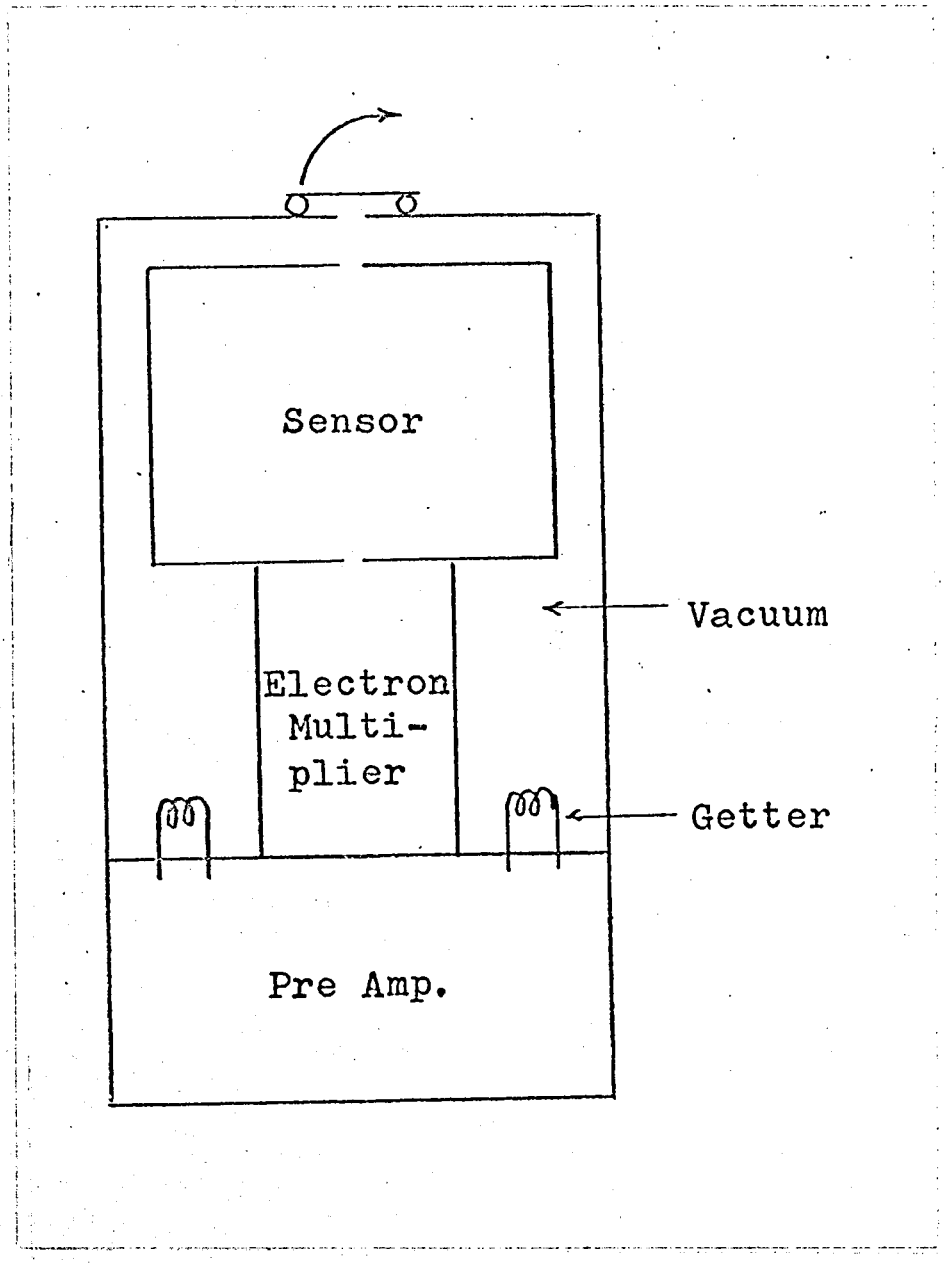

Figure 4.18 Schematic diagram of sensor part for Lamda-3H-7, which is improved to avoid discharge.

CHAPTER 5

CONCLUDING REMARKS

Before starting the observation of the upper-atmospheric composition by rocket borne mass spectrometer, the auther had made a study for all sorts of mass spectrometer about their merit and demerit as an instrument for direct measurement.

From the scientific and technical standpoints the Bennett type of mass spectrometer was adopted. It has been used to measure the ion composition of the ionosphere and it will be used for measuring ion composition of the principal part of the ionosphere on account of unnecessity of secondary electron multiplier.

Recently, with progress of various field of science, especially of semiconductor technique such as development of transistors for high voltage and high frequency or field effect transistor, the quadrupole type mass spectrometer became available. It is introduced for the measurement of ion composition in the lower ionosphere and of neutral composition.

It was decided to use a Bennett type of mass spectrometer for the first satellite experiment owing to have much experience. A static mass spectrometer, however, is desirable because of many problems such as power consumption, stable operation reliability of the system and so on. The static mass spectrometer, namely,

magnetic sector type is able to change its resolution and transparency by changing its mechanical slits. If a mass spectrometer which has the characteristics similar to a static mass spectrometer and is able to vary electronically its resolution and transparency is developed, it will be very convinient for a satellite experiment.

In order to achieve this purpose, investigations for motions of charged particles in various periodic static fields in basic case were carried out. In consequence of the investigation, a configuration of mass spectrometer which is expected to satisfy our request, was proposed. Studies for practical cases impressed its realization. The laboratory experiments with its trial production model give satisfactory results. Though the first flight experiment was not successful because of careless mistake of installation method, a normal operation of the mass spectrometer was confirmed in the final stage of the flight and the cause of the trouble was ascertained by a supplemental simulation experiment in laboratory. After improvement of the installing method, it will be used again in future experiment and will be adopted to use in future satellite projects.

At the same time, it is very important to calibrate the instruments to get the correct results from the measured data. Various problems which occured in direct experiments with space vehicle and its calibrations were investigated on mass spectrometry. According to the result, a system for calibration of mass spectrometers of space use has been constructed. The performance is satisfactory. There is not such a consistent calibration system from gas supplier to data processor as this apparatus so far as the author knows. It is able to supply various atoms, molecules and ions, and to change various parameter of them. Therefore, it will be able to use not only for mass spectrometer but also various instruments for direct measurement such as energy analyser, particle detector, various probes so on. Moreover, it was planned and designed to be able to use for plasma beam experiment and simulation experiment for chemical reaction in the upper-atmosphere in future.

ACKNOWLEDGEMENTS

The author wishes to express his hearty thanks to Proffessor K. Hirao of the Institute of Space and Areronautical Science, University of Tokyo, who was a head of the research section, to which the author belonged, of Radio Research Laboratories, Ministry Posts and Telecommunications, for his valuable guidance, discussion and support throughout the study and for the opportunity of direct measurement by rocket given. He also wishes to express his gratitude to Proffessor K. Maeda of Kyoto University, for his important suggestion and support to the study and offer of opportunity of rocket observation. The author is deeply indepted to Mr. K. Aikyo, colleague of him, for co-operation, especially for programing of electronic computer. He is owe to Mr. T. Suitsu, colleague of him, for sincere asistance. The study and rocket observation was supported by the Institute of Space and Aeronautical Science, University of Tokyo. The rocket borne instrument was accomplished by aid of Messrs. K. Watanabe, T. Kuboi and K. Umehashi of Matsushita Communication Industry Co..

REFERENCES

(1) COSPAR International Reference Atmosphere 1965, North-Holland Pub. Co., Amsterdam.

(2) Bates, D.R. and Patterson, T.N.L., "Helium Ions in the Upper Atmosphere", Planet.Space Sci., 9, 599, Oct. 1962.

(3) Geisler, J.E. and Bowhill, S.A. "Ionospheric Temperature at Sunspot Minimum", J. Atmosph. Terrest. Phys., 27, 457, 1965.

(4) Carlson, H.C. and Gordon, W.E. "Radar Spectrographic Estimates of Ionic Composition from 225 to 1400 Kilometers for Solar Minimum Winter and Summer Conditions", J. Geophys. Res., 71, 5573, 1966.

(5) Shawhan, S.D. "Negative Ion Detection in the Ionosphere from Effects on ELF Waves", J. Geophys. Res., 71, 5585, 1966.

(6) Maier, E.J.R. "Sounding Rocket Measurements of Ion Composition and Charged Particle Temperatures in the Topside Ionosphere", J. Geophys. Res., 74, 815, 1969.

(7) Evans, J.V. and Cox, L.P. "Seasonal Variation of the F_1-Region Ion Composition", J. Geophys. Res., 75, 159, 1970.

(8) Prasad, S.S. "Ionic Composition and Temperature over Arecibo 2", J. Geophys. Res., 75, 1911, 1970.

(9) D'Angelo, N. "Negative Ions in the Night Ionosphere and the Continuous Sub-ELF Emission", J. Geophys. Res., 75, 1541, 1970.

(10) Taylor, H.A., Brinton, H.C. and Deshmukh, A.R. "Observation of Irregular Structure in Thermal Ion Distributions in the Duskside Magnetosphere", J. Geophys. Res., 75, 2481, 1970.

(11) Lehmann, H.-R. and Wagner, Chr. -Ulr. "Meteoric Atomic Ions in the Lower Ionosphere", J. Atmos. Terr. Phys., 28, 617, 1966.

(12) Lebedinets, V.N. "On the Mechanism of Formation of a Region of Higher Atomic Density with Atoms of Meteoric Origin at 100~110 km", Space Res., IV, 553, 1964.

(13) Jones, A.V. "Abundance of Metallic Atoms in the Atmosphere", Ann. Geophysique, 22, 189, 1966.

(14) Bowen, P.J., Boyd, R.L.F., Raitt, W.J. and Willmore, A.P. "Ion Composition of the Upper F-Region", Proc. Roy. Soc., A.281, 504, 1964.

(15) Thomas, J.O. and Dufour, S.W. "Electron Density in the Whistler Medium", Nature, No.4984, 567, 1965.

(16) Gadsden, M. "Sodium in the Upper Atmosphere Meteoric Origin", J. Atmos. Terr. Phys., 30, 151, 1968.

(17) Sullivan, H.M. and Hunten, D.M. "Lithium, Sodium and Potassium in the Twilight Airglow", Can. J. Phys., 42, 937, 1964.

(18) Narcisi, R.S. "Ion Composition of the Mesosphere", Space Research VII, Noth Holland Pub. Co., Amsterdam.

(19) Narcisi, R.S., Bailey, A.D. and Della Lucca, L. "Composition Measurements of Sporadic E in the Nighttime Lower Ionosphere", Space Res., VII, 123, 1967.

(20) Narcisi, R.S., Bailey, A.D. and Della Lucca, L. "The Composition of the Lower Ionosphere during the 1965 Leonid Meteor Shower", Space Res., VII, 446, 1967.

(21) Nier, A.O., Hoffman, J.H., Johnson, C.Y. and Holmes, J.C. "Neutral Composition of the Atmosphere in the 100- to 200-Kilometer Range", J. Geophys. Res., 69, 979, 1964.

(22) Hedin, A.E. and Nier, A.O. "Diffusive Separation in the Upper Atmosphere", J. Geophys. Res., 70, 1273, 1965.

(23) Nier, A.O., Hoffman, J.H., Johnson, C.Y. and Holmes, J.C. "Neutral Constituent of the Upper Atmosphere: The Minor Peaks Observed in a Mass Spectrometer", J. Geophys. Res., 69, 4629, 1964.

(24) Hoffman, J.H., Johnson, C.Y., Holmes, J.C. and Young, J.M. "Daytime Midlatitude Ion Composition Measurements", J. Geophys. Res., 74, 6281, 1969.

(25) Krankowsky, D., Kasprzak, W.T. and Nier, A.O. "Mass Spectrometric Studies of the Composition of the Lower Thermosphere during Summer 1967", J. Geophys. Res., 73, 7291, 1968.

(26) Hoffman, J.H. "Mass Spectrometer Measurements of Ionospheric Composition", International Conference on Mass Spectroscopy, Kyoto Japan 1969.

(27) Hoffman, J.H. "Ion Mass Spectrometer on the Explorer XXXI Satellite", Proc. IEEE, 57, 1969.

(28) Hoffman, J.H. "Composition Measurement of Topside Ionosphere", Science 155, 322, 1967.

(29) Townsend, J.W.Jr., Meadows, E.B. and Pressly, E.C. "A Mass Spectrometric Study of the Upper Atmosphere", in Rocket Exploration of the Upper Atmosphere, Edited by R.L.F.Boyd and M.J.Seaton, Pergamon Press Ltd., London, 1954.

(30) Johnson, C.Y. and Meadows, E.B. "First Investigation of Ambient Positive-Ion Composition to 219 km by Rocket Borne Spectrometers", J. Geophys. Res., 60, 193, 1955.

(31) Meadows, E.B. and Townsend, J.W.Jr. "Diffusive Separation in the Winter Night-time Arctic Upper Atmosphere 112 to 150 km", Ann. Geophysique, 14, 80, 1958.

(32) Johnson, C.Y., Meadows, E.B. and Holmes, J.C. "Ion Composition of the Arctic Ionosphere", J. Geophys. Res., 63, 443, 1958.

(33) Meadows, E.B. and Townsend, J.W.Jr. "IGY Rocket Measurements of Arctic Atmospheric Composition above 100 km", Space Res.,I, 175, 1961.

(34) Taylor, H.A.Jr., Brace, L.H., Brinton, H.C. and Smith, C.R. "Direct Measurements of Helium and Hydrogen Ion Concentration and Total Ion Density to an Altitude of 940 Kilometers", J. Space Res., 63, 5339, 1963.

(35) Johnson, C.Y. "Aeronomic Parameters from Mass Spectrometry", Ann. Geophysique, 17, 100, 1961.

(36) Meadows-Read, E. and Smith, C.R. "Mass Spectrometric Investigations of the Atmosphere between 100 and 227 Kilometers above Wallops Island, Virginia", J. Geophys. Res., 69, 3199, 1964.

(37) Holmes, J.C. and Johnson, C.Y. "Probing the Upper Atmosphere", Anal. Chem., 30, 19, 1958.

(38) Johnson, C.Y., Heppner, J.P., Holmes, J.C. and Meadows, E.B. "Results Obtained with Rocket-Borne Ion Spectrometers", Ann. Geophysique, 14, 475, 1958.

(39) Taylor, H.A.Jr., Brinton, H.C. and Smith, C.R. "Positive Ion Composition in the Magnetoionosphere Obtained from the OGO-A Satellite", J. Geophys. Res., 70, 5769, Dec. 1965.

(40) Pokhunkov, A.A. "Gravitational Separation, Composition and Structural Parameters of the between 100 and 210 km", Planet. Space Sci., 11, 441, 1963.

(41) Pokhunkov, A.A. "Gravitational Separation, Composition and Structural Parameters of the Atmosphere at Altitudes above 100 km", Space Res., III, 132, 1963.

(42) Pokhunkov,A.A. "On the Variation in the Mean Molecular Weight of Air in the Night Atmosphere at Altitudes of 100 to 210 km from Mass Spectrometer Measurements", Planet. Space Sci., 11, 297, 1963.

(43) Istomin, V.G. "Magnesium and Calsium in the Earth's Upper Atmosphere", NASA. Tech. Trans. F-69, 1961.

(44) Istomin, V.G. "Ions of Extra-Terrestrial Origin in the Earth Ionosphere", Planet. Space Sci.,11, 173, 1963. and Space Res., III, 209, 1963.

(45) Istomin, V.G. "Absolute Concentrations of Ion Components of the Earth's Atmosphere at Altitudes between 100 and 200 km", Planet. Space Sci., 11, 169, 1963.

(46) Istomin, V.G. and Pokhunkov, A.A. "Mass Spectrometer Measurements of Atmospheric Composition in the USSR", Space Res., III,117, 1963.

(47) Istomin, V.G. "Observational Results on Atmospheric Ions in the Region of the Outer Ionosphere", Ann. Geophysique, 22, 255, 1966.

(48) Istomin, V.G. "Some Results of the Measurement of the Spectrum Mass of Positive Ions by the 3rd Artificial Earth Satellite", NASA., Tech. Trans., F-7, 1960.

(49) Pokhunkov, A.A. "Mass-Spectrometer Investigations of the Structural Parameters of the Earth's Atmosphere at Altitudes from 100 to 210 km", Planet. Space Sci., 10, 269, 1962.

(50) Young, J.M., Johonson, C.Y. and Holmes, J.C. "Positive Ion Composition of a Temperature-Latitude Sporadic E Layer as Observed during a Rocket Flight", J. Geophys. Res., 72, 1473, 1967.

(51) Brinton, H.C., Pickett, R.A. and Taylor, H.A.Jr. "Diurnal and Seasonal Variation of Atmospheric Ion Composition; Correlation with Solar Zenith Angle", J. Geophys. Res., 74, 4064, 1969.

(52) Brinton, H.C., Pharo, M.W., Mayr, H.G. and Taylor, H.A.Jr.," Implication for Ionospheric Chemistry and Dynamics of a Direct Measurement of Ion Composition", J.Geophys. Res., 74, 2941, 1969.

(53) Goldberg, R.A. and Blumle, L.J. "Positive Ion Composition from a Rocket-Borne Mass Spectrometer", J.Geophys. Res., 75, 133, 1970.

(54) von Zahn, U. and Gross, J. "Mass Spectrometric Investigation of the Thermosphere at High Latitudes", J.Geophys. Res., 74, 4055, 1969.

(55) Schaefer, E.J. "Composition and Temperature of the Neutral Tropic Lower Thermosphere", J.Geophys. Res., 74, 3488, 1969.

(56) Müller, D. and Hartmann, G. "A Mass Spectrometric Investigation of the Lower Thermosphere above Fort Churchill with Special Emphasis on the Helium Content", J. Geophys. Res., 74, 1287, 1969.

(57) Narcisi, R.S. and Bailey, A.D. "Mass Spectrometry in the D-Region Ionosphere-Apparatus, Techniques and First Measurements", AFCRL. Env. Res. Paper, No.82, 1965.

(58) Narcisi, R.S. "Ion Composition Measurements and Related Ionospheric Processes in the D and Lower E Region", AFCRL. Env. Res. Paper, No.230, 1966.

(59) Narcisi, R.S. and Bailey, A.D. "Mass Spectrometric Measurements of Positive Ions at Altitudes from 64 to 112 Kilometers", J. Geophys. Res., 70, 3687, 1965.

(60) Schaefer, E.J. and Nichols, M.H. "Upper Air Neutral Composition Measurements by a Mass Spectrometer", J. Geophys. Res., 69, 4649, 1964.

(61) Schaefer, E.J. and Nichols, M.H. "Neutral Composition Obtained from a Rocket-Borne Mass Spectrometer", Space Res., IV, 205, 1964.

(62) Schaefer, E.J. "The Dissociation of Oxygen Measured by a Rocket-Borne Mass Spectrometer", J. Geophys. Res., 68, 1175, 1963.

(63) Schaefer, E.J. and Brown, J. "Additional Rocket-Borne Mass Spectrometer Measurements of the Dissociation of Oxygen", J. Geophys. Res., 69, 1455, 1964.

(64) Hall, L.A., Schweizer, W. and Hinteregger, H.E. "Improved Extreme Ultraviolet Absorption Measurements in the Upper Atmosphere", J.Geophys. Res., 70, 105, 1965.

(65) Carver, J.H., Mitchell, P. and Murray, E.L. "Molecular Oxygen Density and Lyman-α Absorption in the Upper Atmosphere", J. Geophys. Res., 69, 3755, 1964.

(66) Rawcliff, R.D., Meloy, G.E., Friedman, R.M. and Rogers, E.H., "Measurement of Vertical Distribution of Ozone from a Polar Orbiting Satellite", J. Geophys. Res., 68, 6425, 1963.

(67) Oshio, T. "Instruments for Observation of $\lambda < 2000$ Å", Proceeding of Symposium on Instruments for Scientific Observation of the Space. Institute of Space and Aeronautical Science, Univ. of Tokyo. Feb., 1967 (in Japanese).

(68) Jones, R.A., Bruner, E.C.Jr. and Rense, W.A. "Absorption Measurements of Earth's Hydrogen Atmosphere from Solar Hydrogen Lyman Alpha Rocket Data", J. Geophys. Res., 75, 1849, 1970.

(69) Quessette, J.-A. "On the Measurement of Molecular Oxygen Concentration by Absorption Spectroscopy", J. Geophys. Res., 75, 839, 1970.

(70) Zipf, E.C.Jr. and Fastie, W_M.G. "An Observation of the (O,O) Negative Band of N_2^+ in the Dayglow", J. Geophys. Res., 69, 2357, 1964.

(71) Zipf, E.C.Jr. and Fastie, W_M. G. "An Observation of Day Airglow Emission at 6300 Å", J. Geophys. Res., 68, 6208, 1963.

(72) Barth, C.A. "Rocket Measurement of the Nitric Oxyde Dayglow", J. Geophys. Res., 69, 3301, 1964.

(73) Golomb, D., Rosenberg, N.W. and Aharonian, C. "Oxygen Atom Determination in the Upper Atmosphere by Chemiluminescence", J. Geophys. Res., 70, 1155, 1965.

(74) Nakamura, J. "Chemical Release", Proceeding of Symposium on Instruments for Scientific Observation of the Space. Institute of Space and Aeronautical Science, Univ. of Tokyo. 1967 (in Japanese).

(75) Nier, A.O. "Application of Mass Spectroscopy to Upper Atmosphere and Space Research", International Conference on Mass Spectroscopy Kyoto Japan 1969.

(76) Nier, A.O. "Small Grneral Purpose Double Focusing Mass Spectrometer", Rev. Sci. Instr., 31, 1127, 1960.

(77) Hedin, A.E., Avery, C.P. and Tschetter, C.D. "An Analysis of Spin Modulation Effects on Data Obtained with a Rocket-Borne Mass Spectrometer", J. Geophys. Res., 69, 4637, 1964.

(78) Spencer, N.W. and Reber, C.A. "A Mass Spectrometer for an Aeronony Satellite", Space Res., III, North-Holland Pub. Co., 1963.

(79) Hinteregger, H.H. and Damon, K.R. "Analysis of Photoelectrons from Solar Extreme Ultraviolet", J. Geophys. Res., 64, 961, 1959.

(80) Mckibbin, D.D. "A Direct Measurement of Charge Density in the F_2 Region", IRE. Trans. Instr., 96, Dec. 1962.

(81) Whipple, E.C.Jr. "The Ion-Trap Results in Exploration of the Upper Atmosphere with the Help of the Third Soviet Sputnik", Proc. IRE. 47, 2023, 1959.

(82) Hanson, W.B. and Mckibbin, D.D. "An Ion-Trap Measurement of the Ion Concentration Profile above the F_2 Peak", J. Geophys. Res., 66, 1667, 1961.

(83) Sharp, G.W., Hanson, W.B. and Mckibbin, D.D. "Some Ionospheric Measurements with Satellite-Borne Ion Traps", Space Res., IV, 454, 1964.

(84) Bourdeau, R.E. and Bauer, S.J. "Structure of the Upper Atmosphere Deduced from Charged Particle Measurements on Rockets and the Explorer VIII Satellite", Space Res., III, 173, 1963.

(85) Gringauz, K.I., Gorozhankin, B.N., Shutte, N.M. and Gdalevich, G.L. "Changes of the Distribution of Charged Particle Density with Height and of the Ionic Composition of the Outer Ionosphere Scince the Solar Activity Maximum According to Data Collected by Ion Traps on the COSMOS 2 Satellite", Space Res., IV, 473, 1964.

(86) Niemann, H.B. and Kennedy, B.C. "Omegatron Mass Spectrometer for Partial Pressure Measurements in Upper Atmosphere", Rev. Sci. Instr., 37, 722, 1966.

(87) Jayaram, R. "Mass Spectrometry Theory and Applications", Plenum Press New York, 1966.

(88) Kiser, R.W. "Introduction of Mass Spectrometry and Its Application", Prentice-Hall, Inc. Englewood Cliffs, N.J., 1965.

(89) Barrington, A.E. "Aerospace Mass Spectrometry", Aerospace Measurement Technique NASA SP-132, 1966.

(90) Blauth, E.W. "Dynamic Mass Spectrometers", Elsevier Pub. Co., Amsterdam.

(91) Bennett, W.H. "Radiofrequency Mass Spectrometer", J. Appl. Phys. 21, 143, 1950.

(92) Wherry, T.C. and Karasek, F.W. "Performance of the Nonmagnetic Radiofrequency Mass Spectrometer Tube", J.Appl. Phys., 26, 682, 1955.

(93) Cannon, W.W. and Testerman, M.K. "Accurate Mathematical Treatment of Analyzer of the RF Mass Spectrometer Tube", J. Appl. Phys., 27, 1283, 1956.

(94) Johnson, C.Y. "Mass Determination of Ions Detected by Bennett Ion RF Mass Spectrometer", J. Appl. Phys., 29, 740, 1958.

(95) Townsend, J.W.Jr. "Radiofrequency Mass Spectrometer for Upper Air Research", Rev. Sci. Instr., 23, 538, 1952.

(96) Johnson, C.Y. "Two-Stage Single Cycle Radio Frequency Mass Spectrometer", Space Res., III, 1144, 1963.

(97) Pokhunkov, A.A. "On the Variation in the Mean Molecular Weight of Air in the Night Atmosphere at Altitudes of 100 to 210 km from Mass Spectrometer Measurements", Planet. Space Sci., 11, 297, 1963.

(98) Pokhunkov, A.A. "Mass Spectrometer Measurements of Helium Nitrogen and Argon Distribution in the Earth's Atmosphere above 130 km", Space Res., IV, 325, 1964.

(99) Zarkhin, B.I., Istomin, V.G., Rafalson, A.E. and Slutskii, M.E. "Radio-Frequency Mass Spectrometer for "ELEKTRON" Satellites", Cosmic Res., 3, 626, 1965.

(100) Shcherbakova, M.Ya. "Optimum Analyzer Designs for Radio-Frequency Mass Spectrometers with Two and Three Drift Spaces", Cosmic Res., 3, 221, 1965.

(101) Istomin, V.G. "Radio-Frequency Mass Spectrometer for the Investigation of the Ionic Composition of the Upper Atmosphere", NASA. Tech. Trans. F-53, 1961.

(102) Paul, W. and Steinwedel, H. "Ein Neues Massenspektrometer Ohne Magnetfeld", Z. Naturforsch., 89, 44, 1953.

(103) Paul, W. and Raether, M. "Das Electrische Massenfilter", Z. Phys., 140, 262, 1955.

(104) Paul, W., Reinhard, H.P. and von Zahn, U. "Das Electrische Massenfilter als Massenspektrometer und Isotopentrenner", Z. Physik, 152, 143, 1958.

(105) Flowerday, T.W. "An Instrument for Measuring Ion Composition of the Upper Atmosphere", IEEE. Trans. Instr. and Meas., 14, Mar. 1964.

(106) Bailey, A.D. and Narcisi, R.S. "Miniature Mass Spectrometers for Upper Atmosphere Composition Measurements", AFCRL. Instr. Paper, No.95, 1966.

(107) von Zahn, U. "Monopole Spectrometer: a New Electric Field Mass Spectrometer", Rev. Sci. Instr., 34, 1, 1963.

(108) Dawson, P.H. and Whetten, N.R. "Ion Storage in Three-Dimensional, Rotationally Symmetric Quadrupole Field", J.Vac. Sci. Tech., 5, 1, 1968.

(109) Grossmann, U. and Offermann, D. "Neutral Composition Measurements in the Lower Thermosphere by Means of a Cooled Ion Source", COSPAR. 13th, Plenary Meeting, May 1970.

(110) Courant, E.D., Livingston, M.S. and Snyder, H.S. "The Strong-Focusing Synchroton: A New High Energy Accelerator", Phys. Rev., 88, 1190, 1952.

(111) Clogston, A.M. and Heffner, H. "Forcusing of Electron Beam by Periodic Fields", J. Appl. Phys., 25, 437, 1954.

(112) Tien, P.K. "Focusing of Long Cylindrical Electron Stream by Means of Periodic Electrostatic Fields", J. Appl. Phys., 25, 1281, 1954.

(113) von Taubert, R. "Ein Electrostatisches Energiefilter", Z. Naturforschg., 12a, 169, 1957.

(114) Fugono,N. and Aikyo, K. "A Flyable Mass Spectrometer Using the Spatially Periodic Static Field (I)", J. Radio Res. Lab.; 15, 17, 1968. and Rev. Radio Res. Lab., 14, 368, 1968(in Japanese).

(115) Fugono, N. "A mass Spectrometer Using the Spatially Periodic Static Field", Bulletin of the Institute of Space and Aeronautical Science, University of Tokyo, 6, 190, 1970 (in Japanese).

(116) Fugono, N. "Mass Spectrometer Using Alternating Electromagnetic Fields", Record of 38th Convension of Society of Terrestrial Magnetism and Electricity Japan 1965.

(117) Fugono, N. "A Mass Spectrometer Using Spatially Periodic Static Field", Rec. 42th Conv. Soc. Terr. Mag. Elec. Japan. 1967.

(118) Fugono, N. and Aikyo, K. "A Mass Spectrometer Using Spatially Periodic Static Field(II)", Rec. 44th Conv. Soc. Terr. Mag. Elec. Japan. 1968.

(119) Fugono, N. and Aikyo, K. "A Mass Spectrometer Using Spatially Periodic Static Field(III)", Rec. 46th Conv. Soc. Terr. Mag. Elec. Japan. 1969.

(120) Fugono, N. "Ionic Composition of the Upper Atmosphere", Rev. Radio Res. Lab., 14, 193, 1968 (in Japanese).

(121) Fugono, N. "Upper Atmospheric Composition and its Measurements", Rev. Radio Res. Lab., 11, 378, 1965 (in Japanese).

(122) Fugono, N. "Measurement of the Upper Atmosphere Using Rockets and Satellites", J. Vac. Soc. Japan., 12, 1, 1969(in Japanese).

(123) Fugono, N. "Mass Spectrometry ", Proceeding of Symposium on Instruments for Scientific Observation of the Space. Institute of Space and Aeronautical Science, Univ. of Tokyo,1967 (in Japanese).

(124) Fugono, N. "Ionospheric Instrumentation Technique with Space Vehicle: Velocity and Atitude", Rev. Radio Res. Lab., 14, 29, 1968(in Japanese).

(125) Fugono, N,, Aikyo, K., Utagawa, R. and Suitsu, T. "A Mass Spectrometer on the Ionosphere Sounding Satellite and its Calibration(I)", J. Radio Res. Lab., 16, 67, 1969. and Rev. Radio Res. Lab., 14, 579, 1968 (in Japanese).

(126) Fugono, N. "Bennett Type Radio Frequency Mass Spectrometer to be Borne in Rocket", Rev. Radio Res. Lab., 11, 138, 1965 (in Japanese).

(127) Fugono, N. "Simulation Experiments of Chemical Reactions in the Ionosphere", Rev. Radio Res.,Lab., 15, 356, 1969.(in Japanese).

(128) Moon, P. and Spencer, D.E. "Field Theory for Engineers", D. Van Nostrand Co. Princeton, N.J., 1961.

(129) Binns, K.J. and Lawrenson, P.J. "Analysis and Computation of Electric and Magnetic Field Problems", Pergamon Press, 1963.

(130) Vitkovitch, D. "Field Analysis: Experimental and Computational Methods", D. Van Nostrand Co. London, 1966.

(131) Pierce, J.R. "Theory and Design of Electron Beams", D.Van Nostrand Co. Inc. New York,

(132) Mclachlan, N.W. "Theory and Application of Mathieu Function", Dover Pub. Inc. New York,

(133) Whipple, Jr. E.C. "The Equilibrium Electric Potential of a Body in the Upper Atmosphere and in Interplanetary Space", NASA X-615-65-296, 1965.

(134) Al'pert, Ya. L., Gurevich, A.V. and Pitaevskii, L.P., "Space Physics with Artificial Satellites", Consultants Bureau New York, 1965.

(135) Scott, L.R. "The Ion Flux Characteristics at the Surface of a Charged Spherical Satellite", Tech. Rep., 807, Univ. of Maryland

(136) Onchi, M. "Conductivity and Surface Potential Change of Cadmium Film Due to Adsorption", Trans. 10th Nat. Vac. Symp., 1963.

(137) Keii, T. "Adsorption", Kyoritsu Shuppan Co. Tokyo, 1965 (in Japanese).

(138) Whittick, J.S., Muraca, R.F. and Cavanagh, L.H. "Analytical Chemistry Instrumentation", NASA SP - 5083, 1966.

(139) Collins, D.T. and Hoenig, S.A. "Chemisorption Detector for Oxygen", Rev. Sci. Instr., 35, 15, 1964.

(140) Halpert, G. et al. "Analysis for Oxygen by Gas-Phase Polarography at Low Temperature and Low Pressure, A Prototype Assembly", Rev. Sci. Instr., 35, 950, 1964.

(141) Eisenstadt, M.M. and Hoenig, S.A. "Chemisorption Detector for Hydrogen", Rev. Sci. Instr., 36, 66, 1965.

(142) Narcisi, R.S., Schiff, H.I., Morgan, J.E. and Cohen, H.A. "Calibration of a Flyable Mass Spectrometer for N and O Atom Sensitivity", Space Res., III, 1156, 1963.

(143) "Chemical Reactions in the Lower and Upper Atmosphere", Proc. Internat. Symp., Stanford Res. Inst., April 1961, John Wiley and Sons.

(144) Ferguson, E.E. and Fehsenfeld, F.C. "Some Aspects of the Metal Ion Chemistry of the Earth's Atmosphere", J. Geophys. Res., 73, 6215, 1968.

(145) Schmeltakopf, A.L., Fehsenfeld, F.C., Gilman, G.I. and Ferguson, E.E. "Reaction of Atomic Oxygen Ions with Vibrationally Excited Nitrogen Molecules", Planet. Space Sci., 15, 401, 1967.

(146) Kaufman, F. "The Airglow and its Use in the Study of Some Reactions of Atomic Oxygen", Proc. Roy. Soc., A 247, 123, 1958.

(147) Morgan, J.E., Elias, L. and Schiff, H.I. "Recombination of Oxygen Atoms in the Absence of O_2^*", J. Chem. Phys., 33, 930, 1960.

(148) Bately, P.H., Court, G.P. and Sayers, J. "Afterglow Measurements of the Rate Coefficients for the Reactions $O^+ + O_2 \rightarrow O_2^+ + O$ and $O^+ + N_2 \rightarrow NO^+ + N$ ", Planet. Space Sci., 13, 911, 1965.

(149) Fehsenfeld, F.C., Schmeltekopf, A.L. and Ferguson, E.E. "Correction in the Laboratory Measurement of the Rate Constant for $N_2^+ + O_2 \rightarrow N_2 + O_2^+$ at 300°K", Planet. Space Sci., 13, 919, 1965.

(150) Fehsenfeld, F.C., Schmeltekopf, A.L. and Ferguson, E.E. "Some Measured Rates for Oxygen and Nitrogen Ion-Molecule Reactions of Atmospheric Importance, Including $O^+ + N_2 \rightarrow NO^+ + N$ ", Planet. Space Sci., 13, 219, 1965.

(151) Fehsenfeld, F.C., Schemeltekopf, A.L., Schiff, H.I. and Ferguson, E.E. "Laboratory Measurements of Negative Ion Reactions of Atmospheric Interest", Planet. Space Sci., 15, 373, 1967.

(152) Fehsenfeld, F.C., Schmeltekopf, A.L., Goldan, P.D., Schiff, H.I. and Ferguson, E.E. "Thermal Energy Ion-Neutral Reaction Rates(I): Some Reactions of Helium Ions", J. Chem. Phys., 44, 4087, 1966.

(153) Goldan, P.D., Schmeltekopf, A.L., Fehsenfeld, F.C., Schiff, H.I. and Ferguson, E.E. "Thermal Energy Ion-Neutral Reaction Rates(II): Some Reactions of Ionospheric Interest", J.Chem. Phys., 44, 4095, 1966.

(154) Fehsenfeld, F.C., Ferguson, E.E. and Schmeltekopf, A.L. "Thermal-Energy Ion-Neutral Reaction Rates (III): The Measured Rate Constant for the Reaction $O^+(^4S) + CO_2(^1\Sigma) \longrightarrow O_2^+(^2\Pi) + CO(^1\Sigma)$ ", J. Chem. Phys., 44, 1966.

(155) Ferguson E.E., Fehsenfeld, F.C., Goldan, P.D. and Schmeltekopf, A.L. "Positive Ion-Neutral Reactions in the Ionosphere", J.Geophys. Res., 70, 4323, 1965.

APPENDIX

1. Equations Governing Ionic Trajectories

$$\frac{d^2x}{dt^2} + (a + 2q\phi(t))x = 0 \qquad (1)$$

In case of $\phi(t) = \cos 2t$, Equation (1) is known as Mathieu equation. In order to investigate the behavior of trajectories, we assume three types of functions as $\phi(t)$: that is,

① cosine function $\phi(t) = \cos 2t$

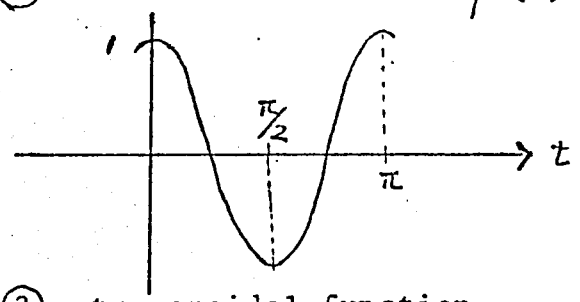

② trapezoidal function

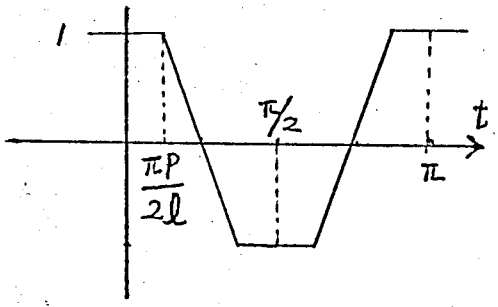

p : width of a pole

ℓ : interval of adjacent pole

$t = t' + n \qquad (n = 0, 1, 2, ...)$

$0 \leqq t' < \pi$

$$
\begin{aligned}
\phi(t) &= 1 && \text{for } 0 \le t' < \frac{\pi p}{2\ell} \\
&= \frac{\ell}{2p-\ell}\left(\frac{4}{\pi}t' - 1\right) && \text{for } \frac{\pi p}{2\ell} \le t' \le \frac{\pi}{2}\left(1-\frac{p}{\ell}\right) \\
&= -1 && \text{for } \frac{\pi}{2}\left(1-\frac{p}{\ell}\right) \le t' \le \frac{\pi}{2}\left(1+\frac{p}{\ell}\right) \qquad (2) \\
&= \frac{\ell}{\ell-2p}\left(\frac{4}{\pi}t' - 3\right) && \text{for } \frac{\pi}{2}\left(1+\frac{p}{\ell}\right) \le t' \le \frac{\pi}{2}\left(2-\frac{p}{\ell}\right) \\
&= 1 && \text{for } \frac{\pi}{2}\left(2-\frac{p}{\ell}\right) \le t' \le \pi
\end{aligned}
$$

(3) triangular function

special case of 2 i.e. p = 0

2. Numerical Analysis of Ionic Trajectories

Equation (1) can be changed into the simultaneous ordinary differential equation of 4-th order as follows.

$$
\begin{aligned}
\frac{dx_1}{dt} &= f_1(t,x_1,x_2,x_3,x_4) = x_2 \\
\frac{dx_2}{dt} &= f_2(t,x_1,x_2,x_3,x_4) = -(a+2q\phi(t))x_1 \qquad (3) \\
\frac{dx_3}{dt} &= f_3(t,x_1,x_2,x_3,x_4) = x_4 \\
\frac{dx_4}{dt} &= f_4(t,x_1,x_2,x_3,x_4) = (a+2q\phi(t))x_3
\end{aligned}
$$

Although there are several methods of solution of the above equations, we adopted the modified Adams method due to a short time for computation. This method, sometimes known as the Adams-Moulton method, is refered to as one of the closed type of predictor-corrector formulas [A 1]. It is particularly efficient for the investigations of the behavior of ions, that is, criterion of divergence of trajectories of ions. Written to apply to a system of equations (3), the predictor values are calculated by

$$x^{p}_{i,n+1} = x_{i,n} + \frac{h}{24}(9f_{i,n+1} + 19f_{i,n} - 5f_{i,n-1} + f_{i,n-2})$$

where $f_{i,s} = f_i(t_0 + (S-1)h, x_{1,s-1}, x_{2,s-1}, x_{3,s-1}, x_{4,s-1})$

with $i = 1,2,3,4$. The corrected values can now be calculated by

$$x^{c}_{i,n+1} = x_{i,n} + \frac{h}{24}(9f^{p}_{i,n+1} + 19f_{i,n} - 5f_{i,n-1} + f_{i,n-2})$$

where $f^{p}_{i,n+1} = f_i(t_0 + nh, x^{p}_{1,n+1}, x^{p}_{2,n+1}, x^{p}_{3,n+1}, x^{p}_{4,n+1})$

The four starting values required for this method are supplied by the Runge-Kutta method, which described

below. The increment of x_i, due to step increment from n to (n+1)th, is given as

$$x_{i,n+1}-x_{i,n}=\frac{1}{6}(k_{1,i}+2k_{2,i}+2k_{3,i}+k_{4,i})$$

where $k_{1,i}=hf_i(t_0+h(n-1),x_{1,n},x_{2,n},x_{3,n},x_{4,n})$

$$k_{2,i}=hf_i(t_0+h(n-\tfrac{1}{2}),x_{1,n}+\frac{k_{0,1}}{2},x_{2,n}+\frac{k_{0,2}}{2},x_{3,n}+\frac{k_{0,3}}{2},x_{4,n}+\frac{k_{0,4}}{2})$$

$$k_{3,i}=hf_i(t_0+h(n-\tfrac{1}{2}),x_{1,n}+\frac{k_{1,1}}{2},x_{2,n}+\frac{k_{1,2}}{2},x_{3,n}+\frac{k_{1,3}}{2},x_{4,n}+\frac{k_{1,4}}{2})$$

$$k_{4,i}=hf_i(t_0+hn,x_{1,n}+k_{2,1},x_{2,n}+k_{2,2},x_{3,n}+k_{2,3},x_{4,n}+k_{2,4})$$

and $i = 1,2,3,4$

Reference

[A.1] Hildelrrand, F.B., "Introduction to Numerical Analysis", McGraw-Hill, Inc., 1956.

Main Program

Initialization

XO(I) : initial value of dependent valuable x_i (I=1,2,3,4)

TO : initial value of independent valuable t

TF : final value of independent valuable t

H : integration interval

WP : interval of printing-out

Subroutine

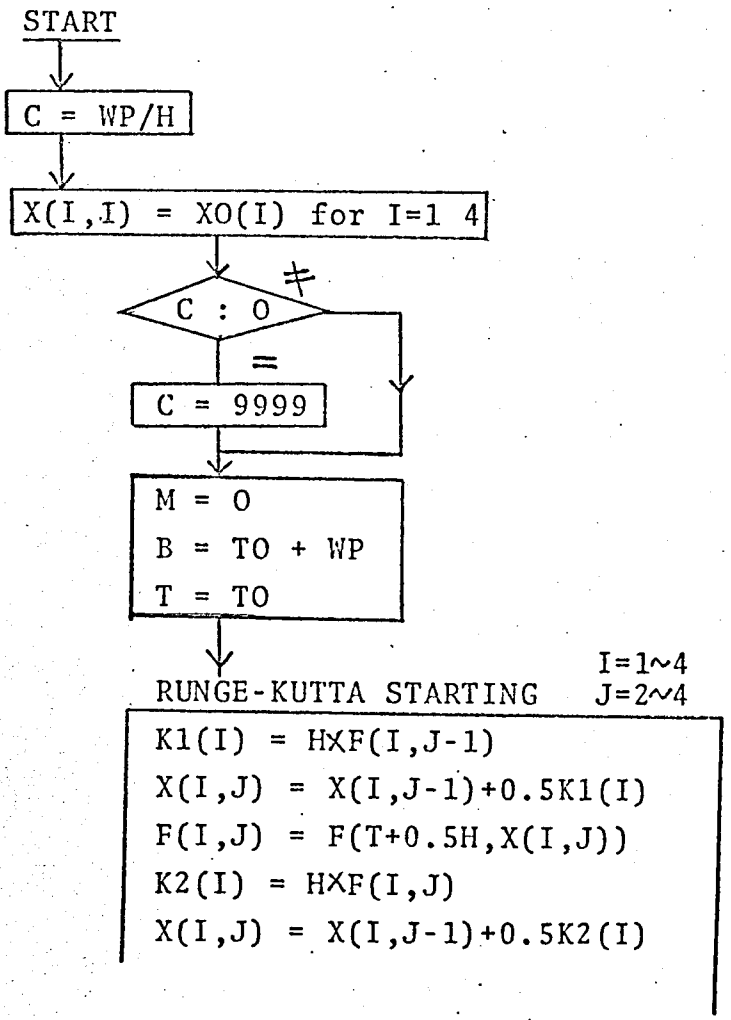

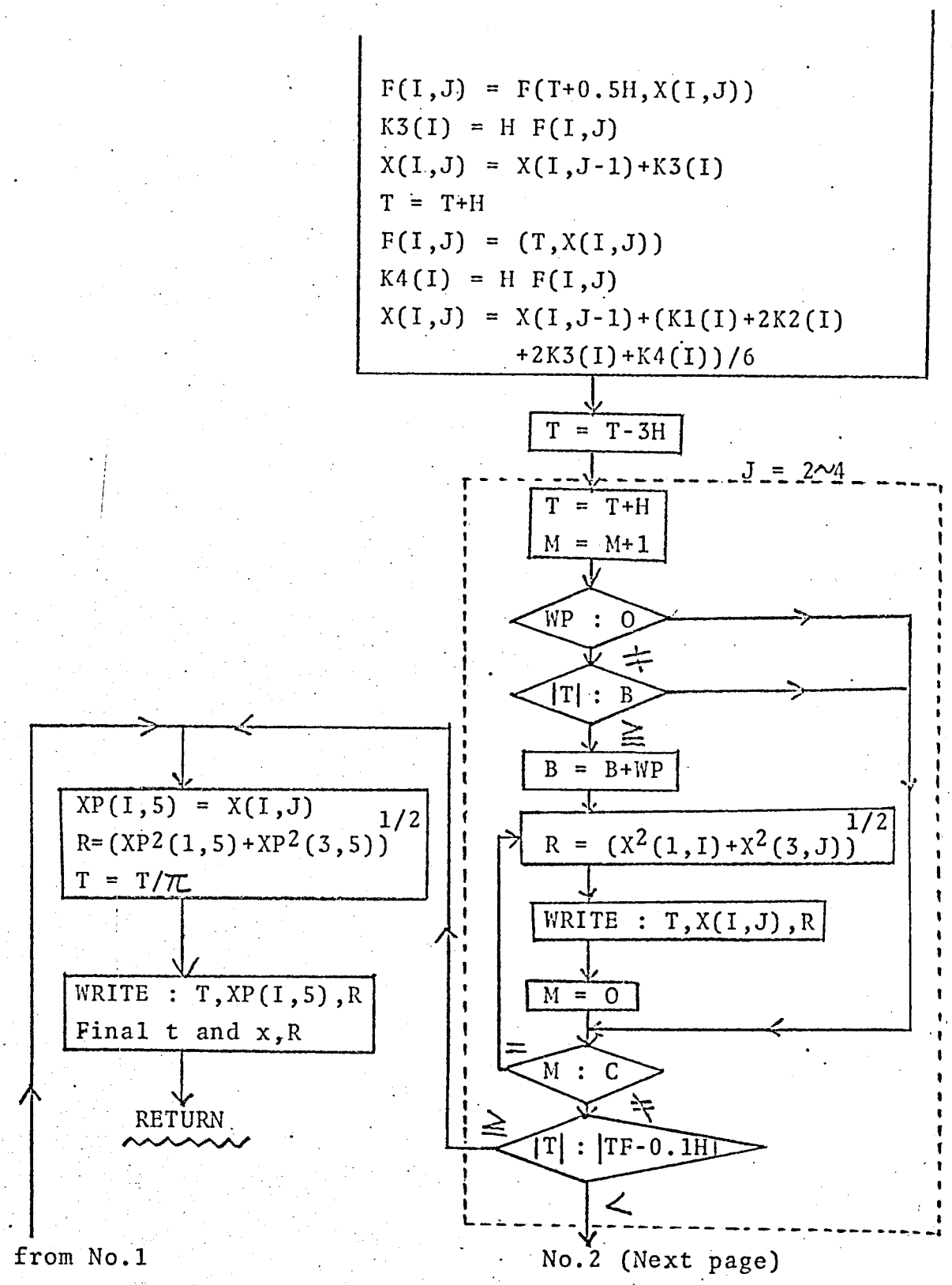
F(I,J) = F(T+0.5H,X(I,J))
K3(I) = H F(I,J)
X(I,J) = X(I,J-1)+K3(I)
T = T+H
F(I,J) = (T,X(I,J))
K4(I) = H F(I,J)
X(I,J) = X(I,J-1)+(K1(I)+2K2(I)
+2K3(I)+K4(I))/6
T = T-3H
J = 2~4
T = T+H
M = M+1
WP : 0
≠
|T| : B
≧
B = B+WP
R = (X²(1,I)+X²(3,J))^1/2
WRITE : T,X(I,J),R
M = 0
=
M : C
≠
≧
|T| : |TF-0.1H|
<
XP(I,5) = X(I,J)
R=(XP²(1,5)+XP²(3,5))^1/2
T = T/π
WRITE : T,XP(I,5),R
Final t and x,R
RETURN
from No.1
No.2 (Next page)

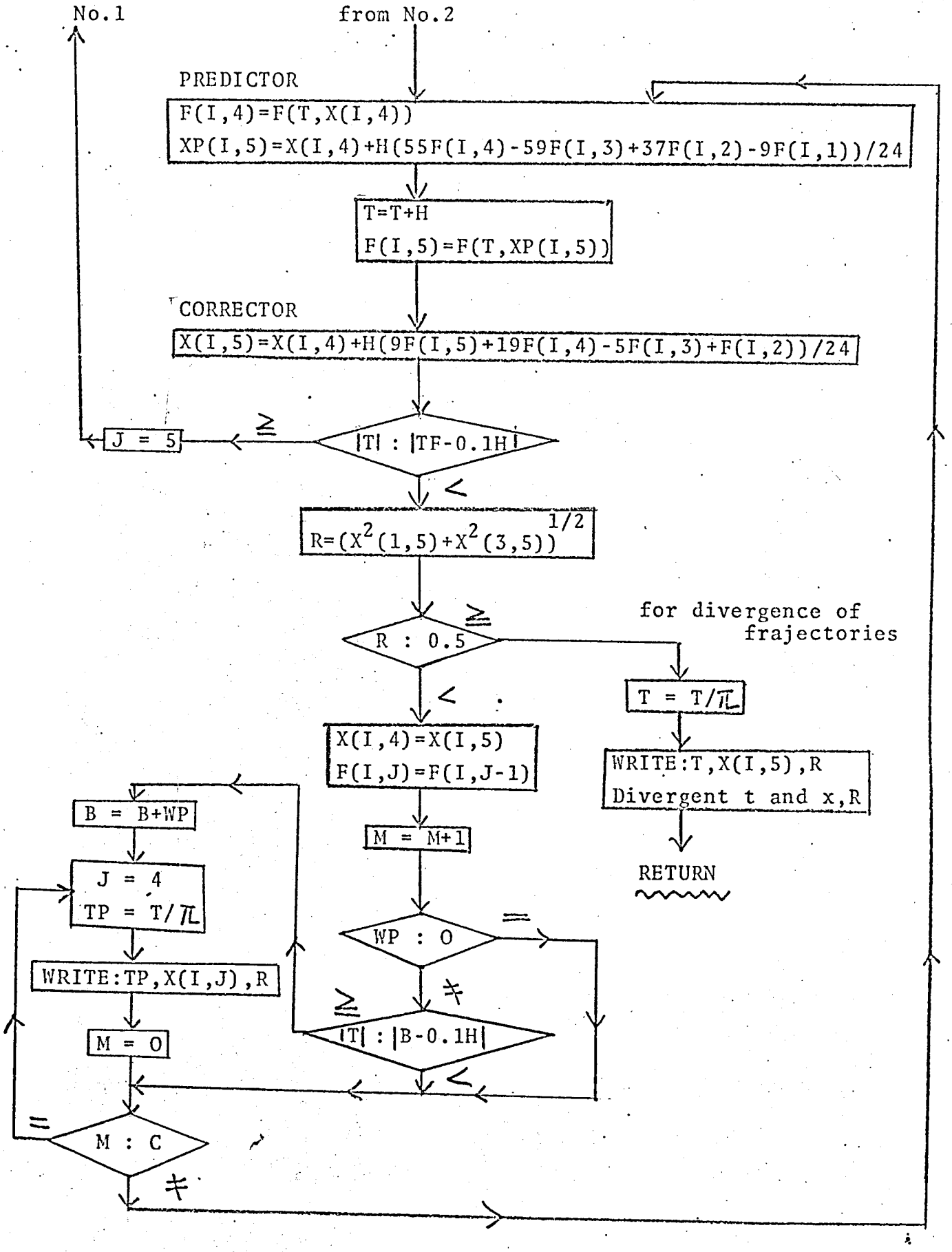
No.1
from No.2
PREDICTOR
F(I,4)=F(T,X(I,4))
XP(I,5)=X(I,4)+H(55F(I,4)-59F(I,3)+37F(I,2)-9F(I,1))/24
T=T+H
F(I,5)=F(T,XP(I,5))
CORRECTOR
X(I,5)=X(I,4)+H(9F(I,5)+19F(I,4)-5F(I,3)+F(I,2))/24
|T| : |TF-0.1H|
≧
J = 5
<
R=(X²(1,5)+X²(3,5))^1/2
R : 0.5
≧
for divergence of frajectories
T = T/π
WRITE:T,X(I,5),R
Divergent t and x,R
RETURN
<
X(I,4)=X(I,5)
F(I,J)=F(I,J-1)
M = M+1
WP : 0
=
≠
≧
|T| : |B-0.1H|
<
B = B+WP
J = 4
TP = T/π
WRITE:TP,X(I,J),R
M = 0
M : C
=
≠